MICROBIOME IN IBD: FROM COMPOSITION TO THERAPY

EDITED BY: Ruixin Zhu, Peijian He, Zhanju Liu, Ning-Ning Liu, Yinglei Miao, Chenggong Yu and Lixin Zhu

PUBLISHED IN: Frontiers in Pharmacology and Frontiers in Immunology

frontiers Research Topics

ISSN 1664-8714
ISBN 978-2-88971-223-6
DOI 10.3389/978-2-88971-223-6

About Frontiers

Frontiers is more than just an open-access publisher of scholarly articles: it is a pioneering approach to the world of academia, radically improving the way scholarly research is managed. The grand vision of Frontiers is a world where all people have an equal opportunity to seek, share and generate knowledge. Frontiers provides immediate and permanent online open access to all its publications, but this alone is not enough to realize our grand goals.

Frontiers Journal Series

The Frontiers Journal Series is a multi-tier and interdisciplinary set of open-access, online journals, promising a paradigm shift from the current review, selection and dissemination processes in academic publishing. All Frontiers journals are driven by researchers for researchers; therefore, they constitute a service to the scholarly community. At the same time, the Frontiers Journal Series operates on a revolutionary invention, the tiered publishing system, initially addressing specific communities of scholars, and gradually climbing up to broader public understanding, thus serving the interests of the lay society, too.

Dedication to Quality

Each Frontiers article is a landmark of the highest quality, thanks to genuinely collaborative interactions between authors and review editors, who include some of the world's best academicians. Research must be certified by peers before entering a stream of knowledge that may eventually reach the public - and shape society; therefore, Frontiers only applies the most rigorous and unbiased reviews.
Frontiers revolutionizes research publishing by freely delivering the most outstanding research, evaluated with no bias from both the academic and social point of view. By applying the most advanced information technologies, Frontiers is catapulting scholarly publishing into a new generation.

What are Frontiers Research Topics?

Frontiers Research Topics are very popular trademarks of the Frontiers Journals Series: they are collections of at least ten articles, all centered on a particular subject. With their unique mix of varied contributions from Original Research to Review Articles, Frontiers Research Topics unify the most influential researchers, the latest key findings and historical advances in a hot research area! Find out more on how to host your own Frontiers Research Topic or contribute to one as an author by contacting the Frontiers Editorial Office: frontiersin.org/about/contact

MICROBIOME IN IBD: FROM COMPOSITION TO THERAPY

Topic Editors:
Ruixin Zhu, Tongji University, China
Peijian He, Emory University, United States
Zhanju Liu, Tongji University, China
Ning-Ning Liu, Shanghai Jiao Tong University, China
Yinglei Miao, The First Affiliated Hospital of Kunming Medical University, China
Chenggong Yu, Nanjing Medical University, China
Lixin Zhu, The Sixth Affiliated Hospital of Sun Yat-sen University, China

Citation: Zhu, R., He, P., Liu, Z., Liu, N.-N., Miao, Y., Yu, C., Zhu, L., eds. (2021). Microbiome in IBD: From Composition to Therapy. Lausanne: Frontiers Media SA. doi: 10.3389/978-2-88971-223-6

Table of Contents

frontiers in Pharmacology

EDITORIAL
published: 24 June 2021
doi: 10.3389/fphar.2021.721992

Editorial: Microbiome in IBD: From Composition to Therapy

Ruixin Zhu[1], Peijian He[2], Zhanju Liu[3], Ningning Liu[4], Yinglei Miao[5], Chenggong Yu[6] and Lixin Zhu[7]*

[1]Department of Gastroenterology, The Shanghai Tenth People's Hospital, Department of Bioinformatics, School of Life Sciences and Technology, Tongji University, Shanghai, China, [2]Division of Digestive Diseases, Department of Medicine, Emory University School of Medicine, Atlanta, GA, United States, [3]Center for IBD Research, Department of Gastroenterology, The Shanghai Tenth People's Hospital, Tongji University, Shanghai, China, [4]State Key Laboratory of Oncogenes and Related Genes, Center for Single-Cell Omics, School of Public Health, Shanghai Jiao Tong University School of Medicine, Shanghai, China, [5]Department of Gastroenterology, First Affiliated Hospital of Kunming Medical University, Yunnan Institute of Digestive Diseases, Kunming, China, [6]Department of Gastroenterology, Nanjing Drum Tower Hospital, The Affiliated Hospital of Nanjing University Medical School, Nanjing, China, [7]Guangdong Institute of Gastroenterology, Guangdong Provincial Key Laboratory of Colorectal and Pelvic Floor Diseases, Department of Colorectal Surgery, The Sixth Affiliated Hospital, Sun Yat-sen University, Guangzhou, China

Keywords: inflammatory bowel disease, microbiome, ulcerative colitis, crohn's disease, interaction

Editorial on the Research Topic

Microbiome in IBD: From Composition to Therapy

Inflammatory bowel disease (IBD) is a chronic, non-specific, inflammatory intestinal disease with a high relapse rate. It has become a huge burden worldwide (Kaplan and Ng, 2017). IBD is characterized by changes in the gut microbiome. However, the role of the gut microbiome in the pathogenesis of IBD is still unclear. Therefore, this theme issue aims to discuss the changes of gut microbiome in IBD and its relevance for the treatment of IBD.

Currently, many studies have found that the composition of the gut microbiome in IBD were significantly altered which is considered to contribute to this immune disorder (Glassner et al., 2020). A probable mechanism is that the metabolites of the microbiota regulate metabolic pathways and inflammatory signal transduction thereby affecting the host immune system. On the other hand, the gut microbiota may affect the gut immunity through adherent bacteria. In this issue, Chen et al. reported that in pediatric IBD, adherent bacteria attached to the terminal ileum were associated with elevated Th17 cells and SIgA responses (Chen et al.). The limitation of this study was the lack of intervention approach. Previous studies of adherent bacteria mainly rely on models of immortal cell lines, which cannot reproduce the tissue-like environment. To address limitations, Mayorgas et al. established a human colonic organoids model which represents a promising tool to study the cross talk between Adherent-invasive *Escherichia coli* and intestinal epithelial cells (Mayorgas et al., 2021).

Studies on the microbial change in pharmaceutical treatment of IBD provided additional evidence for the microbial contribution in IBD pathogenesis. Dai et al. investigated the pharmaceutical mechanism of mesalamine in the treatment of UC through 16S sequencing and metabolomics (Dai et al.). Mesalamine is a radical scavenger and antioxidant, often used to treat UC. The authors observed that the abundance of some bacteria and metabolites were reversed toward the healthy status after mesalamine treatment. Similarly, as summarized in this issue by Li et al., many natural products may exert their therapeutic effects on the gut microbiota in the treatment of IBD (Li et al.). These studies reveal possible molecular mechanisms of naturally derived polysaccharides from plants, seaweeds, and mushrooms in the treatment of IBD, and also identified many potential clinical therapeutic targets. In the same direction, Guo et al. reported that ginger can significantly increase the diversity of intestinal microbiome and alleviate the severity of UC (Guo et al.). This study suggests that the abnormality of the microbiome is closely related to amino acid metabolism, oxidative

OPEN ACCESS

Edited and reviewed by:
Angelo A. Izzo,
University of Naples Federico II, Italy

****Correspondence:***
Ruixin Zhu
*rxzhu@tongji.edu.cn *

Specialty section:
This article was submitted to Gastrointestinal and Hepatic Pharmacology, a section of the journal Frontiers in Pharmacology

Received: *08 June 2021*
Accepted: *14 June 2021*
Published: *24 June 2021*

Citation:
Zhu R, He P, Liu Z, Liu N, Miao Y, Yu C and Zhu L (2021) Editorial: Microbiome in IBD: From Composition to Therapy. Front. Pharmacol. 12:721992. doi: 10.3389/fphar.2021.721992

phosphorylation, protein translation, and ribosome biogenesis. Also in this issue, the study of Zhao et al. is unique in utilizing a nano-targeted drug delivery system to achieve a highly efficient delivery of berberine (Zhao et al.), which effectively regulated inflammation and reconstructed the intestinal microbial community.

One surprising report by Liu et al. explored the effect of metformin in the treatment of IBD from the perspective of drug repurposing (Liu et al.). Although metformin is commonly used to treat type 2 diabetes, some studies report that metformin affect the intestinal microbiome and thus may have a beneficial effect on IBD (Sanchez-Rangel and Inzucchi, 2017). Liu et al. demonstrated a positive effect of metformin on IBD and its association with altered microbiota, that is, significantly increased abundance of the anti-inflammatory bacterium *A. muciniphlia* in the metformin treatment group. Interestingly, Silverstri et al. reported that the anti-inflammatory effects of fish oil and cannabidiol are also associated with increased abundance of *A. muciniphlia* in mouse enteritis models (Silvestri et al.). These studies suggest that microbial intervention could be an effective strategy to control inflammation.

Recently, fecal microbiota transplantation (FMT) gains popularity as an intervention to restore the community of the intestinal microbiota and to treat several gastrointestinal diseases (Weingarden and Vaughn, 2017), including IBD, which was reviewed by Tan et al. in this issue (Tan et al.). This review provided an overview of the effectiveness of FMT in the treatment of IBD. Further, the authors summarized the therapeutic mechanisms of FMT in IBD.

The research topic of "Microbiome in IBD: From Composition to Therapy" discuss not only the role of intestinal microbiome in the pathological mechanisms of IBD, but also in the pharmaceutical mechanisms of multiple drugs. We expect that this collection of inspiring work will stimulate new avenues of thinking, approaches, and collaborations in exploring the complex pathogenesis of IBD and lead to novel therapeutic targets for IBD.

AUTHOR CONTRIBUTIONS

All authors listed have made a substantial, direct and intellectual contribution to the work, and approved it for publication.

ACKNOWLEDGMENTS

The guest editors would like to personally thank all the authors and reviewers who contributed to this research topic. We also greatly appreciate the help of the Frontiers editorial office.

REFERENCES

Glassner, K. L., Abraham, B. P., and Quigley, E. M. M. (2020). The Microbiome and Inflammatory Bowel Disease. *J. Allergy Clin. Immunol.* 145, 16–27. Epub 2020/01/09. doi:10.1016/j.jaci.2019.11.003

Kaplan, G. G., and Ng, S. C. (2017). Understanding and Preventing the Global Increase of Inflammatory Bowel Disease. *Gastroenterology* 152, 313–321. e312Epub 2016/10/30. doi:10.1053/j.gastro.2016.10.020

Mayorgas, A., Dotti, I., Martínez-Picola, M., Esteller, M., Bonet-Rossinyol, Q., Ricart, E., et al. (2021). A Novel Strategy to Study the Invasive Capability of Adherent-Invasive *Escherichia coli* by Using Human Primary Organoid-Derived Epithelial Monolayers. *Front. Immunol.* 12, 646906, 2021 . Epub 2021/04/16. doi:10.3389/fimmu.2021.646906

Sanchez-Rangel, E., and Inzucchi, S. E. (2017). Metformin: Clinical Use in Type 2 Diabetes. *Diabetologia* 60, 1586–1593. Epub 2017/08/05. doi:10.1007/s00125-017-4336-x

Weingarden, A. R., and Vaughn, B. P. (2017). Intestinal Microbiota, Fecal Microbiota Transplantation, and Inflammatory Bowel Disease. *Gut Microbes* 8, 238–252. Epub 2017/06/14. doi:10.1080/19490976.2017.1290757

Conflict of Interest: The authors declare that the research was conducted in the absence of any commercial or financial relationships that could be construed as a potential conflict of interest.

frontiers in Pharmacology

REVIEW
published: 18 September 2020
doi: 10.3389/fphar.2020.574533

Fecal Microbiota Transplantation for the Treatment of Inflammatory Bowel Disease: An Update

Pufang Tan[1], *Xiaogang Li*[1], *Jun Shen*[1,2*] *and Qi Feng*[3]

[1] Division of Gastroenterology and Hepatology, Baoshan Branch, Renji Hospital, School of Medicine, Shanghai Jiao Tong University, Shanghai, China, [2] Division of Gastroenterology and Hepatology, Key Laboratory of Gastroenterology and Hepatology, Ministry of Health, Inflammatory Bowel Disease Research Center, Renji Hospital, School of Medicine, Shanghai Jiao Tong University, Shanghai Institute of Digestive Disease, Shanghai, China, [3] Department of Radiology, Renji Hospital, School of Medicine, Shanghai Jiao Tong University, Shanghai, China

Fecal microbiota transplantation (FMT) has successfully been applied for the treatment of recurrent *Clostridioides difficile* infection (CDI), which has led to studies on its application to other gastrointestinal diseases and extraintestinal diseases associated with gut microbiota dysbiosis. Recently, the results of FMT for patients with inflammatory bowel disease (IBD) have been encouraging. However, studies have not fully clarified the clinical application of this emerging therapy. Here, we aimed to review the current knowledge in this fast-growing field and characterize the effectiveness, safety and mechanisms of FMT for the treatment of IBD patients.

Keywords: fecal microbiota transplantation, inflammatory bowel disease, ulcerative colitis, Crohn's disease, microbiome

OPEN ACCESS

Edited by:
Zhanju Liu,
Tongji University, China

Reviewed by:
Faming Zhang,
Nanjing Medical University, China
Yinglei Miao,
Kunming Medical University, China

***Correspondence:**
Jun Shen
shenjun79@sina.cn

Specialty section:
This article was submitted to Gastrointestinal and Hepatic Pharmacology, a section of the journal Frontiers in Pharmacology

Received: *20 June 2020*
Accepted: *20 August 2020*
Published: *18 September 2020*

Citation:
Tan P, Li X, Shen J and Feng Q (2020) Fecal Microbiota Transplantation for the Treatment of Inflammatory Bowel Disease: An Update. Front. Pharmacol. 11:574533. doi: 10.3389/fphar.2020.574533

INTRODUCTION

Fecal microbiota transplantation (FMT) refers to the therapeutic procedure of transplanting fecal bacteria from healthy persons into patients (Gupta and Khanna, 2017). FMT is aimed at restoring the colonic microbiota through the introduction of fit bacterial population by infusing the gut microbiota, for example *via* colonoscopy, the orogastric tube, enema, or orally in the form of a capsule that contains the freeze-dried substance, to obtain an intestinal microbiota from a suitable donor. This therapeutic method has been proven to be incredibly successful for the treatment of recurrent *Clostridioides difficile* infection (CDI). (Drekonja et al., 2015)

The techniques of FMT deal with three key aspects, including donor selection, together with preparation of donor substance, and FMT delivery (Kelly et al., 2015; Mullish et al., 2018). Appropriate donors should include those of the age range of 18–60 years (Anand et al., 2017; Mullish et al., 2018), in addition to those with a BMI from 18 to 30 kg/m^2 (Alang and Kelly, 2015). The employment of multiple donors was more effective compared with single donor, because that multiple donors increase the microbial diversity in the fecal suspension compared with that of single donor (Levy and Allegretti, 2019). In each of the FMT preparations, the stool requires a weight of at least 25 g for lower gastrointestinal delivery and 12.5 g for upper gastrointestinal delivery (Cammarota et al., 2019). The final fecal substance preserved frozen at a temperature of −80°C is considered to have a maximum shelf life of 2 years (Cammarota et al., 2019). Prior to utilisation, the frozen fecal material should be thawed at 37°C, followed by use within a period of 6 h of thawing (Costello et al., 2015). The fecal microbiota

could be supplied *via* the upper GI route (endoscopically or with the use of a nasogastric tube, nasoduodenal tube, or nasojejunal tube), the lower GI route (retention enema, colonoscopy), or through capsules (which contain either the freeze-dried or lyophilised fecal substance) (Mullish et al., 2018). Proton pump inhibitor and prokinetics (for example, metoclopramide) should be considered before FMT *via* the upper GI route (De Jager et al., 2012; Cohen et al., 2016). Bowel lavage must be performed before FMT *via* the lower GI route. Specifically, Polyethylene glycol preparations are preferred (Kelly et al., 2016). A single dose of loperamide (or other anti-exercise drugs) could be considered subsequent to the lower GI FMT delivery. Further, a minimum 24-h washing period is required from the last dose of antibiotics to FMT treatment (Cammarota et al., 2015). When recipients also show signs of long-term antibiotic use within 8 weeks after FMT, it is necessary to consult infectious disease experts or medical microbiologists for advice (Terveer et al., 2017).

FMT is considered approximately 90% success rate for individuals with recurrent or refractory CDI (Quraishi et al., 2017). In 2013, FMT was approved by the USA Food and Drug Administration for clinical applications of recurrent or refractory CDI (Surawicz et al., 2013). In addition to CDI, there are some studies that have proven that FMT could emerge as a productive method to treat inflammatory bowel disease (IBD). IBD refers to an intestinal disorder, including ulcerative colitis (UC) as well as Crohn's disease (CD). IBD is characterized by chronic inflammation of the gastrointestinal tract, as well as the periodicity of disease progression and remission. During disease activity, patients are likely to present with diarrhoea, coupled with nausea, loss of weight, anepithymia, fever, and celialgia (White et al., 2018). However, the precise pathophysiology is not entirely clear and the aetiology is multifactorial, influenced by individual genetic susceptibility, the external environment, internal gut microbiota, and the host immune response (Zhou et al., 2017). The imbalance of the gut microbiota has been suggested to markedly impact IBD progression (Zuo and Ng, 2018). Metabolomic and metagenomics research has identified the characteristics of IBD microbiota, in addition to finding a general decline in bacterial diversity, with a particular decline in members of *Lachnospiraceae*, as well as the *Bacteroidetes phylum*, coupled with an increase in *Proteobacteria* and *Actinobacteria* (Henson and Phalak, 2017). Biopsy samples attained from patients with CD were found a decline in *Fecalibacterium prausnitzii* which has the effects of anti-inflammatory (Sokol et al., 2008).

FMT is currently regarded as a productive intervention for recurring CDI (Bakken et al., 2011). Meanwhile, the use of FMT in IBD does not result in the same exceptional outcomes. However, emerging data have suggested the possibility that this therapy could have a better effect on these diseases. Reviewing the current evidence on the utility of FMT for the treatment of IBD, we focus on the effectiveness, safety and mechanisms of this new treatment, as well as ongoing research in this growing field.

EFFICACY AND SAFETY OF FMT FOR IBD

The traditional methodology of treating IBD was aimed at reducing the inflammatory. Nevertheless, the latest insights focus on the microbiome, in addition to the idea of dysbiosis and its latent role in IBD pathogenesis, resulting in irreplaceable therapeutic methodologies like FMT, a fascinating area of investigation. FMT was identified as a standard therapy for recurrent CDI, but its efficacy for IBD therapy is controversial (Basso et al., 2018). Most of the researches did not indicated key negative events or severe negative events that were considered medically associated with FMT treatment (Paramsothy et al., 2017b). Sood et al. (2020) performed a retrospective analysis of 101 active UC patients receiving multiple FMT *via* colonoscopy. The study found that the most common short-term adverse events of FMT included abdominal discomfort (30.8%), flatulence (15.9%), abdominal distension (9.8%), borborygmi (7.9%), and low-grade fever (7.6%). The long-term adverse events were arthritis/arthralgia (6.5%), urticaria (4.3%), depression (2.2%), allergic bronchitis (2.2%), and partial sensorineural hearing loss (2.2%). FMT appears to be a safe procedure.

IBD With CDI

Patients who get IBD are easily infected by *C. difficile* (Rodemann et al., 2007). Khoruts et al. (2016) suggested that FMT could be successful for clearing CDI form both IBD and non-IBD patients. Nevertheless, in patients with underlying IBD, the efficiency of single FMT therapy for this application was lower than that in patients without IBD (74.4% *vs.* 92.1%; P = 0.0018). More than 1/4 of patients with IBD (25.6%) related to CDI experienced a significant flare of IBD after treatment with FMT. The latest study including 56 CDI patients (22 UC and 13 CD) who received FMT procedures *via* colonoscopy was successful for 48/56 (85.7%) of cases. In contrast, more than 50% of patients with UC experienced a sudden outbreak of IBD activity (Newman et al., 2017). The largest study of IBD patients with recurrent or refractory CDI included 67 patients (35 CD, 31 UC, and one indeterminate colitis). Respectively, the success rates of the first, second, and third fecal microbiota transplantation were 79%, 88%, and 90%. After FMT, 25 patients (37%) reported improvements in IBD disease activity, 20 patients (30%) had no change, and for nine patients (13%), disease worsened. Serious adverse events included CDI hospitalisation (2.9%), hospitalisation for IBD flares (2.9%), colectomy (1.4%), small bowel obstruction (1.4%), pancreatitis (1.4%), and cytomegalovirus colitis (1.4%) (Fischer et al., 2016). In conclusion, FMT has shown safety and efficacy in clearing CDI from patients with IBD, but the results need to be further evaluated systematically.

Ulcerative Colitis

To date, there have been five published randomised controlled trials (RCT) that assessed the effectiveness of FMT in UC (**Table 1**) (Moayyedi et al., 2015; Rossen et al., 2015; Paramsothy et al., 2017a; Costello et al., 2019; Sood et al., 2019). In July 2015, the first research using a nasoduodenal tube for FMT found that there is no statistically significant difference in the rate of endoscopic and clinical remission between FMT and control groups (Rossen et al., 2015). However, the other four trials using lower gastrointestinal microbiota transplantation showed encouraging results (Moayyedi et al., 2015; Paramsothy et al.,

TABLE 1 | Characteristics of randomized controlled trials on fecal microbiota transplantation (FMT) for ulcerative colitis.

Study	N (FMT/ Control)	Disease activity	Control	Delivery	Frequency	Donor	Dosage	Primary end-point	Follow up	Remission	Response
Rossen et al., 2015	48 (23/ 25)	SCCAI ≥ 4 and ≤ 11	Autologous fecal microbiota	Nasoduodenal	2 (weeks 0 and 3)	Single	Minimum 60 g stool in 500 ml saline	SCCAI ≤ 2 and ≥ 1 point decrease in Mayo endoscopic score	12 weeks	FMT 30.4%, control 20%, p= 0.51	FMT 47.8%, Control 52%
Moayyedi et al., 2015	75 (38/ 37)	Mayo Clinic score ≥ 4 with endoscopic score ≥ 1.	Water enema	Enema	6 (weekly)	Single	50 g stool in 300 ml water	Total Mayo score ≤ 2 with endoscopic score 0.	7 weeks	FMT 24%, control 5%, p=0.03*	FMT 39%, Control 24%, p = 0.16
Paramsothy et al., 2017a	81 (41/ 40)	Mayo Clinic score 4–10 with endoscopic score ≥ 1.	Saline enema	Initial colonoscopy then enema	40 (5/week for 8 weeks)	Pooled multi-donor	37.5 g stool in 150 ml	Total Mayo score ≤ 2, all subscores ≤ 1, and ≥ 1 point reduction in endoscopic score	8 weeks	FMT 27%, control 8%, p = 0.02*	FMT54%, Control 23%, p = 0.004*
Costello et al., 2019	73 (38/ 35)	Mayo Clinic score 310 with endoscopic score ≥2.	Autologous fecal microbiota	Initial colonoscopy then enema	3 (week 0 colonoscop-y, 2 enemas week 1)	Pooled multi-donor	Colonoscopy 50 g stool in 200 ml saline and glycerol, enema 25 g stool in 100 ml	Total Mayo score ≤ 2 and endoscopic score ≤ 1	8 weeks	FMT 32%, Contro l 9%, p = 0.02*	FMT 55%, Control 20%, p ≤ 0.01*
Sood et al., 2019	61(31/ 30)	Mayo score ≤ 2 with each subscore ≤ 1	NR	colonoscopic	7 (Weeks 0, 8, 16, 24, 32, 40, and 48)	Single and unrelated	100g in 200 ml	Mayo score ≤ 2, all subscores ≤ 1	48 weeks	FMT 87.1%, control 6.7%, p= 0.11	NR

*SSCAI, simple clinical colitis activity index. *Statistically significant.*

2017a; Costello et al., 2019; Sood et al., 2019). Moayyedi et al. (2015) found that patients with UC for less than 1 year, but not longer, could enter a state of remission after treatment with FMT. These different findings are likely due to dissimilarities in the routes of administration, in addition to the stool donors and dosing schedules. Sood et al. (2019) conducted a study among 61 UC patients in clinical remission. Participants were randomly assigned to receive either FMT or placebo. Maintaining clinical remission at 48 weeks was achieved in 87.1% patients receiving FMT compared with 66.7% receiving placebo. There was a statistically significant impact of FMT on Endoscopic remission (FMT: 58.1% compared with placebo: 26.7%, p = 0.026) and histological remission (FMT: 45.2% compared with placebo: 16.7%, p = 0. 033). It is indicated that maintenance FMT in UC patients with clinical remission could help sustain endoscopic, histological, and clinical remission.

One recently published meta-analysis assessing the aforementioned four RCTs indicated that 39 of 140 (28%) patients achieved clinical remission in the FMT groups compared to 13 of 137 (9%) patients in the placebo groups, with an odds ratio of 3.67 (95% CI: 1.82–7.39, P < 0.01). Compared to 38 of 137 (28%) placebo patients, 69 of 140 (49%) patients in FMT groups achieved clinical responses, and the odds ratio was 2.48 (95% CI: 1.18–5.21, P = 0.02) (Costello et al., 2017). The latest systematic review and meta-analysis considered 27 research papers, which included 596 adult and paediatric IBD patients, and 459 patients were treated with FMT. During the follow-up period, 132 of 459 (28.8%) patients achieved clinical remission. The clinical effective rate was 53% (241/ 459). The overall clinical remission rate for UC was 21% (95% CI: 8–37%). As subgroup analyses revealed, the clinical remission rate prevailing in adult UC patients amounted to 26% (95% CI: 10%–48%), whereas paediatric patients showed a rate of 10% (95% CI: 0%–43%) (Fang et al., 2018). Hence, the therapeutic effect of FMT for patients with UC is very promising, particularly for patients with multiple transfusions through the lower digestive tract.

Crohn's Disease

The evidence on the effect of FMT in CD has recently been presented. There are currently several active trials studying the effectiveness of FMT for CD, and the results are diverse (**Table 2**) (Cui et al., 2015; Suskind et al., 2015; Wei et al., 2015; Vaughn et al., 2016; Vermeire et al., 2016; Goyal et al., 2018; Gutin et al., 2019; Sokol et al., 2020; Xiang et al., 2020). Xiang et al. (2020) studied 174 CD patients treated with FMT *via* Mid-gut including nasojejunal tube, endoscopy and mid-gut TET (except one through colonic TET). At 1 month after FMT, 76% (19/25), 72.7% (101/139), 70.6% (12/17) and 61.6% (90/146) of patients achieved improvement in hematochezia, abdominal pain, fever and diarrhoea respectively. At the final follow-up, the clinical remission was achieved in 20.1% (35/174) and the clinical

TABLE 2 | Characteristics of fecal microbiota transplantation for Crohn's disease.

Study	N	Age (y)	Disease Activity	Delivery	Frequency	Donor	Dosage	Primary end-point	Follow up	Remission	Response
Vaughn et al., 2016	19	> 18	HBI ≥ 5	Colonoscopy	1	Unrelated	50 g stool in 250 ml solution	HBI < 5 at 4weeks	26 weeks	53%	58%
Vermeire et al., 2016	6	28–53	Widespread involvement of the colon and/or ileum.	Nasojejunal or rectal tube	2 (daily for consecutive days)	Patient-directed donor	200 g stool in 400 ml saline	SES-CD < 3	8 weeks	0%	0%
Cui et al., 2015	30	15–71	HBI ≥ 7	Duodenum *via* gastroscope	1	Patient-directed donor	150–200 ml	HBI ≤ 4	15 months	76.7%	86.7%
Wei et al., 2015	3	16–70	CDAI 150–400 and CRP > 10 mg/L	Nasojejunal or colonoscopy	1	Unrelated	60 g stool in 350 ml saline	CDAI < 150 and CRP < 10 mg/l	4 weeks	0%	NR
Goyal et al., 2018	4	2–22	PCDAI 10–40 or lactoferrin/calprotectin 2×upper limit of normal	Distal duodenum or jejunum *via* gastroscopy or colonoscopy	1	Patient-directed donor	150 g stool in 250–300 ml saline	PDAI<10 or normalization of lactoferrin/calprotectin at 1 month	6 months	50%	75%
Suskind et al., 2015	9	12–19	PCDAI 10–29	Nasogastric tube	1	Related	30 g stool in 100–200 ml saline	PCDAI < 10	12 weeks	78% at 2 weeks, 56% at 6 and 12 weeks	NR
Gutin et al., 2019	10	18-70	HBI ≥ 3	Colonoscopy	1	Unrelated donors	NR	decrease in HBI ≥ 3 at 1 month	12 months	10%	30%
Xiang et al., 2020	174	Median was 33 (IQR: 23–43)	The median of HBI was 8 (IQR: 6–10)	Mid-gut including endoscopy, nasojejunal tube, and mid-gut TET (except one through colonic TET)	Median was 3.5 (IQR: 2–5)	Related and unrelated donors	NR	The rate of improvement in each therapeutic target	Median was 43 months (IQR: 28–59)	20.1%	43.7%
Sokol et al., 2020	17	18–70	HBI > 4	Colonoscopy	1	Unrelated donor	50–100g	successful colonization of donor microbiota	24 weeks	FMT group: 87.5% at 10 weeks; control group 44.4%	NR

HBI, Harwey Bradshaw Index; CDAI, Crohn's Disease Activity Index; PCDAI, Pediatric Crohn's Disease Activity Index; TET, transendoscopic enteral tubing; IQR, interquartile range; NR, not recorded.

response was achieved in 43.7% (76/174). Sokol and colleagues conducted a randomized controlled study of FMT in CD patients. Participants were randomly assigned either to the FMT group or the control group. The incidence of flare in the FMT group was lower than in the control group but there was not a statistically significant impact of FMT on clinical remission. The clinical remission at 10 and 24 weeks was 7/8 (87.5%) and 4/8 (50.0%) in the FMT group and 4/9 (44.4%) and 3/9 (33.3%) in the control group. Crohn's Disease Endoscopic Index of Severity decreased at 6 weeks in the FMT group ($p = 0.03$) but not in the control group ($p = 0.8$). On the contrary, the CRP level increased at 6 weeks in the control group ($p = 0.008$) but not in the FMT group ($p = 0.5$) (Sokol et al., 2020).

Xiang et al. (2020) believed that FMT in CD against targeted therapeutics was efficient, especially hematochezia, abdominal pain, diarrhoea and fever. Whereas, Further research needs to be conduced to gain more high-quality data and provide conclusions with respect to the use of FMT for these patients and subsequently which CD phenotypes are most likely to benefit.

Pouchitis

Pouchitis is the most common complication of patients with refractory UC with ileal pouch-anal anastomosis, and morbidity can reach nearly 50%. Similar to that with UC and CD, a decrease in intestinal microbial diversity plays a critical role in its pathogenesis. Antibiotics might induce remission of pouchitis but can lead to recurrence (Shen, 2012; Maharshak et al., 2017). Probiotics can prevent recurrence, which might be related to recovery of the mucosal barrier (Persborn et al., 2013). Five studies have been conducted to evaluate FMT in patient with pouchitis (**Table 3**) (Landy et al., 2015; Stallmach et al., 2016;

TABLE 3 | Characteristics of fecal microbiota transplantation for pouchitis.

Study	N	Age (y)	Disease Activity	Delivery	Frequency	Donor	Dosage	Primary end-point	Follow up	Remission	Response
Landy et al., 2015	8	24–63	Chronic antibiotic refractory Pouchetis,PDAI ≥ 7	Nasogastric	1	NR	18 g stool/ 30 ml saline solution)	PDAI ≤ 4	4 weeks	0%	25%
Nishida et al., 2019	3	24–52	PDAI ≥ 7	Colonoscopy	1	Related	NR	Reduction in total PDAI ≥ 3 at 8 weeks	8 weeks	0%	33%
Stallmach et al., 2016	5	26–40	Chronic antibiotic refractory pouchitis, PDAI 9–14	Jejunum *via* upper gastrointestinal tract endoscopy	1–7 (3–4 weeks intervals)	Two unrelated	75 g stool in 200 ml saline	NR	3 months	80% at 4 weeks, 60% at 3 months	100%
Herfarth et al., 2019	6	22–60	Chronic antibiotic refractory pouchi-tis (mPDAI≥5 and a history of ≥4 antibiotic therapies for pouchitis in the last 12 months)	Endoscopic (eFMT) and oral encapsulated (oFMT)	eFMT: 2; oFMT: daily for 14 days	Unrelated	eFMT: 12 g stool in 30 ml; oFMT: 4.2 g stool	The safety of the combined eFMT and oFMT	16 weeks	17%	17%
Selvig et al., 2020	19	18-74	Chronic pouchitis (pouch symptoms > 4 weeks and endoscopic evaluation con-frming infamma-tion of the pouch	Pouchoscopy	1–2	12 months	250 ml donor fecal suspen-sion (25 g stool)	Clinical improvement at week 4.	12 months	0	9% (among patients receiving double FMT)

PDAI, Pouchitis Disease Activity Index; FMT, fecal microbiota transplantation; eFMT, endoscopic FMT; oFMT, oral encapsulated FMT.

Herfarth et al., 2019; Nishida et al., 2019; Selvig et al., 2020). In the four studies using a single-source fecal bacteria, none of the patients achieved remission of clinical symptoms (Landy et al., 2015; Herfarth et al., 2019; Nishida et al., 2019; Selvig et al., 2020). Stallmach et al. (2016) used multi-source fecal bacteria and many transplantations, and 80% of the patients achieved clinical remission, with the rest attaining a clinical response. It was lacked of available data and randomized controlled trials to demostrate the efficiency of FMT in treating Pouchitis. Recently, A prospective randomized controlled trial assessing the efficacy of FMT in pouchitis patients was prematurely stopped for low donor FMT engraftment (Selvig et al., 2020). Larger randomized controlled trials are needed to validate the effectiveness of FMT in pouchitis.

IMMUNOMODULATORY EFFECTS AND MECHANISMS OF FMT

FMT therapy has been used for CDI for decades, whereas its use for IBD began since the year 2012. Reviewed from current researches, the immunomodulatory effects and mechanisms of FMT have been concluded:

Intestinal Microbial Ecology

Various gastrointestinal disorders, which include IBD, are linked to changes in the intestinal microbiota composition and metabolic dysbiosis. It is not known if tissue impairment is caused by abnormal immune responses to normal microbiota or by a normal immune response to abnormal microbiota or if dysbiosis constitutes a cause or outcome of IBD (Sheehan et al., 2015; Ni et al., 2017). FMT is considered a promising therapeutic methodology for IBD patients, primarily to achieve outcomes of intestinal microbial restoration (Burrello et al., 2019).

FMT can increase the diversity of intestinal microorganisms, together with rebuilding the immune system and maintaining the balance of intestinal microecology. Even though comprehensive studies on increasing the microbial diversity of the intestines are continually being updated, many current studies could provide such proof-of-concept. Zeng et al. (2019) carried out a study analyzing the latest trials dealing with the immunomodulatory effects and underlying processes of probiotics and FMT, in addition to examining the effectiveness and safety of probiotics and FMT for medical experiments. Their group concluded that the intestinal microbiota from the donors limited intestinal permeability, inhibited intestinal epithelial cell apoptosis, re-established the function of the intestinal barrier, mitigated the production of proinflammatory cytokines and restored the metabolism of secondary bile acids in the intestinal tract. Further, FMT could compete with or antagonise pathogenic bacteria, in addition to enhancing insulin resistance. As a result, the patient's immunity is improved. The IBD microbiome was discovered to promote inflammation and show signs of augmented oxidative stress, in addition to the enhanced secretion of type II toxins and the elevated level of virulence-associated bacterial genes (Erickson et al., 2012).

T-Cell Populations

The populations of gut-linked immune cells make a critical contribution to initiating and sustaining intestinal inflammation, which occurs in patients with IBD and in experimental models of intestinal inflammation (Blumberg et al., 1999; Kaser et al., 2010). Natividad et al. (2015) showed that mice colonized with microbial populations from UC patients that were low in *Firmicutes* were more sensitive to colitis than mice colonized with *Firmicutes*-rich faeces or synthetic ecosystems. Here, *Firmicutes* bacteria were not abundant, the expression of Th17-related genes was increased, and the CD^{4+} cells expressing IL-17A were expanded. Further, bacterial isolates supplemented with *Firmicutes* can eliminate the enhanced Th17 response *in vitro*, and the results support the use of ecotherapy strategies rich in *Firmicutes* to prevent or treat UC.

Populations of T cells that are separated from the colons of mice treated by FMT exhibit a decrease in their ability to proliferate compared to those isolated from colitis mice without FMT treatment. Phenotypically, FMT-treated mice show lower percentages of CD^{8+} T and CD^{4+} T cells, which express the cytotoxicity-related molecule CD107a. This further supports the observation of a decrease in the pro-inflammatory phenotype of colonic T cells in mice treated with FMT (Burrello et al., 2019).

Inflammatory Cytokines

UC has been linked to abnormal Th2 cell response-mediated inflammation (Oh et al., 2017). Burrello and colleges induced intestinal inflammation in mice using the chronic infusion of dextran sodium sulphate (DSS), which is similar to that observed in patients with IBD. Both the mucus and faeces from normal biological donors were given orally to the mice with established chronic colitis induced by DSS. Normoxic FMT therapy was found to lower the intestinal inflammation, as suggested by a robust decline in not only the colonic expression of the pro-inflammatory marker interferon (IFN)-γ but also tumor necrosis factor (TNF), interleukin (IL)-1β, IL-17, and IL-6. Restoring a main ecology of normal organisms contributed to resolving inflammation (Burrello et al., 2019). Wei et al. (2018) identified that FMT could alleviate the acute colitis stimulated by DSS in mice and FMT results in the upregulation of not only aryl hydrocarbon receptor (AHR) but also transforming growth factor beta (TGF-β) and IL-10 in colon tissues. Wang et al. (2020) carried out a study on active UC patients who received three times FMT from a single donor at an interval of 2–3 months. The clinical response was achieved in 14/16 (87.5%) patients. Compared to those before FMT, serum levels of IL-6, IL-1Ra, epithelial neutrophil activating peptide (ENA)-78, and interferon-inducible protein (IP)-10 significantly decreased after the second FMT ($P < 0.05$), and serum levels of vascular cell adhesion molecule (VCAM)-1, granulocyte-colony stimulating factor (G-CSF) and mucosae-associated epithelial chemokine (MEC) significantly decreased after both the first and second FMT ($P < 0.05$). Those findings shed light on the fact that FMT has the potential to control IBD through augmenting anti-inflammation cytokines and reducing pro-inflammatory cytokines.

CONCLUSION AND FUTURE PERSPECTIVES

The understanding of FMT effectiveness for IBD is in its infancy even today. The preliminary findings from medical experiments are conflicting, perhaps owing to the dissimilarities existing in patient populations among various research works, disease seriousness in participants, the delivery processes of FMT, FMT preparations, and the follow-up after transplantation (Rubin, 2015). Nevertheless, the latent potential of FMT for the treatment of IBD should be addressed. It is not clear why some patients with IBD respond impressively following FMT, whereas other patients fail to respond. Nonetheless, it is evident that FMT does not refer to a "one size fits all" and many determinants seem to contribute to its successful use for the treatment of IBD. The host genotype, the course of disease, the use of antibiotics linked to illness onset, the specific types of IBD-linked dysbiosis, and/or donor attributes are all determinants that can potentially dictate the ultimate result. Accordingly, further investigations and a better understanding of this application are required (Rossen et al., 2015). To conclude, applying FMT to manage IBD is likely to constitute an intriguing treatment choice; nonetheless, large and methodical studies are lacking. Further, many concerns related to pathophysiological, methodological, and mechanistic factors require an explanation.

FMT refers to a new potential option for treating IBD; nonetheless, there are many issues that still exist. More research is required to build a more comprehensive and deeper knowledge base, with respect to the entire treatment process ranging from FMT methodologies to FMT immunomodulatory impacts and mechanisms. Being a new treatment for IBD, its efficacy and safety are still not certain, and patient acceptability is also not high; accordingly, longer-term follow-up investigations are required. Standards regarding donor selection are also required. Through further studies, better methodologies and more effective protocols to prepare fecal substances and administer FMT will be realized. Moreover, related laws and regulations need to be formulated to standardise and limit all aspects of the treatment.

AUTHOR CONTRIBUTIONS

PT and XL collected the papers and data, analyzed the conclusions, drafted the manuscript. JS and QF presented the idea of this paper, supported the funding, analyzed the conclusions, drafted, and revised the manuscript.

FUNDING

Supported by grants from National Natural Science Foundation of China (No. 81770545 & 81701746) and MDT Project of Clinical Research Innovation Foundation, Renji Hospital, School of Medicine, Shanghai Jiaotong University (PYI-17-003), and North Shanghai Medical Star Talent Training Program of Baoshan Branch Renji Hospital (rbxxrc-2019-008).

REFERENCES

Alang, N., and Kelly, C. R. (2015). Weight gain after fecal microbiota transplantation. *Open Forum Infect. Dis.* 2, ofv004. doi: 10.1093/ofid/ofv004

Anand, R., Song, Y., Garg, S., Girotra, M., Sinha, A., Sivaraman, A., et al. (2017). Effect of Aging on the Composition of Fecal Microbiota in Donors for FMT and Its Impact on Clinical Outcomes. *Dig. Dis. Sci.* 62, 1002–1008. doi: 10.1007/s10620-017-4449-6

Bakken, J. S., Borody, T., Brandt, L. J., Brill, J. V., Demarco, D. C., Franzos, M. A., et al. (2011). Treating Clostridium difficile infection with fecal microbiota transplantation. *Clin. Gastroenterol. Hepatol.* 9, 1044–1049. doi: 10.1016/j.cgh.2011.08.014

Basso, P. J., Camara, N. O. S., and Sales-Campos, H. (2018). Microbial-Based Therapies in the Treatment of Inflammatory Bowel Disease - An Overview of Human Studies. *Front. Pharmacol.* 9:1571. doi: 10.3389/fphar.2018.01571

Blumberg, R. S., Saubermann, L. J., and Strober, W. (1999). Animal models of mucosal inflammation and their relation to human inflammatory bowel disease. *Curr. Opin. Immunol.* 11, 648–656. doi: 10.1016/S0952-7915(99)00032-1

Burrello, C., Giuffrè, M. R., Macandog, A. D., Diaz-Basabe, A., Cribiù, F. M., Lopez, G., et al. (2019). Fecal Microbiota Transplantation Controls Murine Chronic Intestinal Inflammation by Modulating Immune Cell Functions and Gut Microbiota Composition. *Cells* 8, 517. doi: 10.3390/cells8060517

Cammarota, G., Masucci, L., Ianiro, G., Bibbò, S., Dinoi, G., Costamagna, G., et al. (2015). Randomised clinical trial: fecal microbiota transplantation by colonoscopy vs. vancomycin for the treatment of recurrent Clostridium difficile infection. *Aliment Pharmacol. Ther.* 41, 835–843. doi: 10.1111/apt.13144

Cammarota, G., Ianiro, G., Kelly, C. R., Mullish, B. H., Allegretti, J. R., Kassam, Z., et al. (2019). International consensus conference on stool banking for fecal microbiota transplantation in clinical practice. *Gut* 68, 2111–2121. doi: 10.1136/gutjnl-2019-319548

Cohen, N. A., Livovsky, D. M., Yaakobovitch, S., Ben Yehoyada, M., Ben Ami, R., Adler, A., et al. (2016). A Retrospective Comparison of Fecal Microbial Transplantation Methods for Recurrent Clostridium Difficile Infection. *Isr. Med. Assoc. J.* 18, 594–599.

Costello, S. P., Conlon, M. A., Vuaran, M. S., Roberts-Thomson, I. C., and Andrews, J. M. (2015). Fecal microbiota transplant for recurrent Clostridium difficile infection using long-term frozen stool is effective: clinical efficacy and bacterial viability data. *Aliment Pharmacol. Ther.* 42, 1011–1018. doi: 10.1111/apt.13366

Costello, S. P., Soo, W., Bryant, R. V., Jairath, V., Hart, A. L., and Andrews, J. M. (2017). Systematic review with meta-analysis: fecal microbiota transplantation for the induction of remission for active ulcerative colitis. *Aliment Pharmacol. Ther.* 46, 213–224. doi: 10.1111/apt.14173

Costello, S. P., Hughes, P. A., Waters, O., and Boryant, R. V. (2019). Effect of Fecal Microbiota Transplantation on 8-Week Remission in Patients With Ulcerative Colitis: A Randomized Clinical Trial. *JAMA* 321, 156–164. doi: 10.1001/jama.2018.20046

Cui, B., Feng, Q., Wang, H., Wang, M., Peng, Z., Li, P., et al. (2015). Fecal microbiota transplantation through mid-gut for refractory Crohn's disease: Safety, feasibility, and efficacy trial results *J. Gastroenterol. Hepatol.* 30, 51–58. doi: 10.1111/jgh.12727

De Jager, C. P., Wever, P. C., Gemen, E. F., Van Oijen, M. G., Van Gageldonk-Lafeber, A. B., Siersema, P. D., et al. (2012). Proton pump inhibitor therapy predisposes to community-acquired Streptococcus pneumoniae pneumonia. *Aliment Pharmacol. Ther.* 36, 941–949. doi: 10.1111/apt.12069

Drekonja, D., Reich, J., Gezahegn, S., Greer, N., Shaukat, A., Macdonald, R., et al. (2015). Fecal Microbiota Transplantation for Clostridium difficile Infection: A Systematic Review. *Ann. Intern Med.* 162, 630–638. doi: 10.7326/M14-2693

Erickson, A. R., Cantarel, B. L., Lamendella, R., Darzi, Y., Mongodin, E. F., Pan, C., et al. (2012). Integrated metagenomics/metaproteomics reveals human host-microbiota signatures of Crohn's disease. *PloS One* 7, e49138. doi: 10.1371/journal.pone.0049138

Fang, H., Fu, L., and Wang, J. (2018). Protocol for Fecal Microbiota Transplantation in Inflammatory Bowel Disease: A Systematic Review and Meta-Analysis. *BioMed. Res. Int.* 2018, 8941340. doi: 10.1155/2018/8941340

Fischer, M., Kao, D., Kelly, C., Kuchipudi, A., Jafri, S. M., Blumenkehl, M., et al. (2016). Fecal Microbiota Transplantation is Safe and Efficacious for Recurrent or Refractory Clostridium difficile Infection in Patients with Inflammatory Bowel Disease. *Inflammation Bowel Dis.* 22, 2402–2409. doi: 10.1097/MIB.0000000000000908

Goyal, A., Yeh, A., Bush, B. R., Firek, B. A., Siebold, L. M., Rogers, M. B., et al. (2018). Safety, Clinical Response, and Microbiome Findings Following Fecal Microbiota Transplant in Children With Inflammatory Bowel Disease. *Inflammation Bowel Dis.* 24, 410–421. doi: 10.1093/ibd/izx035

Gupta, A., and Khanna, S. (2017). Fecal Microbiota Transplantation. *JAMA* 318, 102. doi: 10.1001/jama.2017.6466

Gutin, L., Piceno, Y., Fadrosh, D., Lynch, K., Zydek, M., Kassam, Z., et al. (2019). Fecal microbiota transplant for Crohn disease: A study evaluating safety, efficacy, and microbiome profile. *U. Eur. Gastroenterol. J.* 7, 807–814. doi: 10.1177/2050640619845986

Henson, M. A., and Phalak, P. (2017). Microbiota dysbiosis in inflammatory bowel diseases: in silico investigation of the oxygen hypothesis. *BMC Syst. Biol.* 11, 145. doi: 10.1186/s12918-017-0522-1

Herfarth, H., Barnes, E. L., Long, M. D., Isaacs, K. L., Leith, T., Silverstein, M., et al. (2019). Combined Endoscopic and Oral Fecal Microbiota Transplantation in Patients with Antibiotic-Dependent Pouchitis: Low Clinical Efficacy due to Low Donor Microbial Engraftment. *Inflammation Intest Dis.* 4, 1–6. doi: 10.1159/000497042

Kaser, A., Zeissig, S., and Blumberg, R. S. (2010). Inflammatory Bowel Disease. *Annu. Rev. Immuno* 28, 573–621. doi: 10.1146/annurev-immunol-030409-101225

Kelly, C. R., Kahn, S., Kashyap, P., Laine, L., Rubin, D., Atreja, A., et al. (2015). Update on Fecal Microbiota Transplantation 2015: Indications, Methodologies, Mechanisms, and Outlook. *Gastroenterology* 149, 223–237. doi: 10.1053/j.gastro.2015.05.008

Kelly, C. R., Khoruts, A., Staley, C., Sadowsky, M. J., Abd, M., Alani, M., et al. (2016). Effect of Fecal Microbiota Transplantation on Recurrence in Multiply Recurrent Clostridium difficile Infection: A Randomized Trial. *Ann. Intern Med.* 165, 609–616. doi: 10.7326/M16-0271

Khoruts, A., Rank, K. M., Newman, K. M., Viskocil, K., Vaughn, B. P., Hamilton, M. J., et al. (2016). Inflammatory Bowel Disease Affects the Outcome of Fecal Microbiota Transplantation for Recurrent Clostridium difficile Infection. *Clin. Gastroenterol. Hepatol.* 14, 1433–1438. doi: 10.1016/j.cgh.2016.02.018

Landy, J., Walker, A. W., Li, J. V., Al-Hassi, H. O., Ronde, E., English, N. R., et al. (2015). Variable alterations of the microbiota, without metabolic or immunological change, following fecal microbiota transplantation in patients with chronic pouchitis. *Sci. Rep.* 5, 12955. doi: 10.1038/srep12955

Levy, A. N., and Allegretti, J. R. (2019). Insights into the role of fecal microbiota transplantation for the treatment of inflammatory bowel disease. *Therap. Adv. Gastroenterol.* 12, 1756284819836893. doi: 10.1177/1756284819836893

Maharshak, N., Cohen, N. A., Reshef, L., Tulchinsky, H., Gophna, U., and Dotan, I. (2017). Alterations of Enteric Microbiota in Patients with a Normal Ileal Pouch Are Predictive of Pouchitis. *J. Crohns. Colitis* 11, 314–320. doi: 10.1093/ecco-jcc/jjw157

Moayyedi, P., Surette, M. G., Kim, P. T., Libertucci, J., Wolfe, M., Onischi, C., et al. (2015). Fecal Microbiota Transplantation Induces Remission in Patients With Active Ulcerative Colitis in a Randomized Controlled Trial. *Gastroenterology* 149, 102–109.e106. doi: 10.1053/j.gastro.2015.04.001

Mullish, B. H., Quraishi, M. N., Segal, J. P., Mccune, V. L., Baxter, M., Marsden, G. L., et al. (2018). The use of fecal microbiota transplant as treatment for recurrent or refractory Clostridium difficile infection and other potential indications: joint British Society of Gastroenterology (BSG) and Healthcare Infection Society (HIS) guidelines. *Gut* 67, 1920–1941. doi: 10.1136/gutjnl-2018-316818

Natividad, J. M., Pinto-Sanchez, M. I., Galipeau, H. J., Jury, J., Jordana, M., Reinisch, W., et al. (2015). Ecobiotherapy Rich in Firmicutes Decreases Susceptibility to Colitis in a Humanized Gnotobiotic Mouse Model. *Inflammation Bowel Dis.* 21, 1883–1893. doi: 10.1097/MIB.0000000000000422

Newman, K. M., Rank, K. M., Vaughn, B. P., and Khoruts, A. (2017). Treatment of recurrent Clostridium difficile infection using fecal microbiota transplantation in patients with inflammatory bowel disease. *Gut. Microbes* 8, 303–309. doi: 10.1080/19490976.2017.1279377

Ni, J., Wu, G. D., Albenberg, L., and Tomov, V. T. (2017). Gut microbiota and IBD: causation or correlation? *Nat. Rev. Gastroenterol. Hepatol.* 14, 573–584. doi: 10.1038/nrgastro.2017.88

Nishida, A., Imaeda, H., Inatomi, O., Bamba, S., Sugimoto, M., and Andoh, A. (2019). The efficacy of fecal microbiota transplantation for patients with chronic pouchitis: A case series. *Clin. Case Rep.* 7, 782–788. doi: 10.1002/ccr3.2096

Oh, S. R., Ok, S., Jung, T. S., Jeon, S. O., Park, J. M., Jung, J. W., et al. (2017). Protective effect of decursin and decursinol angelate-rich Angelica gigas Nakai extract on dextran sulfate sodium-induced murine ulcerative colitis. *Asian Pac. J. Trop. Med.* 10, 864–870. doi: 10.1016/j.apjtm.2017.08.017

Paramsothy, S., Kamm, M. A., Kaakoush, N. O., Walsh, A. J., Van Den Bogaerde, J., Samuel, D., et al. (2017a). Multidonor intensive fecal microbiota transplantation for active ulcerative colitis: a randomised placebo-controlled trial. *Lancet* 389, 1218–1228. doi: 10.1016/S0140-6736(17)30182-4

Paramsothy, S., Paramsothy, R., Rubin, D. T., Kamm, M. A., Kaakoush, N. O., Mitchell, H. M., et al. (2017b). Fecal Microbiota Transplantation for Inflammatory Bowel Disease: A Systematic Review and Meta-analysis. *J. Crohns. Colitis* 11, 1180–1199. doi: 10.1093/ecco-jcc/jjx063

Persborn, M., Gerritsen, J., Wallon, C., Carlsson, A., and Akkermans, L. M. A. (2013). The effects of probiotics on barrier function and mucosal pouch microbiota during maintenance treatment for severe pouchitis in patients with ulcerative colitis. *Aliment Pharmacol. Ther.* 38, 772–783. doi: 10.1111/apt.12451

Quraishi, M. N., Widlak, M., Bhala, N., Moore, D., Price, M., Sharma, N., et al. (2017). Systematic review with meta-analysis: the efficacy of fecal microbiota transplantation for the treatment of recurrent and refractory Clostridium difficile infection. *Aliment Pharmacol. Ther.* 46, 479–493. doi: 10.1111/apt.14201

Rodemann, J. F., Dubberke, E. R., Reske, K. A., Seo, D. H., and Stone, C. D. (2007). Incidence of Clostridium difficile infection in inflammatory bowel disease. *Clin. Gastroenterol. Hepatol.* 5, 339–344. doi: 10.1016/j.cgh.2006.12.027

Rossen, N. G., Fuentes, S., Van Der Spek, M. J., Tijssen, J. G., Hartman, J. H. A., Duflou, A., et al. (2015). Findings From a Randomized Controlled Trial of Fecal Transplantation for Patients With Ulcerative Colitis. *Gastroenterology* 149, 110–118.e114. doi: 10.1053/j.gastro.2015.03.045

Rubin, D. T. (2015). Fecal Microbiota Transplantation for the Treatment of Inflammatory Bowel Disease. *Gastroenterol. Hepatol. (N. Y.)* 11, 618–620.

Selvig, D., Piceno, Y., Terdiman, J., Zydek, M., Umetsu, S. E., Balitzer, D., et al. (2020). Fecal Microbiota Transplantation in Pouchitis: Clinical, Endoscopic, Histologic, and Microbiota Results from a Pilot Study. *Dig. Dis. Sci.* 65 (4), 1099–1106. doi: 10.1007/s10620-019-05715-2

Sheehan, D., Moran, C., and Shanahan, F. (2015). The microbiota in inflammatory bowel disease. *J. Gastroenterol.* 50, 495–507. doi: 10.1007/s00535-015-1064-1

Shen, B. (2012). Bacteriology in the etiopathogenesis of pouchitis. *Dig. Dis.* 30, 351–357. doi: 10.1159/000338125

Sokol, H., Pigneur, B., Watterlot, L., Lakhdari, O., Bermúdez-Humarán, L. G., Gratadoux, J. J., et al. (2008). Fecalibacterium prausnitzii is an anti-inflammatory commensal bacterium identified by gut microbiota analysis of Crohn disease patients. *Proc. Natl. Acad. Sci. U.S.A.* 105, 16731–16736. doi: 10.1073/pnas.0804812105

Sokol, H., Landman, C., Seksik, P., Berard, L., Montil, M., Nion-Larmurier, I., et al. (2020). Fecal microbiota transplantation to maintain remission in Crohn's disease: a pilot randomized controlled study. *Microbiome* 812 (1). doi: 10.1186/s40168-020-0792-5

Sood, A., Mahajan, R., Singh, A., Midha, V., Mehta, V., Narang, V., et al. (2019). Role of Faecal Microbiota Transplantation for Maintenance of Remission in Patients With Ulcerative Colitis: A Pilot Study. *J. Crohns. Colitis* 13, 1311–1317. doi: 10.1093/ecco-jcc/jjz060

Sood, A., Singh, A., Mahajan, R., Midha, V., Mehta, V., Gupta, Y. K., et al. (2020). Acceptability, tolerability, and safety of fecal microbiota transplantation in patients with active ulcerative colitis (AT&S Study). *J. Gastroenterol. Hepatol.* 35, 418–424. doi: 10.1111/jgh.14829

Stallmach, A., Lange, K., Buening, J., Sina, C., Vital, M., and Pieper, D. H. (2016). Fecal Microbiota Transfer in Patients With Chronic Antibiotic-Refractory Pouchitis. *Am. J. Gastroenterol.* 111, 441–443. doi: 10.1038/ajg.2015.436

Surawicz, C. M., Brandt, L. J., Binion, D. G., Ananthakrishnan, A. N., Curry, S. R., Gilligan, P. H., et al. (2013). Guidelines for diagnosis, treatment, and prevention of Clostridium difficile infections. *Am. J. Gastroenterol.* 108, 478–498. doi: 10.1038/ajg.2013.4

Suskind, D. L., Brittnacher, M. J., Wahbeh, G., Shaffer, M. L., Hayden, H. S., Qin, X., et al. (2015). Fecal Microbial Transplant Effect on Clinical Outcomes and Fecal Microbiome in Active Crohn's Disease. *Gastroenterol. Hepatol. (N. Y.)* 21, 556–563. doi: 10.1097/MIB.0000000000000307

Terveer, E. M., Van Beurden, Y. H., Goorhuis, A., Seegers, J., Bauer, M. P., Van Nood, E., et al. (2017). How to: Establish and run a stool bank. *Clin. Microbiol. Infect.* 23, 924–930. doi: 10.1016/j.cmi.2017.05.015

Vaughn, B. P., Vatanen, T., Allegretti, J. R., Bai, A., Xavier, R. J., Korzenik, J., et al. (2016). Increased Intestinal Microbial Diversity Following Fecal Microbiota Transplant for Active Crohn's Disease. *Inflamm. Bowel Dis.* 22, 2182–2190. doi: 10.1097/MIB.0000000000000893

Vermeire, S., Joossens, M., Verbeke, K., Wang, J., Machiels, K., Sabino, J., et al. (2016). Donor Species Richness Determines Fecal Microbiota Transplantation Success in Inflammatory Bowel Disease. *J. Crohns. Colitis* 10, 387–394. doi: 10.1093/ecco-jcc/jjv203

Wang, Y., Ren, R., Sun, G., Peng, L., Tian, Y., and Yang, Y. (2020). Pilot study of cytokine changes evaluation after fecal microbiota transplantation in patients with ulcerative colitis. *Int. Immunopharmacol.* 85, 106661. doi: 10.1016/j.intimp.2020.106661

Wei, Y., Zhu, W., Gong, J., Guo, D., Gu, L., Li, N., et al. (2015). Fecal Microbiota Transplantation Improves the Quality of Life in Patients with Inflammatory Bowel Disease. *Gastroenterol. Res. Pract.* 2015, 517597. doi: 10.1155/2015/517597

Wei, Y. L., Chen, Y. Q., Gong, H., Li, N., Wu, K. Q., Hu, W., et al. (2018). Fecal Microbiota Transplantation Ameliorates Experimentally Induced Colitis in Mice by Upregulating AhR. *Front. Microbiol.* 9, 1921. doi: 10.3389/fmicb.2018.01921

White, C., Thakor, A., and Goel, R. (2018). Recommended drug therapies for inflammatory bowel disease. *Prescriber* 29, 17–22. doi: 10.1002/psb.1701

Xiang, L., Ding, X., Li, Q., Wu, X., Dai, M., Long, C., et al. (2020). Efficacy of faecal microbiota transplantation in Crohn's disease: a new target treatment? *Microb. Biotechnol.* 13, 760–769. doi: 10.1111/1751-7915.13536

Zeng, W., Shen, J., Bo, T., Peng, L., Xu, H., Nasser, M.II, et al. (2019). Cutting Edge: Probiotics and Fecal Microbiota Transplantation in Immunomodulation. *J. Immunol. Res.* 2019, 1603758. doi: 10.1155/2019/1603758

Zhou, M., He, J., Shen, Y., Zhang, C., Wang, J., and Chen, Y. (2017). New Frontiers in Genetics, Gut Microbiota, and Immunity: A Rosetta Stone for the Pathogenesis of Inflammatory Bowel Disease. *BioMed. Res. Int.* 2017, 8201672. doi: 10.1155/2017/8201672

Zuo, T., and Ng, S. C. (2018). The Gut Microbiota in the Pathogenesis and Therapeutics of Inflammatory Bowel Disease. *Front. Microbiol.* 9:2247. doi: 10.3389/fmicb.2018.02247

Conflict of Interest: The authors declare that the research was conducted in the absence of any commercial or financial relationships that could be construed as a potential conflict of interest.

frontiers in Pharmacology

ORIGINAL RESEARCH
published: 08 October 2020
doi: 10.3389/fphar.2020.585096

Fish Oil, Cannabidiol and the Gut Microbiota: An Investigation in a Murine Model of Colitis

Cristoforo Silvestri[1,2†], Ester Pagano[3†], Sébastien Lacroix[4], Tommaso Venneri[3], Claudia Cristiano[3], Antonio Calignano[3], Olga A. Parisi[3], Angelo A. Izzo[3], Vincenzo Di Marzo[1,2,4,5,6,7,8] and Francesca Borrelli[3*]*

[1] Centre de recherche de l'Institut universitaire de cardiologie et de pneumologie de Québec (IUCPQ), Québec, QC, Canada, [2] Département de médecine, Faculté de Médecine, Université Laval, Québec, QC, Canada, [3] Department of Pharmacy, School of Medicine and Surgery, University of Naples Federico II, Naples, Italy, [4] Institut sur la nutrition et les aliments fonctionnels (INAF), Québec, QC, Canada, [5] Institute of Biomolecular Chemistry, National Research Council (CNR) of Italy, Pozzuoli, Italy, [6] Centre Nutriss, École de nutrition, Faculté des sciences de l'agriculture et de l'alimentation (FSAA), Université Laval, Québec, QC, Canada, [7] Joint International Unit between the National Research Council (CNR) of Italy and Université Laval on Chemical and Biomolecular Research on the Microbiome and its Impact on Metabolic Health and Nutrition (UMI-MicroMeNu), Institute of Biomolecular Chemistry, CNR, Pozzuoli, Italy, [8] Canada Research Excellence Chair on the Microbiome-Endocannabinoidome Axis in Metabolic Health (CERC-MEND), Université Laval, Québec, QC, Canada

OPEN ACCESS

Edited by:
Ruixin Zhu,
Tongji University, China

Reviewed by:
Ling Liu,
Sichuan University, China
Yanling Wei,
Army Medical University, China

***Correspondence:**
Vincenzo Di Marzo
vincenzo.di-marzo.1@ulaval.ca
Francesca Borrelli
franborr@unina.it

†These authors have contributed equally to this work

Specialty section:
This article was submitted to Gastrointestinal and Hepatic Pharmacology, a section of the journal Frontiers in Pharmacology

Received: *19 July 2020*
Accepted: *14 September 2020*
Published: *08 October 2020*

Citation:
Silvestri C, Pagano E, Lacroix S, Venneri T, Cristiano C, Calignano A, Parisi OA, Izzo AA, Di Marzo V and Borrelli F (2020) Fish Oil, Cannabidiol and the Gut Microbiota: An Investigation in a Murine Model of Colitis. Front. Pharmacol. 11:585096. doi: 10.3389/fphar.2020.585096

Inflammatory bowel disorders can be associated with alterations in gut microbiota (dysbiosis) and behavioral disturbances. In experimental colitis, administration of fish oil (FO) or cannabinoids, such as cannabidiol (CBD), reduce inflammation. We investigated the effect of combined FO/CBD administration on inflammation and dysbiosis in the dextran sulphate sodium (DSS) model of mouse colitis, which also causes behavioral disturbances. Colitis was induced in CD1 mice by 4% w/v DSS in drinking water for five consecutive days followed by normal drinking water. FO (20–75 mg/mouse) was administered once a day starting two days after DSS, whereas CBD (0.3–30 mg/kg), alone or after FO administration, was administered once a day starting 3 days after DSS, until day 8 (d8) or day 14 (d14). Inflammation was assessed at d8 and d14 (resolution phase; RP) by measuring the Disease Activity Index (DAI) score, change in body weight, colon weight/length ratio, myeloperoxidase activity and colonic interleukin (IL)-1β (IL-1β), IL-10, and IL-6 concentrations. Intestinal permeability was measured with the fluorescein isothiocyanate-dextran. Behavioral tests (novel object recognition (NOR) and light/dark box test) were performed at d8. Fecal microbiota composition was determined by ribosomal 16S DNA sequencing of faecal pellets at d8 and d14. DSS-induced inflammation was stronger at d8 and accompanied by anxiety-like behavior and impaired recognition memory. FO (35, 50, 75 mg/mouse) alone reduced inflammation at d8, whereas CBD alone produced no effect at any of the doses tested; however, when CBD (3, 10 mg/kg) was co-administered with FO (75 mg/mouse) inflammation was attenuated. FO (20 mg/mouse) and CBD (1 mg/kg) were ineffective when given alone, but when co-administered reduced all inflammatory markers and the increased intestinal permeability at both d8 and d14, but not the behavioral impairments. FO, CBD, and their

combination affected gut bacteria taxa that were not affected by DSS *per se*. *Akkermansia muciniphila*, a species suggested to afford anti-inflammatory action in colitis, was increased by DSS only at d14, but its levels were significantly elevated by all treatments at d8. FO and CBD co-administered at *per se* ineffective doses reduce colon inflammation, in a manner potentially strengthened by their independent elevation of *Akkermansia muciniphila.*

Keywords: colitis, cannabinoid, gut-brain axis, fish oil, microbiome

INTRODUCTION

Ulcerative colitis (UC) and Crohn's disease (CD), the two most common inflammatory bowel diseases (IBDs), are chronic, relapsing, and lifelong ailments characterized by strong inflammation of the colon. They affect millions of people worldwide with increasing incidence (Kaplan and Ng, 2017; Ng et al., 2018). IBDs result from the interaction between environmental, genetic, and epigenetic risk factors causing an excessive immune response in the mucosa leading to uncontrolled inflammation, and represent, in turn, a risk factor for the development of colorectal cancer (Keller et al., 2019). Recent evidence suggests that the imbalance of the gut microbiota ecosystem, also known as gut dysbiosis, is linked to the initiation and progression of IBDs (De Musis et al., 2020). In fact, dysbiosis, through disruption of the intestinal epithelial barrier and ensuing entry of gram-negative bacteria-derived pro-inflammatory molecules such as lipopolysaccharide (LPS) into the blood stream may contribute to systemic inflammation. However, it is still unclear whether gut dysbiosis is one of the primary causes of IBD, or if it is secondary to IBD-induced mucosal inflammation and exacerbates its consequences (Ananthakrishnan et al., 2018; Pittayanon et al., 2020).

Fish oil (FO), mostly thanks to its high content in omega-3 polyunsaturated fatty acids (n-3-PUFAs), i.e., eicosapentaenoic (EPA; C20:5) and docosahexaenoic (DHA; C22:6) fatty acids, has been suggested to produce important anti-inflammatory actions both in pre-clinical and clinical studies [see (Calder, 2017) for review]. Several mechanisms have been proposed for this property of FO, including, but not limited to, the capability of EPA and DHA to: 1) replace arachidonic acid (AA) in membrane phospholipids, and hence reduce the amounts of this omega-6 PUFA that can act as direct or indirect biosynthetic precursors for endocannabinoids and pro-inflammatory eicosanoids (Calder, 2017; Innes and Calder, 2018); and 2) affect the gut microbiota to ameliorate gut dysbiosis and counteract, among others, its contribution to chronic, lowgrade inflammation (Costantini et al., 2017). As a consequence, it has been suggested that FO may provide therapeutic relief for IBDs (Marton et al., 2019). Also, plant cannabinoids from *Cannabis sativa*, and in particular: 1) Δ^9-tetrahydrocannabinol (THC), which activates cannabinoid receptor of type-1 (CB1) or, particularly, type-2 (CB2) [see (Ibeas Bih et al., 2015; Turner et al., 2017) for review], and 2) cannabidiol (CBD), which modulates several pro-inflammatory targets [see (Burstein, 2015) for review] have been shown to produce anti-inflammatory effects in animal models of several inflammatory disorders, including IBDs (Gotfried et al., 2020; Williamson et al., 2020). Importantly, purified plant-derived CBD is now currently approved in both the USA (as Epidiolex®) and Europe (as Epidyolex®, as an adjunctive therapy with clobazam) as an effective treatment for seizures associated with Dravet syndrome and Lennox-Gastaut syndrome (intractable rare pediatric epilepsies); while generally well tolerated, diarrhea is a common adverse event (Pauli et al., 2020).

We have shown that, in the dinitrobenzenesulphonic acid (DNBS) and croton oil models of lower and upper intestinal inflammation, CBD can produce beneficial effects, although often with lower potency/efficacy than other cannabinoids (Borrelli et al., 2009; Borrelli et al., 2013; Romano et al., 2013; Pagano et al., 2019) or CBD-enriched *Cannabis* extracts (Pagano et al., 2016). A CBD-rich extract was indeed tested in an open label phase II trial against UC and, although promising results were seen on some secondary endpoints (subjective physician's global assessment of illness severity, subject global impression of change and patient-reported quality-of-life outcomes), it did not achieve statistically significant results for the primary endpoint (percentage of patients in remission after treatment) (Irving et al., 2018). Given the potential advantages afforded by the use in IBDs of a drug already approved for other indications, we hypothesized that a possible way to improve CBD efficacy and potency at counteracting inflammation would be through its oral co-administration with dietary FO. To test this, we developed a co-administration protocol of the two treatments in a widely used animal model of IBD, and UC in particular, i.e., the dextran sulphate sodium (DSS)-induced colitis in mice. This model has been described to: 1) produce effects on the gut microbiota composition that could contribute to colonic inflammation, and hence has been employed to investigate the anti-inflammatory potential of treatments targeting gut dysbiosis (Munyaka et al., 2016; Ke et al., 2020; Liu et al., 2020); and 2) be accompanied by behavioral cognitive and affective impairments (Reichmann et al., 2015), which, in view of the ever increasing evidence in favor of the microbiota-gut-brain axis [see (Emge et al., 2016) for review], could also be the consequence of DSS-induced dysbiosis. We co-administered different oral doses of FO and CBD during the development of colonic inflammation by administration of DSS until either its peak, at day 8 (d8), or the inflammatory resolution phase (RP), at d14. We also investigated if the potentially stronger effects of

combined FO and CBD treatment was accompanied by effects on DSS-induced gut dysbiosis at d8 and d14, or on behavioral impairments at d8.

MATERIALS AND METHODS

Drugs and Reagents

Dextran Sulfate Sodium (DSS, molecular weight 36,000–50,000) and myeloperoxidase (MPO) from human leucocytes were purchased from MP Biomedical (Illkirch, France) and Sigma Aldrich S.r.l. (Milan, Italy), respectively. Purified, botanically derived CBD (≥98%), was supplied by GW Research Ltd (Cambridge, UK). FO (Marco Viti Farmaceutici S.p.A (Mozzate, Como, Italy)] and sesame oil [SO, Il fiore di Loto S.r.l. (Orbassano, Torino, Italy)] were obtained from a local pharmacy. All chemicals and reagents employed in this study were of analytical grade. CBD was dissolved in sesame oil (90 µl/mouse). Sesame oil had no significant effects on the responses under study.

Animals

Male CD1 mice (weighing 28–30 g) were obtained from Charles River Laboratories (Calco, Lecco, Italy) and housed per experimental group in polycarbonate cages (Tecniplast S.p.A), under a 12-h light/dark cycle, controlled temperature (23 ± 2°C) and constant humidity (60%). Mice had free access to tap water and standard rodent diet (Mucedola srl, Milan, Italy). All mice were fasted 2 h before the oral gavage of CBD and FO. Mice were randomly allocated to different experimental groups (at least six animals for each group, five to six for each cage) of equal size and outcome assessments were performed in blind. All the experimental protocols were evaluated and approved by the Institutional Animal Ethics Committee for the use of experimental animals and conformed to guidelines for the safe use and care of experimental animals in accordance with the Italian D.L. no. 116 of 27 January 1992 and associated guidelines in the European Communities Council (86/609/ECC and 2010/63/UE). Animal studies are reported in compliance with the ARRIVE guidelines (Kilkenny et al., 2010; McGrath and Lilley, 2015) and with the recommendations made by the *British Journal of Pharmacology* (Curtis et al., 2018). G Power was used for sample size calculation (Faul et al., 2007).

Induction of Murine Colitis and Pharmacological Treatments

Colitis was induced in CD1 mice by providing 4% w/v DSS in drinking water for five consecutive days followed by normal drinking water for another 3 or 9 days (DSS water was changed every 2 days) (Chassaing et al., 2014). FO was administered once a day starting two days after DSS and continued every day until d8 or d14. CBD, dissolved in sesame oil, was administered once a day starting one day after the administration of FO (i.e., 3 days after DSS), in order not to overstress the mice with two administrations in the initial phase of the pro-inflammatory treatment and continued every day until euthanasia on d8 or d14 (see **Figure 1A**). Additionally, in preliminary experiments FO was given either simultaneously or one day before CBD; results showed a greater beneficial effect of CBD when it was given one day after FO (data not shown). Therefore, all the experiments were carried out according to this schedule of administration. All animals were euthanized by asphyxiation with CO2.

Four experiments were carried out (**Figure 1A**): Experiment 1) a dose-response curve for FO (20–50 mg/mouse each mouse weighing 28–30 g), to find the highest inactive dose of FO; Experiment 2) a dose-response curve for CBD (0.3–10 mg/kg by gavage in sesame oil) in the presence or absence of FO (20 mg/mouse), to find the highest inactive dose of CBD; Experiment 3) a co-administration of an inactive dose of FO (20 mg/mouse) with an inactive dose of CBD (1 mg/kg), to assess the potential stronger anti-inflammatory effects of a combination treatment in the acute and remission phases of DSS-induced colitis; and Experiment 4) a co-administration of FO at a dose of 75 mg/mouse with different doses (0.3–30 mg/kg) of CBD, to determine even potentially stronger effects on markers of inflammation through the combination of non-inactive doses. In the first, second and fourth experiments, animals were sacrificed at d8, and in the third at both d8 (immediately after behavioral tests) and d14 (RP), (see **Figure 1**). In the third set of experiments, intestinal inflammatory parameters were evaluated at both d8 and d14, whereas behavioral tests were performed at d8 only. In the other experiments, only intestinal inflammatory parameters were evaluated at d8 (**Figure 1**). Stools were collected within 1 h directly from mice previously kept in clean separate cages at d0, d8 and d14 (immediately before the sacrifice) and quickly stored at −80°C. The results of each experimental group were pooled.

For Experiment 1, animals were divided into the following groups: (1) Control (no vehicle or treatment); (2) DSS; (3) DSS + FO 20 mg/mouse; (4) DSS + FO 35 mg/mouse; (5) DSS + FO 50 mg/mouse.

For Experiment 2, animals were divided into the following groups: (1) Control (no vehicle or treatment); (2) DSS; (3) DSS + vehicle (sesame oil, 90 µl/mouse); (4) DSS+ FO 20 mg/mouse; (5) DSS+ CBD 0.3 mg/kg; (6) DSS+ CBD 1 mg/kg; (7) DSS+ CBD 3 mg/kg; (8) DSS+ CBD 10 mg/kg; (9) DSS+ FO 20 mg/mouse+ CBD 0.3 mg/kg; (10) DSS+ FO 20 mg/mouse+ CBD 1 mg/kg; (11) DSS+ FO 20 mg/mouse+ CBD 3 mg/kg; (12) DSS+ FO 20 mg/mouse+ CBD 10 mg/kg.

For Experiment 3, animals were divided into the following groups: (1) Control (no vehicle or treatment) (2) vehicle (sesame oil, 90 µl/mouse); (3) FO 20 mg/mouse; (4) CBD 1 mg/kg; (5) CBD + 1 mg/kg +FO 20 mg/mouse; (6) DSS; (7) DSS + vehicle; (8) DSS + FO 20 mg/mouse; (9) DSS+ 1 mg/kg CBD; (10) DSS+ 20 mg/mouse FO + 1 mg/kg CBD.

For Experiment 4, animals were divided into the following groups: (1) Control (no vehicle or treatment); (2) DSS; (3) DSS + vehicle (sesame oil, 90 µl/mouse); (4) DSS + FO 75 mg/mouse; (5) DSS + CBD 0.3 mg/kg; (6) DSS + CBD 3 mg/kg; (7) DSS + CBD 10 mg/kg; (8) DSS + CBD 30 mg/kg; (9) DSS+ FO 75 mg/mouse + CBD 0.3 mg/kg; (10) DSS+ 75 mg/mouse+ 75 mg/mouse FO+ CBD 3 mg/kg; (11) DSS+ 75 mg/mouse FO+ CBD 10 mg/kg; (12) DSS + 75 mg/mouse FO + CBD 30 mg/kg.

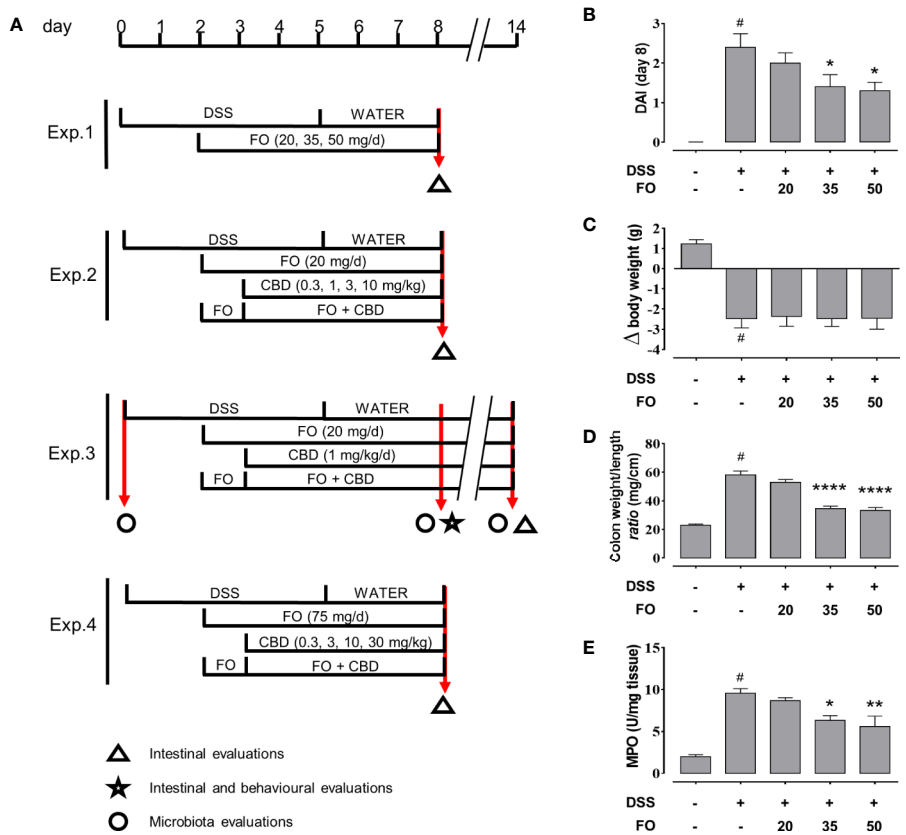

FIGURE 1 | **(A)** Experimental protocols and time points of intestinal, inflammation and microbiota evaluations. **(B–E)** Fish oil (FO) reduces inflammation in a dose-dependent manner in DSS-treated mice (Experiment 1). Effect of FO (20, 35, and 50 mg/mouse, by oral gavage) on disease activity index (DAI) score **(B)**, colon weight/colon length ratio **(C)**, MPO activity **(D)**, and body weight **(E)**, in DSS-treated mice (weighing 28–30 g). Bars are mean ± SEM of 10 animals for **(B, C, E)** and five tissues for **(D)** for each experimental group. Data in **(B)** [$F_{(4,45)} = 12.94$; $p < 0.0001$], **(C)** [$F_{(4,45)} = 14.91$; $p < 0.0001$], **(D)** [$F_{(4,20)} = 18.95$; $p < 0.0001$], and **(E)** [$F_{(4,45)} = 57.33$; $p < 0.0001$] were statistically analyzed using one-way ANOVA followed by the Dunnett's multiple comparisons test $^{\#}p < 0.0001$ vs. control; $^{*}p < 0.05$, $^{**}p < 0.01$, and $^{****}p < 0.0001$ vs. DSS. V, vehicle (sesame oil).

Assessment of Colitis

Body weight, food, and water consumption were measured daily throughout the experiment. Stool consistency and visible blood in faeces were also examined to determine the Disease Activity Index (DAI) score [**Table 1**, (Nishiyama et al., 2012)]. At the time of sacrifice, colons were removed and colon weight/colon length *ratio* was measured. Colons were then snap frozen at −80°C for determination of myeloperoxidase (MPO) activity and interleukin (IL) levels.

TABLE 1 | Disease activity index (DAI) scoring system [adapted from (Nishiyama et al., 2012)].

Score	Diarrheal stool score	Bloody stool score
0	Normal stool	Normal colored stool
1	Midly soft stool	Brown stool
2	Very soft stool	Reddish stool
3	Watery stool	Bloody stool

The sum of the scores of two parameters was defined as the DAI score.

Myeloperoxidase Activity

MPO activity, a marker used to quantify the extent of neutrophil accumulation in whole-tissue colons (Krawisz et al., 1984), was determined in full-thickness colons. Briefly, tissues were homogenized in an appropriate lysis buffer composed of 0.5% hexadecyltrimethylammonium bromide in 3-(N-morpholino) propanesulfonic acid (MOPS) 10 mM in a ratio of 50 mg tissue/1 ml MOPS. The samples were then centrifuged for 20 min at 15,000 x g at 4°C. An aliquot of the supernatant was then incubated with NaPB (sodium phosphate buffer pH 5.5) and 3,3′,5,5′-tetramethylbenzidine (16 mM). After 5 min, H_2O_2 (1mM) in NaPB was added and the reaction stopped by adding acetic acid. The rate of change in absorbance was measured by a spectrophotometer at 650 nm. Different dilutions of human MPO enzyme of known concentration were used to obtain a standard curve (representative $R^2 = 0.94$). MPO activity was expressed as unit(U)/mg of tissue.

Interleukin Levels Determination

Interleukin (IL)-1β (IL-1β), IL-10, and IL-6 concentrations were determined in homogenates obtained from full-thickness mice

colonic tissues using commercial ELISA kits (ThermoFisher Scientific, Milano) according to manufacturer's instructions.

Intestinal Permeability Assay

Intestinal permeability was examined using a fluorescein isothiocyanate (FITC)-labelled-dextran method (Pagano et al., 2019). Briefly, the day before sacrifice (day 7 and day 13), mice received fluorescein isothiocyanate (FITC)-conjugated dextran (molecular mass 3–5 kDa; 600 mg/kg) by oral gavage. One day later, blood was collected by cardiac puncture, and the serum was immediately analyzed for FITC-derived fluorescence using a fluorescent microplate reader (excitation-emission wavelengths: 485–520 nm). Serially diluted FITC-dextran was used to generate a standard curve. Intestinal permeability was expressed as nM FITC found in the serum.

Behavioral Tests

Behavioral tests: novel object recognition (NOR) task to evaluate recognition memory and Light/Dark box test to evaluate anxiety (Guida et al., 2017; Zhu et al., 2018) were performed at d8 only.

NOR task was done as described previously with some modifications (Zhu et al., 2018). Mice were placed on at a time in a cage (40 cm × 25 cm × 18 cm) in the presence of two identical objects (training phase) and filmed for 10 min. Successively, one object was replaced with a new object and mice were placed again in the cage for 10 min (testing phase). The tests were automatically detected by a video camera coupled with video-tracking software (Any-maze, Stoelting Co., Wood Dale, IL, USA). Video clips were analyzed considering the number of explorations of the new object and the meters traveled in the cage (spontaneous locomotion). Mice with cognition disorders spend less time with the new object. After each trial, the cages and the objects were cleaned with 70% ethanol in order to remove odor cues.

Light/Dark box was performed as previously reported (Guida et al., 2017). Mice, one at a time, were placed for 10 min in a light and dark box apparatus, i.e., a box (60 cm × 30 cm × 30 cm) divided in a dark area and a light area (equally sized compartments, 30 x 30 cm each). Mice were placed in the light area and allowed to move freely. Time spent in dark side (mice with anxiety spent more time in dark) and number of transitions between light side and dark side (in order to observe mouse movements) were evaluated.

Statistical Analysis

The data and statistical analysis comply with the British Journal of Pharmacology's recommendations and requirements on experimental design and analysis (Curtis et al., 2018). Results are expressed as mean ± SEM. Data were analyzed for normality using the Anderson-Darling method (http://www.kevinotto.com/RSS/templates/Anderson-DarlingNormalityTestCalculator.xls). Group comparisons were assessed using one-way ANOVA (followed by the Dunnett's or Tukey-Kramer multiple comparisons test). *Post-hoc* tests were conducted only if F achieved $P < 0.05$ and there was no significant variance in homogeneity. Analysis was performed using GraphPad Prism 7.00 (La Jolla, USA). According to recent preclinical guidelines in pharmacology, statistical analysis was undertaken only when each group size (i.e., number of independent values) had a minimum of n = 5 independent animals/samples. Statistical analysis was performed using independent values and technical replicates were not considered independent values. A P value less than 0.05 was considered significant.

Analysis of the Faecal Microbiome

DNA was extracted from faeces using the QIAmp PowerFecal DNA kit (Qiagen, Hilden, Germany) according to the manufacturers' instructions. The DNA concentrations of the extracts were measured fluorometrically with the Quant-iT PicoGreen dsDNA Kit (Thermo Fisher Scientific, MA, USA) and the DNAs were stored at −20°C until 16S rDNA library preparation. Briefly, 1 ng of DNA was used as template and the V3-V4 region of the 16S rRNA gene was amplified by polymerase chain reaction (PCR) using the QIAseq 16S Region Panel protocol in conjunction with the QIAseq 16S/ITS 384-Index I (Sets A, B, C, D) kit (Qiagen, Hilden, Germany) (Rausch et al., 2019). The 16S metagenomic libraries were eluted in 30 µl of nuclease-free water and 1 µl was qualified with a Bioanalyzer DNA 1000 Chip (Agilent, CA, USA) to verify the amplicon size (expected size ~600 bp) and quantified with a Qubit (Thermo Fisher Scientific, MA, USA). Libraries were then normalized and pooled to 2 nM, denatured and diluted to a final concentration of 6 pM and supplemented with 5% PhiX control (Illumina, CA, USA). Sequencing (2 × 275 bp paired-end) was performed using the MiSeq Reagent Kit V3 (600 cycles) on an Illumina MiSeq System. Sequencing reads were generated in less than 65 h. Image analysis and base calling were carried out directly on the MiSeq. Data was processed using the DADA2 pipeline and taxonomic assignation with reference to the RDP database (Callahan et al., 2016). All sequences were cumulative sum scaled (CSS) (Paulson et al., 2013).

Statistical Analysis of Faecal Microbiome Data

The primary objective of the analysis was to evaluate the impact of DSS-induced colitis on gut microbiota composition in comparison to control and to evaluate the potential that CBD, FO or a combination of both have on reversing the DSS-associated disturbances. Vehicle (sesame oil) treated mice were used as control for DSS-Vehicle, and the latter as a control for DSS-CBD, DSS-FO, or DSS-CBD + FO.

Outliers were defined as samples outside the 95% CI ellipse by a PCA. Following this analysis, no samples were defined as outliers and analyses were therefore carried on all samples of interest.

The *Firmicutes* to *Bacteroidetes* ratio is often, but not always, positively associated to diet-induced obesity and dysmetabolism as well as other inflammatory conditions (Ley et al., 2006; Turnbaugh et al., 2008; Boulange et al., 2016; Forbes et al., 2016; Santoru et al., 2017). Asterisks (if none: ns) displayed above boxes represent Kruskal Wallis p-values * $p < 0.05$. Wilcoxon

p-values for pairwise comparisons (within group) are displayed above brackets.

The heatmap.2 package for R was used to represent bacterial family composition between treatment groups and time points using CSS-normalized bacterial counts. Bacterial families or treatment groups and time points were clustered using unsupervised hierarchical clustering.

Differential abundance testing was assessed using two-way ANOVA (taxa ~ Group*Day) and Tukey HSD *post-hoc* p-values. Data is represented in box plots with boxes showing first, second and third quartiles and whiskers indicating samples within 1.5 times the interquartile range. Samples outside this range are indicated by dots.

RESULTS

FO Reduces Inflammatory Colitis in Mice in a Dose Dependent Manner (Experiment 1)

FO, administered at 20, 35, or 50 mg/mouse (by oral gavage) to DSS-treated mice, significantly attenuated the DAI score (**Figure 1B**), colon weight/colon length ratio (**Figure 1C**) and MPO activity (**Figure 1D**), in a dose-dependent manner. Despite this, DSS-induced loss of body weight was unaffected by any FO dose (**Figure 1E**).

Combined Administration of FO and CBD at *Per Se* Ineffective Doses Is Associated With Reduced Colon Inflammation in DSS-Treated Mice (Experiment 2)

CBD, given by oral gavage at the dose range of 0.3-10 mg/kg did not affect DSS-induced intestinal inflammation for any of the four endpoints measured (**Figure 2**). However, co-administration of a *per se* ineffective dose of FO (20 mg/mouse; **Figure 1**) with CBD reduced DAI score (**Figure 2A**), colon weight/colon length ratio (**Figure 2C**) and MPO activity (**Figure 2D**), but not the loss of body weight (**Figure 2B**) in DSS-treated mice; a numerical reduction was observed for the latter with CBD 1 mg/kg but this did not reach significant levels. While the effects appeared to be consistent across all concentrations above CBD 1 mg/kg, this was the most effective dose and was therefore, selected for Experiment 3.

Co-Administered *Per Se* Ineffective Doses of FO and CBD Reduce Colon Inflammation and Epithelial Barrier Permeability in DSS-Treated Mice, but Do Not Affect Behavioral Impairments (Experiment 3)

We confirmed the results of experiments 1 and 2 that FO (20 mg/mouse), CBD (1 mg/kg) or CBD vehicle (sesame oil' SO), all given alone by oral gavage, did not affect DSS-induced intestinal inflammation (**Figure 3**). However, combined treatment with

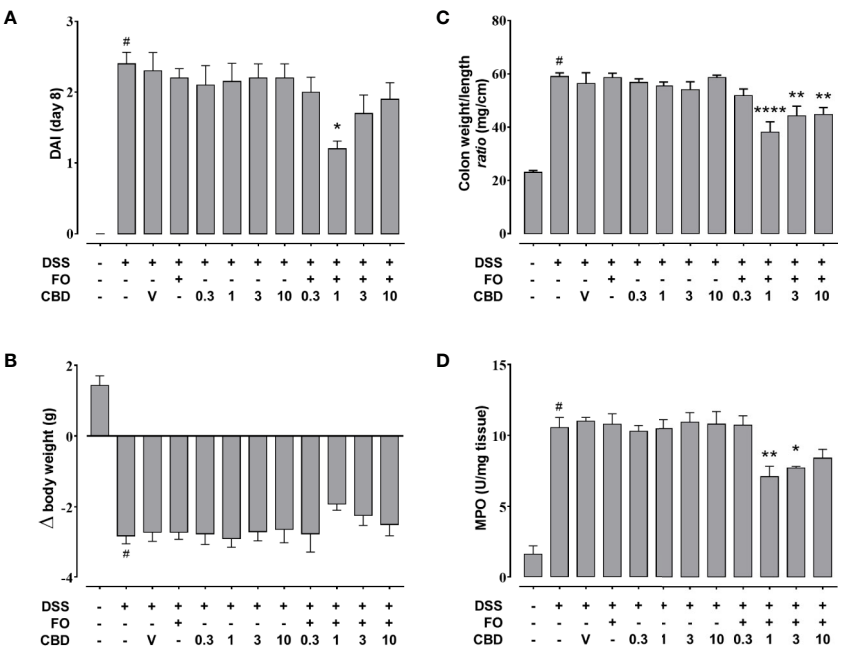

FIGURE 2 | Effect of fish oil (20 mg/mouse) and CBD (0.3–10 mg/kg), both alone and in combination, on intestinal inflammation in DSS-treated mice (Experiment 2). Effect of sesame oil (V, 90 µl/mouse, by oral gavage, used as a vehicle control), fish oil [FO, 20 mg/mouse, by oral gavage], CBD (0.3–10 mg/kg, by oral gavage) and FO + CBD on disease activity index (DAI) score **(A)**, body weight **(B)**, colon weight/colon length ratio **(C)**, and MPO activity **(D)** in DSS-treated mice (weighting 28–30 g). On the *x*-axis the doses shown are for CBD. Bars are mean ± SEM of 10 animals **(A–C)** or of five tissues **(D)** for each experimental group. Data in **(A)** [$F_{(11,108)}$=10.41; $p < 0.0001$], **(B)** [$F_{(11,108)}$ = 16.14; $p < 0.0001$], **(C)** [$F_{(11,108)}$=18.3; $p < 0.0001$], and **(D)** [$F_{(11,48)}$ = 19.36; $p < 0.0001$] were statistically analyzed using one-way ANOVA followed by the Dunnett's multiple comparisons test $^{\#}p < 0.0001$ vs. control, $^{*}p < 0.05$, $^{**}p < 0.01$, and $^{****}p < 0.0001$ vs. DSS + FO.

CBD (1 mg/kg) and FO (20 mg/mouse) significantly reduced the changes induced by DSS administration at d8 (corresponding to active disease phase) on DAI score (**Figure 3A**), colon weight/colon length ratio (**Figure 3B**), and MPO activity (**Figure 3C**), but there was no effect on the loss of mice body weight (**Figure 3D**). Some of these effects were also present at the RP (d14), when the overall degree of inflammation was lower than at d8 (**Figures 3E–H**), and the combination restored almost all intestinal parameters to control levels. When given in combination, but not alone, CBD and FO also significantly reduced DSS-induced increases in intestinal permeability at d8 and d14, and increases in IL-6 and IL-1β and decreases in IL-10 levels at d8. At d14 the combined treatment only reduced the DSS-induced increase of IL-1β levels (**Figure 4**).

CBD (1 mg/kg) and FO (20 mg/mouse), either given alone or in combination, did not affect the DSS-induced behavioral changes in the light-dark box (anxiety test) and NOR (cognitive ability test) at d8 (**Supplementary Figure 1**).

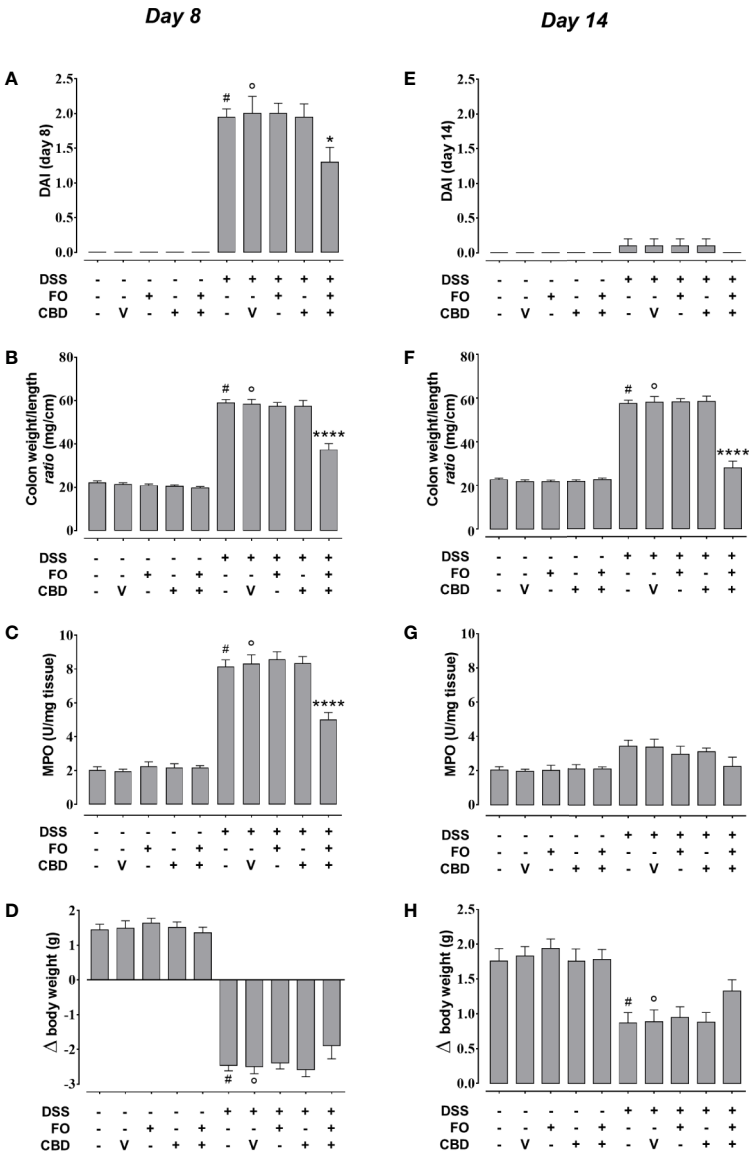

FIGURE 3 | Effect of fish oil (20 mg/mouse) and CBD (1 mg/kg), both alone and in combination, on intestinal inflammation at its peak (day 8) and during remission (day 14) in DSS-treated mice (Experiment 3). Effect of sesame oil (V, 90 µl/mouse, by oral gavage, used as CBD vehicle), fish oil (FO, 20 mg/mouse, by oral gavage), CBD (1 mg/kg, by oral gavage) and FO + CBD on disease activity index (DAI) score **(A, E)**, weight/colon length ratio (B,F), MPO activity (C,G) and body weight (D,H) in control mice (without DSS treatment) and in animals with colitis (induced by DSS) at day 8 **(A–D)** or day 14 **(E–H)** from the first injection of DSS. Bars are mean ± SEM of 10 animals **(A, B, D–F, H)** or five tissues **(C, G)** for each experimental group. Data in **(A)** [$F_{(9,90)} = 54.88$; $p < 0.0001$], **(B)** [$F_{(9,90)} = 121.3$; $p < 0.0001$], **(C)** [$F_{(9,40)} = 84.75$; $p < 0.0001$], **(D)** [$F_{(9,90)}$=98.41; $p < 0.0001$], **(E)** [$F_{(9,90)} = 0.653$; $p = 0.7485$], **(F)** [$F_{(9,90)} = 109.9$; $p < 0.0001$], **(G)** [$F_{(9,40)} = 3.277$; $p = 0.0045$], and **(H)** [$F_{(9,90)} = 8.823$; $p < 0.0001$] were statistically analyzed using one-way ANOVA followed by the Tukey-Kramer multiple comparisons test $^{\#}p < 0.0001$ **(A–D, F)** or $p < 0.01$ **(H)** vs. control; $^{\circ}p < 0.0001$ **(A–D, F)** or $p < 0.01$ **(H)** vs. vehicle; $^{*}p < 0.05$ and $^{****}p < 0.0001$ vs. DSS + vehicle and DSS + FO and DSS + CBD.

Per Se Ineffective Doses of FO and CBD, Alone or in Combination, Produce Profound Effects on the Gut Microbiome of DSS-Treated Mice (Experiment 3)

Neither DSS nor the treatments or their combination with DSS affected in a statistically significant manner Shannon diversity of mouse fecal microbiome (data not shown). At the level of phyla, the Firmicutes:Bacteroidetes ratio increased with time after DSS, but significantly only at the RP (d14). All treatments (i.e., CBD, FO, and CBD + FO) prevented this time-related increase (**Figure 5A**). No statistically significant difference among treatments was observed at either d8 or d14.

Hierarchical clustering of sequencing counts at the family level revealed that all d0 and vehicle-alone groups (irrespective of day) clustered together as did the DSS and DSS + Veh groups at

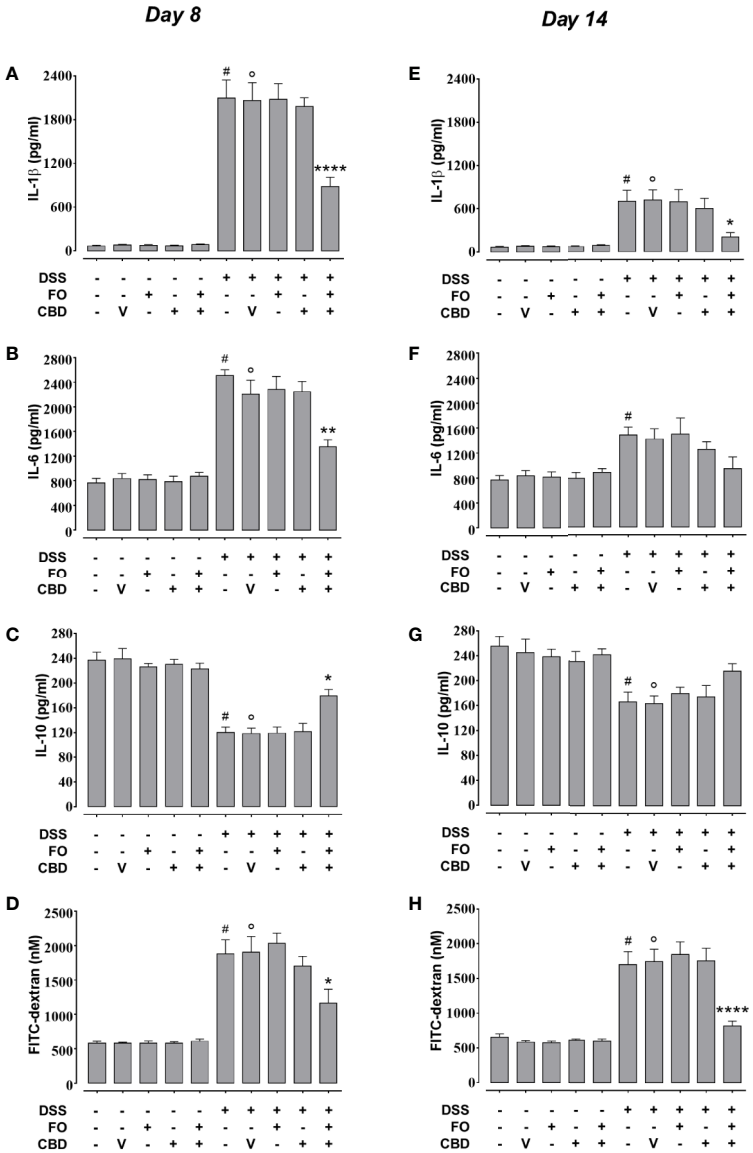

FIGURE 4 | Effect of fish oil (20 mg/mouse) and CBD (1 mg/kg), both alone and in combination, on DSS-induced changes in interleukin-1β, interleukin-6, and interleukin-10 levels and intestinal permiability (Experiment 3). Effect of sesame oil (V, 90 µl/mouse, by oral gavage, used as a control), fish oil (FO, 20 mg/mouse, by oral gavage), CBD (1 mg/kg, by oral gavage) and FO + CBD on interleukin-1β **(A, E)**, interleukin-6 **(B, F)**, interleukin-10 **(C, G)** and serum FICT-dextran concentration (a measure of intestinal barrier function; **D, H**) in control and DSS-treated mice (weighing 28–30 g) at day 8 **(A–D)** and day 14 **(E–H)** from DSS injection. Bars are mean ± SEM of five tissues **(A–D, E, F)** or 6 serum samples **(D, H)** for each experimental group. Data in **(A)** [$F_{(9,40)} = 48.44$; $p < 0.0001$], **(B)** [$F_{(9,40)} = 31.52$; $p < 0.0001$], **(C)** [$F_{(9,40)} = 25.34$; $p < 0.0001$], **(D)** [$F_{(9,50)} = 22.99$; $p < 0.0001$], **(E)** [$F_{(9,40)} = 9.521$; $p < 0.0001$], **(F)** [$F_{(9,40)} = 4.837$; $p = 0.0002$], **(G)** [$F_{(9,40)} = 5.822$; $p < 0.0001$], and **(H)** [$F_{(9,50)} = 23.78$; $p < 0.0001$] were statistically analyzed using one-way ANOVA followed by the Tukey-Kramer multiple comparisons test. $^{\#}p < 0.05$ **(F)** or $p < 0.01$ **(E, G)** or $p < 0.0001$ vs. control **(A–D, H)**; °$p < 0.05$ **(G)**, 0.001 **(E)**, or $p < 0.0001$ **(A–D, H)** vs. vehicle; *$p < 0.05$, **$p < 0.01$, and ****$p < 0.0001$ vs. DSS + vehicle or DSS + FO or DSS + CBD.

d8 (i.e., during the inflammatory peak; **Figure 5B**). Most notably, all DSS-treated groups at d14 (i.e., the RP) clustered together independently but within a larger cluster than included the experimental treatments (CBD, FO, and CBD + FO) at d8.

DSS treatment (DSS + Veh vs. Veh) affected several families, genera and species of gut bacteria mostly at RP (d14) (**Figures 5C**, **6** and **Supplementary Figures 2**–**5**; see **Supplementary Tables 1**–**3** for statistical details).

The only families that showed numerical alterations without reaching statistical differences at d8 were *Saccharimonadaceae* (P = 0.06) and *Streptococcaceae* (P = 0.096), which were reduced, with the latter family being increased by CBD (DSS + CBD vs. DSS + Veh, **Figure 5C** and **Supplementary Figure 2**). On the other hand, at RP (d14), *Akkermansiaceae* and *Tannerellaceae* were increased in the DSS + Veh vs. Veh group, and this increase was significant also at d14 with all three treatments and clustered together within the heatmap in which family sequencing counts were subjected to hierarchical clustering (**Figure 5C** and **Supplementary Figure 2**).

Several families that were not modified by DSS, were instead modified from their relative abundancies in DSS + Veh mice by one or more of the three treatments at either d8 or d14. These included: *Clostridiaceae_1* (reduced by CBD at d8), *Defluviitaleaceae* (increased by CBD and FO at d8), *Marinifilaceae* (decreased by CBD + FO at d8), *Christensenellaceae* (increased in a statistically significant manner by FO at d14 but not d8), *Desulfovibrionaceae* (decreased by CBD + FO at d14). A numerical decrease, which did not reach statistical significance (P = 0.1), was also seen at d14 with *Ruminococcaceae* in the presence of CBD + FO (**Supplementary Figure 3**).

At the genus level (**Supplementary Figure 4**), the only taxa for which a numerical increase, which did not reach statistical

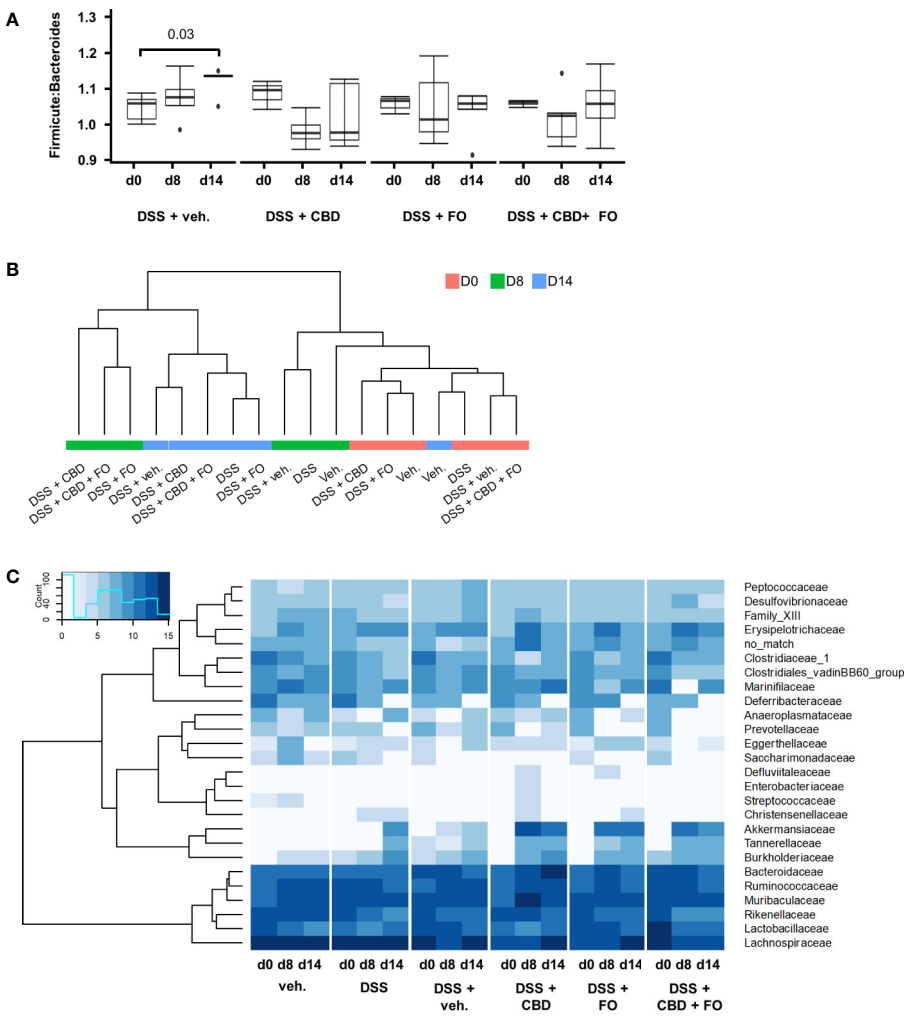

FIGURE 5 | Effect of fish oil (20 mg/mouse) and CBD (1 mg/kg), both alone and in combination, both at day 8 and day 14, on microbiota in faecal samples collected from DSS-treated mice belonging to the same treatment groups as – (Experiment 3). **(A)** Firmicutes:Bacteroidetes ratio. Wilcoxon P-values for pairwise comparisons are displayed above brackets. **(B)** Hierarchical clustering of treatment groups using CSS-normalized bacterial family counts. **(C)** Heat map and hierarchical clustering of family composition using CSS-normalized bacterial counts.

significance, was observed at d8 following DSS was *Akkermansia* (P = 0.09). This increase was however, further increased in a statistically significant manner by all treatment groups at d8. *Akkermansia* was increased by DSS at d14, and as for d8 all treatments resulted in even greater increases. The genus *Acetitomaculum*, instead, was significantly decreased only at d14, and none of the treatments could reverse this effect (**Supplementary Figure 4**). There were, however, several genera that were not affected by DSS but were significantly different from DSS + Veh following treatments (**Supplementary Figure 5**): *Anaerotruncus* and *Candidatus_Arthromitus* were both decreased at d8 by CBD, whereas, at the same time point, *Odoribacter* was decreased by CBD + FO, and *Defluviitaleaceae-UCG011* was increased by CBD and FO. On the other hand, at d14, *Christensenellaceae_R7-group* was increased by FO, *Ruminococcaceae-UCG-005* was decreased by CBD, and *Tyzzerella_3* was decreased by FO and CBD + FO.

Finally, although the method used does not usually allow identification of species, we could identify *Akkermansia muciniphila* and *Parabacteroides goldsteinii* as being increased by DSS at d14, and, in the presence of all treatments, also at d8 (**Figure 6**).

An Effective Dose of FO Administered Together With CBD Abolishes Colon Inflammation (Experiment 4)

FO administration at 75 mg/mouse, numerically reduced colon weight/length ratio and DAI score (**Figures 7A, B**), but this did not reach significant levels, and had no effect on the loss of body weight (**Figure 7C**) in DSS-treated mice. However, it significantly attenuated MPO activity (**Figure 7D**) as observed above. CBD, given by oral gavage at the dose range of 0.3–30 mg/kg did not affect DSS-induced intestinal inflammation, but when administered in FO-treated mice strongly, but variedly, reduced the DAI score (0.3, 3, and 10 mg/mouse only), the colon weight/colon length *ratio* (all doses of CBD tested) the loss of body weight (3 and 10 mg/mouse only) and MPO activity (all doses of CBD tested) (**Figures 7A–D**).

DISCUSSION

Inflammatory bowel diseases represent widespread and increasing chronic pathological conditions that still lack effective treatments. A plethora of recent studies have highlighted the role of gut dysbiosis in these conditions (Pittayanon et al., 2020). FO and its n-3-PUFAs have been suggested as a potential adjunctive treatment for IBDs, although the clinical data that have been obtained so far come from small cohorts of patients using variable modes of consumption (types of foods or types of formulation) and are therefore still controversial (Marton et al., 2019). On the other hand, while various *Cannabis* preparations have been tested in IBD patients as a potential treatment, purified cannabinoids have been mostly tested in animal models of colitis (Couch et al., 2018). Approximately 15% of IBD patients use *Cannabis* to ameliorate CD symptoms (i.e., abdominal pain, abdominal cramps, joint pain, and diarrhea), although so far there have been only three small placebo-controlled studies regarding the use of *Cannabis* in this disorder, involving 93 subjects altogether. Two of these studies showed overall significant clinical improvement but no amelioration in markers of inflammation (Naftali, 2020). With regard to UC, Kafil et al. recently reviewed the literature of the small clinical trials performed for this type of IBD, and stated that "no firm conclusions regarding the efficacy and safety of *Cannabis* or cannabidiol in adults with active ulcerative colitis can be drawn" (Kafil et al., 2018). This may be due, among other reasons, to the use of small numbers of patients, difficulties in obtaining a real placebo, or the relatively high dropout of patients in the active arm of the study. Nevertheless, several studies in animal models of colitis have highlighted that purified plant-derived cannabinoids can be

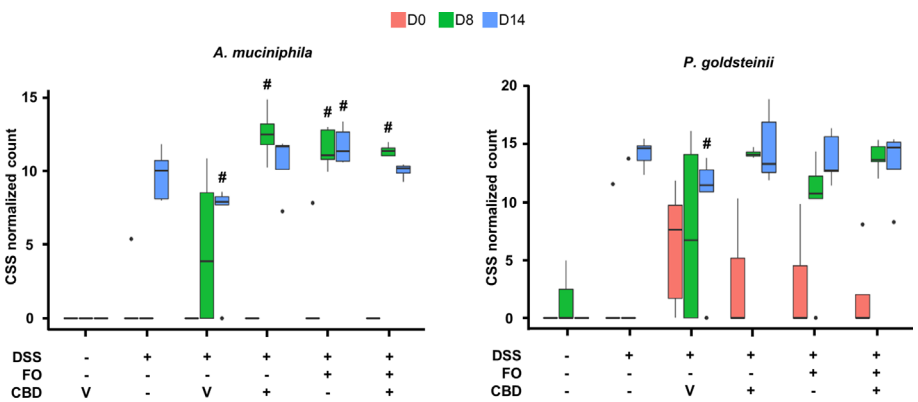

FIGURE 6 | Effect of fish oil (20 mg/mouse) and CBD (1 mg/kg), both alone and in combination, both at day 8 and day 14, on the relative abundance of *Akkermansia muciniphila* and *Parabacteroides goldsteinii* in faecal samples collected from DSS-treated mice belonging to the same treatments groups as – (Experiment 3). Only the species for which statistically significant differences were observed between DSS-Veh and Veh at day 14 are shown. Data were analyzed by two-way ANOVA followed by Tukey HSD *post-hoc* tests #, P < 0.05 vs. relevant control of the same day. For F values, please see **Supplementary Tables 1**.

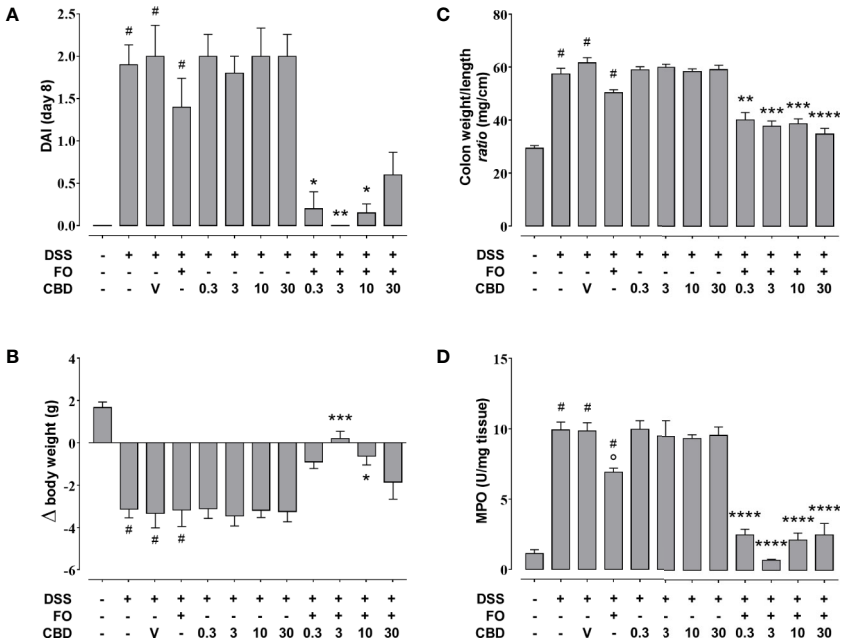

FIGURE 7 | Effect of fish oil (75 mg/mouse) and CBD (0.3–30 mg/kg), both alone and in combination, on DSS-induced inflammation (Experiment 4). Effect of sesame oil (V, 90 µl/mouse, by oral gavage, used as a control), fish oil (FO, 75 mg/mouse corresponding to 70 µl/mouse, by oral gavage), CBD (0.3–30 mg/kg, by oral gavage), and FO (75 mg/mouse) + CBD on disease activity index (DAI) score **(A)**, body weight **(B)**, colon weight/colon length ratio **(C)**, and MPO activity **(D)** in DSS-treated mice (weighting 28–30 g). On the *x*-axis the doses shown are for CBD. Bars are mean ± SEM of 10 animals **(A–C)** and of five tissues **(D)** for each experimental group. Data in **(A)** [$F_{(11,108)} = 13.48$; $p < 0.0001$], **(B)** [$F_{(11,108)} = 11.13$; $p < 0.0001$], **(C)** [$F_{(11,108)} = 44.81$; $p < 0.0001$], and **(D)** [$F_{(11,48)} = 48.28$; $p < 0.0001$] were statistically analyzed using one-way ANOVA followed by the Tukey-Kramer multiple comparisons test $^{\#}p < 0.01$–0.0001 vs. control; $^{\circ}p < 0.05$ vs. DSS alone; $^{*}p < 0.05$, $^{**}p < 0.01$, $^{***}p < 0.001$ and $^{****}p < 0.0001$ vs. DSS + FO.

efficacious, although, of these compounds, purified plant-derived CBD, appeared to be the most studied and the least promising (Borrelli et al., 2009; Borrelli et al., 2013; Romano et al., 2013; Pagano et al., 2016; Couch et al., 2018; Pagano et al., 2019). However, a formulation of highly purified plant-derived CBD was recently approved by the Food and Drug Administration (as Epidiolex®) and European Medicines Authority (as Epidyloex®, as an adjunctive therapy with clobazam) for the treatment of seizures associated with Dravet and Lennox Gastaut syndromes (two rare forms of pediatric epilepsy); while generally well tolerated, diarrhea is a common adverse event (Pauli et al., 2020). Importantly, while FO and n-3 PUFAs have been tested in experimental colitis also with regard to their effects on the gut microbiota, no preclinical or clinical study has ever been conducted with CBD in this context.

The major finding of the present study is that, when co-administered with inactive or minimally active doses of FO in the DSS murine model of colitis, oral purified botanically derived CBD (≥98%) attenuates inflammation even at relatively low doses. The second major finding of our study is that the potentiating effect on colon inflammation of *per se* ineffective doses of FO and CBD does not appear to be dependent on their effects on the gut microbiota. Finally, we have shown that DSS-induced behavioral alterations, which have been previously described in mice (Reichmann et al., 2015), were not affected by the combination of *per se* ineffective doses of FO and CBD despite its anti-inflammatory effects. However, it must be emphasized that the two behavioral tests used here, although used in previous studies on DSS-induced colitis in mice, cannot be considered sufficient alone to fully evaluate cognitive impairment and anxiety behavior in rodents (Kafil et al., 2018).

When tested in two different sets of experiments of DSS-treated mice, oral FO showed moderate and statistically significant efficacy at counteracting several parameters of DSS-induced colon inflammation, with a maximal effect being observed between 50 and 75 mg/mouse. Conversely, in two separate sets of experiments, oral CBD (0.3–30 mg/kg) produced no significant effect on the same parameters, in partial agreement with previous data obtained using the DNBS and croton oil models of lower and upper intestinal inflammation, where this compound showed only weak activity (Borrelli et al., 2009; Pagano et al., 2016). However, when CBD was administered to mice concurrently treated with FO, it produced an amelioration in most macroscopic measures of inflammation. CBD in conjunction with a *per se* ineffective (20 mg/mouse) dose of FO resulted in partial remission, whereas in conjunction with an effective dose (75 mg/mouse) of FO resulted in full remission. Interestingly, similar results have also been obtained with the DNBS model of colitis (Pagano et al., in press).

DSS-treated mice co-administered with *per se* ineffective doses of FO (20 mg/mouse) and CBD (1 mg/kg) also exhibited a recovery from their elevations in colonic inflammatory cytokine levels and permeability. Such general amelioration was observed both during the apex of inflammation, at d8, and during the RP, at d14. However, this combined treatment did not ameliorate the anxiety-like behavior and cognitive deficits of DSS-treated mice, which are known to be maximal at d8 (Emge et al., 2016) and were only assessed at this time point.

The gut microbiota has been suggested to be both one of the underlying causes of IBDs, when dysfunctional (gut dysbiosis) (Manichanh et al., 2012; Khan et al., 2019; Alam et al., 2020), and a mediator of the anti-inflammatory and therapeutic effects of several different types of pharmacological, nutraceutical and nutritional interventions that proved beneficial against these disorders when investigated in preclinical models (and in the DSS model, in particular) (Wu M. et al., 2019; Fernandez et al., 2020; Gu et al., 2020). Gut dysbiosis is also known to accompany, and possibly underlie, some behavioral disturbances, such as those that are observed in DSS-treated mice, i.e., anxiety and cognitive deficits (Reichmann et al., 2015; Emge et al., 2016). In the present study, only few gut microbiota phyla, families, genera and species were affected by DSS at day 8, possibly suggesting that commensal bacteria may not play an important role in DSS-associated inflammatory and behavioral disturbances under our experimental conditions. Conversely, several taxa were significantly altered at day 14, thus indicating that gut bacteria may play a role in the late effects of DSS, in terms of either residual/resolved inflammation or potential residual behavioral disturbances (which we did not assess at this time point). Interestingly, the anti-inflammatory effect of the combination of *per se* ineffective doses of FO (20 mg/mouse) or CBD (1 mg/kg) was accompanied by changes in several gut bacterial taxa, some of which have been suggested to play a beneficial role in inflammation (see below). However, we found that also when administered alone, these non-anti-inflammatory doses of FO or CBD often similarly modified the relative abundances of commensal bacterial taxa that were either affected or not by DSS at d8. This indicates that the observed effects of FO or CBD on the gut microflora were independent from their effects on inflammation and *vice versa*. Nevertheless, some of these effects on the gut microbiota, as in the case of those of the FO/CBD combination, may have reinforced the anti-inflammatory actions, whereas others, as in the case of those of FO or CBD administered *per se*, may have opposed them. Likewise, the fact that the effects of FO, CBD and their combination on gut microbiota taxa were in some cases only observed at RP (day 14), when resolution of inflammation was ongoing, is indicative of either inflammation-independent effects, or effects that were synergistic/antagonistic with those of endogenous inflammation resolution factors.

In particular, at the phyla level, the Firmicutes:Bacteroidetes ratio was previously reported to be increased in some models of colonic inflammation and in human IBDs (Manichanh et al., 2012; Santoru et al., 2017). In the present study, this biomarker of gut inflammation, typical also of obesity-induced dysbiosis (Ley et al., 2006), was increased by DSS only at RP. The combination of *per se* ineffective doses of FO and CBD, but also the single treatments that exerted no effect on inflammation, counteracted this increase, suggesting that at least the effects of the combination of the two substances may have been reinforced by, but was not dependent on, their action on the Firmicutes: Bacteroidetes ratio.

Of note, the combination of CBD + FO specifically decreased the levels of a small number of bacterial families (*Marinifilaceae* at d8 and *Desulfovibrionaceae* and *Ruminococcaceae* at d14) and one genus (*Odoribacter* at d8) in DSS-treated mice, all of which have previously been shown by others to be modified either in patients with IBDs or their preclinical models. *Desulfovibrionaceae* has been reported to be increased in abundance in the faeces of IBD patients (Berry and Reinisch, 2013) and *Ruminococcaceae* have been reported to be increased in those with UC, but decreased in patients with CD (Morgan et al., 2012; Alam et al., 2020). Pre-clinical studies in addition to ours suggest that these families may have functional roles in IBDs. Indeed, DSS-induced increases of *Desulfovibrionaceae* in mice were abrogated through treatment with the probiotic *Bifidobacterium breve* (Yang and Yang, 2018). However, *Desulfovibrionaceae* and *Ruminococcaceae* were both increased by gentamicin in DSS-treated mice in association with an improved DAI and inflammatory profile (Zhai Z. et al., 2019). Most interestingly, *Ptpn22*$^{-/-}$ mice, which are resistant to faster recovery in response to cohousing-mediated faecal microbiota transfer, have decreased *Desulfovibrionaceae* levels (Spalinger et al., 2019). These data are counterintuitive in the light of our data presented here and given that this family may be an indicator of colitis disease activity. In contrast, in the study by Zhai Z. et al. (2019), *Marinifilaceae* positively correlated with inflammatory status in the mice, which is in line with our study describing significant decreases in this family at d8 by CBD (1 mg/kg) + FO (20 mg/mouse), concomitant to decreased inflammation. Furthermore, both *Marinifilaceae* and *Ruminococcaceae* were decreased in rats fed an acorn-fed cured ham diet (having high levels of the mono-unsaturated fatty acid oleic acid), in conjunction with significant prevention of DSS-induced colitis symptoms (Fernandez et al., 2020).

The short chain fatty acid-producing genus *Odoribacter* is generally considered to play a beneficial role against inflammation and is reduced in CD and UC (Morgan et al., 2012). However, its levels have been shown to increase in response to DSS and decrease in response to electroacupuncture and moxibustion treatment that improved the DAI (Wei et al., 2019). Furthermore, *Odoribacter* is increased in azoxymethane (AOM) and DSS-induced colitis-associated cancer in mice, and its levels are reduced in response to treatment with a probiotic in conjunction with decreased tumor formation (Song et al., 2018). Here we found that the abundance of this genus was not altered by DSS, and was decreased by the FO + CBD combination, an effect that, depending on the role of these bacteria, could either contribute to inhibition of inflammation or represent an adaptive consequence of the latter.

A. muciniphila, a species that plays a beneficial role in inflammation and was previously reported to be increased in murine models of IBDs and to mediate the anti-inflammatory

effects of several treatments on these models (Bian et al., 2019; Li et al., 2019; Zhai R. et al., 2019; Zhang et al., 2019), was increased by DSS only at d14, suggesting that this effect might represent a potentially adaptive and protective mechanism intervening the resolution of inflammation. Importantly, this effect was rendered statistically significant also at d8 by a combination of *per se* ineffective doses of FO and CBD, but also by the single treatments. This bacterial species may, therefore, participate in some of the beneficial effects of the FO/CBD combination on DSS-induced inflammation, but does not seem to be sufficient to induce such effects. However, the exact role of *A. muciniphila* in colitis remains to be confirmed, as colonization with this gram-negative species has also been shown to increase intestinal inflammation in both specific-pathogen-free and germ-free $Il10^{-/-}$ mice (Seregin et al., 2017). Interestingly, the effects of the treatments observed here on *A. muciniphila* were also observed at the level of its family (*Akkermansiaceae*) and genus (*Akkermansia*), suggesting that this species is the main, if not only, component of its family in the fecal microbiome of DSS-treated mice, and possibly explaining why we could identify this species even though the sequencing method used normally only allows to detect taxa down to the level of genera.

We could also detect at least another species, *P.goldsteinii*, whose abundance, like with *A. muciniphila*, was increased in DSS-treated mice during the RP, and which is known to play a beneficial action in gut inflammation as well obesity (Chang et al., 2019; Wu T. R. et al., 2019). Accordingly, this increase was observed already at d8 following co-treatment with the anti-inflammatory combination of FO and CBD (but, again, also with the single treatments).

Finally, it should be noted that in the present study we have not measured gut motility changes associated with inflammation, an UC clinical phenomenon (Ohama et al., 2007). However, previous studies have demonstrated that CBD does not affect motility under physiological conditions, but it normalizes intestinal motility when this is perturbed by a pro-inflammatory stimulus (Capasso et al., 2008; Lin et al., 2011), and ameliorated motility changes in a TNBS-induced colitis model (Wei et al., 2020). Although CBD has been shown to reduce acetylcholine- and prostaglandin F2α-induced contractions in the isolated ileum (Capasso et al., 2008), there is no evidence that CBD may slow colonic transit under physiological conditions. This is relevant in the light of the observation that drugs able to slow colonic motility (e.g., narcotic, antidiarrheal, or anticholinergic preparations) are contraindicated in toxic megacolon (Gan and Beck, 2003).

In conclusion, we have shown here that FO in combination with CBD can produce strong intestinal anti-inflammatory effects on DSS-induced colitis in mice, and that both FO and CBD, alone or in combination, can also affect the gut microbiota in these mice in a manner partly independent from their anti-inflammatory actions. Future studies should investigate the possibility of using combinations of low doses of FO and CBD, two clinically used substances with very few undesired side effects, for the treatment of colonic inflammation in IBDs. Understanding the functional/biological relevance of the changes induced by the FO/CBD combination on gut microbiota (both murine and human) also merits further research.

DATA AVAILABILITY STATEMENT

The raw data supporting the conclusions of this article will be made available by the authors, without undue reservation. The datasets analyzed for this study can be found in the NCBI GenBank under BioProject ID PRJNA662783.

ETHICS STATEMENT

The animal study was reviewed and approved by Institutional Animal Ethics Committee of the University of Naples Federico II. The use of animals conformed to guidelines for the safe use and care of experimental animals in accordance with the Italian D.L. no. 116 of 27 January 1992 and associated guidelines in the European Communities Council (86/609/ECC and 2010/63/UE).

AUTHOR CONTRIBUTIONS

CS, AI, VD, and FB conceived and designed the study. EP, TV, CC, AC, and OP performed experiments. CS, EP, SL, and FB analyzed data. VD wrote the manuscript. CS, EP, SL, AI, and FB edited the manuscript. All authors contributed to the article and approved the submitted version.

FUNDING

This work was supported by GW Research Ltd, Cambridge, UK, the Canada Research Excellence Chair in the Microbiome-Endocannabinoidome Axis in Metabolic Health (CERC-MEND), which is funded by the Tri-Agency of the Canadian Federal Government (The Canadian Institutes of Health Research (CIHR), the Natural Sciences and Engineering Research Council of Canada (NSERC), and the Social Sciences and Humanities Research Council of Canada (SSHRC), as well as by the Canadian Foundation of Innovation (to VD, grant numbers 37392 and 37858) and the Sentinelle Nord-Apogée program (to Université Laval). TV acknowledges the Joint International Research Unit for Chemical and Biomolecular Research on the Microbiome and its impact on Metabolic Health and Nutrition (UMI-MicroMeNu), between Université Laval and the CNR of Italy, which is supported by the Sentinelle Nord program.

SUPPLEMENTARY MATERIAL

The Supplementary Material for this article can be found online at: https://www.frontiersin.org/articles/10.3389/fphar.2020.585096/full#supplementary-material

REFERENCES

Alam, M. T., Amos, G. C. A., Murphy, A. R. J., Murch, S., Wellington, E. M. H., and Arasaradnam, R. P. (2020). Microbial imbalance in inflammatory bowel disease patients at different taxonomic levels. *Gut Pathog* 12, 1. doi: 10.1186/s13099-019-0341-6

Ananthakrishnan, A. N., Bernstein, C. N., Iliopoulos, D., Macpherson, A., Neurath, M. F., Ali, R. A. R., et al. (2018). Environmental triggers in IBD: a review of progress and evidence. *Nat. Rev. Gastroenterol. Hepatol.* 15 (1), 39–49. doi: 10.1038/nrgastro.2017.136

Berry, D., and Reinisch, W. (2013). Intestinal microbiota: a source of novel biomarkers in inflammatory bowel diseases? *Best Pract. Res. Clin. Gastroenterol.* 27 (1), 47–58. doi: 10.1016/j.bpg.2013.03.005

Bian, X., Wu, W., Yang, L., Lv, L., Wang, Q., Li, Y., et al. (2019). Administration of Akkermansia muciniphila Ameliorates Dextran Sulfate Sodium-Induced Ulcerative Colitis in Mice. *Front. Microbiol* 10, 2259. doi: 10.3389/fmicb.2019.02259

Borrelli, F., Aviello, G., Romano, B., Orlando, P., Capasso, R., Maiello, F., et al. (2009). Cannabidiol, a safe and non-psychotropic ingredient of the marijuana plant Cannabis sativa, is protective in a murine model of colitis. *J. Mol. Med. (Berl)* 87 (11), 1111–1121. doi: 10.1007/s00109-009-0512-x

Borrelli, F., Fasolino, I., Romano, B., Capasso, R., Maiello, F., Coppola, D., et al. (2013). Beneficial effect of the non-psychotropic plant cannabinoid cannabigerol on experimental inflammatory bowel disease. *Biochem. Pharmacol.* 85 (9), 1306–1316. doi: 10.1016/j.bcp.2013.01.017

Boulange, C. L., Neves, A. L., Chilloux, J., Nicholson, J. K., and Dumas, M. E. (2016). Impact of the gut microbiota on inflammation, obesity, and metabolic disease. *Genome Med.* 8 (1), 42. doi: 10.1186/s13073-016-0303-2

Burstein, S. (2015). Cannabidiol (CBD) and its analogs: a review of their effects on inflammation. *Bioorg Med. Chem.* 23 (7), 1377–1385. doi: 10.1016/j.bmc.2015.01.059

Calder, P. C. (2017). Omega-3 fatty acids and inflammatory processes: from molecules to man. *Biochem. Soc. Trans.* 45 (5), 1105–1115. doi: 10.1042/BST20160474

Callahan, B. J., McMurdie, P. J., Rosen, M. J., Han, A. W., Johnson, A. J., and Holmes, S. P. (2016). DADA2: High-resolution sample inference from Illumina amplicon data. *Nat. Methods* 13 (7), 581–583. doi: 10.1038/nmeth.3869

Capasso, R., Borrelli, F., Aviello, G., Romano, B., Scalisi, C., Capasso, F., et al. (2008). Cannabidiol, extracted from Cannabis sativa, selectively inhibits inflammatory hypermotility in mice. *Br. J. Pharmacol.* 154 (5), 1001–1008. doi: 10.1038/bjp.2008.177

Chang, C. J., Lin, T. L., Tsai, Y. L., Wu, T. R., Lai, W. F., Lu, C. C., et al. (2019). Next generation probiotics in disease amelioration. *J. Food Drug Anal.* 27 (3), 615–622. doi: 10.1016/j.jfda.2018.12.011

Chassaing, B., Aitken, J. D., Malleshappa, M., and Vijay-Kumar, M. (2014). Dextran sulfate sodium (DSS)-induced colitis in mice. *Curr. Protoc. Immunol.* 104, 15 25 1–15 25 14. doi: 10.1002/0471142735.im1525s104

Costantini, L., Molinari, R., Farinon, B., and Merendino, N. (2017). Impact of Omega-3 Fatty Acids on the Gut Microbiota. *Int. J. Mol. Sci.* 18 (12), 2645. doi: 10.3390/ijms18122645

Couch, D. G., Maudslay, H., Doleman, B., Lund, J. N., and O'Sullivan, S. E. (2018). The Use of Cannabinoids in Colitis: A Systematic Review and Meta-Analysis. *Inflammation Bowel Dis.* 24 (4), 680–697. doi: 10.1093/ibd/izy014

Curtis, M. J., Alexander, S., Cirino, G., Docherty, J. R., George, C. H., Giembycz, M. A., et al. (2018). Experimental design and analysis and their reporting II: updated and simplified guidance for authors and peer reviewers. *Br. J. Pharmacol.* 175 (7), 987–993. doi: 10.1111/bph.14153

De Musis, C., Granata, L., Dallio, M., Miranda, A., Gravina, A. G., and Romano, M. (2020). Inflammatory bowel diseases: the role of gut microbiota. *Curr. Pharm. Des.* 26 (25), 2951–2961. doi: 10.2174/1381612826666200420144128

Emge, J. R., Huynh, K., Miller, E. N., Kaur, M., Reardon, C., Barrett, K. E., et al. (2016). Modulation of the microbiota-gut-brain axis by probiotics in a murine model of inflammatory bowel disease. *Am. J. Physiol. Gastroint Liver Physiol.* 310 (11), G989–G998. doi: 10.1152/ajpgi.00086.2016

Faul, F., Erdfelder, E., Lang, A. G., and Buchner, A. (2007). G*Power 3: a flexible statistical power analysis program for the social, behavioral, and biomedical sciences. *Behav. Res. Methods* 39 (2), 175–191. doi: 10.3758/bf03193146

Fernandez, J., de la Fuente, V. G., Garcia, M. T. F., Sanchez, J. G., Redondo, B. I., Villar, C. J., et al. (2020). A diet based on cured acorn-fed ham with oleic acid content promotes anti-inflammatory gut microbiota and prevents ulcerative colitis in an animal model. *Lipids Health Dis.* 19 (1), 28. doi: 10.1186/s12944-020-01205-x

Forbes, J. D., Van Domselaar, G., and Bernstein, C. N. (2016). The Gut Microbiota in Immune-Mediated Inflammatory Diseases. *Front. Microbiol* 7, 1081. doi: 10.3389/fmicb.2016.01081

Gan, S. I., and Beck, P. L. (2003). A new look at toxic megacolon: an update and review of incidence, etiology, pathogenesis, and management. *Am. J. Gastroenterol.* 98 (11), 2363–2371. doi: 10.1111/j.1572-0241.2003.07696.x

Gotfried, J., Naftali, T., and Schey, R. (2020). Role of Cannabis and Its Derivatives in Gastrointestinal and Hepatic Disease. *Gastroenterology* 159 (1), 62–80. doi: 10.1053/j.gastro.2020.03.087

Gu, Z., Zhu, Y., Jiang, S., Xia, G., Li, C., Zhang, X., et al. (2020). Tilapia head glycolipids reduce inflammation by regulating the gut microbiota in dextran sulphate sodium-induced colitis mice. *Food Funct.* 11 (4), 3245–3255. doi: 10.1039/d0fo00116c

Guida, F., Boccella, S., Iannotta, M., De Gregorio, D., Giordano, C., Belardo, C., et al. (2017). Palmitoylethanolamide Reduces Neuropsychiatric Behaviors by Restoring Cortical Electrophysiological Activity in a Mouse Model of Mild Traumatic Brain Injury. *Front. Pharmacol.* 8, 95. doi: 10.3389/fphar.2017.00095

Ibeas Bih, C., Chen, T., Nunn, A. V., Bazelot, M., Dallas, M., and Whalley, B. J. (2015). Molecular Targets of Cannabidiol in Neurological Disorders. *Neurotherapeutics* 12 (4), 699–730. doi: 10.1007/s13311-015-0377-3

Innes, J. K., and Calder, P. C. (2018). Omega-6 fatty acids and inflammation. *Prostaglandins Leukot Essent Fatty Acids* 132, 41–48. doi: 10.1016/j.plefa.2018.03.004

Irving, P. M., Iqbal, T., Nwokolo, C., Subramanian, S., Bloom, S., Prasad, N., et al. (2018). Double-blind, Placebo-controlled, Parallel-group, Pilot Study of Cannabidiol-rich Botanical Extract in the Symptomatic Treatment of Ulcerative Colitis. *Inflammation Bowel Dis.* 24 (4), 714–724. doi: 10.1093/ibd/izy002

Kafil, T. S., Nguyen, T. M., MacDonald, J. K., and Chande, N. (2018). Cannabis for the treatment of ulcerative colitis. *Cochrane Database Syst. Rev.* 11, CD012954. doi: 10.1002/14651858.CD012954.pub2

Kaplan, G. G., and Ng, S. C. (2017). Understanding and Preventing the Global Increase of Inflammatory Bowel Disease. *Gastroenterology* 152 (2), 313–321e2. doi: 10.1053/j.gastro.2016.10.020

Ke, J., Li, Y., Han, C., He, R., Lin, R., Qian, W., et al. (2020). Fucose Ameliorate Intestinal Inflammation Through Modulating the Crosstalk Between Bile Acids and Gut Microbiota in a Chronic Colitis Murine Model. *Inflammation Bowel Dis.* 26 (6), 863–873. doi: 10.1093/ibd/izaa007

Keller, D. S., Windsor, A., Cohen, R., and Chand, M. (2019). Colorectal cancer in inflammatory bowel disease: review of the evidence. *Tech Coloproctol* 23 (1), 3–13. doi: 10.1007/s10151-019-1926-2

Khan, I., Ullah, N., Zha, L., Bai, Y., Khan, A., Zhao, T., et al. (2019). Alteration of Gut Microbiota in Inflammatory Bowel Disease (IBD): Cause or Consequence? IBD Treatment Targeting the Gut Microbiome. *Pathogens* 8 (3), 126. doi: 10.3390/pathogens8030126

Kilkenny, C., Browne, W., Cuthill, I. C., Emerson, M., Altman, D. G., and Group, N.C.R.R.G.W. (2010). Animal research: reporting in vivo experiments: the ARRIVE guidelines. *Br. J. Pharmacol.* 160 (7), 1577–1579. doi: 10.1111/j.1476-5381.2010.00872.x

Krawisz, J. E., Sharon, P., and Stenson, W. F. (1984). Quantitative assay for acute intestinal inflammation based on myeloperoxidase activity. Assessment of inflammation in rat and hamster models. *Gastroenterology* 87 (6), 1344–1350. doi: 10.1016/0016-5085(84)90202-6

Ley, R. E., Turnbaugh, P. J., Klein, S., and Gordon, J. I. (2006). Microbial ecology: human gut microbes associated with obesity. *Nature* 444 (7122), 1022–1023. doi: 10.1038/4441022a

Li, S., Fu, C., Zhao, Y., and He, J. (2019). Intervention with alpha-Ketoglutarate Ameliorates Colitis-Related Colorectal Carcinoma via Modulation of the Gut Microbiome. *BioMed. Res. Int.* 2019, 8020785. doi: 10.1155/2019/8020785

Lin, X. H., Yuece, B., Li, Y. Y., Feng, Y. J., Feng, J. Y., Yu, L. Y., et al. (2011). A novel CB receptor GPR55 and its ligands are involved in regulation of gut movement in rodents. *Neurogastroenterol Motil* 23 (9), 862–e342. doi: 10.1111/j.1365-2982.2011.01742.x

Liu, Y., Wang, X., Chen, Q., Luo, L., Ma, M., Xiao, B., et al. (2020). Camellia sinensis and Litsea coreana Ameliorate Intestinal Inflammation and Modulate

Gut Microbiota in Dextran Sulfate Sodium-Induced Colitis Mice. *Mol. Nutr. Food Res.* 64 (6), e1900943. doi: 10.1002/mnfr.201900943

Manichanh, C., Borruel, N., Casellas, F., and Guarner, F. (2012). The gut microbiota in IBD. *Nat. Rev. Gastroenterol. Hepatol.* 9 (10), 599–608. doi: 10.1038/nrgastro.2012.152

Marton, L. T., Goulart, R. A., Carvalho, A. C. A., and Barbalho, S. M. (2019). Omega Fatty Acids and Inflammatory Bowel Diseases: An Overview. *Int. J. Mol. Sci.* 20 (19), 4851. doi: 10.3390/ijms20194851

McGrath, J. C., and Lilley, E. (2015). Implementing guidelines on reporting research using animals (ARRIVE etc.): new requirements for publication in BJP. *Br. J. Pharmacol.* 172 (13), 3189–3193. doi: 10.1111/bph.12955

Morgan, X. C., Tickle, T. L., Sokol, H., Gevers, D., Devaney, K. L., Ward, D. V., et al. (2012). Dysfunction of the intestinal microbiome in inflammatory bowel disease and treatment. *Genome Biol.* 13 (9), R79. doi: 10.1186/gb-2012-13-9-r79

Munyaka, P. M., Rabbi, M. F., Khafipour, E., and Ghia, J. E. (2016). Acute dextran sulfate sodium (DSS)-induced colitis promotes gut microbial dysbiosis in mice. *J. Basic Microbiol* 56 (9), 986–998. doi: 10.1002/jobm.201500726

Naftali, T. (2020). An overview of cannabis based treatment in Crohn's disease. *Expert Rev. Gastroenterol. Hepatol.* 14 (4), 253–257. doi: 10.1080/17474124.2020.1740590

Ng, S. C., Shi, H. Y., Hamidi, N., Underwood, F. E., Tang, W., Benchimol, E. I., et al. (2018). Worldwide incidence and prevalence of inflammatory bowel disease in the 21st century: a systematic review of population-based studies. *Lancet* 390 (10114), 2769–2778. doi: 10.1016/S0140-6736(17)32448-0

Nishiyama, Y., Kataoka, T., Yamato, K., Taguchi, T., and Yamaoka, K. (2012). Suppression of dextran sulfate sodium-induced colitis in mice by radon inhalation. *Mediators Inflammation* 2012, 239617. doi: 10.1155/2012/239617

Ohama, T., Hori, M., and Ozaki, H. (2007). Mechanism of abnormal intestinal motility in inflammatory bowel disease: how smooth muscle contraction is reduced? *J. Smooth Muscle Res.* 43 (2), 43–54. doi: 10.1540/jsmr.43.43

Pagano, E., Capasso, R., Piscitelli, F., Romano, B., Parisi, O. A., Finizio, S., et al. (2016). An Orally Active Cannabis Extract with High Content in Cannabidiol attenuates Chemically-induced Intestinal Inflammation and Hypermotility in the Mouse. *Front. Pharmacol.* 7, 341. doi: 10.3389/fphar.2016.00341

Pagano, E., Romano, B., Iannotti, F. A., Parisi, O. A., D'Armiento, M., Pignatiello, S., et al. (2019). The non-euphoric phytocannabinoid cannabidivarin counteracts intestinal inflammation in mice and cytokine expression in biopsies from UC pediatric patients. *Pharmacol. Res.* 149, 104464. doi: 10.1016/j.phrs.2019.104464

Pauli, C. S., Conroy, M., Vanden Heuvel, B. D., and Park, S. H. (2020). Cannabidiol Drugs Clinical Trial Outcomes and Adverse Effects. *Front. Pharmacol.* 11:63:63. doi: 10.3389/fphar.2020.00063

Paulson, J. N., Stine, O. C., Bravo, H. C., and Pop, M. (2013). Differential abundance analysis for microbial marker-gene surveys. *Nat. Methods* 10 (12), 1200–1202. doi: 10.1038/nmeth.2658

Pittayanon, R., Lau, J. T., Leontiadis, G. I., Tse, F., Yuan, Y., Surette, M., et al. (2020). Differences in Gut Microbiota in Patients With vs Without Inflammatory Bowel Diseases: A Systematic Review. *Gastroenterology* 158 (4), 930–946 e1. doi: 10.1053/j.gastro.2019.11.294

Rausch, P., Ruhlemann, M., Hermes, B. M., Doms, S., Dagan, T., Dierking, K., et al. (2019). Comparative analysis of amplicon and metagenomic sequencing methods reveals key features in the evolution of animal metaorganisms. *Microbiome* 7 (1), 133. doi: 10.1186/s40168-019-0743-1

Reichmann, F., Hassan, A. M., Farzi, A., Jain, P., Schuligoi, R., and Holzer, P. (2015). Dextran sulfate sodium-induced colitis alters stress-associated behaviour and neuropeptide gene expression in the amygdala-hippocampus network of mice. *Sci. Rep.* 5, 9970. doi: 10.1038/srep09970

Romano, B., Borrelli, F., Fasolino, I., Capasso, R., Piscitelli, F., Cascio, M., et al. (2013). The cannabinoid TRPA1 agonist cannabichromene inhibits nitric oxide production in macrophages and ameliorates murine colitis. *Br. J. Pharmacol.* 169 (1), 213–229. doi: 10.1111/bph.12120

Santoru, M. L., Piras, C., Murgia, A., Palmas, V., Camboni, T., Liggi, S., et al. (2017). Cross sectional evaluation of the gut-microbiome metabolome axis in an Italian cohort of IBD patients. *Sci. Rep.* 7 (1), 9523. doi: 10.1038/s41598-017-10034-5

Seregin, S. S., Golovchenko, N., Schaf, B., Chen, J., Pudlo, N. A., Mitchell, J., et al. (2017). NLRP6 Protects Il10(-/-) Mice from Colitis by Limiting Colonization of Akkermansia muciniphila. *Cell Rep.* 19 (4), 733–745. doi: 10.1016/j.celrep.2017.03.080

Song, H., Wang, W., Shen, B., Jia, H., Hou, Z., Chen, P., et al. (2018). Pretreatment with probiotic Bifico ameliorates colitis-associated cancer in mice: Transcriptome and gut flora profiling. *Cancer Sci.* 109 (3), 666–677. doi: 10.1111/cas.13497

Spalinger, M. R., Schwarzfischer, M., Hering, L., Shawki, A., Sayoc, A., Santos, A., et al. (2019). Loss of PTPN22 abrogates the beneficial effect of cohousing-mediated fecal microbiota transfer in murine colitis. *Mucosal Immunol.* 12 (6), 1336–1347. doi: 10.1038/s41385-019-0201-1

Turnbaugh, P. J., Backhed, F., Fulton, L., and Gordon, J. I. (2008). Diet-induced obesity is linked to marked but reversible alterations in the mouse distal gut microbiome. *Cell Host Microbe* 3 (4), 213–223. doi: 10.1016/j.chom.2008.02.015

Turner, S. E., Williams, C. M., Iversen, L., and Whalley, B. J. (2017). Molecular Pharmacology of Phytocannabinoids. *Prog. Chem. Org Nat. Prod* 103, 61–101. doi: 10.1007/978-3-319-45541-9_3

Wei, D., Xie, L., Zhuang, Z., Zhao, N., Huang, B., Tang, Y., et al. (2019). Gut Microbiota: A New Strategy to Study the Mechanism of Electroacupuncture and Moxibustion in Treating Ulcerative Colitis. *Evid Based Complement Alternat Med.* 2019, 9730176. doi: 10.1155/2019/9730176

Wei, D., Wang, H., Yang, J., Dai, Z., Yang, R., Meng, S., et al. (2020). Effects of O-1602 and CBD on TNBS-induced colonic disturbances. *Neurogastroenterol Motil* 32 (3), e13756. doi: 10.1111/nmo.13756

Williamson, E. M., Liu, X., and Izzo, A. A. (2020). Trends in use, pharmacology, and clinical applications of emerging herbal nutraceuticals. *Br. J. Pharmacol.* 177 (6), 1227–1240. doi: 10.1111/bph.14943

Wu, M., Li, P., An, Y., Ren, J., Yan, D., Cui, J., et al. (2019). Phloretin ameliorates dextran sulfate sodium-induced ulcerative colitis in mice by regulating the gut microbiota. *Pharmacol. Res.* 150, 104489. doi: 10.1016/j.phrs.2019.104489

Wu, T. R., Lin, C. S., Chang, C. J., Lin, T. L., Martel, J., Ko, Y. F., et al. (2019). Gut commensal Parabacteroides goldsteinii plays a predominant role in the anti-obesity effects of polysaccharides isolated from Hirsutella sinensis. *Gut* 68 (2), 248–262. doi: 10.1136/gutjnl-2017-315458

Yang, J., and Yang, H. (2018). Effect of Bifidobacterium breve in Combination With Different Antibiotics on Clostridium difficile. *Front. Microbiol* 9, 2953. doi: 10.3389/fmicb.2018.02953

Zhai, Z., Zhang, F., Cao, R., Ni, X., Xin, Z., Deng, J., et al. (2019). Cecropin A Alleviates Inflammation Through Modulating the Gut Microbiota of C57BL/6 Mice With DSS-Induced IBD. *Front. Microbiol* 10, 1595. doi: 10.3389/fmicb.2019.01595

Zhai, R., Xue, X., Zhang, L., Yang, X., Zhao, L., and Zhang, C. (2019). Strain-Specific Anti-inflammatory Properties of Two Akkermansia muciniphila Strains on Chronic Colitis in Mice. *Front. Cell Infect. Microbiol* 9, 239. doi: 10.3389/fcimb.2019.00239

Zhang, T., Li, Q., Cheng, L., Buch, H., and Zhang, F. (2019). Akkermansia muciniphila is a promising probiotic. *Microb Biotechnol.* 12 (6), 1109–1125. doi: 10.1111/1751-7915.13410

Zhu, W., Gao, Y., Wan, J., Lan, X., Han, X., Zhu, S., et al. (2018). Changes in motor function, cognition, and emotion-related behavior after right hemispheric intracerebral hemorrhage in various brain regions of mouse. *Brain Behav. Immun.* 69, 568–581. doi: 10.1016/j.bbi.2018.02.004

Conflict of Interest: CS, FB, VD, and AI receive research grants from GW Research Ltd, UK. CS was an employee of GW Research Ltd, UK. The authors declare that this study received funding from GW Research Ltd, UK. The funder had the following involvement with the study: has read, edited, and approved of the manuscript for submission.

The remaining authors declare that the research was conducted in the absence of any commercial or financial relationships that could be construed as a potential conflict of interest.

frontiers in Pharmacology

ORIGINAL RESEARCH
published: 30 November 2020
doi: 10.3389/fphar.2020.588560

Adhesive Bacteria in the Terminal Ileum of Children Correlates With Increasing Th17 Cell Activation

*Bo Chen[1], Diya Ye[1], Lingling Luo[1], Weirong Liu[1,2], Kerong Peng[1], Xiaoli Shu[1], Weizhong Gu[1], Xiaojun Wang[2], Charlie Xiang[3] and Mizu Jiang[1]**

[1]Gastrointestinal Lab, Children's Hospital, Zhejiang University School of Medicine, National Clinical Research Center for Child, National Children's Regional Medical Center, Hangzhou, China, [2]Shaoxing People's Hospital, Shaoxing, China, [3]Collaborative Innovation Center for Diagnosis and Treatment of Infectious Diseases, State Key Laboratory for Diagnosis and Treatment of Infectious Diseases, The First Affiliated Hospital, School of Medicine, Zhejiang University, Hangzhou, China

Humans and symbiotic bacteria are interdependent and co-evolved for millions of years. These bacteria communicate with human hosts in the gut in a contact-independent metabolite. Because most intestinal bacteria are non-adhesive, they do not penetrate the mucus layer and are not directly in contact with epithelial cells (ECs). Here, we found that there are adhesive bacteria attached to the Children's terminal ileum. And we compared the immune factors of non-adhesive bacteria in the children ileum with adhesive bacteria as well. Stimulated Th17 cell associated with adherent bacteria in the ileum ECs. SIgA responses are similar to those roles in mouse experiments. Immunohistochemical analysis confirmed that the expression of *SAA1, IL-2, IL-17A, foxp3, RORγt, TGFβ*, and protein increased in Th17 cells. Finally, we used 16S rRNA genes 454 pyrosequencing to analyze the differences in bacterial communities between adhesive and non-adhesive bacteria in the ileum. Ileum with adherent bacteria demonstrated increased mucosa-related bacteria, such as *Clostridium, Ruminococcus, Veillonella, Butyricimonas*, and *Prevotella*. We believe that adhesive bacteria in children's terminal ileum associated with an increased Th17 cell activation and luminal secretory IgA. Adhesive bacteria very closely adhere to terminal ileum of children. They may play important role in human gut immunity and Crohn's disease.

Keywords: Th17 cells, adhesive bacteria, terminal ileum, Crohn's disease, SIgA

OPEN ACCESS

Edited by:
Lixin Zhu,
The Sixth Affiliated Hospital of Sun Yat-sen University, China

Reviewed by:
Sitang Gong,
Guangzhou Medical University, China
Wei Cai,
Xinhua Hospital, China

****Correspondence:***
Mizu Jiang
mizu@zju.edu.cn

Specialty section:
This article was submitted to Gastrointestinal and Hepatic Pharmacology, a section of the journal Frontiers in Pharmacology

Received: *29 July 2020*
Accepted: *07 October 2020*
Published: *30 November 2020*

Citation:
Chen B, Ye D, Luo L, Liu W, Peng K, Shu X, Gu W, Wang X, Xiang C and Jiang M (2020) Adhesive Bacteria in the Terminal Ileum of Children Correlates With Increasing Th17 Cell Activation. Front. Pharmacol. 11:588560. doi: 10.3389/fphar.2020.588560

INTRODUCTION

Trillions of bacteria are present in our bodies (Sender et al., 2016). These bacteria genomes encode a number of genes not naturally existing in the host, regulate host gut gene expression and affect the differentiation and maturation of the host immune system (Mazmanian et al., 2005). The intestinal walls in humans are joined between the luminal contents and the epithelium, and the mucus layer is separated from the gut bacteria in the intestinal epithelial cells (Meddings, 2008). Past research has found that penetrating bacteria in the intestinal mucosa may cause diseases in humans, such as ulcerative colitis (van der Waaij et al., 2005; Caselli et al., 2013; Johansson et al., 2014). The adhesion features of intestinal bacteria are key factors for inducing Th17 cells (Atarashi et al., 2015). One individual-based model demonstrated that hosts select specific bacteria using adhesion (McLoughlin et al., 2016), because adhesion provides a competitive advantage within host-associated communities

(Schluter et al., 2015). However, whether bacteria in intestinal mucosal tissue are both penetrative and adhesive, as well as the effect human gut immunity like SFB induce Th17 cells in mice (Gaboriau-Routhiau et al., 2009; Ivanov et al., 2009), is unknown.

Segmented filamentous bacteria (SFB), or *Candidatus Savagella* (Fernández et al., 2013) in mice are both penetrative and adhesive. A large number of SFB penetrated the villi of wild-type mice during weaning, and induced Th17 cell differentiation and secretory immunoglobulin (SIgA) secretion (Ivanov et al., 2009). SFB enhanced the maturity of the immune system and regulated the immune balance in mice. However, to our knowledge, no study has yet tried to identify that SFB and other bacteria penetrate or adhere to the human ileum. To better understand this issue, we used Scanning Electron Microscopy (SEM) images and observed adhesive bacteria and other mucosa-associated bacteria that penetrate and adhere to the ileum in human. We hypothesized that these bacteria play an important role in human gut immunity, are similar to that of SFB and other adhesive bacteria in mice. We examined Th17 cells associated cytokines *SAA1, IL-17, foxp3, TGFβ, IL-22, RORγt* and host B cells associated cytokine SIgA. To understand the main roles of the mucosa-associated bacteria, we identified the microbiota flora structure non-adhesive and adhesive bacteria of terminal ileum by using 16S rDNA 454 pyrosequencing.

MATERIALS AND METHODS

Subjects

We profiled 106 specimens from the terminal ileum in patients ranging from 6 to 180 months of age by colonic endoscopy because of digestive symptoms such as diarrhea, hematochezia, and abdominal pain. Exclusion criteria: antibiotics used in the last 2 weeks. Recruitment was conducted in the clinic under the protocol approved by the Ethics Committee of Children's Hospital of Zhejiang University School of Medicine. Written informed consent was provided by the parents and from the children as appropriate.

Scanning Electron Microscopy

The terminal ileum biopsies obtained from endoscopy was directly fixed in 4% glutaraldehyde buffer, sample preparation process is described in the documentation (Brandi et al., 1996; Yu et al., 2013). After coating the gold-palladium film (Chen et al., 2018) on the sample, observe the sample at 20 kV under the H-9500 Hitachi SEM microscope.

DNA Extraction 16s rRNA Gene 454 Pyrosequencing

QIAamp DNA Stool mini kit (Qiagen, Germany) was used for DNA extractions according to the instructions, and then PCR amplified with bacterial genomic DNA. NanoDrop ND-2000 (NanoDrop Products, United States) was used to quantify DNA. For each DNA sample, the 16S rRNA gene was amplified using a fusion primer set specific for V3–V5 hypervariable regions (F: 5-′TCCTACGGGAGGCAGCAG-3′ and R: 5′-TGTGCGGGCCCCCGTCAATT-3′) and contained adaptors, key sequences and barcode (Multiple Identifier) sequences as described by the 454 Sequencing System Guidelines for Amplicon Experimental Design (Roche), according to the following protocol: 5 min at 94°C, 27 cycles of 30 s at 94°C, 45 s at 55°C and 1 min at 72°C, followed by a final extension of 7 min at 72°C. The 454 pyrosequencing was determined using the GS FLX+ system and the XL+ chemistry following the manufacturer's recommendations (Roche 454). Further processing was conducted in a data curation pipeline implemented in QIIME 1.7.0 as pick_closed_reference_otus.py (Caporaso et al., 2010). In summary, this pipeline chose OTUs using a reference-based method and constructs from an OTU table. Taxonomy was assigned using the Green genes predefined taxonomy map of the reference sequence OTUs to taxonomy (McDonald et al., 2012; Vazquez-Baeza et al., 2013). The resulting OTU tables were checked for mislabeling (Knights et al., 2011) and contamination, and further microbial community analysis and principal coordinates beta diversity visualizations were created using Emperor (Knights et al., 2011). A mean sequence depth of 19,914 sequences per sample was obtained, and samples with fewer than 3,000 filtered sequences were excluded from analysis. Alpha- and beta-diversity were calculated using QIIME 1.6.0 (Caporaso et al., 2010), and PcoA plots were produced using Emperor (http://qiime.org/emperor).

Immunohistochemistry

Biopsy specimens were cut at 5 μm and fixed in 4% paraformaldehyde overnight. For the staining process, tissues were cryoprotected with 30% sucrose in PBS overnight. Two unacquainted pathologists, Weizhong Gu and Xiaojun Wang, who are blinded to score evaluated the results of immunohistochemical staining. Only nuclear staining was considered positive. The scoring rules are as follows: 0 (no detectable staining); 1 (25% positive cells); 2 (25–49% positive cells); 3 (50–74% positive cells); and 4 (75% positive cells). The densities of IL-22, IL-17, foxp3, TGFβ, IL-22, and RORγt positive cells in the surface epithelium and lamina propria were determined by numbers of stained cells per mm^2 of lamina propria. All data were expressed as mean ± SD (standard deviation) using SPSS 20.0.

Enzyme Linked Immunosorbent Assay

Measure the total concentration of the fluid in the SIgA chamber, centrifuge approximately 500 μl of sample for 1,000 min at 1,000 × g at 4°C. The sample was diluted 1/10 and serially diluted two times. Human immunoglobulin IgA ELISA kit (Elabscience, China) was used to quantify total SIgA according to the manufacturer's instructions (Chen et al., 2018).

RNA Extraction and Gene Expression Analysis

Total RNA was extracted from Biopsy specimens of the terminal ileum using Trizol reagent (Life Technologies, United States) and purified using RNeasy mini Kit (Qiagen, Germany).

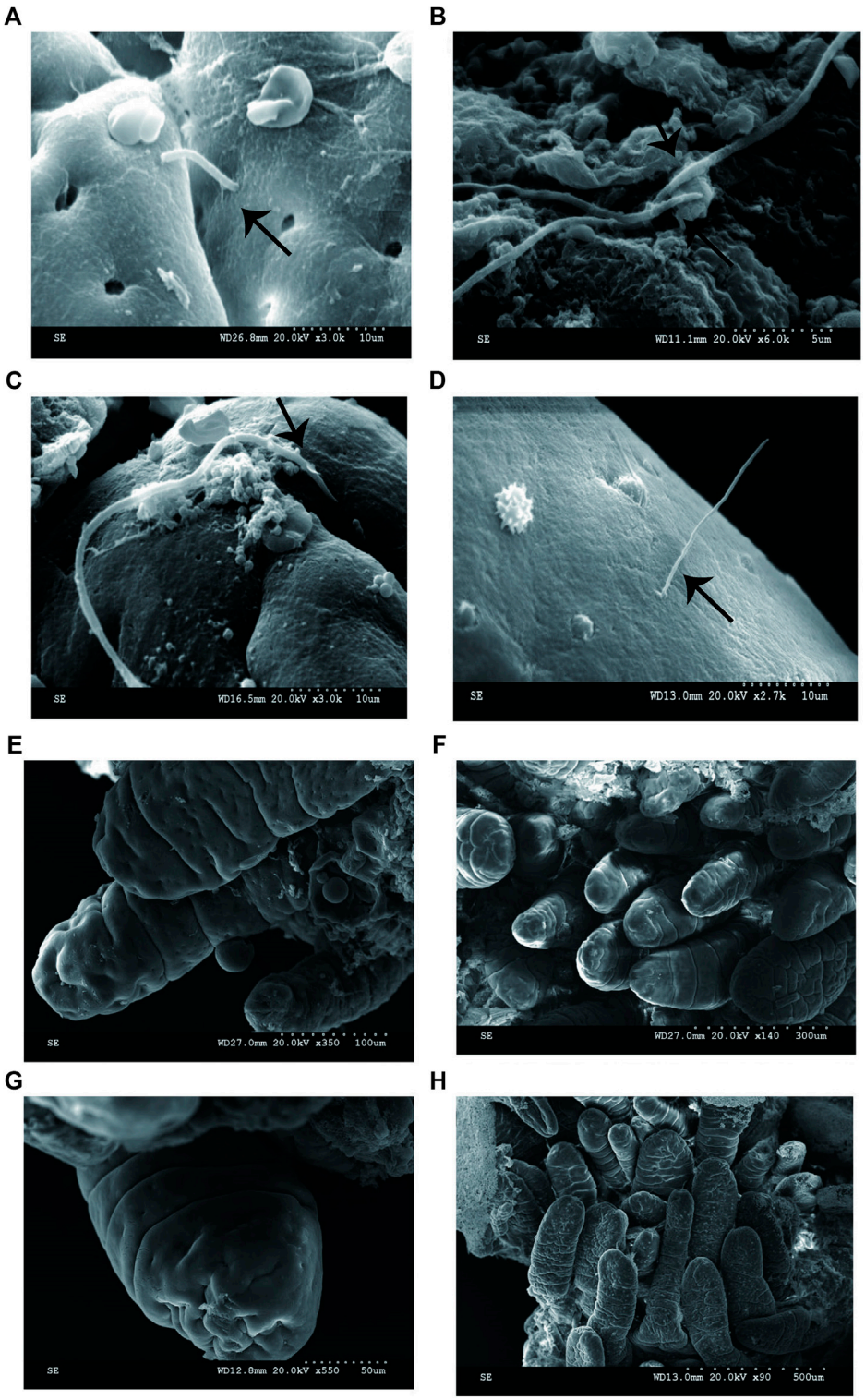

FIGURE 1 | SEM micrographs of human ileal biopsies. The specimens were processed for the observation of microbiota by SEM and as described in Methods. **(A)** SFB-like bacteria inserted and attached tightly to epithelial cell in the terminal ilea by penetrating mucous layer. Sample ID 12,×3000; **(B)** SFB-like bacteria adhered to the ileal mucosa ×6000; **(C)** SFB-like bacteria adhered tightly to the epithelial cell of villi, ×3000; **(D)** SFB-like bacteria superficially penetrated the epithelium of the villi of ilea with both ends outside, ×2700; and **(E–H)** Non-adhesive bacteria observed in the villous epithelium.

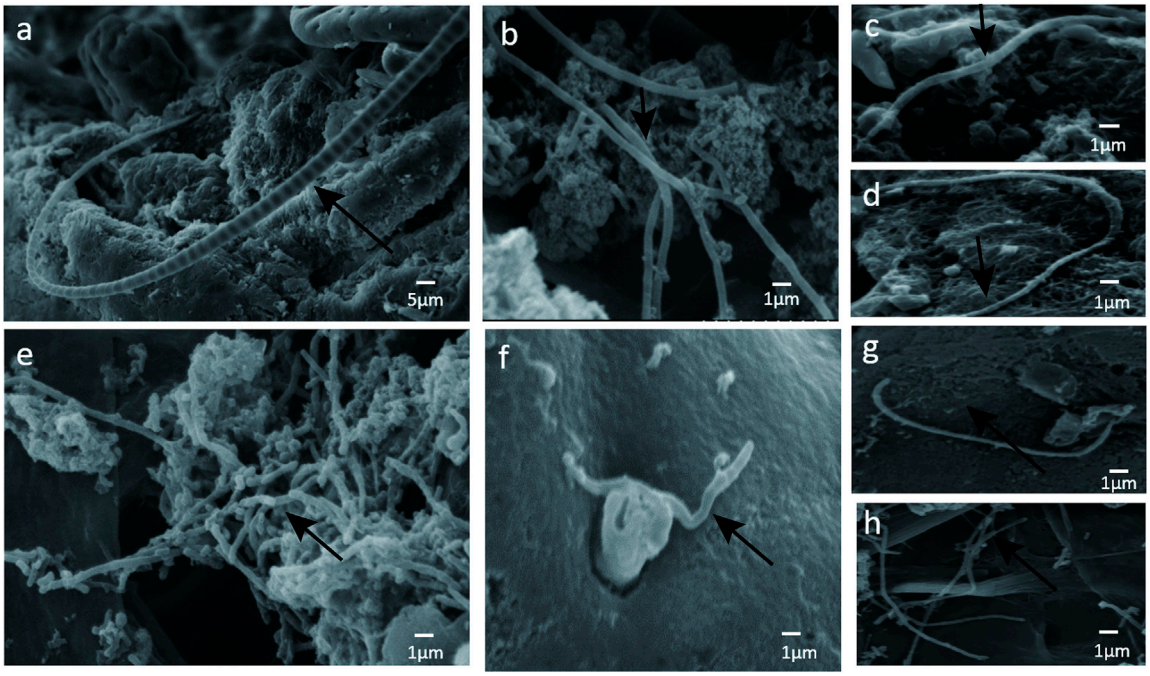

FIGURE 2 | (A) SFB-like bacteria attached to epithelial cell in the terminal ilea. Sample ID 12, ×600; **(B –H)** numerous adhesive bacteria observed in the ileal mucosa and epithelial cell ×2500.

The amount of gene expression was determined by real-time fluorescent quantitative PCR. RNA was purified from intestinal tissues and qRT-PCR was performed using TaqMan gene expression detection, TaqMan universal PCR master mix (Applied Biosystems) or human-specific primers using SYBR-Green PCR master mix (Applied Biosystems). IL-22 was generated, RORγt IL-17, foxp3 TGFβ, and SAA1 primer sequences were added to the S1 shown in the table. The endogenous control gene is beta actin. Repeated DNA sample assays, each sample normalized to related gene expression and 2-ΔCtβ-actin calculations. The two-tailed *t*-test of unpaired students was statistically significant unless otherwise stated. The *p* value is shown in the graph and the table, and the bar indicates SD (standard deviation). To compare the differences in SIgA levels between adhesive and non-adhesive flora, a non-linear fit curve was introduced into the data using GraphPad Prism 6 (Chen et al., 2018).

TABLE 1 | Age distribution of children with adhesive bacteria on their ileum.

Age (months)	Gender (F/M)	Adhesive bacteria (%)	Adhesive bacteria/total samples
2–10	8/9	5.89	1/17
11–36	16/18	35.29	12/34
37–72	9/10	5.26	1/19
73–108	9/9	0	0/18
109–180	8/10	0	0/18
Total	50/56	13.20	14/106

RESULTS

The Adhesive Bacteria That Penetrate and Adhere to Pediatric Ileum Were Age-Dependent

To determine if the bacteria penetrated and adhered to small intestinal mucosal tissue, we used SEM images to visualize adhesive bacteria on the surfaces of 14 ileum mucosal biopsy specimens (**Figures 1A–D**, **2**). These bacteria showed that the adhesion in the ileal mucosa was similar to SFB adhesive to ECs in mice. However, most ileum villi were without adhesive bacteria (**Figures 1E–H**). van der Waaij also did not observe direct contact between bacterial and epithelial cells in adults with normal ileum mucosa (van der Waaij et al., 2005). Among the 14 samples with collected adhesive bacteria, 12 samples were found in the ileum of children 11–36 months. As shown in **Table 1**, 35.29% of ileum samples collected from children under 11–36 months of age had observable adhesive bacteria on the ileal villi. These results suggested that adhesive and adhesive bacteria penetrated and adhered to 11–36 months pediatric ileum (shortly after weaning).

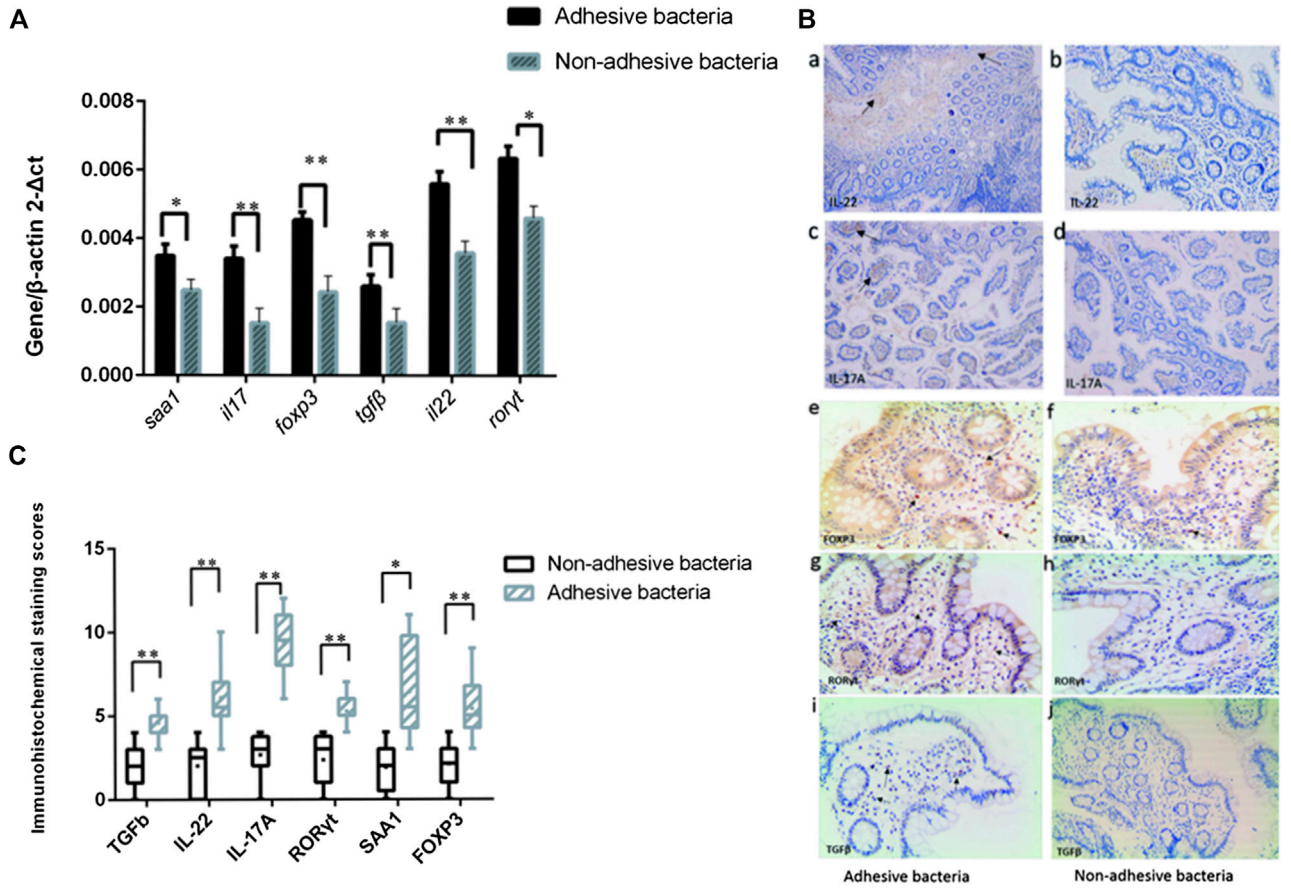

FIGURE 3 | Induction of Th17 cell genes related to the presence of adhesive bacteria. **(A)** qRT-PCR analysis of Th17 cell genes related to the presence of adhesive bacteria. Data are expressed as means (n = 28) and standard deviations. P-values are calculated using the Student's t-test. qRT-PCR was performed as described in the Methods section of this paper. **(B) (a–j)** Photographs of the immunohistochemistry in adhesion bacteria and non-adhesion bacteria, IL22, IL17, Foxp3, and RORγt,TGFβ (brown). **(C)** A total score (ranging from 1-25) was obtained by multiplying the staining intensity score (1-5) in the terminal ileum epithelial cells with the positive fraction score (1-5). The densities of IL-22, IL-17, foxp3, TGFβ, IL-22, and RORγt positive cells in the lamina propria and in the surface epithelium were determined by counting the number of stained cells per mm^2 of lamina propria with adhesive bacteria and non-adhesive bacteria.

The Presence of Adhesive Bacteria Correlated With Induced Th17-Mediated Immune Response Programs in Pediatric Ileum

Since SFB and adhesive bacteria play key roles in the induction of Th17 cells (Gaboriau-Routhiau et al., 2009; Ivanov et al., 2009). We next examined the influence of adhesive bacteria compared with non-adhesive bacteria in ileum EC immunity gene expression profiles using real-time PCR and immunohistochemical staining (**Figure 3**). We measured the mRNA *SAA1, IL-17, foxp3, TGFβ, IL-22, RORγt* in 32 of the biopsied samples. qRT-PCR data were expressed as the mean ± SD ($n = 32$). p Values were calculated using the Student's t-test. The upregulated transcripts, including the Th17 cell effector cytokines, exhibited increased transcripts SAA1 (a member of the SAA family), interleukin IL-17 and interleukin IL-22 in ileal mucosa with adhesive bacteria (**Figure 3**). An abundance of SAA1 in adhesive bacteria samples suggested that SAA induction required bacteria adhesion to epithelial cells (ECs). The Th17 cell effector cytokines, such as IL-22 and IL-17, which were required for Th17 cell function, were considered to guard against infections with *Salmonella* and *Citrobacter rodentium* (Atarashi et al., 2015). We next found that the Th17 cell specific transcription regulatory factors, *RORγt* (retinoic acid-related orphan receptor family), Treg specific transcription factors, *F*oxp3 (Fork head box P3), TGFβ (transforming growth factor β) are upregulated in ileum with adhesive bacteria.

These upregulated immunity gene expressions showed that, as in mice, many samples had adhesive microbes that adhered to epithelial cells, and the qRT-PCR of the total ileal tissue exhibited increased amounts of genes participating in T cell differentiation and responses in the adherence bacteria samples.

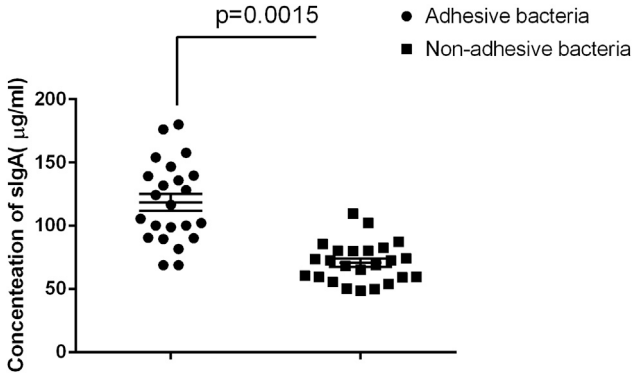

FIGURE 4 | Comparison of SIgA in luminal fluids collected from the adhesive and non-adhesive ileum (n = 12 vs 20). Approximately 500 μl of luminal fluids from each patient were used for the measurement of SIgA as previously described. The supernatants were assayed for total secretory IgA using ELISA with a Human Secretory IgA ELISA Detection Kit as previously described. The SIgA was expressed as μg/ml of fecal materials. Statistical analysis and boxed-plot was performed with the Student's *t-test* using the Graph Pad Prism 6.

The Presence of Adhesive Bacteria Activating SIgA Secretions in the Human Ileum

Secretory immunoglobulin is an important component of the epithelial barrier because it maintains host intestinal homeostasis (Peterson et al., 2007; Derebe et al., 2014). Many bacteria in the gut are covered by SIgA, and certain adhesive species, such as helicobacter spp. and SFB, are particularly heavily covered by SIgA (Palm et al., 2014). We also quantified SIgA concentrations in intestinal fluids using ELISA age-matched individuals. The results showed that adhesive bacteria ileum fluid had an abundance of SIgA 105.8 μg/ml ± 10.25 μg/ml (mean ± SD, n = 12) compared to that of the non-adhesive bacteria ileum fluid 68.53 μg/ml ± 7.24 μg/ml (mean ± SD, n = 20) ($p < 0.001$, **Figure 4**). This indicated that the host secrete more SIgA to maintain intestinal homeostasis.

The Difference of Microbiota in the Ileum With Adhesive Bacteria and Non-Adhesive Bacteria

A supervised analysis of the 16S rRNA gene sequencing data with LDA effect size compared the bacterial community structure in the ileum with adhesive bacteria to the ileum with non-adhesive bacteria by using an LDA threshold score of 4 ($n \geq 5$). Adhesive bacteria ileum samples increased the mucosa-associated bacteria *Clostridium, Veillonella, Ruminococcus, Butyricimonas* and *Prevotella,* and decreased *Escherichia, Fusobacterium, Klebsiella, Bacteroides* (**Figure 5A**). An unweighted UniFrac-based was used to compare the adhesive microbiota and non-adhesive microbiota from pediatric ileum (**Figure 5B**). The PCoA analysis indicated that the overall diversity in the adhesive microbial composition had greater differences in the samples with non-adhesive microbiota (**Table 2**). qRT-PCR data were confirmed these findings (**Table 3**).

DISCUSSION

The ileum epithelial cells and the mucus layer usually separate from the bacteria in the small intestinal. Also, small intestinal bacteria usually cannot penetrate the mucosal layer (van der Waaij et al., 2005), and some bacteria avoid it, such as SFB and pathogenic invasive bacteria. The bacteria had direct contact with the colonic epithelial cells and showed significant associations with ulcerative colitis in humans and mice (Caselli et al., 2013; Johansson et al., 2014). We hypothesized that adhesive and adhesive bacteria also have immunostimulatory and gut immune system maturation roles in humans like that in mice.

Commensal Bacteria Typically Living in Luminal Fluid and Avoid Direct

Contact with epithelial cells in the human terminal ileum. Atarashi et al. (2015) found that the adhesion of microbes such as *Citrobacter rodentium, Escherichia coli* O157, and 20 bacterial strains from human feces induced Th17 cells in mouse models, are similar to the SFB's role in the maturation of the host gut immune system (Goto et al., 2014; Lee and Cua, 2014; Schnupf et al., 2015). Based on the individual model which is a hybrid between an individual based model of microbes and a continuum model of solutes (McLoughlin et al., 2016), the results indicated that the host-mediated adhesion increased the competitive advantage of microbes and created a rendezvous for ecological species with slow growth rates (Schnupf et al., 2015). Positive selection through the adhesive can be converted into the negative if the host secreted large amounts of mucus in the matrix. Therefore, the penetration and adhesion bacteria in the human ileum should be studied to understand the impact on the development of the human immune system. Considering that the tight attachment of SFB or other adhesive bacteria, the results showed that host released serum amyloid A (SAA). SAA1 was induced by SFB in the terminal ileum of germ-free (GF) mice. SAA1 induced Th17 cell differentiation in a concentration-dependent manner *in vitro* (Curtiss et al., 2009; Schnupf et al., 2015).

We also investigated whether adhesion was another potential mechanism of the host positive selective. Our findings suggested that microorganisms on the surface of intestinal epithelial cells used adhesion to correlate with immune responses (Schluter et al., 2015).

Our results showed that Th17 cells in the lamina propria were correlated with adhesive microbiota in the human gut. We also observed similar effects in Th17 cells differentiation in mice monocolonized with SFB (Gaboriau-Routhiau et al., 2009; Ivanov et al., 2009). Signals from adhesive bacteria provide a secondary effect, such as the polarization reaction of T helper cells of the Th17 extraction without tissue damage in cases of intestinal immune suppression. Attached SFB stimulated the development of a subset of T helper cells (Faith et al., 2013). Similarly, in that study *Clostridium*

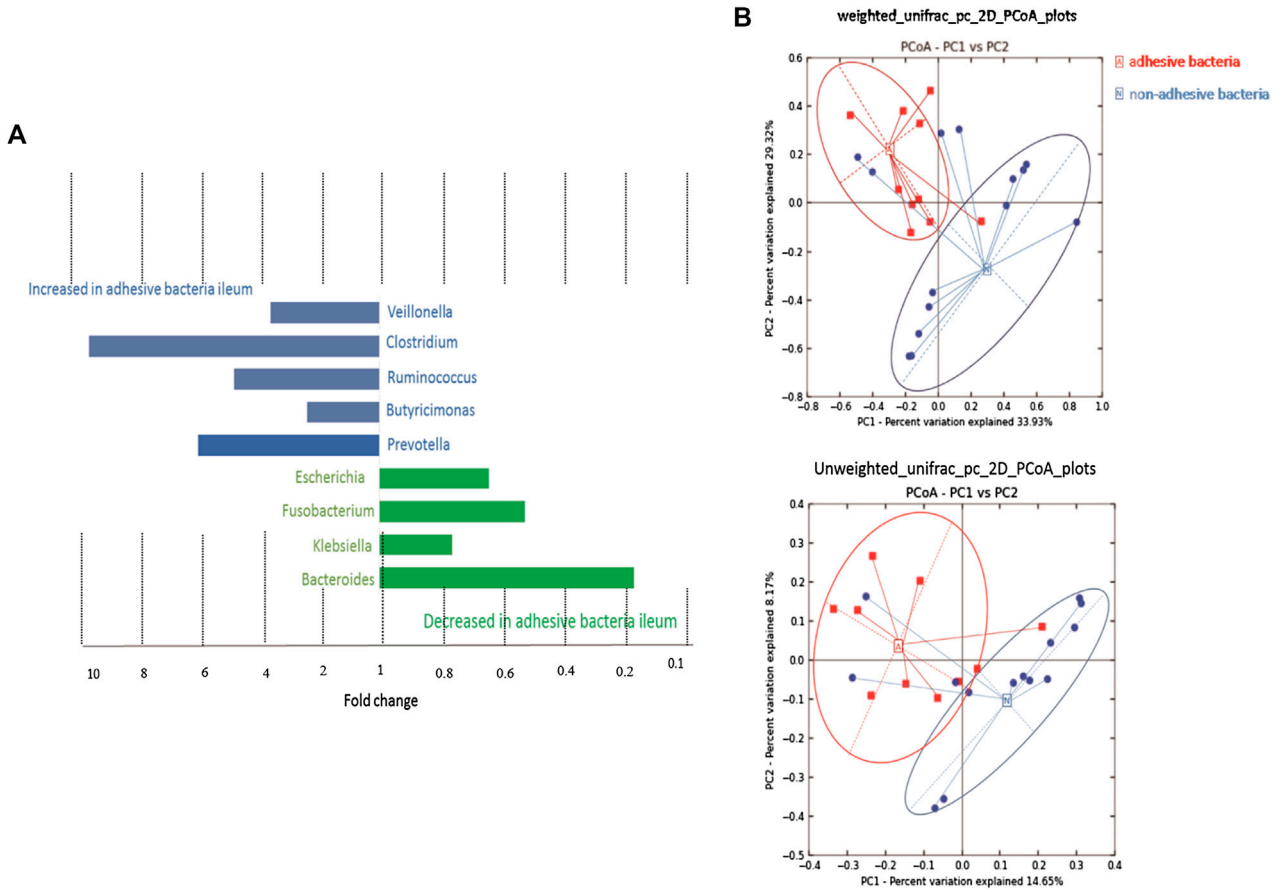

FIGURE 5 | 16s rRNA gene 454 pyrosequencing analysis of the gut microbiota. Approximately 500 μg of gut contents from 24 patients were used for the extraction of genomic DNA. Approximately 2 μg of genomic DNA from each patient was used for de novo sequencing and the principal coordinate analysis (PCoA) of the genus profile. The top four genera as the main contributors were determined and plotted by their loadings in these two components. **(A)** Differences in abundance are shown for the taxonomic biomarkers that were detected using a multivariate statistical approach. The fold change for each taxon was calculated by dividing the mean abundance in the cases by that of the controls. Several taxonomic biomarkers measured at both the ileal and the rectal sites were found to be significantly correlated with the adhesive bacteria. **(B)** A set of principal coordinate plots of the unweighted UniFrac distance. PC1, PC2, and PC3 represented the top three principal coordinates that captured most of the diversity, with a fraction of diversity captured by the coordinate, shown as a percent.

also induced regulatory T cells, but the population of many species was more effective than a single isolated or a combination of several species by the reaction of the regulatory T cells. As a result, many other beneficial microbes promoted stable long-term co-existence within the immune system.

Through localized, immune-facilitated and adherence-dependent interactions, the diverse community of microbial symbionts distribution had spatial-temporal heterogeneity in human intestines (Donaldson et al., 2016). The 16S gene rRNA sequencing study of the colonic crypt microbiome demonstrated that the intestinal crypt community included many aerobic bacteria and had a distinct profile relative to the luminal bacteria (Pedron et al., 2012). The human small intestine exhibited lower microbiota diversity than in the colon, and was

TABLE 2 | Comparison of phylotype coverage and diversity estimation of the 16S rRNA gene libraries at 3% dissimilarity from the pyrosequencing analysis.

Group	Reads	OTUs[a]	Good's[b]	ACE	95% CI		Chao1	95% CI		Shannon[c]
Non-adhesive bacteria	88,485	2,968	0.978	78,488	76,558.6	77,654.5	52,565.4	50,124.8	55,455.8	3.237
Adhesive bacteria	78,458	2,645	0.972	69,484	67,895.8	68,892.4	48,998.5	48,235.6	49,878.1	2.686

[a]*The operational taxonomic units (OTUs) were defined with 3% dissimilarity level.*
[b]*The coverage percentage (Goods), richness estimators (ACE and Chao1) and diversity indices (Shannon) were calculated using Good's method in the mothur program, respectively.*
[c]*The Shannon index of evenness was calculated with formula E = H/ln(S), where H is the Shannon diversity index and S is the total number of sequences in that group.*

TABLE 3 | Primers used in this study.

Gene name	Primer sequence
FOXP3 F/R	5′-ATCCGCCACAACCTGAGTCT-3′/5′-TCCACACAGCCCCCTTCTC-3′
IL-17 F/R	5′-TCCTAGGGCCTGGCTTCTG-3′/5′-AGTTCGTTCTGCCCCATCAG-3′
SAA1	5′-GCTGATCAGGCTGCCAATG-3′/5′-GCCAGCAGGTCGGAAGTG-3′
TGFβ	5′-GCTGAGCGCTTTTCTGATCCT-3′/5′-CGAGTGTGCTGCAGGTAGACA-3′
IL-22	5′-CCCCACTGGGACACTTTCTA-3′/5′-TGGCCCTTTAGGTACTGTGG-3′
RORγt	5′-TGAGAAGGACAGGGAGCCAA-3′/5′-CCACAGATTTTGCAAGGGA3′
Clostridium	CloI-F: TACCHRAGGAGGAAGCCAC CloI-R: GTTCTTCCTAATCTCTACGCAT
Ruminococcus	F: 5′-AGAGTTTGATCMTGGCTCAG-3′ R: 5′-ACGGCTACCTTGTTACGACTT-3′
Veillonella	5′-CAGAAGCAGGTTCCCGTAACTC-3′ 5′-GCCTACCGCAAGTGGCAATA-3′
Butyricimonas	Buty1f;5′-GGTGAGTAACACGTGTGCAAC-3′ Buty1r;5′-TACCCCGCCAACTACCTAATG-3′
Prevotella	303F: 5′-GAAGGTCCCCCACATTG-3′ 708R: 5′-CAATCGGAGTTCTTCGTG-3′
Bacteroides	F: 5′-CGTCCATTAGGCAGTTGGT-3′ R: 5′-CGTAGGAGTTTGGACCGTG-3′
Klebsiella	F: 5′-GACGATCCCTAGCTGGTCTG-3′ R: 5′-GTGCAATATTCCCCACTGCT-3′
E. coli	F: 5′-AATGATACGGCGACCACCGAGATCT-3′ R: 5′-CAAGCAGAAGACGGCATACGAGAT-3′
Fusobacterium	F: 5′CAACCATTACTTTAACTCTACCATGTTCA-3′ R: 5′GTTGACTTTACAGAAGGAGATTATGTAAAAATC-3′

enriched by certain *Clostridium* spp. members (Palm et al., 2014). In mice, *Proteobacteria* and members of the family *Lactobacillaceae* are enriched in the small intestinal (Lee and Cua, 2014).

Intestinal epithelial cells serve as a physical barrier between microbes and the host's body, and mediate mucous immune responses through the direct perception of microbiota immune responses (Goto et al., 2014), including adaptive immune responses such as SIgA (Peterson et al., 2007; Hapfelmeier et al., 2010), and influence the establishment of the microbiota. The immune system selects appropriate microbiota by innate and adaptive mechanisms, such as SIgA (Caselli et al., 2013). In monoclonization SFB mice model, the numbers of SFB in the terminal ileum changed in an age-dependent manner and was particularly influenced by the IgA concentration in maternal milk during the sucking period and in the luminal content produced by the pups after weaning (Jiang et al., 2001). In this study, we also find the adhesive bacteria increased after weaning. These results show that IgA from maternal milk may regulate the composition of adhesive bacteria in the children ileum.

We propose a model where adhesive bacteria strongly colonize on the small intestines since adhesion permits bacteria to resist displacement by others, and non-adhesive bacteria are more likely to be pushed away from the epithelial cells surface. So long as adhesive bacteria grow on the mucosa layer, the adhesive strain will be dominant. Therefore, adhesion may be a bacterial strategy for colonization in the gut and model (Guzman et al., 1997; Grubb et al., 2009; Nowrouzian et al., 2007).

Few studies addressed the role of immunomodulation by non-pathogens, an aspect that requires these bacteria to have access to the tissue. Based on our observations, we found that the host provided limited space to specific bacteria and that the immune system only allowed adhesive bacteria to access these locations. A particular species close to epithelial cells created a protected microbials despite the rapidly changing conditions in the small intestinal lumen. For example, SFB are members of the symbiotic microbes that penetrate the villi during weaning in wild-type mice.

We showed that adhesive bacteria such as adhesive bacteria in human ileum were special because they were adhesive to the ileal mucosa, are similar to SFB in mice. This behavior resembled that of pathogens and was in contrast with that of most other commensals, which instead remained on the mucus. Adhesive microorganisms have striking characteristic in terms of their morphologies and close proximities to the gut wall. Anchorage into host cells is thought to be necessary for adhesive bacteria to obtain nutrients indispensable for growth but also to induce signals that stimulate the post-natal development of the gut immune system. The findings of these Adhesive and adhesion bacteria in humans are valuable to study their effects on the immune system and human health.

CONCLUSION

Adhesive bacteria typically penetrated and adhered to pediatric ileum induced the Th17 cells in the ileum ECs, and triggered SIgA responses. Adhesive bacteria ileum samples exhibited increased amounts of mucosa-associated bacteria, such as *Clostridium, Veillonella, Ruminococcus, Butyricimonas*, and *Prevotella.*

DATA AVAILABILITY STATEMENT

The datasets of the 16S rRNA gene 454 pyrosequencing were available in the NCBI. The accession number was PRJNA343381.

TABLE 4 | Real time PCR results for human intestinal lavage fluid samples.[a]

Sample	*Bacteroides*	*Klebsiella*	*Clostridium*	*E. coli*	*Prevotella*	*Butyricimonas*	*Veillonella*	*Ruminococcus*	*Fusobacterium*
Adhesive bacteria	12.4[a]	11.64[a]	10.7[a]	11.88[a]	12.09[a]	10.65[a]	11.00[a]	11.22[a]	11.02[a]
Non-adhesive bacteria	13.1[a]	12.03[a]	9.74[a]	12.20[a]	11.28[a]	10.29[a]	10.24[a]	10.56[a]	11.52[a]

[a]*Represents log10 bacteria 16S rRNA gene for each ml of liquid. All data repeated three times.*

ETHICS STATEMENT

The studies involving human participants were reviewed and approved by Ethics Committee of Children's Hospital of Zhejiang University School of Medicine. Written informed consent to participate in this study was provided by the participants' legal guardian/next of kin.

AUTHOR CONTRIBUTIONS

Study concept, designs and obtained funding (MJ). Drafting of the manuscript, acquisition of data and statistical analysis (BC). Analysis and interpretation of data (BC, LL, DY). Critical revision of the manuscript for important intellectual content (CX, XS). Colonoscopy and clinical data collection (KP, XW, WG).

FUNDING

The Scientific Research Fund of National Health and the Family Planning Commission-Major Science and Technology Project of the Zhejiang Province Medical and Health (WKJ-ZJ-1622).

ACKNOWLEDGMENTS

We thank LetPub (www.letpub.com) for its linguistic assistance during the preparation of this manuscript.

REFERENCES

Atarashi, K., Tanoue, T., Ando, M., Kamada, N., Nagano, Y., Narushima, S., et al. (2015). Th17 cell induction by adhesion of microbes to intestinal epithelial cells. *Cell* 163, 367–380. doi:10.1016/j.cell.2015.08.058

Brandi, G., Pisi, A., Biasco, G., Miglioli, M., Biavati, B., and Barbara, L. (1996). Bacteria in biopsies of human hypochloridric stomach: a scanning electron microscopy study. *Ultrastruct. Pathol.* 20, 203–209. doi:10.3109/01913129609016316

Caporaso, J. G., Kuczynski, J., Stombaugh, J., Bittinger, K., Bushman, F. D., Costello, E. K., et al. (2010). QIIME allows analysis of high-throughput community sequencing data. *Nat. Methods* 7, 335–336. doi:10.1038/nmeth.f.303

Caselli, M., Tosini, D., Gafà, R., Gasbarrini, A., and Lanza, G. (2013). Segmented filamentous bacteria-like organisms in histological slides of ileo-cecal valves in patients with ulcerative colitis. *Am. J. Gastroenterol.* 108, 860–861. doi:10.1038/ajg.2013.61

Chen, B., Chen, H., Shu, X., Yin, Y., Li, J., Qin, J., et al. (2018). Presence of segmented filamentous bacteria in human children and its potential role in the modulation of human gut immunity. *Front. Microbiol.* 9, 1403. doi:10.3389/fmicb.2018.01403

Curtiss, R., 3rd, Wanda, S.-Y., Gunn, B. M., Zhang, X., Tinge, S. A., Ananthnarayan, V., et al. (2009). *Salmonella enterica* serovar typhimurium strains with regulated delayed attenuation *in vivo*. *Infect. Immun.* 77, 1071–1082. doi:10.1128/iai.00693-08

Derebe, M. G., Zlatkov, C. M., Gattu, S., Ruhn, K. A., Vaishnava, S., Diehl, G. E., et al. (2014). Serum amyloid A is a retinol binding protein that transports retinol during bacterial infection. *eLife* 3, e03206. doi:10.7554/elife.03206

Donaldson, G. P., Lee, S. M., and Mazmanian, S. K. (2016). Gut biogeography of the bacterial microbiota. *Nat. Rev. Microbiol.* 14 (1), 20–32. doi:10.1038/nrmicro3552

Faith, J. J., Guruge, J. L., Charbonneau, M., Subramanian, S., Seedorf, H., Goodman, A. L., et al. (2013). The long-term stability of the human gut microbiota. *Science* 341, 1237439. doi:10.1126/science.1237439

Fernández, L., Langa, S., Martín, V., Maldonado, A., Jiménez, E., Martín, R., et al. (2013). The human milk microbiota: origin and potential roles in health and disease. *Pharmacol. Res.* 69, 1–10. doi:10.1016/j.phrs.2012.09.001.

Gaboriau-Routhiau, V., Rakotobe, S., Lécuyer, E., Mulder, I., Lan, A., Bridonneau, C., et al. (2009). The key role of segmented filamentous bacteria in the coordinated maturation of gut helper T cell responses. *Immunity* 31, 677–689. doi:10.1016/j.immuni.2009.08.020

Goto, Y., Panea, C., Nakato, G., Cebula, A., Lee, C., Diez, M. G., et al. (2014). Segmented filamentous bacteria antigens presented by intestinal dendritic cells drive mucosal Th17 cell differentiation. *Immunity* 40, 594–607. doi:10.1016/j.immuni.2014.03.005

Grubb, S. E. W., Murdoch, C., Sudbery, P. E., Saville, S. P., Lopez-Ribot, J. L., and Thornhill, M. H. (2009). Adhesion of *Candida albicans* to endothelial cells under physiological conditions of flow. *Infect. Immun.* 77, 3872–3878. doi:10.1128/iai.00518-09

Guzman, C. A., Biavasco, F., and Pruzzo, C. (1997). News & notes: adhesiveness of *Bacteroides fragilis* strains isolated from feces of healthy donors, abscesses, and blood. *Curr. Microbiol.* 34, 332–334. doi:10.1007/s002849900191

Hapfelmeier, S., Lawson, M. A. E., Slack, E., Kirundi, J. K., Stoel, M., Heikenwalder, M., et al. (2010). Reversible microbial colonization of germ-free mice reveals the dynamics of IgA immune responses. *Science* 328, 1705–1709. doi:10.1126/science.1188454

Ivanov, I. I., Atarashi, K., Manel, N., Brodie, E. L., Shima, T., Karaoz, U., et al. (2009). Induction of intestinal Th17 cells by segmented filamentous bacteria. *Cell* 139, 485–498. doi:10.1016/j.cell.2009.09.033

Jiang, H.-Q., Bos, N. A., and Cebra, J. J. (2001). Timing, localization, and persistence of colonization by segmented filamentous bacteria in the neonatal mouse gut depend on immune status of mothers and pups. *Infect. Immun.* 69, 3611–3617. doi:10.1128/iai.69.6.3611-3617.2001

Johansson, M. E. V., Gustafsson, J. K., Holmén-Larsson, J., Jabbar, K. S., Xia, L., Xu, H., et al. (2014). Bacteria penetrate the normally impenetrable inner colon mucus layer in both murine colitis models and patients with ulcerative colitis. *Gut* 63, 281–291. doi:10.1136/gutjnl-2012-303207

Knights, D., Kuczynski, J., Koren, O., Ley, R. E., Field, D., Knight, R., et al. (2011). Supervised classification of microbiota mitigates mislabeling errors. *ISME J.* 5, 570–573. doi:10.1038/ismej.2010.148

Lee, J. S., and Cua, D. J. (2014). The emerging landscape of RORγt biology. *Immunity* 40, 451–452. doi:10.1016/j.immuni.2014.04.005

Mazmanian, S. K., Liu, C. H., Tzianabos, A. O., and Kasper, D. L. (2005). An immunomodulatory molecule of symbiotic bacteria directs maturation of the host immune system. *Cell* 122, 107–118. doi:10.1016/j.cell.2005.05.007

McDonald, D., Price, M. N., Goodrich, J., Nawrocki, E. P., DeSantis, T. Z., Probst, A., et al. (2012). An improved Greengenes taxonomy with explicit ranks for ecological and evolutionary analyses of bacteria and archaea. *ISME J.* 6, 610–618. doi:10.1038/ismej.2011.139

McLoughlin, K., Schluter, J., Rakoff-Nahoum, S., Smith, A. L., and Foster, K. R. (2016). Host selection of microbiota via differential adhesion. *Cell Host Microbe* 19, 550–559. doi:10.1016/j.chom.2016.02.021.

Meddings, J. (2008). The significance of the gut barrier in disease. *Gut* 57, 438–440. doi:10.1136/gut.2007.143172

Nowrouzian, F. L., Friman, V., Adlerberth, I., and Wold, A. E. (2007). Reduced phase switch capacity and functional adhesin expression of type 1-fimbriated *Escherichia coli* from immunoglobulin A-deficient individuals. *Infect. Immun.* 75, 932–940. doi:10.1128/iai.00736-06

Palm, N. W., Zoete, M. R., Cullen, T. W., Barry, N. A., Stefanowski, J., Hao, L., et al. (2014). Immunoglobulin A coating identifies colitogenic bacteria in inflammatory bowel disease. *Cell* 158, 1000–1010. doi:10.1016/j.cell.2014.08.006

Pedron, T., Mulet, C., Dauga, C., Frangeul, L., Chervaux, C., Grompone, G., et al. (2012). A crypt-specific core microbiota resides in the mouse colon. *mBio* 3. doi:10.1128/mbio.00116-12

Peterson, D. A., McNulty, N. P., Guruge, J. L., and Gordon, J. I. (2007). IgA response to symbiotic bacteria as a mediator of gut homeostasis. *Cell Host Microbe* 2, 328–339. doi:10.1016/j.chom.2007.09.013.

Schluter, J., Nadell, C. D., Bassler, B. L., and Foster, K. R. (2015). Adhesion as a weapon in microbial competition. *ISME J.* 9, 139–149. doi:10.1038/ismej.2014.174

Schnupf, P., Gaboriau-Routhiau, V., Gros, M., Friedman, R., Moya-Nilges, M., Nigro, G., et al. (2015). Growth and host interaction of mouse segmented filamentous bacteria *in vitro*. *Nature* 520, 99–103. doi:10.1038/nature14027

Sender, R., Fuchs, S., and Milo, R. (2016). Are we really vastly outnumbered? Revisiting the ratio of bacterial to host cells in humans. *Cell* 164, 337–340. doi:10.1016/j.cell.2016.01.013

van der Waaij, L. A., Harmsen, H. J. M., Madjipour, M., Kroese, F. G. M., Zwiers, M., van Dullemen, H. M., et al. (2005). Bacterial population analysis of human colon and terminal ileum biopsies with 16S rRNA-based fluorescent probes: commensal bacteria live in suspension and have no direct contact with epithelial cells. *Inflamm. Bowel Dis.* 11, 865–871. doi:10.1097/01.mib.0000179212.80778.d3

Vazquez-Baeza, Y., Pirrung, M., Gonzalez, A., and Knight, R. (2013). EMPeror: a tool for visualizing high-throughput microbial community data. *GigaScience* 2, 16. doi:10.1186/2047-217x-2-16

Yu, Z.-T., Chen, C., and Newburg, D. S. (2013). Utilization of major fucosylated and sialylated human milk oligosaccharides by isolated human gut microbes. *Glycobiology* 23, 1281–1292. doi:10.1093/glycob/cwt065

Conflict of Interest: The authors declare that the research was conducted in the absence of any commercial or financial relationships that could be construed as a potential conflict of interest.

frontiers in Pharmacology

ORIGINAL RESEARCH
published: 18 January 2021
doi: 10.3389/fphar.2020.620724

Gut Microbiota and Related Metabolites Were Disturbed in Ulcerative Colitis and Partly Restored After Mesalamine Treatment

Liang Dai[1†], *Yingjue Tang*[1†], *Wenjun Zhou*[1], *Yanqi Dang*[1], *Qiaoli Sun*[1], *Zhipeng Tang*[1], *Mingzhe Zhu*[1,2*] *and Guang Ji*[1*]

[1]*Institute of Digestive Diseases, China-Canada Center of Research for Digestive Diseases (ccCRDD), Longhua Hospital, Shanghai University of Traditional Chinese Medicine, Shanghai, China,* [2]*School of Public Health, Shanghai University of Traditional Chinese Medicine, Shanghai, China*

OPEN ACCESS

Edited by:
Ruixin Zhu,
Tongji University, China

Reviewed by:
Hao Wu,
Zhongshan Hospital, Fudan University, China
Luqing Zhao,
Beijing Hospital of Traditional Chinese Medicine, Capital Medical University, China

***Correspondence:**
Mingzhe Zhu
zhumingzhe@sibs.ac.cn
Guang Ji
jiliver@vip.sina.com

[†]*These authors have contributed equally to this work*

Specialty section:
This article was submitted to Gastrointestinal and Hepatic Pharmacology, a section of the journal Frontiers in Pharmacology

Received: *23 October 2020*
Accepted: *14 December 2020*
Published: *18 January 2021*

Citation:
Dai L, Tang Y, Zhou W, Dang Y, Sun Q, Tang Z, Zhu M and Ji G (2021) Gut Microbiota and Related Metabolites Were Disturbed in Ulcerative Colitis and Partly Restored After Mesalamine Treatment. Front. Pharmacol. 11:620724. doi: 10.3389/fphar.2020.620724

Mesalamine has been well used in the improvement of ulcerative colitis (UC) in clinics, however, the underlying mechanisms were not well illustrated. To explore its efficacy from the perspective of gut microbiota and related metabolites, we employed 16S rRNA sequencing and metabolomics approaches in stool samples across 14 normal healthy controls (NC group), 10 treatment-naïve UC patients (UC group) and 14 UC patients responded to mesalamine treatment (mesalamine group). We noted that the gut microbiota diversity and community composition were remarkably perturbed in UC group and partially restored by mesalamine treatment. The relative abundance of 192 taxa in genus level were significantly changed in UC group, and 168 genera were significantly altered after mesalamine intervention. Meanwhile, a total of 127 metabolites were significantly changed in UC group and 129 metabolites were significantly altered after mesalamine treatment. Importantly, we observed that many candidates including 49 genera (such as *Escherichia-shigella, Enterococcus* and *Butyricicoccus*) and 102 metatoblites (such as isoleucine, cholic acid and deoxycholic acid) were reversed by mesalamine. Spearman correlation analysis revealed that most of the candidates were significantly correlated with Mayo score of UC, and the relative abundance of specific genera were significant correlated with the perturbation of metabolites. Pathway analysis demonstrated that genera and metabolites candidates were enriched in many similar molecular pathways such as amino acid metabolism and secondary metabolites biosynthesis. Importantly, ROC curve analysis identified a gut microbiota signature composed of five genera including *Escherichia-Shigella, Streptococcus, Megamonas, Prevotella_9* and [*Eubacterium*] *_coprostanoligenes _group* which might be used to distinguish UC group from both NC and mesalamine group. In all, our results suggested that mesalamine might exert a beneficial role in UC by modulating gut microbiota signature with correlated metabolites in different pathways, which may provide a basis for developing novel candidate biomarkers and therapeutic targets of UC.

Keywords: 16S rRNA sequencing, metabolomics, mesalamine, ulcerative colitis, gut microbiota

INTRODUCTION

Ulcerative colitis (UC) is a chronic inflammatory bowel disease characterized by relapsing and remitting mucosal inflammation. The affected site starts in the rectum and could extend to proximal segments of the colon (Ungaro et al., 2017). The typical symptoms of UC include bloody stools, diarrhoea and fatigue, which may severely impact work capacity and quality of life (Hoivik et al., 2013; Lynch and Hsu, 2020). The global incidence and prevalence of UC experienced a great increase in recent years, posing a significant burden on public health system (Kotze et al., 2020). Hence, it is urgent to explore underlying pathogenesis of UC and discover efficient therapies.

UC is consider as a disease of unknown aetiology, which is a multifactorial disorder (Shen et al., 2018; Kaur and Goggolidou, 2020). It has been reported that a variety of complex factors including genetics, environment, epithelial barrier defects and immune system disorders were related to the pathogenesis of ulcerative colitis (Porter et al., 2020). Meanwhile, abundant evidence have demonstrated that gut microbiota might play a crucial role in ulcerative colitis, and many studies have revealed that biodiversity and composition of gut microbiota were changed in UC patients and animal models (Bajer et al., 2017; Shang et al., 2017). However, the mechanisms of gut microbiota contributing to the pathogenesis of UC and efficient interventions need further investigation. The aim of UC treatment is to induce and maintain remission of the disease (Scaldaferri et al., 2016). Mesalamine has been used in controlling UC, which is recommended as the first-line therapy (Adams and Bornemann, 2013). As a free radical scavenger and an antioxidant, mesalamine could regulate inflammatory response by modulating the production of inflammatory cytokines and the functions of immune cells (Nakashima and Preuss, 2020). However, few studies have reported the influence of mesalamine on gut microbiota and related metabolites in UC patients.

In the present study, we employed 16S rRNA sequencing and LC-MS (liquid chromatography mass spectrometry) metabolomics, observed the changes of gut microbiota composition and the related metabolites among normal healthy controls, UC patients with no treatment and UC patients with mesalamine treatment, reported the effects of mesalamine in restoring perturbance of metabolites and gut microbiota, and identified the underlying functional pathways and biomarkers of UC. The present study will enhance the comprehension of gut microbiota in UC pathogenesis and mechanisms of mesalamine in treating UC, which may benefit development of novel therapeutic agents in future.

MATERIALS AND METHODS

Study Design

This exploratory study composed of two sequential cross-sectional trials. Firstly, we designed a cohort contained 10 treatment-naïve UC patients (UC group) and 14 healthy volunteers (NC group), to investigate the potential difference in gut microbiota and related metabolites between UC and healthy status. Then, another cohort was established, which composed of all patients from UC group and 14 UC patients in mesalamine group who were well responded to mesalamine treatment, to discover underlying gut microbiota and related metabolites that mesalamine could modulate. All patients were screening from inpatient and outpatient of gastroenterology and anorectal departments in Longhua Hospital from January 2019 to August 2020. Healthy controls were recruited voluntarily from health examination department. The present study was approved by the Ethics Committee of Longhua Hospital, and informed consent was obtained from all participants.

Participants and Sample Collection

UC was diagnosed based on a combination of clinical symptoms, endoscopic and histological findings, and absence of other reasons induced colitis according to the Chinese consensus on diagnosis and treatment of inflammatory bowel disease (Beijing, 2018) (Wu et al., 2018). In brief, the following criteria were compulsory: 1) persistent or recurrent diarrhea with mucus and bloody purulent discharge for more than 6 weeks; 2) endoscopic findings of erythema, mucosal congestion, disappearance of vascular pattern, erosions, ulcerations and so on; 3) histological evidences of inflammatory cell infiltration, distortion of crypt architecture and mucosal erosion or ulceration; 4) exclusion of other pathologies including but not limited to infection, medications, radiation and ischemia.

Patients aged 18–65 years old who had mild and moderate UC with a modified Mayo score of 3–10 were screened. The additional inclusion criteria for UC group were treatment-naïve patients, who were defined as patients who were initially diagnosed as UC and received no treatment, or had a complete remission at least 6 months but experienced a recent relapse before any medication administration. On the other hand, the extra inclusion criteria for mesalamine group were mesalamine-responded UC patients. The administration rules should be oral intake of 1.0 g mesalazine enteric-coated tablets, three times a day, 1 h before three meals for at least continuous 3 months. The treatment response was set as a reduction from initial treatment in total Mayo score of at least 30%, with an accompanying decline in the dimension for rectal bleeding of at least one point or an absolute score for rectal bleeding of 0 or 1 (Rutgeerts et al., 2005). Patients were excluded if they met any of following criteria: breastfeeding or pregnant, participation in other clinical trials within the past 6 months, administration of antibiotics within the past 3 months, administration of immunosuppressive agents, biological agents, other non-steroidal (steroidal) anti-inflammatory drugs besides mesalamine, gastrointestinal mucosal protective agents, intestinal probiotics and prebiotics within the past 4 weeks. Besides, patients were also excluded if they combined with severe heart, liver, kidney and other important organ and blood system diseases, as well as gastroduodenal ulcer, history of intestinal surgery, intestinal obstruction, intestinal perforation, perianal abscess, severe hemorrhagic disease and mental disorders. This study also recruited age and gender matched healthy volunteers as NC group. The corresponding eligible criteria contained: 1) no

administration of salicylic acid drugs in the past 4 weeks; 2) no history of gastrointestinal diseases in the past 6 months; 3) no existence of gastrointestinal symptoms such as abdominal distension, abdominal pain, diarrhea and constipation; 4) no combination with severe cardiovascular, hepatic, renal and digestive diseases. Based on above inclusion and exclusion criteria, the first cohort included 10 treatment-naïve UC patients and 14 healthy volunteers, then the second cohort contained 10 treatment-naïve UC patients and 14 mesalamine-responded UC patients.

Age, gender and body mass index (BMI) were recorded for all participants. Disease course, Montreal classification, Mayo score and corresponding disease severity were also documented for UC patients. In addition, Baron index was utilized to quantify the endoscopic activity in UC patients (Baron et al., 1964). Participants were informed to terminate administration of antibiotics, probiotics, prebiotics or other microbiota-related preparations at least 4 weeks before sampling. All participants were instructed to collect 3.0 g morning first feces using sterile fecal collection tubes. The fecal samples should avoid contamination from other mediums such as urine. The collected samples were stored at −80°C for further16S rRNA sequencing and untargeted metabonomics detection.

DNA Extraction and 16S rRNA Sequencing

Fecal samples were performed 16S rRNA sequencing in Shanghai Meiji Biomedical Technology Co., Ltd. (Shanghai, China) following the manufactures' procedures. Briefly, DNA were extracted from fecal samples according to the instructions of E. Z.N.A® soil (Omega Bio-tek, Norcross, GA, United States). The quality of DNA was detected by 1% agarose gel electrophoresis, and the concentration and purity were detected by NanoDrop 2000. 16S rRNA genes were amplified using PCR with primers targeting the V3-V4 region (338F–806R). The amplicons were purified using AxyPrep DNA Gel Extraction Kit (Axygen Biosciences, Union City, CA, United States), and quantified by QuantiFluor™-ST (Promega, United States) to construct libraries and perform paired-end rRNA sequencing on Illumina MiSeq platform (Illumina, San Diego, United States) following the manufactures' instructions.

16S rRNA Sequencing Data Analysis

The adapters and low-quality bases were trimmed using fastp tool to obtain clean reads (Chen et al., 2018), and then merged by FLASH software (Magoc and Salzberg, 2011). Sequences with 97% similarity were clustered in OTUs (operational taxonomic units) using UPARSE software (Edgar, 2013). Taxonomy was annotated and aligned with Silva 16S-rDNA database (v138) using RDP classifier (Wang et al., 2007). The Chao and Shannon index was used to estimate Alpha diversity and principle coordinates analysis (PCoA) using unweighted UniFrac distance was performed to reveal the Beta diversity among samples. ANOSIM (analysis of similarities) analysis was performed to assess the significance of difference in PCoA plots. Kruskal-Wallis H test or Wilcoxon rank-sum test were used to assess the significant difference of bacterial genera abundance among groups. The functional prediction of taxa was performed using PICRUSt analysis (Langille et al., 2013). p value less than 0.05 was considered as significantly different. The signature to discriminate UC group from NC and mesalamine group was identified using ROC (receiving operator curve) analysis by estimating AUC (area under curve) value.

Metabolomics Data Acquisition

Stool samples were performed metabolomics analysis in Shanghai Meiji Biomedical Technology Co., Ltd. (Shanghai, China) following the manufactures' procedures. Briefly, 50 mg stool samples were added 400 Ul of cold methanol solution (methanol: water = 4:1), broken by a high-throughput tissue crusher at low temperature. After vortex mixing, the samples were extracted by ultrasound on ice for 10 min and three times, placed at −20°C for 30 min, centrifuged at 13,000 g, 4°C for 15 min, and the supernatant was performed metabolomics analysis using ultra performance liquid chromatography-triple time of flight mass spectrometry (UPLC-Triple TOF-MS, AB SCIEX Company, United States) following the manufactures' protocols. The chromatographic column was BEHC18 column (100 × 2.1 mm i.d., 1.7 μm; Waters, Milford, United States). Mobile phase A was water (containing 0.1% formic acid), and mobile phase B was acetonitrile/isopropanol (1/1) (containing 0.1% formic acid). The flow rate was 0.4 ml/min, injection volume was 20 μl and column temperature was 40°C. The chromatographic elution gradient was 0.0 min, 95%A and 5% B; 3 min, 80%A and 20% B; 9.0 min, 5%A and 95% B; 13 min, 5% A and 95% B; 13.1 min, 95%A and 5% B and 16 min, 95%A and 5% B. The samples mass spectrometry signal acquisition was used positive and negative ion scanning mode. The electrospray capillary voltage, injection voltage and collision voltage were 1.0 kV, 40 V and 6 eV, respectively. The ion source temperature and desolvation temperature were 120 °C and 500 °C, carrier gas flow was 900 L/h, mass spectrometry scanning range was 50–1,000 m/z and resolution was 30,000. Quality control (QC) samples were pooled from all experimental samples and analyzed with the same procedure.

Metabolomics Data Analysis

Raw data were processed using Progenesis QI software (Waters Corporation, Milford, United States), then a data matrix of retention time, m/z and peak area was obtained. Only variables with a non-zero value of more than 50% in all samples were retained, and the missing values were filled with 1/2 of the minimum value in the original matrix. The total peaks were normalized, and variables with a relative standard deviation (RSD) of QC samples of more than 30% were deleted to obtain a data matrix for further analysis. To identify the structure of metabolites, raw data were imported to Progenesis QI software (Waters Corporation, Milford, United States) and the mass spectra were compared to an in-house standard library and public databases such as The Human Metabolome Database (HMDB) and METLIN.

Using R package ropls (version1.6.2), principle component analysis (PCA) and orthogonal partial least squares discriminant analysis (OPLS-DA) were performed for multivariate statistical analysis, and variable importance of projection (VIP) values were

TABLE 1 | Baseline characteristics of included participants.

	NC group (n = 14)	UC group (n = 10)	Mesalamine group (n = 14)	*p* Value
Age, years	32.50 (10.0)	27.50 (11.0)	42.50 (23)	0.084
Gender, male	7 (50.0%)	5 (50.0%)	9 (64.3%)	0.694
BMI, kg/m^2	22.35 (1.5)	20.15 (4.4)	23.35 (2.5)	0.075
Course, months	—	9.50 (34.0)	48.00 (77.0)	0.007
Montreal classification				0.546
Proctitis	—	3	6	
Left-sided colitis	—	3	4	
Extensive colitis	—	4	4	
Modified mayo score	—	8.00 (3.0)	5.00 (2.0)	0.005
Disease severity[a]	—			0.022
Clinical remission	—	0	2	
Mild	—	3	9	
Moderate	—	6	3	
Severe	—	1	0	
Baron index	—	3.00 (0.0)	1.00 (2.0)	0.002

[a]*Evaluation of disease severity is based on modified Mayo score: 1) Clinical remission: total score ≤2 points, and every sub-dimension score ≤1 point; 2) Mild: total score of three to five points; 3) Moderate: total score of 6–10 points; 4) Severe: total score of 11–12 points.*

obtained. For univariate statistical analysis, Welch's *t* test was used to calculate *p* values between groups. Fold changes of metabolites were calculated between groups based on the ratio of average normalized peak intensity. The differential metabolites between groups were identified with the threshold of VIP > 1 and $p < 0.05$. Venn diagram (R package, version1.6.2) was used to obtain the intersection of differential metabolites between pairwise groups. Hierarchical cluster was performed to reveal the expression patterns of differential metabolites among groups, and pathway enrichment was performed to reveal metabolites related biological functions using scipy (Python, version1.0.0).

Statistical Analysis

For baseline data, data were presented as median with interquartile range or number with percentage. Statistical analysis was performed using SPSS 24.0 software. The qualitative data among three groups were assessed using one-way analysis of variance (ANOVA) or Kruskal-Wallis test based on data distribution. The qualitative data was analyzed by Chi-square test. Difference between two groups were determined by Student's T test or Wilcoxon rank sum test. For correlation analysis, Spearman rank correlation coefficient was calculated. *p* value less than 0.05 was considered as significant difference.

RESULTS

Baseline Characteristic of Participants

A total of 14 normal healthy controls (NC group), 10 UC patients with no treatment (UC group), and 14 UC patients with mesalamine treatment (mesalamine group) were included in the present study. Detailed demographic and clinical characteristics of enrolled participants were shown in **Table 1**. No significant difference was found in age, gender and BMI among three groups. UC phenotypes based on Montreal Classification was comparable between UC group and mesalamine group. Patients in mesalamine group showed milder disease severity and endoscopic activity than UC groups, according to modified Mayo score and Baron index, respectively.

Mesalamine Intervention Improved Gut Microbiota Diversity in UC Patients

The 16S rRNA sequencing of stool samples from three groups was performed to reveal the difference of gut microbial community structure. Analysis of Chao index indicated that there was a significant increase in taxa richness in UC group, while mesalamine could obviously restore the disturbance (**Figure 1A**). The Shannon index of taxa evenness exhibited a decreased trend in UC group, and mesalamine partially improved the perturbance (**Figure 1B**). PCoA plots revealed that there was remarkable difference in bacterial composition between UC group and NC group, while mesalamine intervention could ameliorate the difference (**Figure 1C**).

Mesalamine Intervention Improved Gut Microbiota Abundance in UC Patients

To examine whether relative abundance of gut microbiota was associated with the diversity difference, Circos analysis (**Figure 1D**) and community bar plots (**Figure 1E**) at genus level were performed. The results showed that the relative abundance of various specific microbiotas at genus level were different between groups. For example, the relative abundance of genus *Streptococcus* in UC group, mesalamine group and NC group was 11.24, 1.81, and 1.27%, respectively. To test whether there was a significant difference of specific microbiota between UC group and NC group or between mesalamine group and UC group, the differential microbiota analysis based on relative abundance at genus level was performed using Wilcoxon rank-sum test. Our results showed that there were 192 significantly differential genera between UC group and NC group (Supplementary Table S1), and the representative top 15

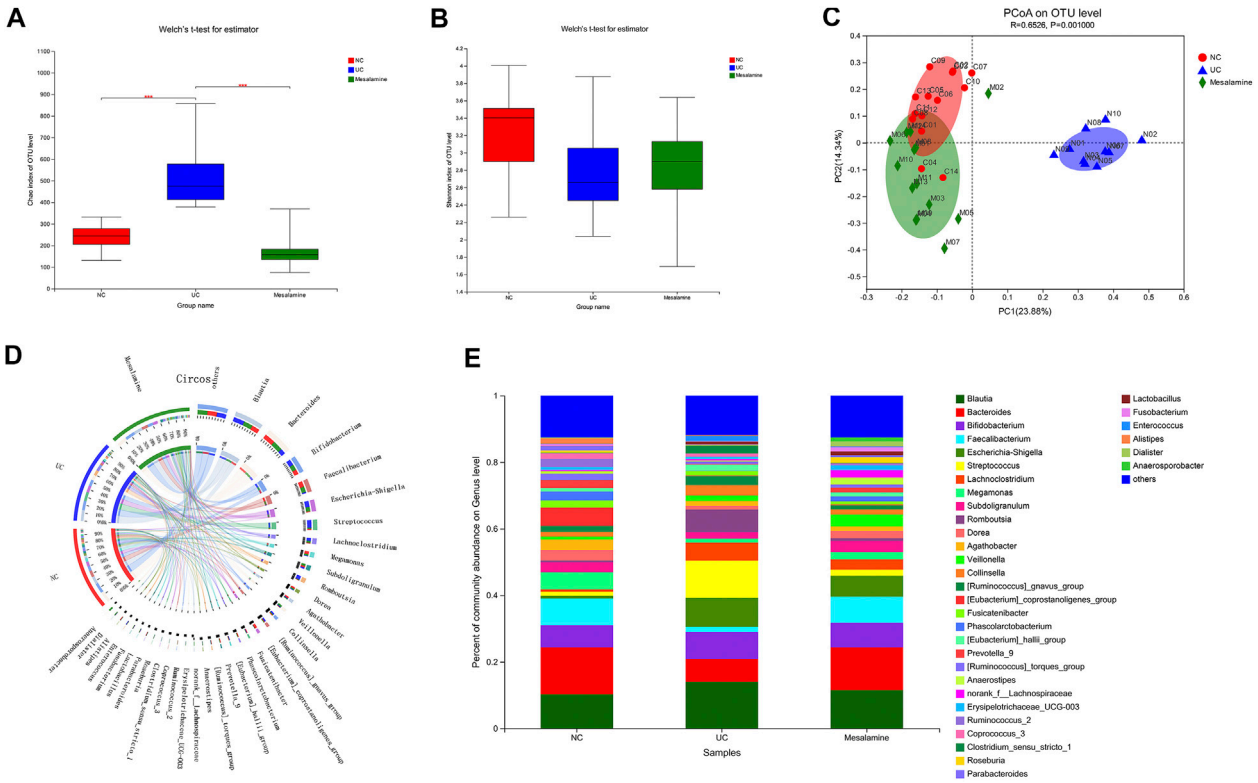

FIGURE 1 | Gut microbiota diversity and composition analysis. **(A)** α-Diversity evaluated by Chao index (***$p < 0.001$) **(B)**. α-Diversity evaluated by Shannon index. **(C)** PCoA plots based on unweighted UniFrac distance **(D)**. Diagram of Circos analysis, the small semicircle **(left half circle)** represents the species composition in the sample, the color of outer ribbon represents the group from which the species came, the color of inner ribbon represents the species, and the length represents the relative abundance of the species in the corresponding samples; the large semicircle **(right half circle)** represents the distribution proportion of species in different samples at the taxonomic level, and the outer layer ribbon represents the species, the inner ribbon color represents different groups, and the length represents the distribution proportion of the sample in a certain species. **(E)** The overall percentage of gut microbiota community abundance on genus level.

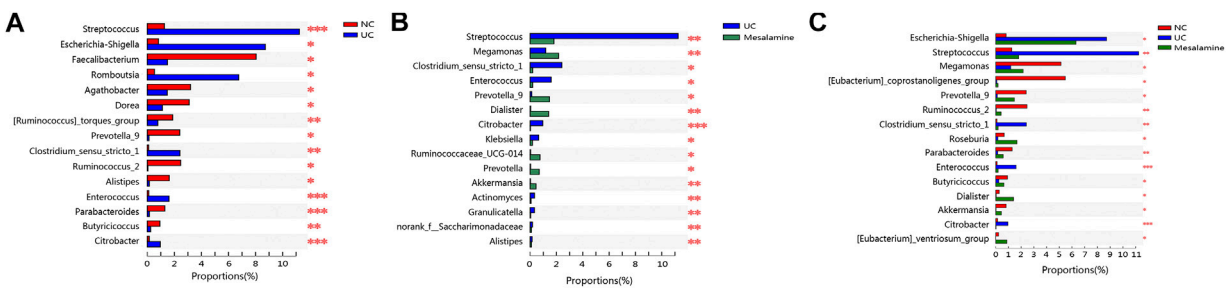

FIGURE 2 | Significantly changed taxa on genus level among groups. **(A)** Top 15 differential genera between UC group and NC group. **(B)** Top 15 differential genera between UC group and mesalamine group **(C)**. Top 15 mesalamine restored genera. *$0.01 < p \leq 0.05$, **$0.001 < p \leq 0.01$, ***$p \leq 0.001$.

genera were presented in **Figure 2A**. Meanwhile, mesalamine intervention significantly changed the relative abundance of 168 genera in UC patients (Supplementary Table S2), and the top 15 differential genera were revealed in **Figure 2B**. Interestingly, we observed that mesalamine intervention could significantly reverse the relative abundance of 49 genera in UC patients (**Table 2**), which were identified as candidate genera for further analysis. The top 15 mesalamine reversed genera were presented in **Figure 2C**, which revealed that the relative abundance of *Escherichia-Shigella, Megamonas, Clostridium_ sensu_stricto_ 1, Enterococcus* and *Citrobacter* was significantly increased in UC group compared to NC, and restored by mesalamine treatment. The relative abundance of genera including *Megamonas* [*Eubacterium*]*_ventriosum_ group, Prevotella_9, Ruminococcus_2, Roseburia, Parabacteroides, Butyricicoccus, Dialister, Akkermansia* and [*Eubacterium*]*_coprostanoligenes_*

TABLE 2 | 49 candidate genera reversed by mesalamine intervention.

Genus name	NC group proportion (%)	UC group proportion (%)	Mesalamine group proportion (%)	*p* Value
g__Escherichia-shigella	0.827	8.721	6.317	0.039
g__Megamonas	5.136	1.185	2.162	0.017
g__Streptococcus	1.266	11.240	1.807	0.001
g__Roseburia	0.669	0.171	1.676	0.042
g__Prevotella_9	2.401	0.128	1.470	0.020
g__Dialister	0.281	0.044	1.406	0.024
g__[Eubacterium]_ventriosum_group	0.229	0.003	0.877	0.020
g__Butyricicoccus	0.931	0.247	0.648	0.017
g__Parabacteroides	1.299	0.158	0.595	0.003
g__Akkermansia	0.824	0.032	0.449	0.010
g__Ruminococcus_2	2.465	0.050	0.431	0.002
g__Clostridium_sensu_stricto_1	0.102	2.413	0.194	0.008
g__Enterococcus	0.109	1.602	0.193	0.001
g__[Eubacterium]_coprostanoligenes_group	5.477	0.092	0.186	0.016
g__Klebsiella	0.228	0.648	0.176	0.026
g__[Clostridium]_innocuum_group	0.007	0.533	0.153	0.008
g__Ruminococcaceae_UCG-002	0.418	0.009	0.153	0.046
g__norank_f__Saccharimonadaceae	0.009	0.180	0.102	0.000
g__*Actinomyces*	0.048	0.335	0.070	0.002
g__Odoribacter	0.152	0.014	0.058	0.046
g__Pseudomonas	0.609	0.012	0.055	0.006
g__Coprococcus_1	0.109	0.029	0.053	0.023
g__Ruminococcaceae_UCG-003	0.085	0.005	0.049	0.045
g__Rothia	0.006	0.131	0.045	0.000
g__Granulicatella	0.015	0.331	0.044	0.001
g__Family_XIII_AD3011_group	0.038	0.008	0.044	0.003
g__*Citrobacter*	0.150	0.963	0.029	0.000
g__Bilophila	0.092	0.005	0.028	0.012
g__unclassified_f__Ruminococcaceae	0.038	0.061	0.020	0.009
g__Gemella	0.004	0.148	0.018	0.000
g__Oribacterium	0.002	0.023	0.014	0.025
g__norank_f__Muribaculaceae	0.080	0.176	0.013	0.000
g__Solobacterium	0.002	0.038	0.008	0.000
g__Morganella	0.000	0.011	0.006	0.004
g__Atopobium	0.003	0.021	0.005	0.026
g__Staphylococcus	0.001	0.149	0.003	0.000
g__Lachnospiraceae_UCG-001	0.144	0.002	0.003	0.008
g__Weissella	0.002	0.030	0.002	0.012
g__*Aeromonas*	0.000	0.049	0.001	0.000
g__Corynebacterium	0.002	0.022	0.001	0.028
g__Lactococcus	0.004	0.021	0.001	0.000
g__Family_XIII_UCG-001	0.031	0.000	0.001	0.003
g__Bacillus	0.000	0.181	0.001	0.000
g__Corynebacterium_1	0.001	0.017	0.001	0.004
g__Finegoldia	0.001	0.012	0.001	0.013
g__*Acinetobacter*	0.001	0.033	0.000	0.000
g__Porphyromonas	0.002	0.021	0.000	0.000
g__Leuconostoc	0.002	0.008	0.000	0.004
g__Anaerofilum	0.001	0.002	0.000	0.028

group were significantly reduced in UC group compared to NC, which was obviously increased by mesalamine intervention.

Mesalamine Intervention Restored the Perturbance of Fecal Metabolites in UC Patients

Using UPLC-Triple TOF-MS, the fecal metabolites across NC, UC and mesalamine groups were profiled. As shown in **Figure 3A**, the PCA plots of three groups revealed that there was distinct separation among groups, and the plots of mesalamine group were close to NC group. The results indicated that the metabolites profile in UC group might be different from both NC and mesalamine group, and the metabolites profile of latter two groups might be similar. To identify the differential metabolites, OPLS-DA model was performed between pairwise groups (UC vs NC group, and mesalamine vs UC group). The results showed that the plots of UC group samples were obviously separated from NC or mesalamine group (**Figures 3B,C**). With the threshold of VIP

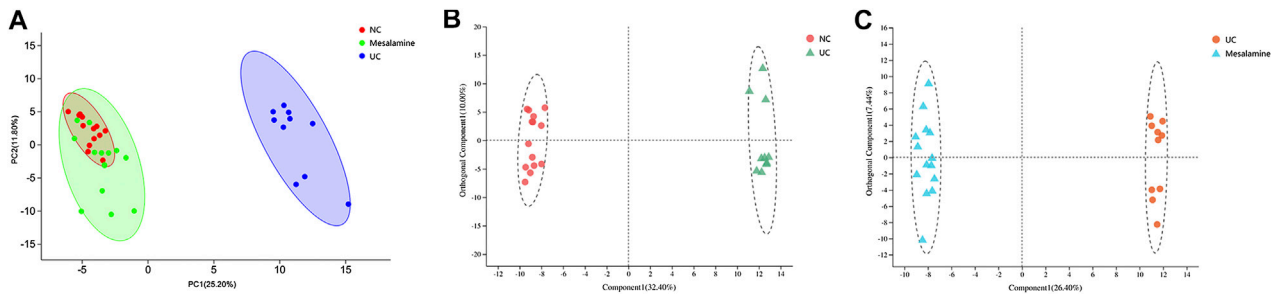

FIGURE 3 | PCA and OPLS-DA plots among groups. **(A)** PCA score plots of NC, UC and mesalamine groups, red dots represented NC group, green dots represented mesalamine group and blue dots represented UC group. **(B)** OPLS-DA score plots of NC and UC groups, red dots represented NC group and green triangles represented UC group. **(C)** OPLS-DA score plots of UC and mesalamine groups, red dots represented UC group and blue triangles represented mesalamine group.

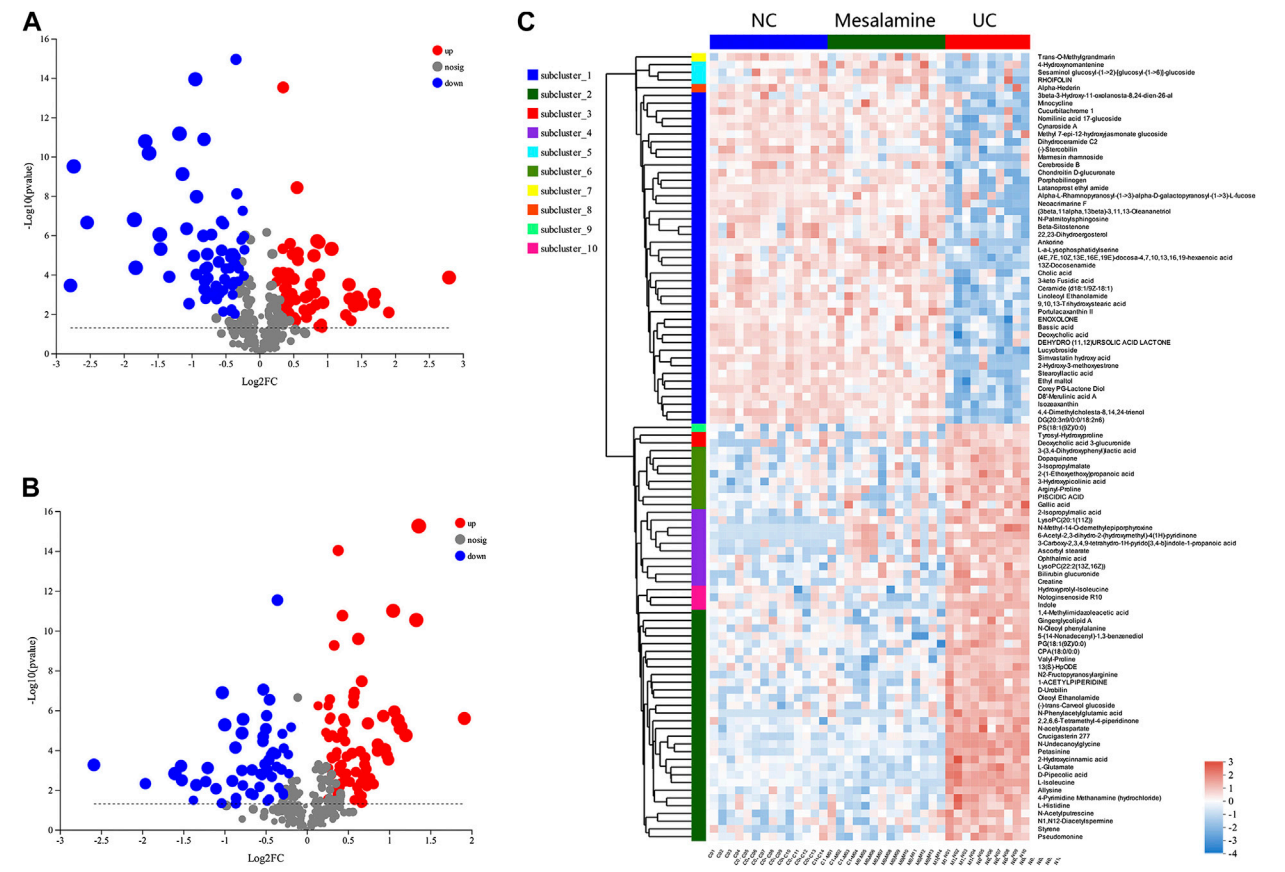

FIGURE 4 | Significantly changed metabolites among groups. **(A)** Volcano plots of differential metabolites between UC group and NC group, grey dots represent metabolites with no significant change, red dots represent up-regulated metabolites and green dots represent down-regulated metabolites. **(B)** Volcano plots of differential metabolites between UC group and mesalamine group, grey dots represent metabolites with no significant change, red dots represent up-regulated metabolites and green dots represent down-regulated metabolites. **(C)** Hierarchical cluster of 102 candidate metabolites. The color indicates the relative expression level of metabolites in this group of samples, red indicates up-regulated and blue indicated down-regulated.

more than 1, *p* value less than 0.05 and fold change not equal to 1, a total of 127 differential metabolites between UC group and NC were obtained, and 129 differential metabolites between mesalamine and UC group were identified (**Figures 4A,B**; Supplementary Table S3, S4). Importantly, a total of 102 metabolites reversed by mesalamine intervention in UC patients were filtered out as candidates for further analysis (**Figure 4C**; **Table 3**). For example, the level of ophthalmic

TABLE 3 | 102 candidate metabolites reversed by mesalamine intervention.

Metabolite	Fold change (UCgroup/ NC group)	UCgroup vs NC group *p* value	Fold change (mesalamine group/UC group)	Mesalamine group vs UC group *p* Value
D8′-merulinic acid A	0.573	0.000	1.726	0.000
(4E,7E,10Z,13E,16E,19E)-docosa-4,7,10,13,16,19-hexaenoic acid	0.731	0.000	1.443	0.000
13(S)-HpODE	1.234	0.000	0.734	0.000
Marmesin rhamnoside	0.309	0.001	2.865	0.003
Cynaroside A	0.570	0.001	1.728	0.001
Methyl 7-epi-12-hydroxyjasmonate glucoside	0.530	0.032	1.819	0.048
2-(1-Ethoxyethoxy)propanoic acid	1.296	0.000	0.761	0.001
Valyl-Proline	1.243	0.000	0.638	0.000
Ophthalmic acid	1.750	0.000	0.587	0.003
Neoacrimarine F	0.400	0.000	2.305	0.001
N-acetylaspartate	1.342	0.000	0.727	0.000
N2-Fructopyranosylarginine	2.104	0.000	0.479	0.000
L-Histidine	1.275	0.000	0.740	0.000
Pseudomonine	1.693	0.000	0.458	0.000
Stearoyllactic acid	0.545	0.000	1.824	0.000
N-Palmitoylsphingosine	0.768	0.000	1.296	0.000
Cerebroside B	0.770	0.000	1.289	0.001
Lucyobroside	0.718	0.001	1.423	0.001
(-)-Stercobilin	0.624	0.001	1.373	0.029
Hydroxyprolyl-isoleucine	1.330	0.006	0.717	0.001
Gallic acid	1.286	0.010	0.774	0.016
3-Hydroxypicolinic acid	1.355	0.000	0.777	0.000
3-Isopropylmalate	1.704	0.000	0.607	0.001
3-(3,4-Dihydroxyphenyl)lactic acid	1.953	0.000	0.624	0.002
Piscidic acid	1.634	0.000	0.503	0.000
Dopaquinone	1.276	0.000	0.810	0.000
Portulacaxanthin II	0.544	0.000	2.037	0.000
2-Isopropylmalic acid	1.327	0.000	0.784	0.000
Rhoifolin	0.546	0.041	2.149	0.009
Cholic acid	0.801	0.007	1.221	0.014
2,2,6,6-Tetramethyl-4-piperidinone	1.204	0.000	0.836	0.000
Nomilinic acid 17-glucoside	0.522	0.003	1.872	0.004
Tyrosyl-Hydroxyproline	1.733	0.002	0.629	0.019
Simvastatin hydroxy acid	0.478	0.000	1.996	0.000
Notoginsenoside R10	1.745	0.000	0.518	0.000
Deoxycholic acid	0.780	0.004	1.218	0.017
DG (20:3n9/0:0/18:2n6)	0.555	0.000	1.711	0.000
Ethyl maltol	0.741	0.000	1.330	0.000
Sesaminol glucosyl-(1->2)-[glucosyl-(1->6)]-glucoside	0.267	0.008	3.894	0.005
Ceramide (d18:1/9Z-18:1)	0.759	0.000	1.349	0.000
N-Oleoyl phenylalanine	1.558	0.000	0.551	0.000
CPA(18:0/0:0)	1.703	0.000	0.464	0.000
LysoPC(20:1 (11Z))	2.195	0.000	0.763	0.001
Ascorbyl stearate	3.090	0.000	0.696	0.004
3beta-3-Hydroxy-11-oxolanosta-8,24-dien-26-aL	0.618	0.015	1.606	0.015
Dihydroceramide C2	0.593	0.006	1.566	0.018
Enoxolone	0.740	0.003	1.397	0.001
Ankorine	0.368	0.001	2.885	0.001
Oleoyl ethanolamide	1.902	0.000	0.598	0.000
2-Hydroxy-3-methoxyestrone	0.144	0.000	6.006	0.001
N-Phenylacetylglutamic acid	6.671	0.000	0.266	0.000
3-keto Fusidic acid	0.721	0.001	1.343	0.002
5-(14-Nonadecenyl)-1,3-benzenediol	1.305	0.000	0.683	0.000
Cucurbitachrome 1	0.397	0.002	2.343	0.004
Bilirubin glucuronide	2.746	0.000	0.635	0.005
13Z-Docosenamide	0.785	0.000	1.281	0.000
Gingerglycolipid A	1.314	0.001	0.552	0.000
Petasinine	2.264	0.000	0.484	0.000
L-isoleucine	1.926	0.000	0.390	0.000
9,10,13-Trihydroxystearic acid	0.675	0.000	1.448	0.000
(-)-trans-Carveol glucoside	1.410	0.000	0.724	0.000

(Continued on following page)

TABLE 3 | (*Continued*) 102 candidate metabolites reversed by mesalamine intervention.

Metabolite	Fold change (UCgroup/ NC group)	UCgroup vs NC group *p* value	Fold change (mesalamine group/UC group)	Mesalamine group vs UC group *p* Value
Indole	1.516	0.000	0.398	0.000
Trans-O-Methylgrandmarin	0.309	0.003	2.599	0.033
N-Methyl-14-O-demethylepiporphyroxine	3.542	0.000	0.670	0.032
4-Hydroxynornantenine	0.737	0.008	1.477	0.002
Styrene	1.740	0.000	0.613	0.000
Alpha-L-Rhamnopyranosyl-(1->3)-alpha-D-galactopyranosyl-(1->3)-L-fucose	0.687	0.019	1.397	0.036
6-Acetyl-2,3-dihydro-2-(hydroxymethyl)-4(1H)-pyridinone	3.212	0.000	0.615	0.001
Arginyl-Proline	1.773	0.000	0.662	0.001
Porphobilinogen	0.560	0.003	1.714	0.006
Chondroitin D-glucuronate	0.609	0.001	1.490	0.007
1-Acetylpiperidine	1.341	0.000	0.715	0.000
N-Acetylputrescine	1.471	0.000	0.812	0.002
N1,N12-Diacetylspermine	1.426	0.000	0.740	0.001
1,4-Methylimidazoleacetic acid	1.298	0.000	0.746	0.001
Creatine	3.589	0.000	0.434	0.000
4-Pyrimidine methanamine (hydrochloride)	1.472	0.000	0.673	0.000
D-Pipecolic acid	1.260	0.000	0.741	0.000
Beta-sitostenone	0.841	0.000	1.169	0.000
Corey PG-Lactone Diol	0.590	0.000	1.586	0.001
L-a-Lysophosphatidylserine	0.799	0.000	1.403	0.000
PG (18:1 (9Z)/0:0)	1.171	0.000	0.813	0.000
Alpha-Hederin	0.413	0.011	2.049	0.046
Linoleoyl ethanolamide	0.677	0.000	1.445	0.000
N-Undecanoylglycine	1.271	0.000	0.768	0.000
Bassic acid	0.822	0.000	1.214	0.000
Minocycline	0.690	0.002	1.459	0.002
Latanoprost ethyl amide	0.353	0.003	3.037	0.001
22,23-Dihydroergosterol	0.787	0.000	1.229	0.000
3-Carboxy-2,3,4,9-tetrahydro-1H-pyrido [3,4-b]indole-1-propanoic acid	5.817	0.000	0.624	0.044
Dehydro (11,12)ursolic acid lactone	0.704	0.000	1.377	0.000
Crucigasterin 277	1.761	0.000	0.649	0.000
D-Urobilin	2.769	0.000	0.465	0.000
L-Glutamate	1.187	0.000	0.795	0.000
4,4-Dimethylcholesta-8,14,24-trienol	0.681	0.000	1.369	0.000
Allysine	1.442	0.000	0.675	0.000
PS(18:1 (9Z)/0:0)	1.673	0.001	0.723	0.004
(3beta,11alpha,13beta)-3,11,13-Oleananetriol	0.379	0.004	2.537	0.006
Deoxycholic acid 3-glucuronide	2.053	0.003	0.509	0.000
LysoPC(22:2 (13Z,16Z))	1.371	0.000	0.775	0.007
Isozeaxanthin	0.712	0.000	1.412	0.000
2-Hydroxycinnamic acid	1.165	0.000	0.824	0.000

acid, isoleucine, styrene and creatine was elevated in treatment-naïve UC patients compared to normal healthy controls, and restored by mesalamine treatment. The level of cholic acid, deoxycholic acid and enoxolone was reduced in treatment-naïve UC patients, and restored by mesalamine intervention.

Mesalamine Restored Gut Microbiota and Metabolites Correlated with UC Clinical Indexes

To explore whether mesalamine restored gut microbiota and metabolites were related to UC clinical features, Spearman correlation analysis was performed. As shown in **Figure 5A** total of 26 genera (such as *Bacillus, Butyricicoccus* and *Streptococcus*) was significantly correlated with both Mayo score and the course of disease (month). Interestingly, the genera decreased by mesalamine in UC patients were positively correlated with Mayo score and the course of disease, and vice versa. For instance, the relative abundance of *Bacillus, Enterococcus* and *Streptococcus* reduced by mesalamine exhibited a significant positive correlation with Mayo score and the course of disease. Whereas, *Butyricicoccus, Parabacteroides* and *Pseudomonas* were increased by mesalamine and had a negative correlation with Mayo score and the course of

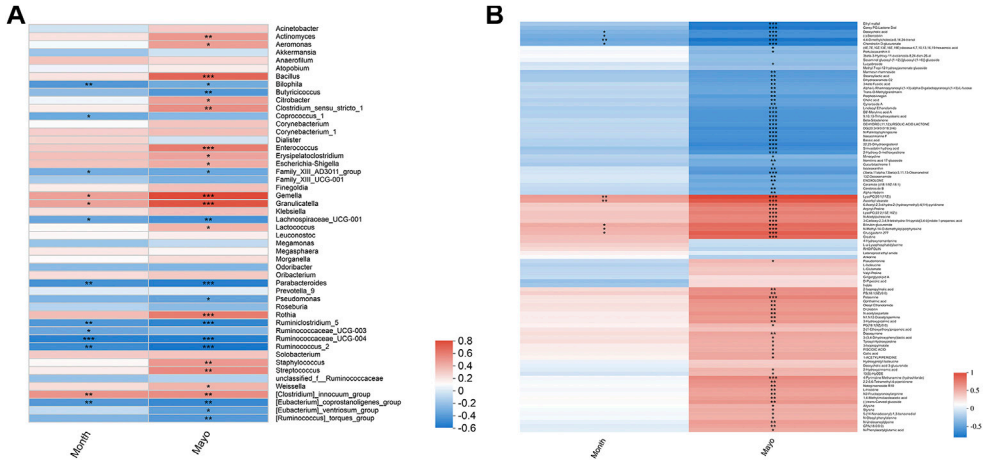

FIGURE 5 | Spearman correlation analysis of candidate genera and metabolites with UC clinical indexes. **(A)** Spearman correlation of candidate genera with UC Mayo score and the course of disease (month). **(B)** Spearman correlation of candidate metabolites with UC Mayo score and the course of disease (month). Different colors represent the value of correlation coefficient, red indicates positive correlation and blue indicated negative correlation. *$0.01 < p \leq 0.05$, **$0.001 < p \leq 0.01$, ***$p \leq 0.001$.

disease. The results indicated mesalamine might exert a beneficial role in UC by restoring the gut microbiota perturbance.

Besides, most of the candidate metabolites (85/102) revealed a significant correlation with UC Mayo score (**Figure 5B**). It was worth noting that the metabolites decreased by mesalamine were also positively correlated with Mayo score, and vice versa. For example, the levels of ophthalmic acid, allysine and styrene were reduced by mesalamine and positively correlated with Mayo score. Whereas, several metabolites increased by mesalamine such as cholic acid, deoxycholic acid and enoxolone exhibited negative correlation with Mayo score. Interestingly, the correlation pattern of metabolites with Mayo score was consistent with that of gut microbiota, which suggested that the perturbance of gut microbiota might correlate with metabolites disturbance in UC.

Gut Microbiota Correlated with Metabolites Changes in Different Pathways

Spearman correlation analysis was also performed for 49 genera and 102 metabolites candidates to examine whether there is a correlation of gut microbiota with metabolites changes (**Figure 6**). Of interest, a batch of mesalamine increased metabolites were negatively correlated with mesalamine decreased genera, and vice versa. The metabolites such as ophthalmic acid and styrene that were reduced by mesalamine were positively correlated with mesalamine decreased *Enterococcus* genus, and mesalamine increased metabolites such as deoxycholic acid and enoxolone were positively correlated with mesalamine increased genera *Butyricicoccus* and *Parabacteroides*, respectively.

Furthermore, the functional correlation between gut microbiota and metabolites changes was explored. Using PICRUSt analysis, the 49 candidate genera were enriched in 24 function classes including carbohydrate transport and metabolism, amino acid transport and metabolism, lipid transport and metabolism, signal transduction mechanisms, secondary metabolites biosynthesis, transport and catabolism, etc (**Figure 7A**). The 102 candidate metabolites were enriched in 14 KEGG pathway related items such as amino acid metabolism, biosynthesis of other secondary metabolites, lipid metabolism, carbohydrate metabolism, etc (**Figure 7B**). We observed that the candidate genera and metabolites were enriched in many similar molecular pathways such as amino acid metabolism and secondary metabolites biosynthesis, which might implicate the high functional correlation of gut microbiota with related metabolites.

The Gut Microbiota Signature Discriminate Treatment-Naïve UC Patients from Both Normal Healthy Control and Mesalamine-Responded UC Patients

To evaluate whether gut microbiota could be used to distinguish treatment-naïve UC patients from normal healthy control or mesalamine-responded UC patients, ROC analysis was performed for 49 candidate genera. Our results indicated that a gut microbiota signature composed of five genera including *Escherichia-Shigella, Streptococcus, Megamonas, Prevotella_9* and [*Eubacterium*]*_coprostanoligenes _group* might be used to distinguish treatment-naïve UC patients from normal healthy controls (AUC = 0.79, 95% CI 0.6–0.98, **Figure 8A**). Meanwhile, the five genera signature might also be used to discriminate treatment-naïve UC patients from mesalamine-responded UC patients (AUC = 0.73, 95% CI 0.52–0.94, **Figure 8B**).

DISCUSSION

In the present study, 16S rRNA sequencing and LC-MS metabolomics were integrated to detect the perturbance of gut

FIGURE 6 | Spearman correlation between candidate genera and metabolites. Different colors represent the value of correlation coefficient, red indicates positive correlation and blue indicated negative correlation. *$0.01 < p \leq 0.05$, **$0.001 < p \leq 0.01$, ***$p \leq 0.001$.

microbiota and metabolites in UC patients and observed the effect of mesalamine. We observed there were significant changes of gut microbiota and metabolites in UC patients, and mesalamine might exert beneficial effects in UC by partially restoring gut microbiota and correlated metabolites in different pathways.

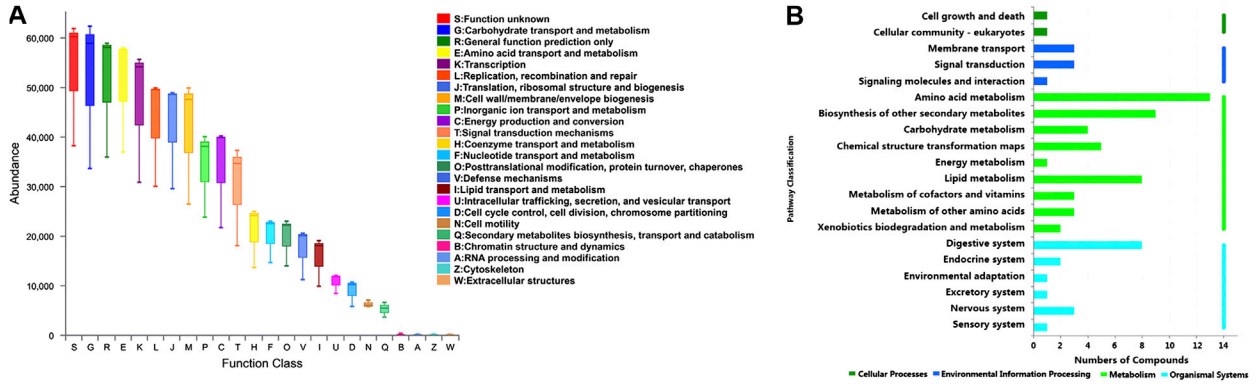

FIGURE 7 | Pathway analysis of candidate genera and metabolites. **(A)** The candidate genera functional prediction by PICRUSt analysis. The horizontal axis represents the function number, and the vertical axis represents the functional abundance. **(B)** Pathway enrichment of candidate metabolites. The horizontal axis represents the number of enriched metabolites, and the vertical axis represents the enriched pathway items.

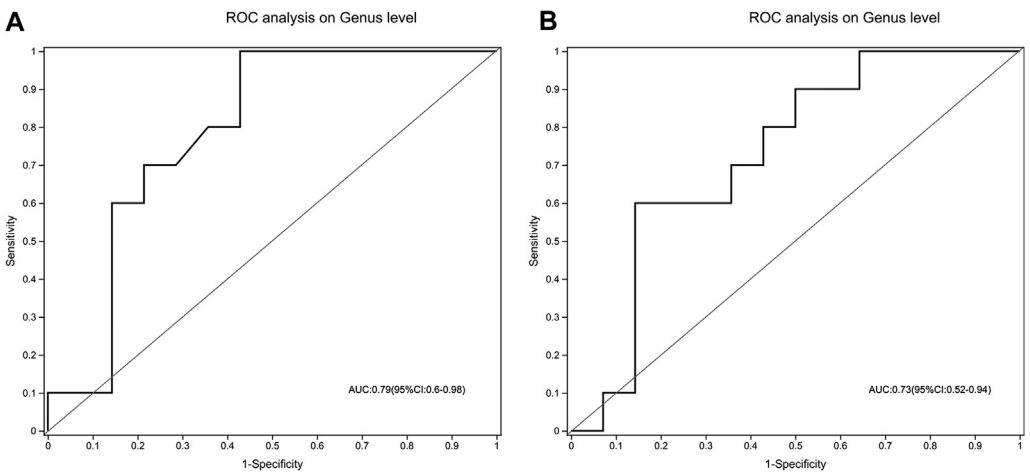

FIGURE 8 | A signature composed of five genera discriminating UC group from both NC and mesalamine groups. **(A)** ROC curve analysis of UC group and NC group. **(B)** ROC analysis of UC group and mesalamine group.

The important role of gut microbiota in UC has been widely accepted, and disruptions to the microbiome have been implicated in the pathogenesis (Derikx et al., 2016). A recent study of fecal microbiota analysis revealed that the relative abundance of *Escherichia-shigella* and *Streptococcus* was elevated, whereas *Bacteroides* and *Prevotella_9* was reduced in UC patients compared to healthy participants (Sun et al., 2019). Another study reported the gut microbial dysbiosis in Chinese inflammatory bowel disease patients, and found that the community of Megamonas and *Butyricicoccus*, which could produce short-chain fatty acids and modulate colonic regulatory T cells, was significantly repressed in UC patients stool samples (Ma et al., 2018). Here, we also observed significant changes of gut microbiota composition in treatment-naïve UC patients using 16S rRNA sequencing bacteria community analysis. We noted that the relative abundance of many genera such as *Escherichia-shigella, Megamonas, Clostridium_sensu_stricto_1, Enterococcus* and *Citrobacter* was increased, while a batch of genera such as *Megamonas, Prevotella_9, Parabacteroides [Eubacterium] _ventriosum_ group, Ruminococcus_2, Roseburia, Butyricicoccus, Dialister, Akkermansia* and [*Eubacterium*] *_coprostanoligenes_group* was reduced in UC patients. The results were partially consistent with previous studies. Importantly, we observed that the relative abundance of 49 candidate genera was significantly reversed by mesalamine intervention. It is interesting that most of the candidate genera were significantly correlated with Mayo score and the course of disease. Of which, several genera such as *Enterococcus* and *Streptococcus* exhibited a significant positive correlation with Mayo score and the course of disease, exerting their adverse effect in UC pathogenesis. Whereas, other genera such as *Butyricicoccus, Parabacteroides* and *Pseudomonas* were negatively correlated with Mayo score and the course of

disease, which implicated their beneficial role in UC. It has been reported the amount of *Enterococcus* was higher in UC patients than in healthy subjects (Nemoto et al., 2012). Another longitudinal analyses of gut mucosal microbiotas in UC patients revealed that high clinical activity indices and sigmoidoscopy scores were associated with *Enterococcus faecalis* (Fite et al., 2013). Our results were partially consistent with these data. However, there were conflicting results concerning the role of *Streptococcus* in UC. For example, it is suggested that infection with highly-virulent specific types of *Streptococcus mutans* might be a potential risk factor in the aggravation of UC (Kojima et al., 2012), whereas, it has been reported that *Streptococcus thermophilus* strain might have the potential to reduce signs of colitis (Bailey et al., 2017). These results indicated that specific strain of *Streptococcus* might have different role in the development of UC. In the present study, we reported the association of *Streptococcus* genus level with UC and did not examine the specific *Streptococcus* species. Further extensive investigation of the identified candidate genera may obtain novel gut microbiota targets for UC treatment.

It is noted that the perturbation of gut microbial community may lead to metabolite alterations. The disordered metabolites may enter the host, then modulate intestine epithelial cells and inflammation in the disease progression (Arpaia et al., 2013). Therefore, we examined the metabolite profiles across fecal samples from normal healthy subjects, treatment-naïve UC patients and mesalamine-responded UC patients. By LC-MS metabolomics, we noted that a batch of metabolites were significantly different in treatment-naïve UC patients, and mesalamine restored the changes of 102 candidate metabolites. Many amino acids in serum such as leucine, isoleucine, glycine and histidine have been implicated in inflammatory bowel diseases (Dawiskiba et al., 2014; Probert et al., 2018). In the present study, L-isoleucine and L-histidine in fecal samples were remarkably changed in treatment-naïve UC patients and could be restored by mesalamine intervention. The findings indicated their potential role in UC and might serve as potential therapeutic targets. Dysmetabolism of bile acids has also been found in UC pathogenesis (Pavlidis et al., 2015). Duboc, et al., 2013 reported that the level of secondary bile acids was decreased in fecal and serum samples of UC patients, and Sinha, et al., 2020 observed lithocholic acid and deoxycholic acid were reduced in stool samples of UC patients (Duboc et al., 2013; Sinha et al., 2020). Our results partially conformed to their findings. We noted that cholic acid and deoxycholic acid concentrations were reduced in UC patients and could be restored by mesalamine intervention. Besides, we also obtained many other mesalamine reversed candidates which had been implicated in UC. For example, styrene is a benzenoid compound produced by decarboxylation of cinnamic acid and has been reported positively correlated with disease activity in UC (De Preter et al., 2015). In present study, we noted that the level of styrene was higher in treatment-naïve UC patients than normal healthy controls and positively correlated with UC Mayo score. It is worth noting that most of the candidate metabolites were not only significantly correlated with UC Mayo score, but also correlated with specific bacteria genera. Furthermore, we observed that the candidate genera and metabolites were enriched in many similar KEGG pathways such as amino acid metabolism and secondary metabolites biosynthesis, indicating their high functional correlation. The results suggested that mesalamine might exert a beneficial role in UC by modulating gut microbiota genera and relevant metabolites in different pathways. In-depth extensive investigation of the identified candidates may provide us novel targets for UC treatment.

Finally, we identified a gut microbiota signature composed of five genera that might be used to discriminate treatment-naïve UC patients from both normal healthy controls and mesalamine-responded UC patients. However, our study has some inherent limitations. Firstly, the findings in the present study were based on the limited samples with no further functional experiments, and the identified genera and metabolites candidates should be further verified in a comprehensive and large scale investigation. Second, this exploratory study composed of two cross-sectional trials. Current results could only support correlation, not the causality. Besides, the cross-sectional design ignored the pre-treatment clinical information of mesalamine group. Potential imbalance may exist between UC group and mesalamine group, which may affect the results. Longitudinal design should be considered in future studies. Third, the course of disease might affect the gut microbiota and metabolites, and further study should be performed in UC patients with matched course of disease to validate our findings.

CONCLUSION

In summary, 16S rRNA sequencing and metabolomics approaches were integrated to detect the perturbance of gut microbiota and metabolites in stool samples across normal healthy controls, treatment-naïve UC patients and mesalamine-responded UC patients. We observed significant changes of gut microbiota and metabolites in UC patients. Mesalamine might exert beneficial effects in UC by modulating gut microbiota and correlated metabolites in different pathways. We also identified a gut microbiota signature to discriminate treatment-naïve UC from normal healthy controls and mesalamine-responded UC patients. Our results may shed new lights on the mechanism of mesalamine in UC treatment and provide us novel therapeutic targets.

DATA AVAILABILITY STATEMENT

The datasets presented in this study can be found in online repositories. The names of the repository/repositories and accession number(s) can be found below: NCBI SRA database, under the accession (BioProject PRJNA681685).

ETHICS STATEMENT

The studies involving human participants were reviewed and approved by Ethics Committee of Longhua Hospital. The

patients/participants provided their written informed consent to participate in this study.

AUTHOR CONTRIBUTIONS

LD and YT collected and prepared the samples, analyzed the data and wrote the manuscript. WZ, YD, and QS collected the samples. ZT interpreted the data. MZ and GJ designed the study, interpreted the data, wrote and revised the manuscript. All authors contributed to the article and approved the submitted version.

FUNDING

This work was supported by Three Year Action Plan of Shanghai Hygiene (ZY(2018-2020)-CCCX-2002-01) and Evidence-based Special Project of National Traditional Chinese Medicine (2019xzzx-xh012).

SUPPLEMENTARY MATERIAL

The Supplementary Material for this article can be found online at: https://www.frontiersin.org/articles/10.3389/fphar.2020.620724/full#supplementary-material.

REFERENCES

Adams, S. M., and Bornemann, P. H. (2013). Ulcerative colitis *Am. Fam. Physician* 87, 699–705.

Arpaia, N., Campbell, C., Fan, X., Dikiy, S., Van Der Veeken, J., Deroos, P., et al. (2013). Metabolites produced by commensal bacteria promote peripheral regulatory T-cell generation. *Nature* 504, 451–455. doi:10.1038/nature12726

Bailey, J. R., Vince, V., Williams, N. A., and Cogan, T. A. (2017). Streptococcus thermophilus NCIMB 41856 ameliorates signs of colitis in an animal model of inflammatory bowel disease. *Benef. Microbes*. 8, 605–614. doi:10.3920/BM2016.0110

Bajer, L., Kverka, M., Kostovcik, M., Macinga, P., Dvorak, J., Stehlikova, Z., et al. (2017). Distinct gut microbiota profiles in patients with primary sclerosing cholangitis and ulcerative colitis. *World J. Gastroenterol*. 23, 4548–4558. doi:10.3748/wjg.v23.i25.4548

Baron, J. H., Connell, A. M., and Lennard-Jones, J. E. (1964). Variation between observers in describing mucosal appearances in proctocolitis. *Br. Med. J.* 1, 89–92. doi:10.1136/bmj.1.5375.89

Chen, S., Zhou, Y., Chen, Y., and Gu, J. (2018). Fastp: an ultra-fast all-in-one FASTQ preprocessor. *Bioinformatics* 34, i884–i890. doi:10.1093/bioinformatics/bty560

Dawiskiba, T., Deja, S., Mulak, A., Ząbek, A., Jawień, E., Pawełka, D., et al. (2014). Serum and urine metabolomic fingerprinting in diagnostics of inflammatory bowel diseases. *World J. Gastroenterol*. 20, 163–174. doi:10.3748/wjg.v20.i1.163

De Preter, V., Machiels, K., Joossens, M., Arijs, I., Matthys, C., Vermeire, S., et al. (2015). Faecal metabolite profiling identifies medium-chain fatty acids as discriminating compounds in IBD. *Gut* 64, 447–458. doi:10.1136/gutjnl-2013-306423

Derikx, L. A., Dieleman, L. A., and Hoentjen, F. (2016). Probiotics and prebiotics in ulcerative colitis. *Best Pract. Res. Clin. Gastroenterol*. 30, 55–71. doi:10.1016/j.bpg.2016.02.005

Duboc, H., Rajca, S., Rainteau, D., Benarous, D., Maubert, M. A., Quervain, E., et al. (2013). Connecting dysbiosis, bile-acid dysmetabolism and gut inflammation in inflammatory bowel diseases. *Gut* 62, 531–539. doi:10.1136/gutjnl-2012-302578

Edgar, R. C. (2013). UPARSE: highly accurate OTU sequences from microbial amplicon reads. *Nat. Methods* 10, 996–998. doi:10.1038/nmeth.2604

Fite, A., Macfarlane, S., Furrie, E., Bahrami, B., Cummings, J. H., Steinke, D. T., et al. (2013). Longitudinal analyses of gut mucosal microbiotas in ulcerative colitis in relation to patient age and disease severity and duration. *J. Clin. Microbiol.* 51, 849–856. doi:10.1128/JCM.02574-12

Hoivik, M. L., Moum, B., Solberg, I. C., Henriksen, M., Cvancarova, M., Bernklev, T., et al. (2013). Work disability in inflammatory bowel disease patients 10 years after disease onset: results from the IBSEN Study. *Gut* 62, 368–375. doi:10.1136/gutjnl-2012-302311

Kaur, A., and Goggolidou, P. (2020). Ulcerative colitis: understanding its cellular pathology could provide insights into novel therapies. *J. Inflamm*. 17, 15. doi:10.1186/s12950-02000246-4

Kojima, A., Nakano, K., Wada, K., Takahashi, H., Katayama, K., Yoneda, M., et al. (2012). Infection of specific strains of Streptococcus mutans, oral bacteria, confers a risk of ulcerative colitis. *Sci. Rep*. 2, 332. doi:10.1038/srep00332

Kotze, P. G., Steinwurz, F., Francisconi, C., Zaltman, C., Pinheiro, M., Salese, L., et al. (2020). Review of the epidemiology and burden of ulcerative colitis in Latin America. *Therap. Adv. Gastroenterol.* 13, 1756284820931739. doi:10.1177/1756284820931739

Langille, M. G., Zaneveld, J., Caporaso, J. G., Mcdonald, D., Knights, D., Reyes, J. A., et al. (2013). Predictive functional profiling of microbial communities using 16S rRNA marker gene sequences. *Nat. Biotechnol*. 31, 814–821. doi:10.1038/nbt.2676

Lynch, W. D., and Hsu, R. (2020). *Ulcerative colitis*. Florida, FL: StatPearls Publishing.

Ma, H. Q., Yu, T. T., Zhao, X. J., Zhang, Y., and Zhang, H. J. (2018). Fecal microbial dysbiosis in Chinese patients with inflammatory bowel disease. *World J. Gastroenterol*. 24, 1464–1477. doi:10.3748/wjg.v24.i13.1464

Magoc, T., and Salzberg, S. L. (2011). FLASH: fast length adjustment of short reads to improve genome assemblies. *Bioinformatics* 27, 2957–2963.

Nakashima, J., and Preuss, C. V. (2020). *Mesalamine (USAN)*. Florida, FL: StatPearls.

Nemoto, H., Kataoka, K., Ishikawa, H., Ikata, K., Arimochi, H., Iwasaki, T., et al. (2012). Reduced diversity and imbalance of fecal microbiota in patients with ulcerative colitis. *Dig. Dis. Sci*. 57, 2955–2964. doi:10.1007/s10620-012-2236-y

Pavlidis, P., Powell, N., Vincent, R. P., Ehrlich, D., Bjarnason, I., and Hayee, B. (2015). Systematic review: bile acids and intestinal inflammation-luminal aggressors or regulators of mucosal defence? *Aliment. Pharmacol. Ther*. 42, 802–817. doi:10.1111/apt.13333

Porter, R. J., Kalla, R., and Ho, G. T. (2020). Ulcerative colitis: recent advances in the understanding of disease pathogenesis F1000Res. 9, F1000 Faculty Rev-294. doi:10.12688/f1000research.20805.1

Probert, F., Walsh, A., Jagielowicz, M., Yeo, T., Claridge, T. D. W., Simmons, A., et al. (2018). Plasma nuclear magnetic resonance metabolomics discriminates between high and low endoscopic activity and predicts progression in a prospective cohort of patients with ulcerative colitis. *J. Crohns. Colitis*. 12, 1326–1337. doi:10.1093/ecco-jcc/jjy101

Rutgeerts, P., Sandborn, W. J., Feagan, B. G., Reinisch, W., Olson, A., Johanns, J., et al. (2005). Infliximab for induction and maintenance therapy for ulcerative colitis. *N. Engl. J. Med*. 353, 2462–2476. doi:10.1056/NEJMoa050516

Scaldaferri, F., Gerardi, V., Mangiola, F., Lopetuso, L. R., Pizzoferrato, M., Petito, V., et al. (2016). Role and mechanisms of action of *Escherichia coli* Nissle 1917 in the maintenance of remission in ulcerative colitis patients: an update. *World J. Gastroenterol*. 22, 5505–5511. doi:10.3748/wjg.v22.i24.5505

Shang, Q., Sun, W., Shan, X., Jiang, H., Cai, C., Hao, J., et al. (2017). Carrageenan-induced colitis is associated with decreased population of anti-inflammatory bacterium, Akkermansia muciniphila, in the gut microbiota of C57BL/6J mice. *Toxicol. Lett*. 279, 87–95. doi:10.1016/j.toxlet.2017.07.904

Shen, Z. H., Zhu, C. X., Quan, Y. S., Yang, Z. Y., Wu, S., Luo, W. W., et al. (2018). Relationship between intestinal microbiota and ulcerative colitis: mechanisms and clinical application of probiotics and fecal microbiota transplantation. *World J. Gastroenterol*. 24, 5–14. doi:10.3748/wjg.v24.i1.5

Sinha, S. R., Haileselassie, Y., Nguyen, L. P., Tropini, C., Wang, M., Becker, L. S., et al. (2020). Dysbiosis-induced secondary bile acid deficiency promotes intestinal inflammation. *Cell Host. Microbe*. 27, 659–e5. doi:10.1016/j.chom.2020.01.021

Sun, M., Du, B., Shi, Y., Lu, Y., Zhou, Y., and Liu, B. (2019). Combined signature of the fecal microbiome and plasma Metabolome in patients with ulcerative colitis. *Med. Sci. Mon. Int. Med. J. Exp. Clin. Res.* 25, 3303–3315. doi:10.12659/MSM.916009

Ungaro, R., Mehandru, S., Allen, P. B., Peyrin-Biroulet, L., and Colombel, J. F. (2017). Ulcerative colitis. *Lancet* 389, 1756–1770. doi:10.1016/S0140-6736(16)32126-2

Wang, Q., Garrity, G. M., Tiedje, J. M., and Cole, J. R. (2007). Naive Bayesian classifier for rapid assignment of rRNA sequences into the new bacterial taxonomy. *Appl. Environ. Microbiol.* 73, 5261–5267. doi:10.1128/AEM.00062-07

Wu, K. C., Liang, J., Ran, Z. H., Qian, J. M., Yang, H., Chen, M. H., and He, Y. (2018). For inflammatory bowel disease group of Chinese society of gastroenterology of Chinese medical association Chinese consensus on diagnosis and treatment of inflammatory bowel disease (Beijing, 2018). *Chin. J. Pract. Intern. Med.* 38, 796–813. doi:10.19538/j.nk2018090106

Conflict of Interest: The authors declare that the research was conducted in the absence of any commercial or financial relationships that could be construed as a potential conflict of interest.

frontiers in Pharmacology

BRIEF RESEARCH REPORT
published: 26 January 2021
doi: 10.3389/fphar.2020.587445

Case Report: IL-21 and Bcl-6 Regulate the Proliferation and Secretion of Tfh and Tfr Cells in the Intestinal Germinal Center of Patients With Inflammatory Bowel Disease

*Youguang Yang[1], Xiaodan Lv[2], Lingling Zhan[2], Lan Chen[1], Hui Jin[1], Xinping Tang[1], Qingqing Shi[1], Qiyuan Zou[1], Jiqiao Xiang[1], WeiWei Zhang[1], Zhaojing Zeng[1], Haixing Jiang[1] and Xiaoping Lv[1]**

[1]Department of Gastroenterology, The First Affiliated Hospital of Guangxi Medical University, Nanning, China, [2]Department of Clinical Experimental Medicine, The First Affiliated Hospital of Guangxi Medical University, Nanning, China

OPEN ACCESS

Edited by:
Yinglei Miao,
First Affiliated Hospital of Kunming Medical University, China

Reviewed by:
Guang Chen,
Huazhong University of Science and Technology, China
Zhanju Liu,
Tongji University, China

***Correspondence:**
Xiaoping Lv
lxxp58@hotmail.com

Specialty section:
This article was submitted to Gastrointestinal and Hepatic Pharmacology, a section of the journal Frontiers in Pharmacology

Received: 26 July 2020
Accepted: 14 December 2020
Published: 26 January 2021

Citation:
Yang Y, Lv X, Zhan L, Chen L, Jin H, Tang X, Shi Q, Zou Q, Xiang J, Zhang W, Zeng Z, Jiang H and Lv X (2021) Case Report: IL-21 and Bcl-6 Regulate the Proliferation and Secretion of Tfh and Tfr Cells in the Intestinal Germinal Center of Patients With Inflammatory Bowel Disease. Front. Pharmacol. 11:587445. doi: 10.3389/fphar.2020.587445

Objective: This study aimed to investigate the effect of interleukin (IL)-21 and B cell lymphoma protein-6 on germinal center follicular helper T (Tfh) cells and follicular regulatory T (Tfr) cells and its relationship with the clinical features of inflammatory bowel disease (IBD).

Methods: The expression of peripheral blood cytokines IL-21 and Bcl-6 mRNA was detected by reverse transcription–polymerase chain reaction. The distribution characteristics of Tfh and Tfr cells were detected using the triple immunofluorescence staining analysis.

Results: The expression of IL-21 and Bcl-6 mRNA was upregulated in the ulcerative colitis (UC) and Crohn disease (CD) groups compared with that in the control group. Triple immunofluorescence staining showed that the number of Tfh cells in the intestinal germinal center obviously increased in the UC and CD groups compared with that in the control group, whereas the number of Tfr cells reduced.

Conclusion: This study suggested that the Tfr and Tfh cells might be involved in the regulation of IBD. Bcl-6 and IL-21 can regulate the Tfh/Tfr ratio in the intestinal germinal center, promoting the occurrence and development of IBD.

Keywords: Bcl-6, follicular helper T cells, follicular regulatory T cells, germinal center, IL-21, inflammatory bowel disease

INTRODUCTION

Inflammatory bowel disease (IBD) is characterized by inflammation and abnormal bowel patterns. However, its etiology and pathogenesis are still not clear, possibly due to intestinal microbial infection or physicochemical factors (such as certain foods and drugs), coupled with a variety of factors related to individual genetic susceptibility, or caused by excessive activation of intestinal mucosal immune response (Baumgart and Sandborn, 2007) IBD includes ulcerative colitis (UC) and Crohn disease (CD). The main difference between UC and CD is that UC is mainly located in the colon and rectum, while CD can affect the entire digestive tract (Baumgart et al., 2012; Ordás et al.,

2012). Two new types of T helper cells have been found in the germinal center of lymphoid tissues: follicular helper T (Tfh) cells and follicular regulatory T (Tfr) cells, which differentiate and proliferate in lymphoid follicles. (Deenick and Ma, 2011; Linterman et al., 2011) These two types of cells are closely related to various autoimmune diseases (Wang et al., 2014; Dhaeze et al., 2015). Despite minimal research on the Tfr/Tfh ratio in patients with IBD, some scholars (Ozaki et al., 2002; Eto et al., 2011) reported that changes in the levels of IL-2 and IL-6 in the local microenvironment of IBD might be involved in the differentiation of Tfh cells and the abnormal expression of transcription factors such as Bcl-6 and c-MAF. Treg cells may also be involved in the abnormal regulation of Tfh cells. Based on the characteristics of IBD with excessive immune damage and autoimmune response, it is reasonable to speculate that Tfh and Tfr cells are involved in the progression of IBD. The proportion of Tfh and Tfr cells in the peripheral blood of patients with IBD and healthy population was detected by flow cytometry to determine the correlation between Tfh/Tfr ratio and IBD. The expression of IL-21 and Bcl-6 was assessed by reverse transcription–polymerase chain reaction (RT-PCR) in patients. Moreover, triple immunofluorescence staining analysis was performed to detect the distribution characteristics of Tfh cells in the germinal center and Tfr cells in the intestinal tissue of patients with IBD by illustration there specia cell phenotype CD57/FoxP3. The present study might provide a theoretical basis for the clinical treatment of IBD by the intervention of Tfh and Tfr cells.

MATERIALS AND METHODS

Materials

Blood samples were collected from 134 patients with IBD in the Department of Gastroenterology, the First Affiliated Hospital of Guangxi Medical University, China. Among them, 79 were males and the remaining 55 were females. The age ranged from 21 to 65 years, with an average age of 38.12 ± 7.23 years colorectal inflammation tissue of 111 patients were collected by endoscopy. Among them, 69 were males and the remaining were females. The age ranged from 21 to 68 years, with an average age of 37.08 ± 6.03 years. In addition, 90 cases of blood samples and 80 cases of colorectal tissue samples were collected from healthy controls. The subjects were healthy people who had been treated in the First Affiliated Hospital of Guangxi Medical University at the same time, who had excluded tumor, autoimmune disease and family history of IBD. There was no significant difference in age and gender between IBD group and healthy control group ($p > 0.05$). All specimens obtained were approved by ethics committee of the First Affiliated Hospital of Guangxi Medical University, and all patients were informed and agreed.

Methods

Expression of Peripheral Blood Cytokines IL-21 and Bcl-6 mRNA Was Detected by RT-PCR in Patients With IBD and Healthy Controls

The total RNA was extracted from the peripheral blood using chloroform and TRIzol solution (TaKaRa Bio Inc., Shiga, Japan). A first-strand cDNA synthesis was performed with 1 μg of total RNA. The cDNA samples were thereafter amplified in the ABI Prism 7500 Sequence Detection System (Applied Biosystems, MA, United States) for 40 cycles (95°C for 3 s and 60°C for 34 s) with specific oligonucleotide primers (TaKaRa Bio Inc.). Each sample was analyzed in triplicate, with β-actin used for normalization. The relative quantification of target genes was determined using the ΔΔCT method. The primers used in RT-PCR analyses are listed in **Table 1**.

Triple Immunofluorescence Staining Analysis of the Distribution Characteristics of Tfh/Tfr Ratio in the Germinal Center

IBD intestinal tissue was taken and fixed with paraformaldehyde. The paraffin-embedded sections were stained with immunohistochemistry. The tissue sections were washed with PBS, water, and then skimmed milk. Two groups of three fluorescent-labeled antibodies were added at room temperature: the first group comprised the primary antibodies to CD4 (BioLegend, United States) , CXCR5, and FOXP3 (eBioscience, United States); the second group comprised the primary antibodies in three different colors: green fluorescent protein labeling, Cy3-labeled red fluorescence, and AMCA blue fluorescence. The secondary antibodies were stained in three different colors, representing different Tfr and Tfh cells. The results were analyzed using average optical density values.

STATISTICAL ANALYSIS

All data were expressed as mean ± standard deviation. Comparisons between groups were performed using one-way analysis of variance followed by the Student–Newman–Keuls post hoc test. p values less than 0.05 were considered statistically significant. All the statistical analyses were performed using the statistical software package SPSS version 16.0 (SPSS Inc., IL, United States).

RESULTS

Effect of IBD on the mRNA Expression of IL-21 and Bcl-6

The expression of IL-21 and Bcl-6 mRNA was examined in the peripheral blood by RT-PCR (**Figures 1**, **2**). The expression of IL-21 and Bcl-6 mRNA was low in the control group, while it significantly increased in the UC and CD groups ($p < 0.05$). The reason probably is that Tfh can secrete IL-21R in an autocrine manner at the same time, IL-21R can also stimulate the production of Bcl-6, which can also secrete Tfh. Therefore, it was hypothesized that IL-21 and Bcl-6 played an important role in the pathogenesis of IBD.

Triple Immunofluorescence Staining Analysis of the Distribution Characteristics of Tfh/Tfr Ratio in the Germinal Center

Triple immunofluorescence staining was performed to analyze the distribution characteristics of Tfh/Tfr ratio in the germinal

TABLE 1 | Primer sequences for PCR.

Gene name	Direction	Sequences (5′–3′)
IL-21	Forward	CACAGACTAACATGCCCTTCAT
	Reverse	GAATCTTCACTTCCGTGTGTTCT
Bcl-6	Forward	CGGAAGGGTCTGGTTAG
	Reverse	TGAGCACGATGAACTTGTAT
B-actin	Forward	CCCATACCCACCATCACACC
	Reverse	GAGAGGGAAATCGTGCGTGAC

β-actin; IL, interleukin; PCR, polymerase chain reaction.

center of intestinal tissues (**Figure 3**). Red fluorescence indicated CXCR5; green fluorescence indicated CD4; and blue fluorescence indicated FOXP3/CD57. The coincidence of white fluorescence with red, blue, or green fluorescence indicated that the site was Tfh or Tfr cells. When the three channels were coincident, the white light appeared in the germinal center of the lymph nodes. We used the average of optical density to evaluate the intensity of cell staining in each groupStaining of the intestinal tissue samples from the normal control group showed that the staining intensity of Tfr cells in the germinal center was obviously upregulated compared with the UC and CD groups ($p < 0.05$). However, the staining intensity of Tfh cells in the germinal center from the UC and CD groups significantly increased compared with the control group ($p < 0.05$).

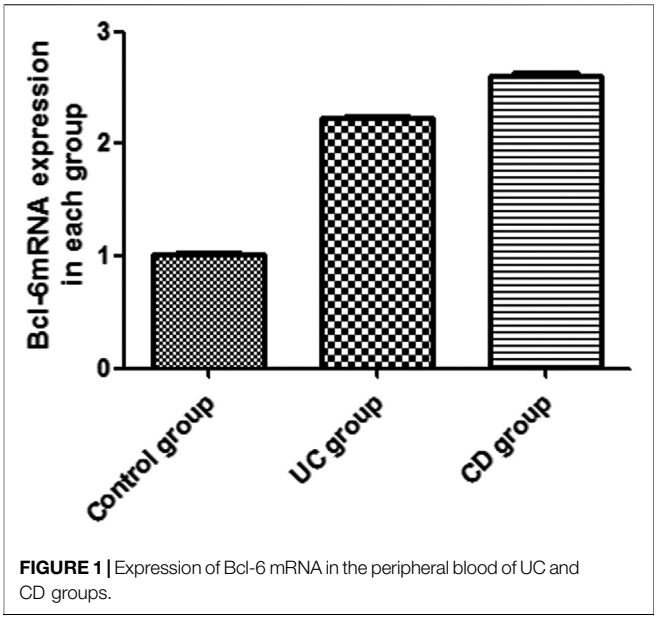

FIGURE 1 | Expression of Bcl-6 mRNA in the peripheral blood of UC and CD groups.

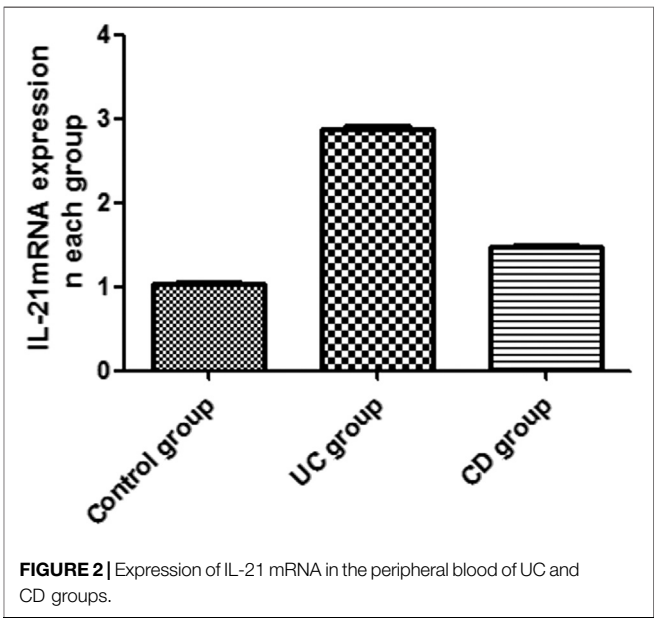

FIGURE 2 | Expression of IL-21 mRNA in the peripheral blood of UC and CD groups.

DISCUSSION

IBD is a disease with autoimmune characteristics because of immune response imbalance. The incidence of IBD is continuously rising; however, its etiology and pathogenesis are not clear.

The Tfh cells are regulated by B cells, Inducible costimulator, SLAM-associated protein, and PD-1, whose surface marker is CD4+CD57+CXCR5. They can secrete IL-21, IL-6, and IL-27 (Auderset et al., 2013). IL-21, a T-cell–derived cytokine, is produced in excess in inflammatory bowel diseases, which can be highly expressed in intestinal mucosa of IBD patients (Chelsky et al., 2007). The main function of Tfh cells is to form B cells with high-affinity antibodies and lack of differentiation into autoreactive plasma cells and memory B cells with high affinity and long-term protective effect against infection. Tfh cells also play a key role in promoting the formation of germinal center, immunoglobulin class switching, and maintaining long-term humoral immune response (Cannons et al., 2013). It has been found that IL-21 and Bcl-6 are the key factors regulating the development and function of Tfh cells. The research shows that Tfh cells form but decline faster in the absence of IL-21 (Linterman et al., 2010). The most probably reason is that IL-21 is involved in the differentiation of B cells, which are produced by the Tfh cells and play a key role in the survival of Tfh cells. It is involved in the transformation of CD4+T cells into Tfh cells, which is essential for the growth and development of Tfh cells (Yu et al., 2015).

Tfr is a newly discovered regulatory T cell subgroup. Tfr surface markers, including Tfh cell-related molecules, play an essential role in the regulation of germinal center response (Linterman et al., 2011; Linterman et al., 2012). Tfr cells can express CD8, CXCR5, Bcl-6, and FOXP3, and are located in the germinal center, inhibiting the immune response (Deaglio et al., 2007). Tfr cells are characterized by the overlap of surface phenotype and Tfh cells, so that Tfr and Tfh have dual functional characteristics. Tfr cells can regulate the number of Tfh cells and the response of germinal centers (Szanya et al., 2002; Borsellino et al., 2007; Deaglio et al., 2007). If FOXP3+Bcl-6+Treg lacks in the follicles, the germinal centers lose the role of inhibiting the immune response, resulting in the secretion of antibodies from a large number of B cells. Therefore, it is believed that FOXP3+Bcl-6+ Treg is an autoimmune regulatory signal (Wollenberg et al., 2011). However, Tfr and Tfh cells have the

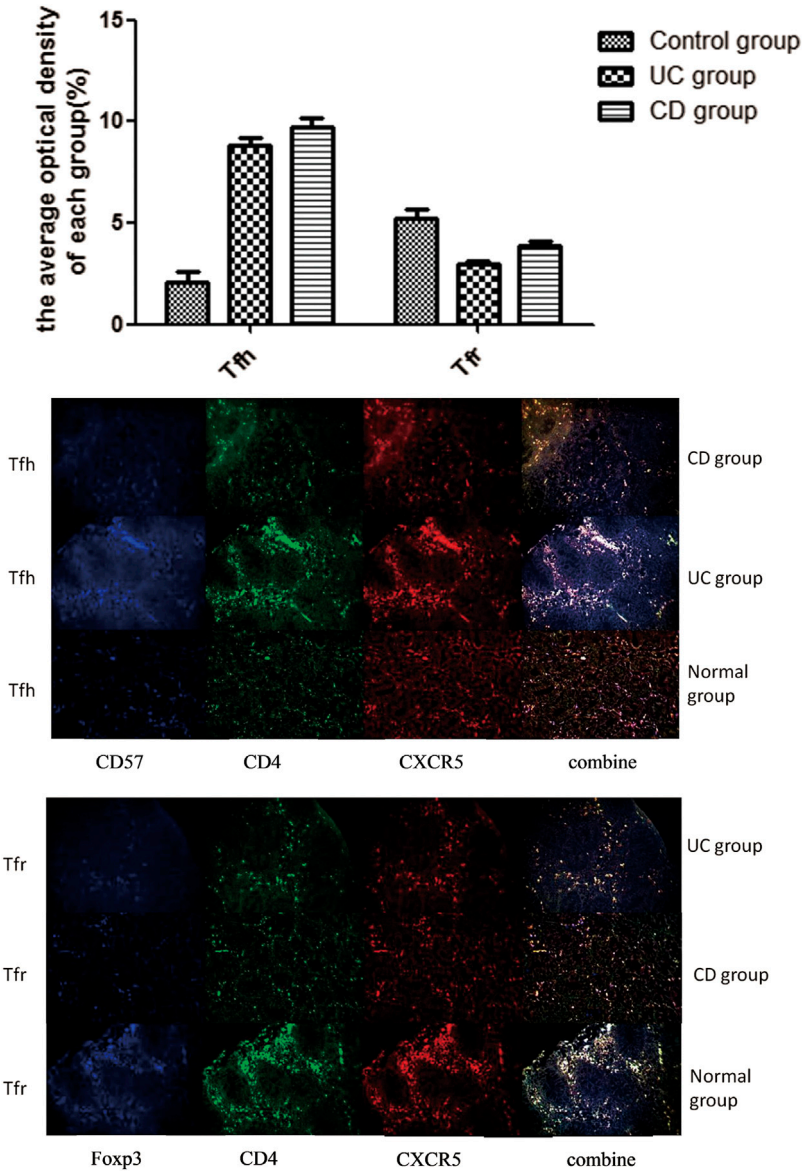

FIGURE 3 | Tfh and Tfr triple immunofluorescence staining (×20).

same phenotypic characteristics, which may be related to the germinal centers (Chung et al., 2011). A certain number of Tfr cells exist in the circulation, which can be activated by CD28 and ICOS and inhibited by PD-1 and PD-L1 (Sage et al., 2012). The specific inhibition needs further investigation. A recent study showed that Tfr cells mediated Tfh cell and B cell responses, regulating the germinal center reaction. Therefore, Tfr cell dysregulation is critical to the development of autoimmune diseases (Sage and Sharpe, 2016).

Tfh can secrete IL-21R in an autocrine manner, which promotes the proliferation of Tfh cells with high expression of CXCR5 and ICOS and their migration to lymph nodes and germinal centers (Sarra et al., 2012; Spolski et al., 2012). However, Tfh cells not only increase the expression of Bcl-6 but also increase the expression of Tfh surface protein gene. The reason may be that Bcl-6 is necessary for the differentiation of CD4+T cells into Tfh cells *in vivo* (Johnston et al., 2009). The high expression of Bcl-6 can induce the formation of Tfh phenotype cells (such as CXCR5, PD-1, and CXCR4) (Nurieva et al., 2009). The initial T cells receive dendritic cells presenting antigen and ICOS stimulation signals and begin to express Bcl-6 at high levels (Choi et al., 2013). It has been confirmed that transcription factors and regulatory factors Bcl-6 and IL-21 are important factors in the regulation of Tfh differentiation (Wollenberg et al., 2011; Ding et al., 2014). The changes in the expression of IL-21 and Bcl-6 mRNA in the peripheral blood were measured in the present study to evaluate the numbers of Tfh cells. The results showed an increase in the expression of IL-21 and Bcl-6 mRNA, suggesting an increase in the

number of Tfh cells. The lack of Tfr cells might be due to the decrease in STAT3 in Treg cells (Hao et al., 2016). The loss of Tfr cells and the corresponding decrease in the cell phenotype FOPX3 lead to a decrease in the number of Treg cells (Aloulou et al., 2016). An increase in the number of Tfh cells promotes the activation of Bcl-6/IL-21, leading to the occurrence and development of IBD.

This study showed two kinds of cells in patients with IBD having abnormal regulation and differentiation: Tfh and Tfr. It was suggested that Tfh and Tfr might be involved in the immune regulation of IBD. These results also suggested that Bcl-6/IL-21 could regulate the changes in Tfh/Tfr ratio and promote the occurrence and development of IBD.

In summary, this study suggested that Tfh cells helped B cells in germinal center formation and produced high-affinity antibodies. However, Tfr cells inhibited B cells, which secreted IL-21, thereby reducing the inflammatory reaction. Tfr cells play a key role in negative immune regulation in the pathogenesis of IBD. This study may provide a theoretical basis for future studies on the pathogenesis and clinical treatment of IBD.

DATA AVAILABILITY STATEMENT

The raw data supporting the conclusions of this article will be made available by the authors, without undue reservation.

ETHICS STATEMENT

The studies involving human participants were reviewed and approved by Medical Ethics Committee of the First Affiliated Hospital of Guangxi Medical University. The patients/participants provided their written informed consent to participate in this study.

AUTHOR CONTRIBUTIONS

XL and LZ: designed and supervised the research. YY, XL, LC, QS, QZ, and JX: performed the experiments. YY, HJ, XT, and WZ: acquired and analyzed the data. YY: drafted and wrote the manuscript. HJ and XL: revised the manuscript for important intellectual content. All the authors have read and approved the final version to be published.

FUNDING

National Natural Science Foundation of China (No. 81860104, 81460114 and 81860120). Natural Science Foundation of Guangxi Zhuang Autonomous Region (No. 2017GXNSFAA198299 and 2017GXNSFBA198134). The Development and Application of Medical and Health Appropriate Technology Project in Guangxi Zhuang Autonomous Region (No. S2018049). The Youth Science Foundation of Guangxi Medical University (No. GXMUYSF201913 and GXMUYSF201908). The Self-financing Project of Health Commission of Guangxi Zhuang Autonomous Region (No. Z20200398).

ACKNOWLEDGMENTS

The authors would like to thank the members of Clinical Trial Service Unit of Guangxi Medical University for their technical support. All authors also wish to express their gratitude to the medical personnel of Department of Gastroenterology and Clinical Experimental Medicine, the First Affiliated Hospital of Guangxi Medical University for their theoretical guidance.

REFERENCES

Aloulou, M., Carr, E. J., Gador, M., Bignon, A., Liblau, R. S., Fazilleau, N., et al. (2016). Follicular regulatory t cells can be specific for the immunizing antigen and derive from naive t cells. *Nat. Commun.* 7, 10579. doi:10.1038/ncomms10579

Auderset, F., Schuster, S., Fasnacht, N., Coutaz, M., Charmoy, M., Koch, U., et al. (2013). Notch signaling regulates follicular helper t cell differentiation. *J. Immunol.* 191 (5), 2344–2350. doi:10.4049/jimmunol.1300643

Baumgart, D. C., and Sandborn, W. J. (2007). Inflammatory bowel disease: clinical aspects and established and evolving therapies, *Lancet* 369 (9573), 1641–1657. doi:10.1016/S0140-6736(07)60751-X

Baumgart, D. C., and Sandborn, W. J. (2012). Crohn's disease. *Lancet* 380, 1590–1605. doi:10.1016/S0140-6736(12)60026-9

Borsellino, G., Kleinewietfeld, M., Di Mitri, D., Sternjak, A., Diamantini, A., Giometto, R., et al. (2007). Expression of ectonucleotidase CD39 by Foxp3+ Treg cells: hydrolysis of extracellular ATP and immune suppression. *Blood* 110, 1225–1232. doi:10.1182/blood-2006-12-064527

Cannons, J. L., Lu, K. T., and Schwartzberg, P. L. (2013). T follicular helper cell diversity and plasticity. *Trends Immunol.* 34 (5), 200–207. doi:10.1016/j.it.2013.01.001

Chelsky, R., Wilson, R. A., Morton, M. J., Burry, K. A., and Giraud, G. D. (2007). A functional role for interleukin-21 in promoting the synthesis of the t-cell chemoattractant, mip-3α, by gut epithelial cells. *J. Crohns Colitis Suppl.* 132 (6), 166–175. doi:10.1053/j.gastro.2006.09.053

Choi, Y. S., Yang, J. A., and Crotty, S. (2013). Dynamic regulation of bcl6 in follicular helper cd4 t (tfh) cells. *Curr. Opin. Immunol.* 25 (3), 366–372. doi:10.1016/j.coi.2013.04.003

Chung, Y., Tanaka, S., Chu, F., Nurieva, R. I., Martinez, G. J., Rawal, S., et al. (2011). Follicular regulatory T cells expressing Foxp3 and Bcl-6 suppress germinal center reactions. *Nat. Med.* 17, 983–988. doi:10.1038/nm.2426

Deaglio, S., Dwyer, K. M., Gao, W., Friedman, D., Usheva, A., Erat, A., et al. (2007). Adenosine generation catalyzed by CD39 and CD73 expressed on regulatory T cells mediates immune suppression. *J. Exp. Med.* 204, 1257–1265. doi:10.1084/jem.20062512

Deenick, E. K., and Ma, C. S. (2011). The regulation and role of t follicular helper cells in immunity. *Immunology* 134 (4), 361–367. doi:10.1111/j.1365-2567.2011.03487.x

Dhaeze, T., Peelen, E., Hombrouck, A., Peeters, L., Van Wijmeersch, B., Lemkens, N., et al. (2015). Circulating follicular regulatory t cells are defective in multiple sclerosis. *J. Immunol.* 195 (3), 832–840. doi:10.4049/jimmunol.1500759

Ding, Y., Li, J., Yang, P. A., Luo, B., and Mountz, J. D. (2014). Il-21 promotes germinal center reaction by skewing the tfr/tfh balance in autoimmune bxd2 mice. *Arthritis Rheumatol.* 66 (9), 2601. doi:10.1002/art.38735

Eto, D., Lao, C., DiToro, D., Barnett, B., Escobar, T. C., Kageyama, R., et al. (2011). Il-21 and il-6 are critical for different aspects of b cell immunity and redundantly induce optimal follicular helper cd4 t cell (tfh) differentiation. *PloS One* 6, e17739. doi:10.1371/journal.pone.0017739

Hao, W., Xie, M. M., Hong, L., Dent, A. L., and Derya, U. (2016). Stat3 is important for follicular regulatory t cell differentiation. *PloS One* 11 (5), e0155040. doi:10.1371/journal.pone.0155040

Johnston, R. J., Poholek, A. C., Ditoro, D., Yusuf, I., Eto, D., Barnett, B., et al. (2009). Bcl6 and blimp-1 are reciprocal and antagonistic regulators of t follicular helper cell differentiation. *Science* 325 (5943), 1006–1010. doi:10.1126/science.1175870

Linterman, M. A., Beaton, L., Yu, D., Ramiscal, R. R., Srivastava, M., Hogan, J. J., et al. (2010). Il-21 acts directly on b cells to regulate bcl-6 expression and germinal center responses. *J. Exp. Med.* 207 (2), 353–363. doi:10.1084/jem.20091738

Linterman, M. A., Liston, A., and Vinuesa, C. G. (2012). T-follicular helper cell differentiation and the co-option of this pathway by non-helper cells. *Immunol. Rev.* 247 (1), 143–159. doi:10.1111/j.1600-065X.2012.01121.x

Linterman, M. A., Pierson, W., Lee, S. K., Kallies, A., Kawamoto, S., Rayner, T. F., et al. (2011). Foxp3+ follicular regulatory t cells control the germinal center response. *Nat. Med.* 17 (8), 975–982. doi:10.1038/nm.2425

Nurieva, R. I., Chung, Y., Martinez, G. J., Yang, X. O., Tanaka, S., Matskevitch, T. D., et al. (2009). Bcl6 mediates the development of t follicular helper cells. *Science* 325, 1001–1005. doi:10.1126/science.1176676

Ordás, I., Eckmann, L., Talamini, M., Baumgart, D. C., and Sandborn, W. J. (2012). Ulcerative colitis. *Lancet* 380 (9853), 1606. doi:10.1016/S0140-6736(12)60150-0

Ozaki, K., Spolski, R., Feng, C. G., Qi, C. F., Cheng, J., Sher, A., et al. (2002). A critical role for IL-21 in regulating immunoglobulin production. *Science* 298, 1630–1634. doi:10.1126/science.1077002

Sage, P. T., Francisco, L. M., Carman, C. V., and Sharpe, A. H. (2012). The receptor pd-1 controls follicular regulatory t cells in the lymph nodes and blood. *Nat. Immunol.* 14 (2), 152–161. doi:10.1038/ni.2496

Sage, P. T., and Sharpe, A. H. (2016). T follicular regulatory cells. *Immunol. Rev.* 271 (1), 246–259. doi:10.1111/imr.12411

Sarra, M., Cupi, M., Pallone, F., and Monteleone, G. (2012). Interleukin-21 in immune and allergic diseases. *Inflamm. Allergy Drug Targets* 11 (4), 313–319. doi:10.2174/187152812800959040

Spolski, R., Wang, L., Wan, C. K., Bonville, C. A., Domachowske, J. B., Kim, H. P., et al. (2012). Il-21 promotes the pathologic immune response to pneumovirus infection. *J. Immunol.* 188 (4), 1924. doi:10.4049/jimmunol.1100767

Szanya, V., Ermann, J., Taylor, C., Holness, C., and Fathman, C. G. (2002). The subpopulation of cd4+cd25+ splenocytes that delays adoptive transfer of diabetes expresses l-selectin and high levels of ccr7. *J. Immunol.* 169 (5), 2461–2465. doi:10.4049/jimmunol.169.5.2461

Wang, Z., Wang, Z., Diao, Y., Qian, X., Zhu, N., and Dong, W. (2014). Circulating follicular helper t cells in crohn's disease (cd) and cd-associated colorectal cancer. *Tumour Biol.* 35 (9), 9355–9359. doi:10.1007/s13277-014-2208-2

Wollenberg, I., Agua-Doce, A., Hernández, A., Almeida, C., Oliveira, V. G., Faro, J., et al. (2011). Regulation of the germinal center reaction by Foxp3+ follicular regulatory T cells. *J. Immunol.* 187, 4553–4560. doi:10.4049/jimmunol.1101328

Yu, J., He, S., Liu, P., Hu, Y., Wang, L., Wang, X., et al. (2015). Interleukin-21 promotes the development of ulcerative colitis and regulates the proliferation and secretion of follicular T helper cells in the colitides microenvironment. *Mol. Med. Rep.* 11 (2), 1049. doi:10.3892/mmr.2014.2824

Conflict of Interest: The authors declare that the research was conducted in the absence of any commercial or financial relationships that could be construed as a potential conflict of interest.

frontiers in Pharmacology

ORIGINAL RESEARCH
published: 22 February 2021
doi: 10.3389/fphar.2021.632569

Ginger Alleviates DSS-Induced Ulcerative Colitis Severity by Improving the Diversity and Function of Gut Microbiota

Shanshan Guo[1,2†], Wenye Geng[3†], Shan Chen[2†], Li Wang[2], Xuli Rong[4], Shuocun Wang[1], Tingfang Wang[1], Liyan Xiong[1], Jinghua Huang[2], Xiaobin Pang[4*] and Yiming Lu[1,2,5*]*

[1]School of Medicine, Shanghai University, Shanghai, China, [2]Eight Plus One Pharmaceutical Co., Ltd, Guilin, China, [3]Institutes of Integrative Medicine, Fudan University, Shanghai, China, [4]School of Pharmacy, Henan University, Kaifeng, China, [5]Department of Critical Care Medicine, Shanghai Tenth People's Hospital, School of Medicine, Tongji University, Shanghai, China

OPEN ACCESS

Edited by:
Lixin Zhu,
The Sixth Affiliated Hospital of Sun Yat-sen University, China

Reviewed by:
Antonella Marino Gammazza,
University of Palermo, Italy
Rinaldo Pellicano,
Molinette Hospital, Italy

***Correspondence:**
Jinghua Huang
Huangjh.81@188.com
Xiaobin Pang
pxb@vip.henu.edu.cn
Yiming Lu
bluesluyi@sina.com

[†]These authors have contributed equally to this work

Specialty section:
This article was submitted to Gastrointestinal and Hepatic Pharmacology, a section of the journal Frontiers in Pharmacology

Received: 23 November 2020
Accepted: 08 January 2021
Published: 22 February 2021

Citation:
Guo S, Geng W, Chen S, Wang L, Rong X, Wang S, Wang T, Xiong L, Huang J, Pang X and Lu Y (2021) Ginger Alleviates DSS-Induced Ulcerative Colitis Severity by Improving the Diversity and Function of Gut Microbiota. Front. Pharmacol. 12:632569. doi: 10.3389/fphar.2021.632569

The effects of ginger on gastrointestinal disorders such as ulcerative colitis have been widely investigated using experimental models; however, the mechanisms underlying its therapeutic actions are still unknown. In this study, we investigated the correlation between the therapeutic effects of ginger and the regulation of the gut microbiota. We used dextran sulfate sodium (DSS) to induce colitis and found that ginger alleviated colitis-associated pathological changes and decreased the mRNA expression levels of interleukin-6 and inducible nitric oxide synthase in mice. 16s rRNA sequencing analysis of the feces samples showed that mice with colitis had an intestinal flora imbalance with lower species diversity and richness. At the phylum level, a higher abundance of pathogenic bacteria, *Proteobacteria* and *firmicutes*, were observed; at the genus level, most samples in the model group showed an increase in *Lachnospiraceae_NK4A136_group*. The overall analysis illustrated an increase in the relative abundance of *Lactobacillus_murinus*, *Lachnospiraceae_bacterium_615*, and *Ruminiclostridium*_sp._*KB18*. These increased pathogenic bacteria in model mice were decreased when treated with ginger. DSS-treated mice showed a lower abundance of *Muribaculaceae*, and ginger corrected this disorder. The bacterial community structure of the ginger group analyzed with Alpha and Beta indices was similar to that of the control group. The results also illustrated that altered intestinal microbiomes affected physiological functions and adjusted key metabolic pathways in mice. In conclusion, this research presented that ginger reduced DSS-induced colitis severity and positively regulated the intestinal microbiome. Based on the series of data in this study, we hypothesize that ginger can improve diseases by restoring the diversity and functions of the gut microbiota.

Keywords: colitis, ginger, 16S rRNA, intestinal microbiota, dextran sodium sulfate

INTRODUCTION

Ulcerative colitis (UC) is an idiopathic chronic inflammatory disease of the colonic mucosa, which starts in the rectum and usually continuously extends proximally through part of or the entire colon. The most common clinical symptoms of UC include diarrhea, abdominal pain and bloody mucoid stools (Silverberg et al., 2005).

The exact cause of UC is still unknown, but extensive research suggested that aberrant responses to environmental factors, genetic susceptibility, abnormal immune regulation, the intestinal mucosal barrier, and intestinal microecological changes contribute to the occurrence and development of UC (Heller et al., 2005; Dong et al., 2019).

The expression of β-defensin produced by intestinal epithelial cells to promote host defense and limit bacterial invasion has also been reported to be upregulated in colon samples of UC patients (Rahman et al., 2010). Recent years, a more popular theory indicted that dysregulation of immune responses to microbes in the gut contributed to the occurrence, progression, and changes of UC (Zheng et al., 2017). The innate and adaptive immunity of the host can prevent the invasion of harmful bacteria, tolerate the normal microflora. However, imbalance intestinal flora reduces intestinal immunity, resulting in overstimulation of intestinal mucosal immune response, finally contributing to the disease (Zhang et al., 2015).

Human gut microbiome disorder is closely related to a variety of human diseases like autism and mood disorders (Mangiola et al., 2016), as well as obesity, diabetes and cardiovascular diseases (Hills et al., 2019). Series of researches proved that gut microbiome played an important role in the etiopathogenesis and treatment of inflammatory bowel disease (IBD) (Masoodi et al., 2019). Colonocyte metabolism regulates the content of anaerobic bacteria, and restoration of this colonocyte metabolism seems to be a novel therapeutic approach for IBD (Litvak et al., 2018). The intestinal microbiome is a diverse combination of bacteria, archaea, fungi, prokaryotes and viruses located in the intestines of all mammals. Fungi and bacteria occupy the main position, with the most abundant and diverse in the distal ileum and colon (Ley et al., 2006). Researchers established that intestinal microbiome was a strong inducer of pro-inflammatory T helper 17 cells (TH17) and regulatory T cells (Tregs) in the intestinal, which regulated type 2 responses and balanced mucosal immune responses by inducing type 3 retinoic acid-related orphan receptor-γt (RORγt) (+) Tregs cells and TH17 cells (Ohnmacht et al., 2015). The fecal microbiome of UC patients showed significantly less biodiversity than that of healthy people (Zhang and Li, 2014). A common difference between Crohn disease (CD) and UC patients was that they showed a decrease in the proportion of *Firmicutes* and a contrasting increase in that of *Proteobacteria* (Marchesi et al., 2016). *Akkermansia muciniphila*, the most abundant bacterial species in the human intestinal flora, has also been observed to decrease significantly in UC patients (Bajer et al., 2017).Various novel therapeutic approaches using prebiotic, probiotic, symbiotic and fecal microbiota transplantation (FMT) as complementary and alternative medicine has improved the condition of IBD patients (Khan et al., 2019). Probiotics can repair the damaged intestinal mucosal barrier in UC patients (Abraham and Quigley, 2017). A randomized controlled trial showed that FMT can be used to relieve the symptoms of UC patients in the short term (Narula et al., 2017).

Ginger (*Zingiber officinael*) is a perennial rhizome herb that has been globally used to treat gastrointestinal disorders such as nausea, dysentery, diarrhea and infections. Recent years, numerous studies proved that ginger exert anti-inflammatory, antioxidant, antitumor and antiulcer effects (Mohd Sahardi and Makpol, 2019; Nikkhah Bodagh et al., 2019). Ginger extract 6-gingerol has been proved to induce the apoptosis of gastric cancer cells through tumor necrosis factor (TNF)-related apoptosis-inducing ligand-(TRAIL-)(Prasad and Tyagi, 2015). The high content of 6-shogaol contributed to the antitumor activity of ginger against breast, cervical and hematological cancer *in vitro* (Sharifi-Rad et al., 2017; Mahomoodally et al., 2019). In addition to gastrointestinal disorders, ginger also alleviated fatty liver and irritable bowel syndrome (Nikkhah Bodagh et al., 2019). Ginger nanoparticles (GDNPs 2) have been shown to relieve colitis by reducing the expression of inflammatory cytokines in FVB/NJ mice colitis model (Zhang et al., 2016) while ginger exosome-like nanoparticles alleviated colitis in mice model via *Lactobacillus rhamnosus* (LGG) (Teng et al., 2018).

In this study, we elucidated the effects of ginger on intestinal microbiome in dextran sulfate sodium (DSS) induced mice. Fecal samples were collected and 16s rRNA sequencing was perform to investigate the changes in the gut microbiota.

MATERIALS AND METHODS

Biological Materials and Reagents

Ginger powder was purchased from Fujian Longzhi Biotechnology Co., Ltd (Fujian, China), and DSS salt (reagent grade) was purchased from MP Biomedicals (Santa Ana, CA, USA). Chloroform was purchased from Sinopharm Chemical Reagent (Co., Ltd.) (Shanghai, China). Sulfasalazine (SASP) was purchased from Dalian Meilun Biotechnology Co., Ltd (Dalian, China). RNAiso Plus, TB Green® Premix Ex Taq™ II, and PrimeScript™ RT Master Mix were purchased from Takara Biomedical Technology Co. (Beijing, China). QIAamp 96 PowerFecal QIAcube HT kit was purchased from Thermo Fisher Scientific Inc (Waltham MA, USA). All other chemicals and reagents used in this study were of analytical grade.

DSS Induced Colitis Mice Model

Male BALB/c mice (weighing 18–22 g) were purchased from the Experimental Animal Center, Second Military Medical University (Shanghai, China) and were maintained under a 12 h light-dark cycle at a temperature of 24°C. After adapting to the environment, 32 mice were divided into four groups. All animal experiments were conducted according to the Guide for the Care and Use of Laboratory Animals published by the National Institutes of Health, and the study protocol was approved by the Animal Care and Use Committee of the Shanghai University. The DSS-induced colitis mice model were established as previously described (Chassaing et al., 2014). Briefly, BALB/c mice were administered 2.5% DSS for 7 days, Weighing body weight and monitoring disease action index (DAI) daily.

After acclimatization for 3 days, mice were randomly divided into four groups as follows: 1) the control group, fed with standard rodent food and water, without any other treatment; 2) the model group provided free access to 2.5% DSS, and orally administered normal saline at 100 μL/20 g daily; 3) provided free

TABLE 1 | Primer sequences of inflammatory factor.

GAPDH	Forward primer	5′-AGG TCG GTG TGA ACG GAT TTG-3′
	Reverse primer	5′-TGT AGA CCA TGT AGT TGA GGT-3′
IL-6	Forward primer	5′-CCA ATG CTC TCC TAA CAG AT-3′
	Reverse primer	5′-TGT CCA CAA ACT GAT ATG CT-3′
iNOS	Forward primer	5′-GCC AGT CAG GTC TCA GCA AG-3′
	Reverse primer	5′- CGC ATG CAA TGT GTG CTT GT-3′

access to 2.5% DSS and orally administered SASP at 400 mg/kg daily; 4) provided free access to 2.5% DSS and orally administered ginger at 500 mg/kg daily. The dose of ginger was determined according to the method by Teng et al. (2018), because we had used the same ginger. Body weight and DAI were noted daily.

Sample Collection

At the end of the experiment, fresh fecal samples were collected from the mice in autoclaved Eppendorf tubes and stored at −80°C before mice were sacrificed. The length of each colon was measured and divided into three parts for real time-PCR, and histopathological studies.

Histopathological Studies

The colon tissues were formalin-fixed, paraffin-embedded, cut into 5 μm sections, and stained with hematoxylin and eosin (H&E). Colonic histological damage was observed under a light microscope.

RNA Extract and Real-Time PCR

Total RNA was extracted from the colon tissue using with RNAiso Plus and chloroform, and then the total RNA concentration and purity were measured using a NanoDrop 2000 spectrophotometer. cDNA was synthesized using the PrimeScript™ RT Master Mix. Real-time PCR was conducted using TB Green® Premix Ex Taq™ II, and the reaction solution contained 5 μL TB Green® Premix Ex Taq™ II, 0.5 μL of each primer (10 μM), 3 μL genomic DNA, and nuclease-free water (total volume 10 μL). The following primer sequences of *glyceraldehyde 3-phosphate dehydrogenase* (*GAPDH*), *interleukin 6* (*IL-6*) and *inducible nitric oxide synthase (iNOS)*, are presented in **Table 1**.

DNA Extraction

Total genomic DNA was extracted using QIAamp 96 PowerFecal QIA cube HT kit (Qiagen), and the integrity and concentration were measured using NanoDrop (Thermo Fisher Scientific) and 1% agarose gel electrophoresis (voltage, 120 V; electrophoresis time, 15 min).

16S rRNA Sequence

16S rRNA sequencing was performed by Oebiotech (Shanghai, China), the amplification of the V3V4 region (343–798) of the 16S rRNA gene was conducted with these primer pairs: 343F-5′-TACGGRAGGCAGCAG-3′, 798R-5′- AGGGTATCTAATCCT-3′. For library construction, the 30 μL PCR mixture consisted of 10–50 ng DNA template, 1 μL each of the forward and reverse PCR primers (5 pmol/μL each), 15 μL 2× Gflex PCR buffer (Takara), 0.6 μL Tks Gflex DNA polymerase (1.25 U/μL, Takara), and an appropriate volume of double distilled water (ddH2O) was added to make up the volume to 30 μL. The PCR program was as follows: initial denaturation at 94°C for 5 min, followed by 26 cycles of denaturation at 94°C for 30 s, annealing at 56°C for 30 s, extension at 72°C for 20 s, and a final extension at 72°C for 5 min.

Bioinformatic Analysis

Raw data were analyzed in the FASTQ format, and Trimmomatic software was used to preprocess paired-end reads. After trimming, paired-end reads were assembled using FLASH software, and reads with chimeras were detected and removed using UCHIME software. Clean reads were clustered into Operational Taxonomic Unit (OTUs) with 97% similarity cutoff using Vsearch software. The representative reads were selected using QIIME and blast against Greengenes or Silva (version 132) using a PDR classifier.

Statistical Analysis

All values are expressed as mean ± standard error of the mean (SEM). All statistical analyses were performed using GraphPad Prism. Differences between groups were analyzed using the two-tailed Student's *t*-test, and results with $p < 0.05$ were considered statistically significant.

Sequence Accession Numbers

The sequences generated in the present study are available through the NCBI Sequence Read Archive (accession number PRJNA680889).

RESULTS

Ginger Alleviates the Symptoms and Inhibits the Inflammation in DSS Induced Mice Colitis

As shown in **Figure 1A**, mice administered ginger and SASP shown a lower weight loss than the model group. The disease activity index (DAI) of mice administered Ginger and SASP were also decreased significantly (**Figure 1B**). Colon length shortening was less in ginger- and SASP-treated mice than the model group mice (**Figure 1C**). The spleen index of the ginger- and SASP-treated mice was significantly lower than the model group mice (**Figure 1D**).

Real-time PCR analysis revealed significantly increased mRNA levels of *IL-6* and *iNOS* in the model mice, whereas SASP and ginger treatment decreased the mRNA expression levels of these inflammatory cytokines. Ginger was less effective than SASP in decreasing the expression of *IL-6* (**Figure 1E**) but they were both equally effective in decreasing the expression level of *iNOS* (**Figure 1F**). Ginger-treated colitis mice exhibited less reduction in colon length than the model group mice (**Figure 1G**). Hematoxylin and eosin (H&E) staining of the colon tissues showed less severe intestinal mucosa injury (destruction of the epithelial structure and inflammatory cell

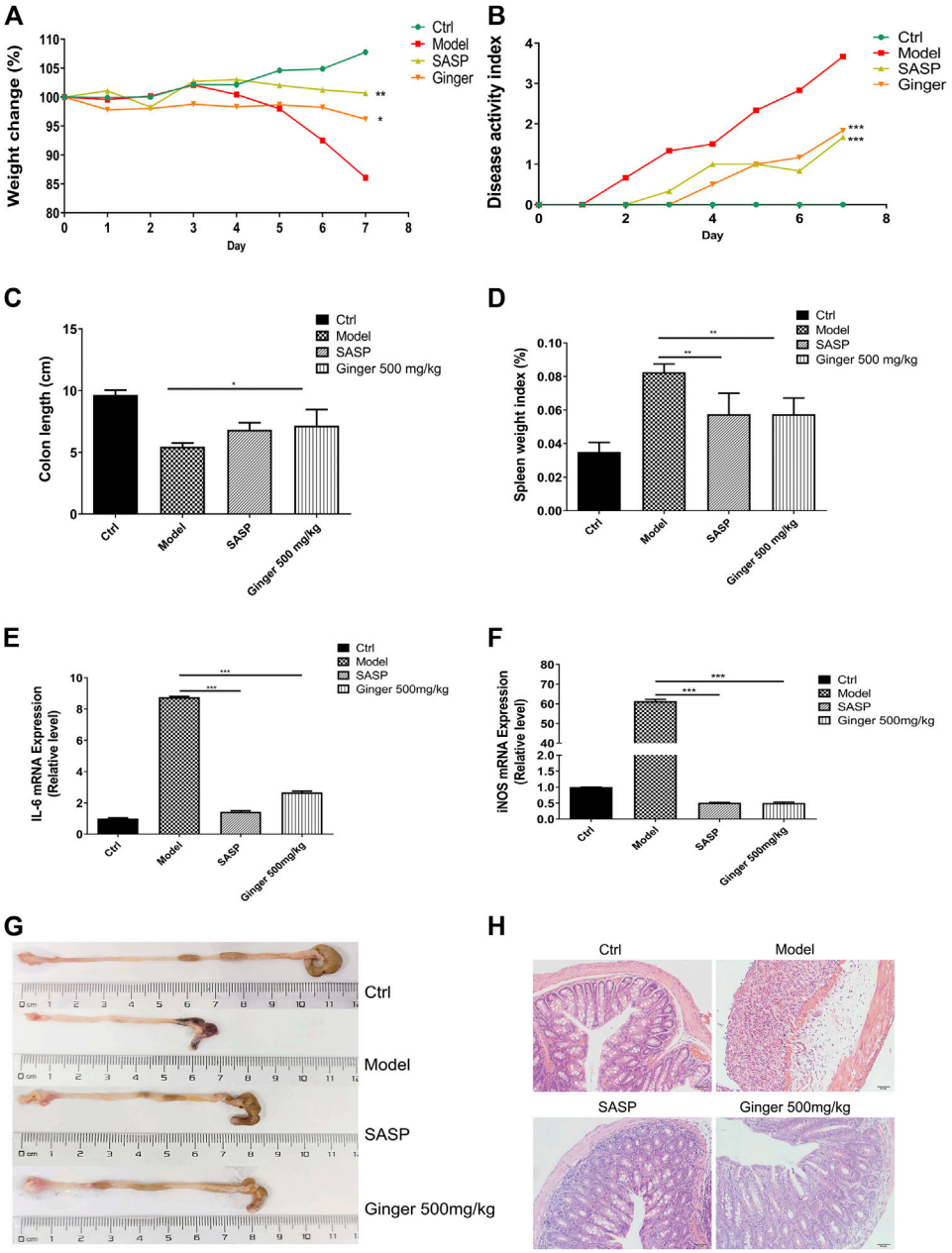

FIGURE 1 | Ginger alleviates the symptoms and reduced the mRNA expression of inflammatory cytokines in DSS induced mice colitis **(A)** Body weight of mice. **(B)** Disease activity index (DAI). **(C)** Colon length. **(D)** Spleen index. **(E)** Interleukin 6 (*IL-6*) expression. **(F)** Inducible nitric oxide synthase (*iNOS*) expression. **(G)** Images of colon samples showing colon length. **(H)** Images of hematoxylin and eosin **(H and E)**-stained colon tissue samples. Magnification, ×200. Values are mean ± standard error of the mean (SEM); $^{*}p < 0.05$, $^{**}p < 0.01$, and $^{***}p < 0.001$ for ginger and SASP vs. model group.

infiltration) in SASP and ginger treatment groups than the model group (**Figure 1H**).

Ginger Restores the Composition of Intestinal Flora in Colitis Mice

The total number of tags in the OTU was collected to obtain the OTU level bar plot of each sample (shown in **Table 2** and **Figure 2A**). After quality control, approximately 41,264 and 74,044 clean tags were obtained; the chimeras were removed and the valid tags obtained were used for the analysis. The average length of valid tags ranged from 405.99–417.12 bp. The number of OTUs in each sample was counted by subtracting the representative sequences from OTU counts, and it ranged from 577–1835 bp (**Figure 2B**).

We further analyzed the community structural distribution and first calculated the relative abundance based on biological taxonomy levels. The differences in abundance between each

TABLE 2 | Sample tag distribution summary table.

#SampleID	Clean_tags	Valid_tags	Valid_percent (%)	Valid minLength	Valid meanLength	Valid maxLength	OTU_counts	Total OTUs
C1.D8	71,734	65,958	91.95	256	416.09	439	1,594	4,135
C2.D8	74,044	68,076	91.94	228	414.24	455	1949	4,135
C3.D8	41,264	37,203	90.16	229	416.22	441	1,429	4,135
C4.D8	72,438	67,264	92.86	228	412.12	440	1733	4,135
C5.D8	71,160	66,202	93.03	228	414.04	437	1,694	4,135
C6.D8	73,320	67,309	91.80	236	414.18	440	1,661	4,135
C8.D8	73,930	68,725	92.96	228	414.27	440	1753	4,135
M1.D8	71,501	67,026	93.74	228	414.38	441	1,441	4,135
M2.D8	72,059	65,866	91.41	228	417.12	442	1,307	4,135
M3.D8	71,152	67,237	94.50	228	415.51	440	1,257	4,135
M4.D8	73,322	68,919	93.99	259	406.4	446	1,152	4,135
M5.D8	72,402	68,246	94.26	248	412.6	440	1,206	4,135
M6.D8	73,007	69,406	95.07	256	405.99	438	1,099	4,135
M7.D8	73,066	67,713	92.67	258	410.17	441	1,312	4,135
M8.D8	73,764	69,241	93.87	222	409.59	441	1,263	4,135
SA1.D8	72,246	67,236	93.07	228	415.88	450	1,100	4,135
SA2.D8	67,957	58,735	86.43	258	415.37	455	691	4,135
SA3.D8	69,731	62,157	89.14	256	414.68	445	930	4,135
SA4.D8	69,355	61,676	88.93	258	416.79	438	1,413	4,135
SA5.D8	71,149	65,883	92.60	228	412.19	441	889	4,135
SA6.D8	71,172	63,337	88.99	228	416.76	437	1,495	4,135
G1.D8	72,469	66,439	91.68	228	413.08	437	1,379	4,135
G2.D8	71,143	66,258	93.13	248	411.4	440	1,438	4,135
G3.D8	72,253	64,874	89.79	229	412.79	442	1,392	4,135
G4.D8	70,144	64,416	91.83	258	415.05	440	1,091	4,135
G5.D8	70,345	63,676	90.52	228	410.17	441	1,402	4,135
G6.D8	70,384	61,150	86.88	258	410.15	441	1,268	4,135
G7.D8	72,754	68,379	93.99	256	411.65	440	1,291	4,135
G8.D8	70,885	65,241	92.04	228	411.71	441	1,420	4,135
G4.D8	70,144	64,416	91.83	258	415.05	440	1,091	4,135

group at the phylum level are shown in **Figure 2C**, where we detected the top 30 representative phyla, in which we observed that colitis mice presented a high relative abundance in *Firmicutes* compared to the other three groups. Subsequently, we focused on the difference in abundance at the family and genus levels (**Figures 2D,E**) in each group. At the phylum level, colitis mice presented a high relative abundance of *Proteobacteria and Firmicutes*, which had been proved to be a signature of dysbiosis of the gut microbiota. Mice treated with ginger and SASP showed completely opposite results. We also observed a slight increase in *Gemmatimonadetes*. At the family level, *Lachnospiraceae* showed a significant increase in mice treated with DSS than in the control group. Ginger and SASP decreased the relative abundance of *Lachnospiraceae*. In contrast, *Muribaculaceae* were reduced in colitis mice, and ginger corrected this disorder. At the genus level, *the Lachnospiraceae_NK4A136_group* showed a sharp increase in the model group. Finally, we calculated the average data in each group and performed a heatmap to illustrate the top 15 different species at the family level (**Figure 2F**). The heatmap showed that *Lactobacillus_murinus*, *Lachnospiraceae_bacterium_615*, and *Ruminiclostridium*_sp._*KB18* levels increased in the model group but decreased in ginger and SASP treatment groups. However, *Bacteroides_acidifaciens_JCM_10,556* showed an opposite trend.

The Diversity of Species in the Microbiological Environment

Alpha diversity analysis was performed to observe the species diversity in each individual sample. The constructed dilution curve of the diversity index presents the differences in species richness, and the goods_coverage in **Figure 3A** shows the sequencing depth with an index value close to 1 that proved the rationality of this analysis. The species richness index was calculated with Chao1 (**Figure 3B**). Mice with colitis showed a lower richness index, which suggested that DSS disrupted the microbiology structure. The administration of ginger and SASP to mice altered this phenomenon. Rank abundance (**Figure 3C**) demonstrated the species richness and evenness of each group. DSS disrupted the balance in the composition of the gut microbiota. Mice treated with ginger and SASP showed a higher species richness and evenness compared to the model group. Furthermore, the specaccum species accumulation curve illustrated in **Figure 3D** showed that the number of species increased with an increasing number of samples, and the gentle curve indicates sufficient sampling. We also obtained the average results in each group and finally obtained an observed species curve in **Figure 3E** to prove the results. Mice in the control group showed the highest diversity in microbiome species, and mice treated with ginger came next. DSS reduced diversity sharply, and it seems SASP could not reverse this.

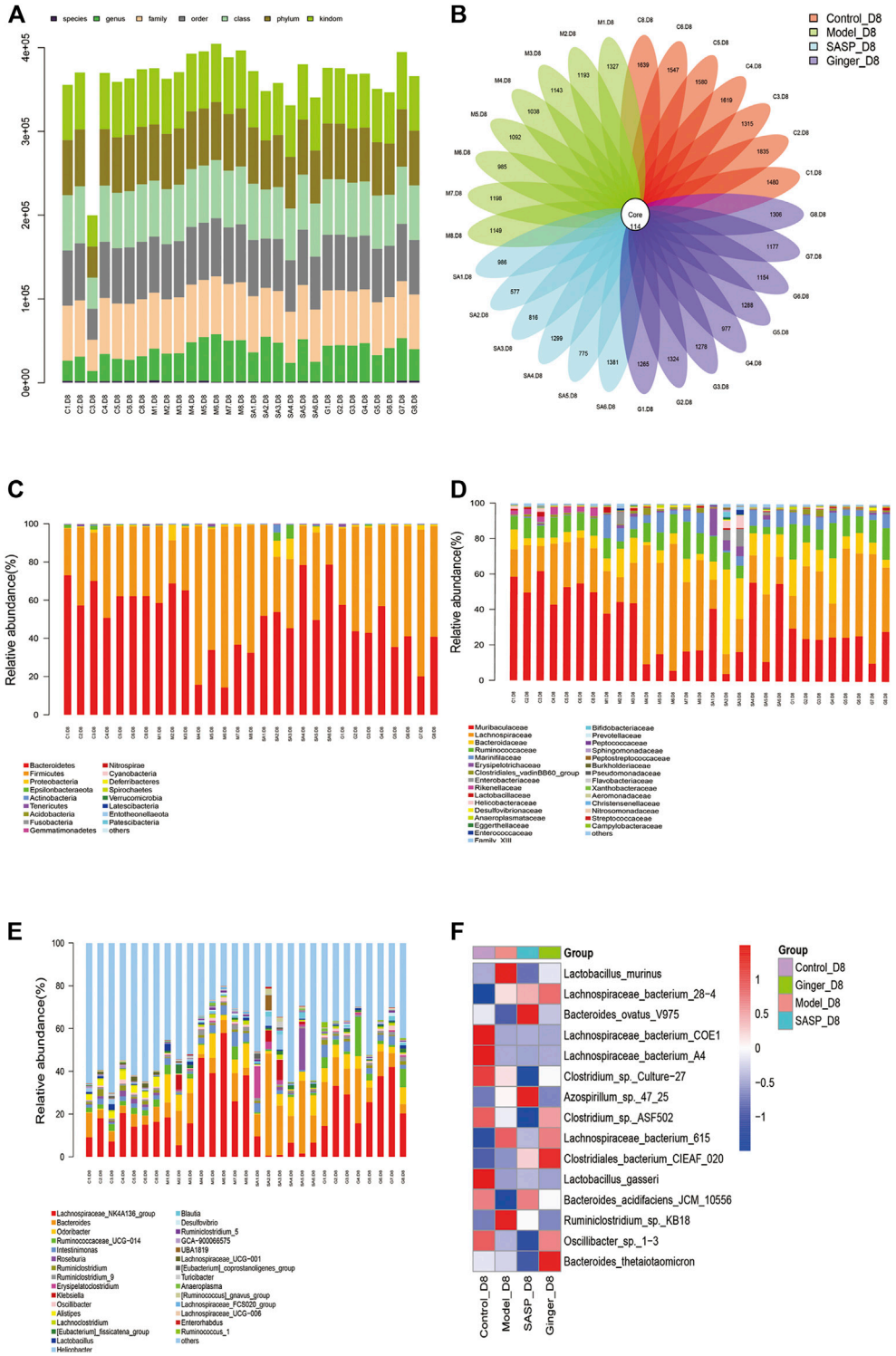

FIGURE 2 | Analysis of the microbial community structure of each group **(A)** Operational taxonomic unit (OTU) level bar plots. The *X*-axis shows the name of each sample, and the *Y*-axis is the total number of tags in OTUs under class. **(B)** Flower plot analysis of the number of OTUs in each sample. The values were obtained by subtracting representative sequences from OTU counts. OTUer ring indicates samples. Values on petals were the exact OTU numbers of each sample. The center of the circle represents sequences. **(C)** Relative abundance of phyla. Each column represents a sample. Different colors indicate different bacteria in phyla. The *X*-axis represents samples, and the *Y*-axis shows relative abundance in phyla. **(D)** Relative abundance of families. Each column represents a sample. Different colors indicate different bacteria in families. The *X*-axis represents samples, and the *Y*-axis is the relative abundance of families. **(E)** Relative abundance of genus. Each column represents a sample. Different colors indicate different bacteria in genus. The *X*-axis represents samples, and the *Y*-axis is the relative abundance of classes. **(F)** Heatmaps illustrate the relative abundance of families in samples, cluster tree on the left represents the clustering of families. The above-clustering branch group represents samples from different groups. Orange and blue indicate higher and lower relative abundance, respectively.

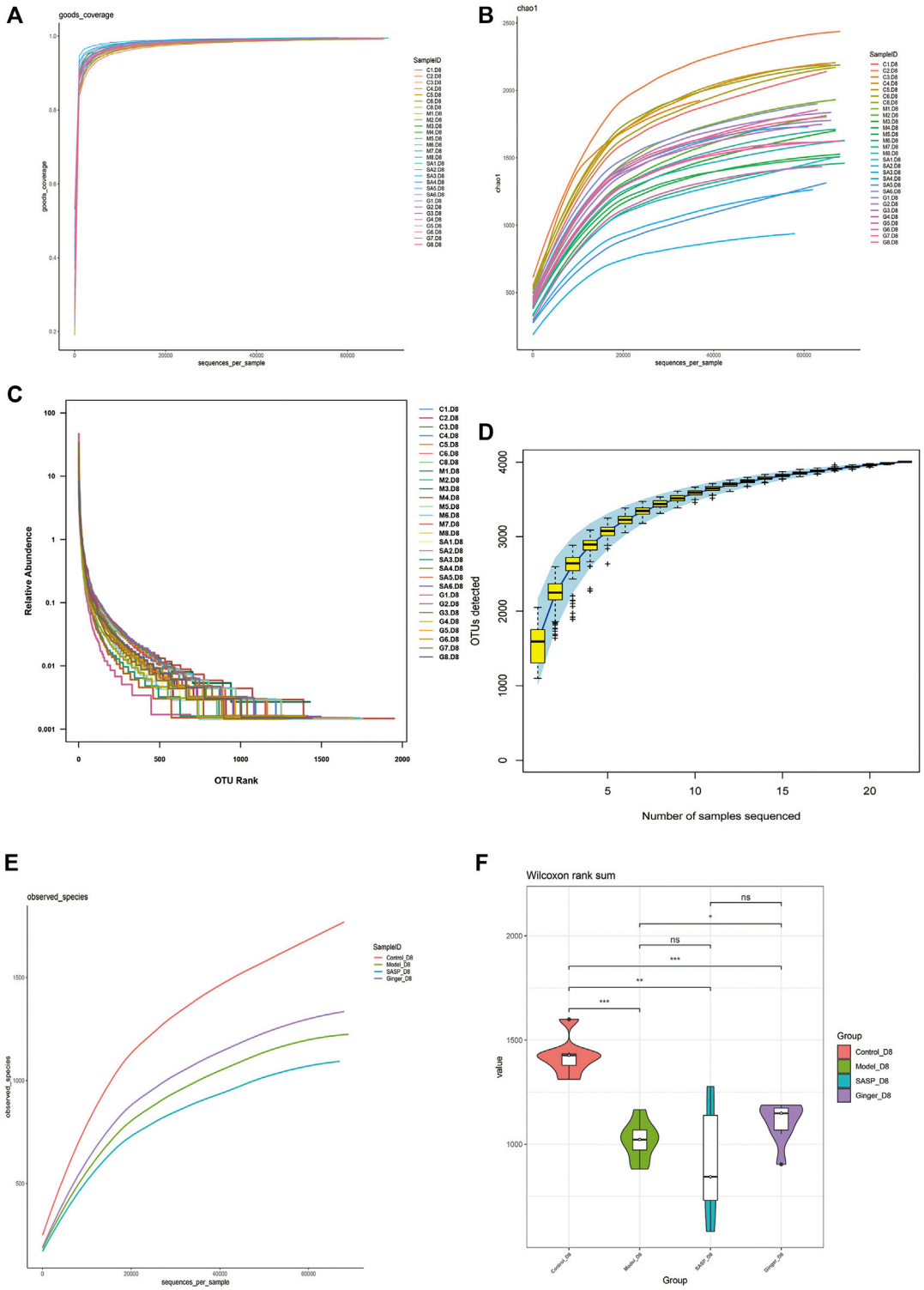

FIGURE 3 | Alpha diversity index calculation statistics correct sequencing depth. **(A)** Goods_coverage analysis of each sample. Each curve represents a sample. The *X*-axis is the depth of random sampling (number of sequences sampled), and the *Y*-axis is the exponential value. An increase in the number of extracted sequences and the gradually flattening curve indicate that the amount of sequencing data is reasonable. **(B)** The chao 1 estimator. The *X*-axis is the depth of random sampling (number of sequences sampled), and the *Y*-axis is the number of OTUs. **(C)** Species richness and evenness of each group. On the *X*-axis, OTUs are sorted according to the number of sequences they contain. For example, "500" represents the 500th most abundant OTU in the sample. On the *Y*-axis, the relative abundance of OTU, such as "0.01", represents 0.01%; eg, "0.1" stands for 0.1%. **(D)** Species accumulation curve. The *X*-axis represents the number of samples, and the *Y*-axis

(*Continued*)

FIGURE 3 | represents detected operational taxonomic unit (OTU) numbers. The flat curve indicates sufficient sampling. **(E)** The average OTUs numbers of observed species in each group. The *X*-axis is the depth of random sampling (number of sequences sampled), and the *Y*-axis is the exponential value. When the curve tends to be flat, it indicates that the amount of sequencing data is large enough to reflect most of the microbial species information in the sample. **(F)** Violin diagram shows alpha diversity index. The *X*-axis represents different groups are distinguished by different colors, and *Y*-axis is the index value.

Finally, we performed Wilcoxon rank-sum, and a violin diagram was obtained, which more clearly indicated the microbial diversity in mice from different groups. (**Figure 3F**). We confirmed that DSS destroyed the microbiology structure in mice colon, and ginger slightly corrected this; however, the influence was not dramatic.

Sequencing Depth Correlation and Multivariate Statistical Analysis of Microorganisms

Beta diversity analysis reflects the diversity among habitats, which means the differences between different samples are often based on OTU sequence similarity or the structure of the community (i.e., species abundance and distribution), or both the evolutionary relationship of the OTU sequence and the structure of the community. First, we obtained the beta-diversity index and found that the microbial diversity observed in mice treated with ginger was similar to that of the control group (**Figure 4A**). We also used principal coordinate analysis (PCoA) of the microbial community to compare the degree of variation between different samples, and the results are shown with a 3D diagram (**Figure 4B**). Here we conclude that, overall, microbial evolution in mice treated with ginger is closer to that in control mice. A larger difference was observed between saline- and SASP-treated mice with colitis. We observed that these two groups possessed a larger difference compared to the control group. Nonmetric multidimensional scaling (NMDS) is often used to compare differences between sample groups, and it is based on evolutionary relationships or quantitative distance matrices. We also obtained an NMDS 3D diagram (**Figure 4C**), and the results were consistent with the PCoA. For clarity, we obtained a circular hierarchical clustering_tree (**Figure 4D**) using the unweighted pair-group method with arithmetic mean (UPGMA) statistics. The distance between the two branches demonstrates the differences between the two samples. Finally, we performed an analysis of variance (ANOVA) and counted the top 10 different abundant microbiomes at the genus level (**Figure 4E**) and species level (**Figure 4F**). We found that most of the microbiomes were similar in the other three groups compared to the control group, but there were also some differences in those three groups. At the genus level, SASP and ginger decreased the abundance of *Odoribacter* compared to colitis mice. Ruminococcaceae_UCG-014 was decreased in colitis mice, and SASP did not reverse this, but mice treated with ginger showed a similarity in abundance with control mice. At the species level, we observed a sharp increase in the relative abundance of *Azospiellum*_sp_*47_25* in the model and SASP groups; mice in the ginger group only had a slight increase. We also found that *Lachnospiraceae_bacterium_615, Ruminiclostridum*_sp._*kb 18, and intestinimonas_gabonensis* were high in colitis mice compared to control mice, and SASP and ginger reduced this change. Meanwhile, *Lactobacillus_gasseri* and *Oscillibacter*_sp._*1-3* showed contrasting trends.

Species Correlation and Phylogenetic Analysis

Random forest is a machine learning algorithm that can effectively and accurately classify microbial community samples and identify different key components (OTUs or species) between regions. We drew a random forest diagram in **Figure 5A** and predicted the outstanding species. The Spearman correlation coefficient was calculated based on the relative abundance between species samples. The interrelations between species within the sample or group of samples were obtained, and the network of species interactions was constructed using a visual software that showed the interrelations between species. We plotted a network map of species in **Figure 5B** to exhibit the species correlation of various classification levels under certain environmental conditions. The abundance of each OTU was calculated. TOP50 with the most tags (most abundant) were selected to construct a phylogenetic tree (**Figure 5C**) and were shown with a heatmap (**Figure 5D**). We observed a lower abundance of bacteria such as *Epsilonbacteraeota* and *Bacteroidetes* and a higher abundance of bacteria such as *Firmicutes, Proteobacteria,* and *Tenericutes* in colitis mice compared to mice treated with ginger and SASP.

Gut Microbiome Disorder Contributed to Metabolic Dysfunction

As shown in **Figure 6A**, Wilcoxon analysis was used, and we eventually found that changes in the intestinal flora in different groups showed a close relationship with human physiological function. The most prominent function focused on human disease, organismal systems, genetic information processing, metabolism, and cellular processes. Kruskal–Wallis analysis using the Kyoto Encyclopedia of Genes and Genomes (KEGG) database identified 30 pathways based on different flora (**Figure 6B**). The predictions revealed that most pathways involved were related to metabolism, including the metabolism of starch, sucrose (and oxidative phosphorylation), and amino acids (alanine, aspartate, and glutamate), as well as genetic information processing (DNA repair and recombination proteins, ribosome, and pyrimidine metabolism). Clusters of Orthologous Groups of proteins (COG) is a database of the NCBI. COG is categorized into two: prokaryotes and eukaryotes. Prokaryotes are generally called COG databases. In this research, cluster analysis of difference results was performed based on COG databases, and the heatmap in **Figure 6C** shows

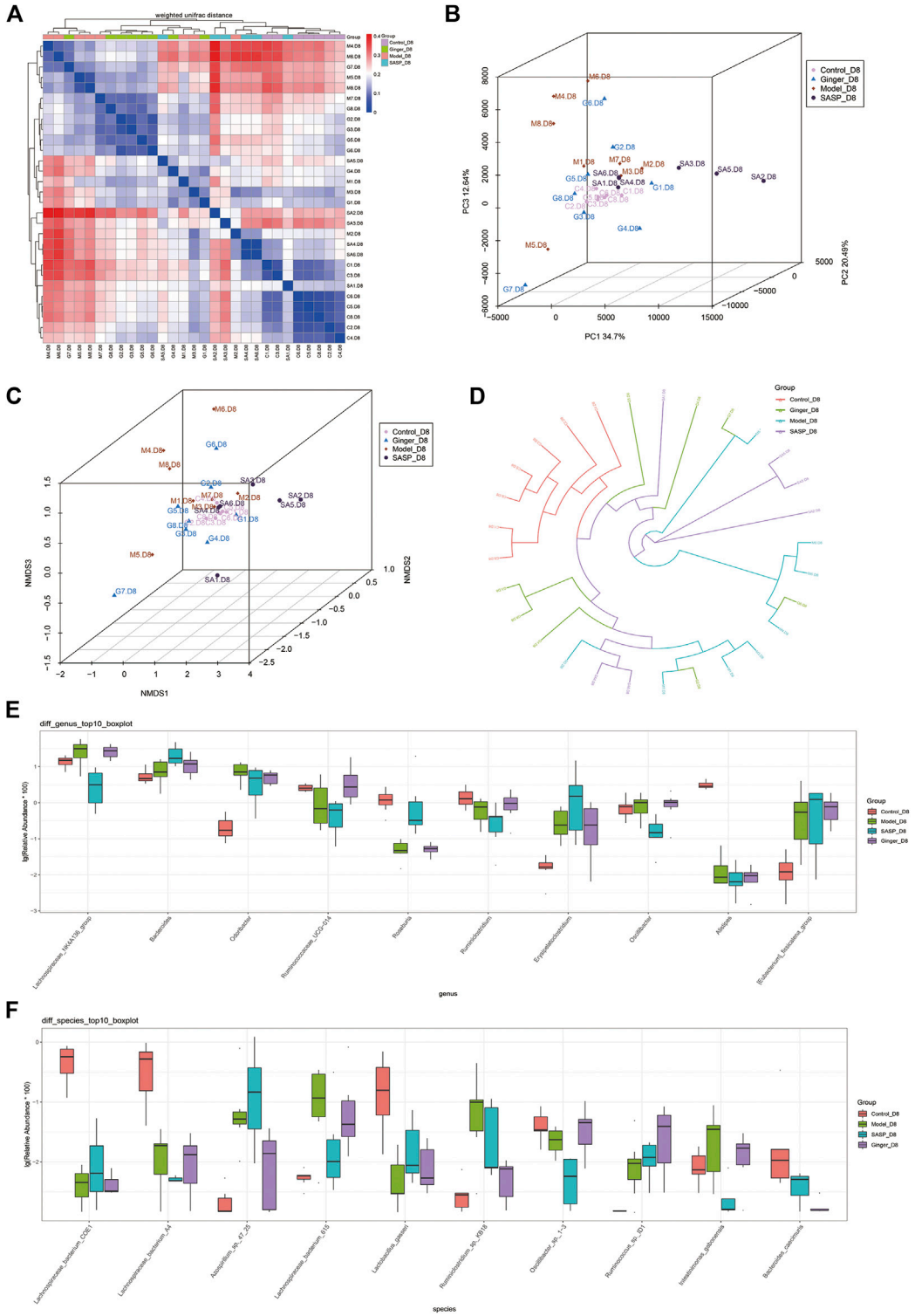

FIGURE 4 | Sequencing depth corrected and multivariate statistical analysis of microorganisms. **(A)** Beta diversity analysis of the variability of each group. In the heatmap (above and left), the clustering branch represents samples from different groups. The deeper the blue, the closer the two groups are. The intensity of the red color indicates the opposite. **(B)** PCoA represents differences between groups. The abscissa (PC1) and the ordinate (PC2) are the two main coordinates with the largest interpretation of the difference between samples. Each point in the figure represents a sample, the same color is the same group, similar samples will be clustered together, if there is a big difference between the samples, the distance will be farther in figure. **(C)** NMDS analysis. Each point in the figure represents a sample, the same color is the same group, similar samples will be clustered together, if there is a big difference between the samples, the distance will be farther in figure. **(D)** UPGMA analysis the differences between samples. Each color represents a group. The closer the branch distance, the more similar the samples. Bar boxes illustrate the relative abundance of dominant species and compared the differences within different groups in **(E)** genus and **(F)** species.

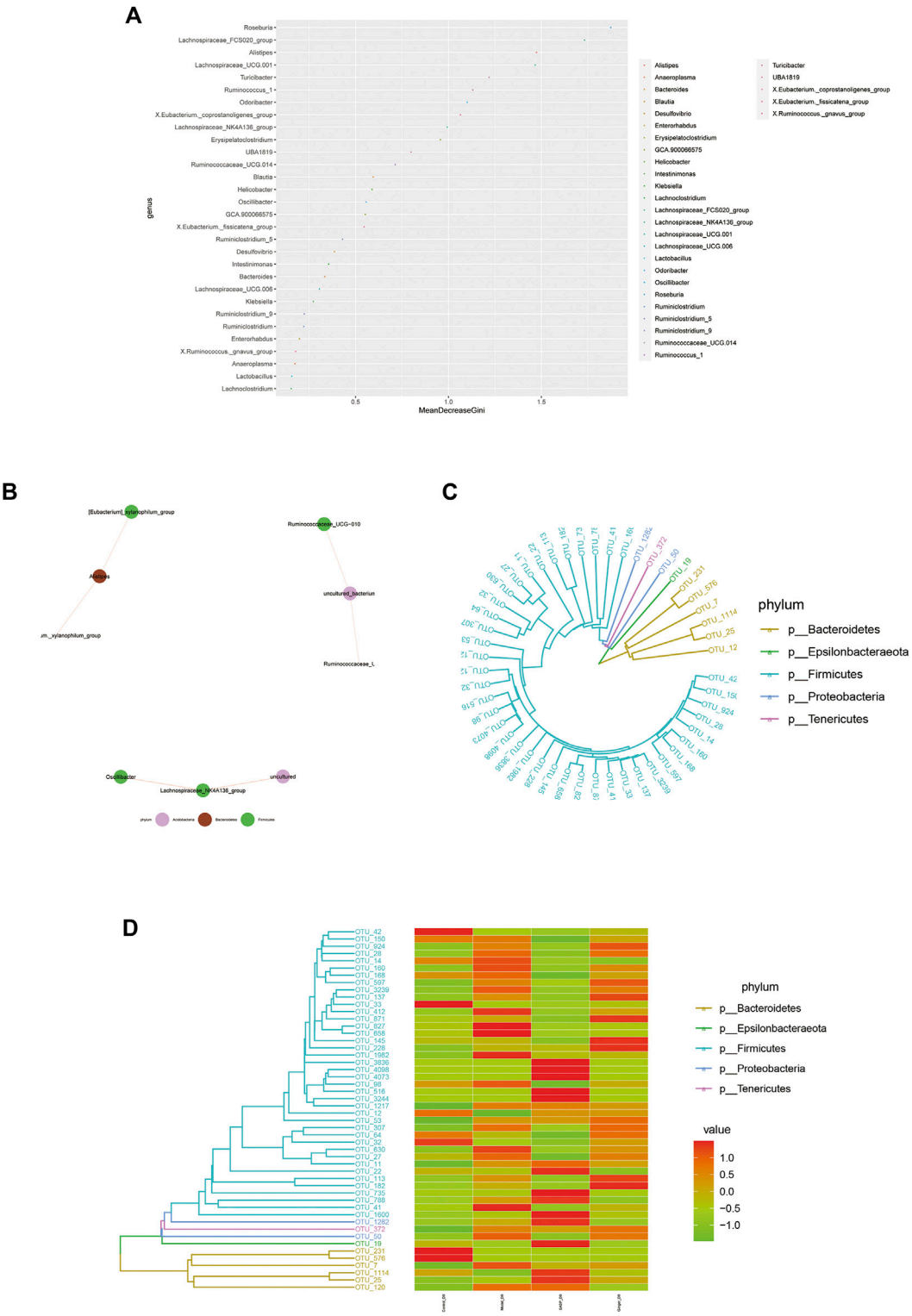

FIGURE 5 | Microbiome community samples classification and phylogeny analysis of phylum. **(A)** Species (variables) importance point map. The abscissa is the importance measurement standard, and the ordinate is the species name sorted by importance. The figure uses standardized importance values by default. **(B)** Species correlation network diagram. The size of the nodes in the figure indicates the abundance of species, and different colors indicate different species; the color of the line indicates positive and negative correlation, red indicates positive correlation, and green indicates negative correlation; the thickness of the line indicates the size of Pearson's correlation coefficient. Thicker line represents more higher the correlation between species. the abundance of OTUs in each sample are shown **(C)** and phylogenetic tree and species abundance combination diagram **(D)** is obtained. The clustering branch represents different bacterial phyla. The abundance graph is shown on the right, which corresponds to the abundance of left operational taxonomic units (OTUs) in each sample.

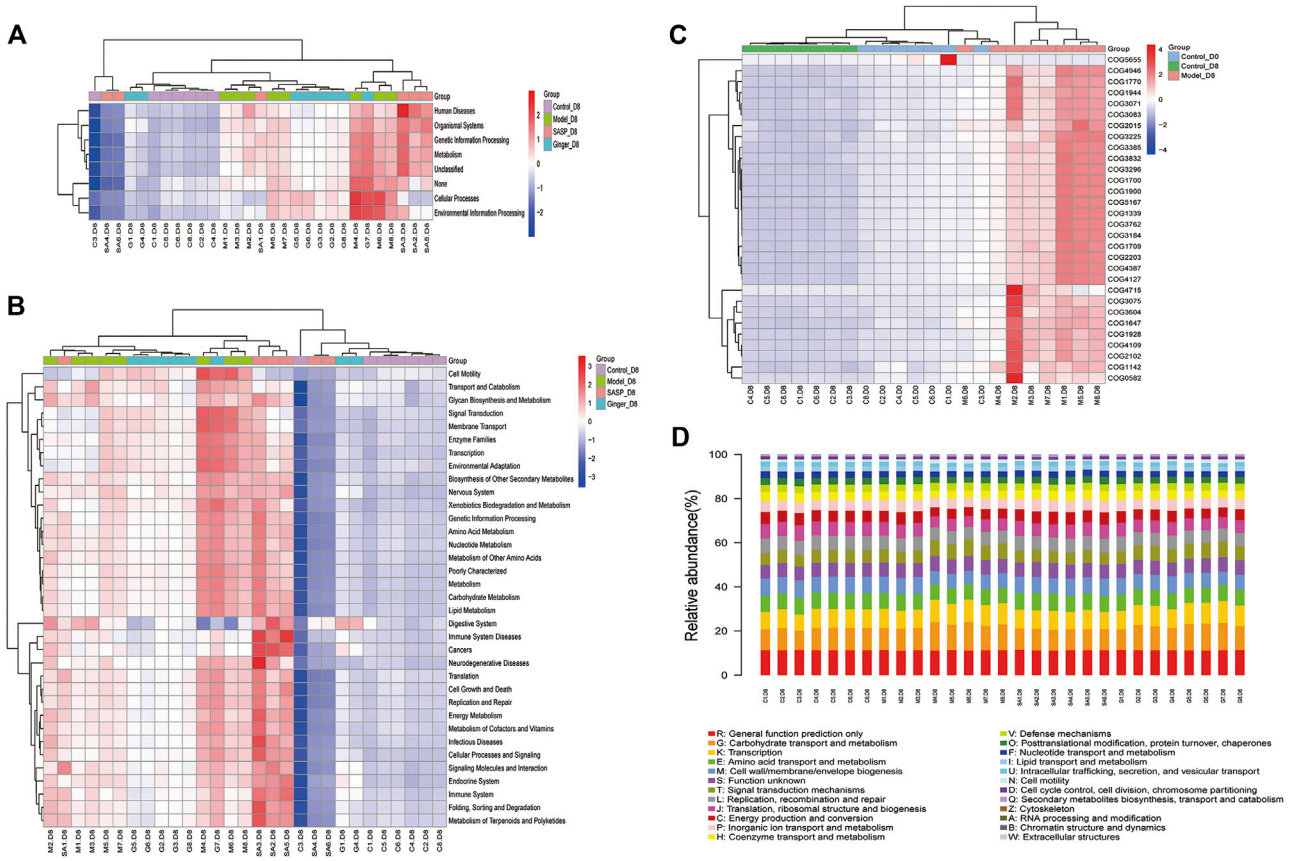

FIGURE 6 | Prediction of the functional composition of the gut microbiome. **(A)** and **(B)** Kruskal–Wallis analysis was performed to predict functions **(A)** and pathways **(B)** the different microbiome species related. The results are shown as a heatmap. **(C)** Clusters of Orthologous Groups of proteins were predicted and shown in the heatmap. The cluster tree on the left represents the clustering of different metabolic pathways, and the above-clustering branch represents samples from different groups **(D)** COG bar plot predicted the microbiome function; the *x*-axis is sample name and the *Y*-axis is relative abundance of predicted COG_category.

the top 30 COG related to different species in the four groups. We also generated a bar blot, as shown in **Figure 6D**, to predict the potential functions microbiomes possess. However, we only found two functions, carbohydrate transport and metabolism and transcription, slightly related to their microbiology.

DISCUSSION

In this study, we established a DSS-induced mice colitis model to determine whether ginger restored the gut microbiome composition or not. We also chose SASP, a sulfa antimicrobial that has been used as a therapy for IBD (Sutherland and Macdonald, 2006), as a positive control. Our findings revealed that ginger inhibited colitis progression, alleviated colon injury, and regulated the fecal microbiome.

In recent years, many investigators have researched the treatment mechanism of SASP, especially its regulatory effect on the intestinal microbiome. It has also been proven that SASP altered the gut microbiome and restored the TNBS-induced gut dysbiosis in TNBS-induced colitis (Zheng et al., 2017). We have also mentioned that SASP is widely chosen as a positive control in research that elaborates on the regulation effect of rhizome herb on intestinal microbiota in experimental IBD (Liu et al., 2018; Jia et al., 2020). In our study, the results indicated that ginger alleviated weight loss and reduced DAI in colitis mice, an effect that is similar to that of SASP. The results also showed similar effects on the changing of colon length and spleen index. Although ginger was slightly disadvantageous in reducing the expression of *IL-6*, it exhibited the same efficiency in regulating the expression of *iNOS*. Therefore, we proved that oral ginger delayed DSS-induced colitis progression in Balb/C mice.

A community structure or a biological community refers to all creatures with a direct or indirect relationship to each other in the communal biological environment or the collection of all organisms. The various groups in a microbial community coexist and have distinct types of nutrition and metabolism (Hooper et al., 2012). Imbalances in the gut microbiome disrupt homeostasis and contribute to UC; therefore, novel treatment approaches such as manipulation of the gut microbiome (Cohen et al., 2019) and FMT have been proposed for treating UC (de Groot et al., 2017). The

microbial diversity results of our study suggested that the ecological structure of the intestinal flora was disrupted as colitis progressed. Our analysis of the community structure revealed a high composition of *Proteobacteria*, *firmicutes*, *Gemmatimonadetes,* and *Lachnospiraceae* in DSS-induced model mice, which was reduced by ginger and SASP. Ginger especially showed a higher efficiency compared to SASP. In contrast, *Muribaculaceae* was decreased in colitis mice. In more detail, we found that *Bacteroides_acidifaciens_JCM_10,556,* a species in the *Bacteroides* phylum, was decreased in the model group; although ginger could also correct this disorder, SASP almost reversed this change.

The presence of *Proteobacteria* is a sign of microbiota disorder, and increased levels contribute to dysbiosis and the risk of disease (Shin et al., 2015). In addition to IBD and other intestinal diseases, asthma and chronic obstructive pulmonary disease have also been observed to be associated with increased *Proteobacteria* composition (Rizzatti et al., 2017). Recent studies have revealed the relationship between a high abundance of firmicutes and IBD risk (Eom et al., 2018). *Gemmatimonadetes*, one of four major families of organisms constituting the human gut microbiota, plays an important role in gastrointestinal and systemic diseases (Binda et al., 2018). Ginger reduced the abundance of these pathogenic bacteria and was an active component that improved colitis via the gut microbe regulation. *Lachnospiraceae* depletion was reported in most research (de Oliveira, 2019), contrasting with our research; this needs more experimentation to explore the changes accurately. *Bacteroides* imbalance was reported in IBD patients who presented with a lower abundance compared to healthy humans (Brown et al., 2019). Bacteroides ovatus monotherapy has also been proven to be more effective than FMT to treat IBD (Ihekweazu et al., 2019). In this study, we also found a decrease in the relative abundance of *Bacteroides_acidifaciens_JCM_10,556* in model groups. Ginger and SASP slightly improved the abundance.

Alpha diversity analysis reflects the diversity of species in the biological environment, and Beta diversity is the degree of diversity between habitats, that is, to compare the differences of samples in different groups. Two methods were used in this research. Colitis mice treated with SASP and ginger all showed a relatively healthy gut microbiome status and similar microbial diversity to mice in the control group. According to Alpha analysis results, ginger was more effective than SASP, suggesting that ginger stabilized the gut microbiome. This observation might explain the use of ginger as a traditional medicine for alleviating gastrointestinal diseases, such as IBD and necrotizing enterocolitis (Cakir et al., 2018). However, some microbiomes showed an opposite trend with the control group, and this needs further verification.

The gut microbiome is well known to play a major role in sustaining human health, and temporal and spatial changes in the gut microbiota occur throughout life (Jandhyala et al., 2015). Important metabolic pathways such as lipid metabolism (Wang et al., 2016), drug metabolism and efficacy (Wilson and Nicholson, 2017) and the production of tryptophan, phenylalanine, and tyrosine (Dodd et al., 2017) have been shown to be modulated by the gut microbiome. In this study, we first analyzed the correlation between different diseases and physiological functions. The results showed that the differences between the four groups contribute to human disease, organismal systems, genetic information processing, metabolism, and cellular processes. For further analysis, we used the KEGG database to explore the metabolic changes caused by different gut microbiome structure in colitis mice and identified 42 pathways related to the different microbiome. We found that gut microbiome disorder disrupts metabolic pathways of amino acid metabolism, as well as oxidative phosphorylation and genetic information processing, such as translation and ribosome biogenesis.

We predicted that gut microbiome disorder significantly contributed to the upsetting of metabolic pathways such as transport and catabolism, oxidative phosphorylation, glycan biosynthesis and metabolism, and biosynthesis of other secondary metabolites. Researchers have shown that changes in carbohydrate metabolism and amino acid biosynthesis are related to nutrient transport and uptakee (Morgan et al., 2012). Epidemiological research has also shown that antibiotics over-scavenge the gut flora, causing macrophages to overreact to bacteria, thereby disrupting oxidative phosphorylation. Hypermutation occurs in 27% of IBD-associated colorectal cancer cases, including DNA repair dysfunction (Din et al., 2018). *Lipopolysaccharide* isolated from *Helicobacter* disrupts intestinal DNA repair, increasing the risk of permanent genotoxic effects, contributing to IBD or colon cancer (Cavallo et al., 2011). The COG prediction results also focus on nucleic acid and metabolism-related functions. We observed a significant relationship between the different species and RNA processing and modification, chromatin structure and dynamics, amino acid transport and metabolism, and nucleotide transport and metabolism.

In conclusion, the results in this research showed that ginger ameliorates the severity of DSS-induced colitis in mice. We also observed that ginger treatment altered the intestinal microbiomes of colitis mice, increasing the relative abundance of some species. According to KEGG and COG analysis, the observed changes have a close relationship with the physiological functions of mice. Therefore, we hypothesize that the IBD alleviation effect of ginger may be related to the function of intestinal bacteria. However, the components of ginger that contribute to its regulatory effects on the gut microbiota and mediate its therapeutic effects still need further exploration.

DATA AVAILABILITY STATEMENT

The data presented in this article are deposited in the NCBI Sequence Read Archive repository, accession number PRJNA680889.

ETHICS STATEMENT

The animal study was reviewed and approved by the Animal Care and Use Committee of the Shanghai University.

AUTHOR CONTRIBUTIONS

YL, XP, JH conceived and designed the research; SG, WG, SC, and XR performed the *in vivo* experiments; SG, LW, TW, and LX analyzed the data; YL, XM, and SW contributed reagents/materials/analysis tools; and SG, WG, and SC wrote the paper.

FUNDING

This work was supported by Shanghai University Scientific Research Achievement Transformation Project (20H00892) and the Key Research and Development Program of Guangxi (AB19259007).

REFERENCES

Abraham, B. P., and Quigley, E. M. M. (2017). Probiotics in inflammatory bowel disease. *Gastroenterol. Clin. N. Am.* 46 (4), 769–782. doi:10.1016/j.gtc.2017.08.003

Bajer, L., Kverka, M., Kostovcik, M., Macinga, P., Dvorak, J., Stehlikova, Z., et al. (2017). Distinct gut microbiota profiles in patients with primary sclerosing cholangitis and ulcerative colitis. *World J. Gastroenterol.* 23 (25), 4548–4558. doi:10.3748/wjg.v23.i25.4548

Binda, C., Lopetuso, L. R., Rizzatti, G., Gibiino, G., Cennamo, V., and Gasbarrini, A. (2018). Actinobacteria: a relevant minority for the maintenance of gut homeostasis. *Dig. Liver Dis.: Off. J. Ital. Soc. Gastroenterol. Ital. Assoc. Stud. Liver* 50 (5), 421–428. doi:10.1016/j.dld.2018.02.012

Brown, E. M., Ke, X., Hitchcock, D., Jeanfavre, S., Avila-Pacheco, J., Nakata, T., et al. (2019). Bacteroides-derived sphingolipids are critical for maintaining intestinal homeostasis and symbiosis. *Cell Host Microbe* 25 (5), 668–680. doi:10.1016/j.chom.2019.04.002e667

Cakir, U., Tayman, C., Serkant, U., Yakut, H. I., Cakir, E., Ates, U., et al. (2018). Ginger (Zingiber officinale Roscoe) for the treatment and prevention of necrotizing enterocolitis. *J. Ethnopharmacol.* 225, 297–308. doi:10.1016/j.jep.2018.07.009

Cavallo, P., Cianciulli, A., Mitolo, V., and Panaro, M. A. (2011). Lipopolysaccharide (LPS) of helicobacter modulates cellular DNA repair systems in intestinal cells. *Clin. Exp. Med.* 11 (3), 171–179. doi:10.1007/s10238-010-0118-1

Chassaing, B., Aitken, J. D., Malleshappa, M., and Vijay-Kumar, M. (2014). Dextran sulfate sodium (DSS)-induced colitis in mice. *Gastroenterology* 15, 11–15. doi:10.1002/0471142735.im1525s104

Cohen, L. J., Cho, J. H., Gevers, D., and Chu, H. (2019). Genetic factors and the intestinal microbiome guide development of microbe-based therapies for inflammatory bowel diseases. *Gastroenterology* 156 (8), 2174–2189. doi:10.1053/j.gastro.2019.03.017

de Groot, P. F., Frissen, M. N., de Clercq, N. C., and Nieuwdorp, M. (2017). Fecal microbiota transplantation in metabolic syndrome: history, present and future. *Gut Microbes* 8 (3), 253–267. doi:10.1080/19490976.2017.1293224

de Oliveira, G. L. V. (2019). "Chapter 33—the gut microbiome in autoimmune diseases," in *Microbiome and metabolome in diagnosis, therapy, and other strategic applications*. Editors J. Faintuch and S. Faintuch (London: Academic Press), 325–332.

Din, S., Wong, K., Mueller, M. F., Oniscu, A., Hewinson, J., Black, C. J., et al. (2018). Mutational analysis identifies therapeutic biomarkers in inflammatory bowel disease-associated colorectal cancers. *Clin. Canc. Res.: Off. J. Am. Assoc. Cancer Res.* 24 (20), 5133–5142. doi:10.1158/1078-0432.CCR-17-3713

Dodd, D., Spitzer, M. H., Van Treuren, W., Merrill, B. D., Hryckowian, A. J., Higginbottom, S. K., et al. (2017). A gut bacterial pathway metabolizes aromatic amino acids into nine circulating metabolites. *Nature* 551 (7682), 648–652. doi:10.1038/nature24661

Dong, J., Liang, W., Wang, T., Sui, J., Wang, J., Deng, Z., et al. (2019). Saponins regulate intestinal inflammation in colon cancer and IBD. *Pharmacol. Res.* 144, 66–72. doi:10.1016/j.phrs.2019.04.010

Eom, T., Kim, Y. S., Choi, C. H., Sadowsky, M. J., and Unno, T. (2018). Current understanding of microbiota- and dietary-therapies for treating inflammatory bowel disease. *J. Microbiol.* 56 (3), 189–198. doi:10.1007/s12275-018-8049-8

Heller, F., Florian, P., Bojarski, C., Richter, J., Christ, M., Hillenbrand, B., et al. (2005). Interleukin-13 is the key effector Th2 cytokine in ulcerative colitis that affects epithelial tight junctions, apoptosis, and cell restitution. *Gastroenterology* 129 (2), 550–564. doi:10.1016/j.gastro.2005.05.002

Hills, R. D., Jr., Pontefract, B. A., Mishcon, H. R., Black, C. A., Sutton, S. C., and Theberge, C. R. (2019). Gut microbiome: profound implications for diet and disease. *Nutrients* 11 (7), 1613. doi:10.3390/nu11071613

Hooper, L. V., Littman, D. R., and Macpherson, A. J. (2012). Interactions between the microbiota and the immune system. *Science* 336 (6086), 1268–1273. doi:10.1126/science.1223490

Ihekweazu, F. D., Fofanova, T. Y., Queliza, K., Nagy-Szakal, D., Stewart, C. J., Engevik, M. A., et al. (2019). Bacteroides ovatus ATCC 8483 monotherapy is superior to traditional fecal transplant and multi-strain bacteriotherapy in a murine colitis model. *Gut Microb.* 10 (4), 504–520. doi:10.1080/19490976.2018.1560753

Jandhyala, S. M., Talukdar, R., Subramanyam, C., Vuyyuru, H., Sasikala, M., and Nageshwar Reddy, D. (2015). Role of the normal gut microbiota. *World Journal of Gastroenterology* 21 (29), 8787–8803. doi:10.3748/wjg.v21.i29.8787

Jia, Y. Q., Yuan, Z. W., Zhang, X. S., Dong, J. Q., Liu, X. N., Peng, X. T., et al. (2020). Total alkaloids of *Sophora* alopecuroides L. ameliorated murine colitis by regulating bile acid metabolism and gut microbiota. *J. Ethnopharmacol.* 255, 112775. doi:10.1016/j.jep.2020.112775

Khan, I., Ullah, N., Zha, L., Bai, Y., Khan, A., Zhao, T., et al. (2019). Alteration of gut microbiota in inflammatory bowel disease (IBD): cause or consequence? IBD treatment targeting the gut microbiome. *Pathogens* 8 (3), 126. doi:10.3390/pathogens8030126

Ley, R. E., Peterson, D. A., and Gordon, J. I. (2006). Ecological and evolutionary forces shaping microbial diversity in the human intestine. *Cell* 124 (4), 837–848. doi:10.1016/j.cell.2006.02.017

Litvak, Y., Byndloss, M. X., and Bäumler, A. J. (2018). Colonocyte metabolism shapes the gut microbiota. *Science (New York, N.Y.)* 362 (6418), eaat9076. doi:10.1126/science.aat9076

Liu, X., Yu, X., Xu, X., Zhang, X., and Zhang, X. (2018). The protective effects of Poria cocos-derived polysaccharide CMP33 against IBD in mice and its molecular mechanism. *Food Funct.* 9 (11), 5936–5949. doi:10.1039/c8fo01604f

Mahomoodally, M. F., Aumeeruddy, M. Z., Rengasamy, K. R. R., Roshan, S., Hammad, S., Pandohee, J., et al. (2019). Ginger and its active compounds in cancer therapy: from folk uses to nano-therapeutic applications. *Semin. Canc. Biol.* 14, 33. doi:10.1016/j.semcancer.2019.08.009

Mangiola, F., Ianiro, G., Franceschi, F., Fagiuoli, S., Gasbarrini, G., and Gasbarrini, A. (2016). Gut microbiota in autism and mood disorders. *World J. Gastroenterol.* 22 (1), 361–368. doi:10.3748/wjg.v22.i1.361

Marchesi, J. R., Adams, D. H., Fava, F., Hermes, G. D., Hirschfield, G. M., Hold, G., et al. (2016). The gut microbiota and host health: a new clinical Frontier. *Gut* 65 (2), 330–339. doi:10.1136/gutjnl-2015-309990

Masoodi, I., Alshanqeeti, A. S., Ahmad, S., Alyamani, E. J., and Alomair, A. O. J. M. G. e. D. (2019). Microbial dysbiosis in inflammatory bowel diseases: results of a metagenomic study in. *Saudi Arab. (Quarterly Forecast Rep.)* 65 (3), 39. doi:10.23736/S1121-421X.19.02576-5

Mohd Sahardi, N. F. N., and Makpol, S. (2019). Ginger (zingiber officinale roscoe) in the prevention of ageing and degenerative diseases: review of current evidence. *Evid Based Complement Alternat. Med.* 7, 5054395. doi:10.1155/2019/5054395

Morgan, X. C., Tickle, T. L., Sokol, H., Gevers, D., Devaney, K. L., Ward, D. V., et al. (2012). Dysfunction of the intestinal microbiome in inflammatory bowel disease and treatment. *Genome Biol.* 13 (9), R79. doi:10.1186/gb-2012-13-9-r79

Narula, N., Kassam, Z., Yuan, Y., Colombel, J. F., Ponsioen, C., Reinisch, W., et al. (2017). Systematic review and meta-analysis: fecal microbiota transplantation for treatment of active ulcerative colitis. *Inflamm. Bowel Dis.* 23 (10), 1702–1709. doi:10.1097/mib.0000000000001228

Nikkhah Bodagh, M., Maleki, I., and Hekmatdoost, A. (2019). Ginger in gastrointestinal disorders: a systematic review of clinical trials. *Food Sci. Nutr.* 7 (1), 96–108. doi:10.1002/fsn3.807

Ohnmacht, C., Park, J.-H., Cording, S., Wing, J. B., Obata, Y., Gaboriau-Routhiau, V., et al. (2015). Mucosal immunology. The microbiota regulates type 2 immunity through RORgammat (+) T cells. *Science* 349 (6251), 989–993. doi:10.1126/science.aac4263

Prasad, S., and Tyagi, A. K. (2015). Ginger and its constituents: role in prevention and treatment of gastrointestinal cancer. *Gastroenterol Res. Pract.* 2015, 142979. doi:10.1155/2015/142979

Rahman, A., Fahlgren, A., Sundstedt, C., Hammarström, S., and Hammarström, M. L. (2010). Chronic colitis induces expression of β-defensins in murine intestinal epithelial cells. *Clin. Exp. Immunol.* 163 (1), 123–130

Rizzatti, G., Lopetuso, L. R., Gibiino, G., Binda, C., and Gasbarrini, A. (2017). Proteobacteria: a common factor in human diseases. *BioMed Res. Int.* 2017, 9351507. doi:10.1155/2017/9351507

Sharifi-Rad, M., Varoni, E. M., Salehi, B., Sharifi-Rad, J., Matthews, K. R., Ayatollahi, S. A., et al. (2017). Plants of the genus zingiber as a source of bioactive phytochemicals: from tradition to pharmacy. *Molecules* 22 (12), 27. doi:10.3390/molecules22122145

Shin, N.-R., Whon, T. W., and Bae, J.-W. (2015). Proteobacteria: microbial signature of dysbiosis in gut microbiota. *Trends Biotechnol.* 33 (9), 496–503. doi:10.1016/j.tibtech.2015.06.011

Silverberg, M. S., Satsangi, J., Ahmad, T., Arnott, I. D., Bernstein, C. N., Brant, S. R., et al. (2005). Toward an integrated clinical, molecular and serological classification of inflammatory bowel disease: report of a Working Party of the 2005 Montreal World Congress of Gastroenterology. *Can. J. Gastroenterol.* 19 (Suppl. l), 5a–36a. doi:10.1155/2005/269076

Sutherland, L., and Macdonald, J. K. (2006). Oral 5-aminosalicylic acid for maintenance of remission in ulcerative colitis. *Cochrane Database Syst. Rev.* 2, Cd000544. doi:10.1002/14651858.CD000544.pub2

Teng, Y., Ren, Y., Sayed, M., Hu, X., Lei, C., Kumar, A., et al. (2018). Plant-derived exosomal MicroRNAs shape the gut microbiota. *Cell Host Microbe* 24 (5), 637–652. doi:10.1016/j.chom.2018.10.001

Wang, Z., Koonen, D., Hofker, M., and Fu, J. (2016). Gut microbiome and lipid metabolism: from associations to mechanisms. *Curr. Opin. Lipidol.* 27 (3), 216–224. doi:10.1097/MOL.0000000000000308

Wilson, I. D., and Nicholson, J. K. (2017). Gut microbiome interactions with drug metabolism, efficacy, and toxicity. *Transl. Res.: J. Lab. Clin. Med.* 179, 204–222. doi:10.1016/j.trsl.2016.08.002

Zhang, M., Viennois, E., Prasad, M., Zhang, Y., Wang, L., Zhang, Z., et al. (2016). Edible ginger-derived nanoparticles: a novel therapeutic approach for the prevention and treatment of inflammatory bowel disease and colitis-associated cancer. *Biomaterials* 101, 321–340. doi:10.1016/j.biomaterials.2016.06.018

Zhang, Y.-J., Li, S., Gan, R.-Y., Zhou, T., Xu, D.-P., and Li, H.-B. (2015). Impacts of gut bacteria on human health and diseases. *Int. J. Mol. Sci.* 16 (4), 7493–7519. doi:10.3390/ijms16047493

Zhang, Y. Z., and Li, Y. Y. (2014). Inflammatory bowel disease: pathogenesis. *World J. Gastroenterol.* 20 (1), 91–99. doi:10.3748/wjg.v20.i1.91

Zheng, H., Chen, M., Li, Y., Wang, Y., Wei, L., Liao, Z., et al. (2017). Modulation of gut microbiome composition and function in experimental colitis treated with sulfasalazine. *Front. Microbiol.* 8. doi:10.3389/fmicb.2017.01703

Conflict of Interest: SG, SC, LW, JH, and YL are employeed Eight Plus One Pharmaceutical Co., Ltd.

The remaining authors declare that the research was conducted in the absence of any commercial or financial relationships that could be construed as a potential conflict of interest.

frontiers in Immunology

METHODS
published: 29 March 2021
doi: 10.3389/fimmu.2021.646906

A Novel Strategy to Study the Invasive Capability of Adherent-Invasive *Escherichia coli* by Using Human Primary Organoid-Derived Epithelial Monolayers

Aida Mayorgas[1], *Isabella Dotti*[1], *Marta Martínez-Picola*[1], *Miriam Esteller*[1], *Queralt Bonet-Rossinyol*[2], *Elena Ricart*[1], *Azucena Salas*[1]* *and Margarita Martínez-Medina*[2]

[1] Department of Gastroenterology, IDIBAPS, Hospital Clínic, CIBER-EHD, Barcelona, Spain, [2] Laboratory of Molecular Microbiology, Department of Biology, Universitat de Girona, Girona, Spain

OPEN ACCESS

Edited by:
Ulisses Gazos Lopes, Federal University of Rio de Janeiro, Brazil

Reviewed by:
Marie-Agnes Bringer, INRA Centre Dijon Bourgogne Franche-Comté, France
Zhengxiang He, Icahn School of Medicine at Mount Sinai, United States

***Correspondence:**
Azucena Salas
asalas1@clinic.cat

Specialty section:
This article was submitted to Microbial Immunology, a section of the journal Frontiers in Immunology

Received: 08 January 2021
Accepted: 08 March 2021
Published: 29 March 2021

Citation:
Mayorgas A, Dotti I, Martínez-Picola M, Esteller M, Bonet-Rossinyol Q, Ricart E, Salas A and Martínez-Medina M (2021) A Novel Strategy to Study the Invasive Capability of Adherent-Invasive Escherichia coli by Using Human Primary Organoid-Derived Epithelial Monolayers. Front. Immunol. 12:646906. doi: 10.3389/fimmu.2021.646906

Over the last decades, Adherent-Invasive *Escherichia coli* (AIEC) has been linked to the pathogenesis of Crohn's Disease. AIEC's characteristics, as well as its interaction with the gut immune system and its role in intestinal epithelial barrier dysfunction, have been extensively studied. Nevertheless, the currently available techniques to investigate the cross-talk between this pathogen and intestinal epithelial cells (IECs) are based on the infection of immortalized cell lines. Despite their many advantages, cell lines cannot reproduce the conditions in tissues, nor do they reflect interindividual variability or gut location-specific traits. In that sense, the use of human primary cultures, either healthy or diseased, offers a system that can overcome all of these limitations. Here, we developed a new infection model by using freshly isolated human IECs. For the first time, we generated and infected monolayer cultures derived from human colonic organoids to study the mechanisms and effects of AIEC adherence and invasion on primary human epithelial cells. To establish the optimal conditions for AIEC invasion studies in human primary organoid-derived epithelial monolayers, we designed an infection-kinetics study to assess the infection dynamics at different time points, as well as with two multiplicities of infection (MOI). Overall, this method provides a model for the study of host response to AIEC infections, as well as for the understanding of the molecular mechanisms involved in adhesion, invasion and intracellular replication. Therefore, it represents a promising tool for elucidating the cross-talk between AIEC and the intestinal epithelium in healthy and diseased tissues.

Keywords: organoid-derived epithelial monolayers (ODM), adherent-invasive *E. coli* (AIEC), bacterial infection, intestinal epithelial cells (IECs), inflammatory bowel disease (IBD)

INTRODUCTION

Escherichia coli (*E. coli*) strains are widely known inhabitants of the healthy human gut microbiota, being one of the first colonizers as well as among the most prevalent microorganisms in the intestines (1, 2). *E. coli* promotes health benefits to its hosts by preventing the colonization of pathogens and thus, positively contributes to intestinal homeostasis (3, 4). However, several *E. coli* strains, including the Adherent-Invasive *E. coli* (AIEC) pathotype, have acquired a virulent nature. Despite the lack of typical enteropathogenic *E. coli* virulent factors in AIEC isolates, these are able not only to adhere to and invade intestinal epithelial cells (IECs), but also to replicate within macrophages without inducing cell death, thus evading protective host immune responses (5–7).

AIEC was first identified in the ileal mucosa of patients with Crohn's Disease (CD) and may constitute more than the 50% of the total number of bacteria both in early and chronic ileal lesions (8, 9). AIEC prevalence in Inflammatory Bowel Disease (IBD) – which comprises CD and Ulcerative Colitis (UC) – patients is significantly higher than in non-IBD subjects and, in general, AIEC strains are found in ileal and colonic samples of CD patients (6, 10–17). In UC, although the prevalence of this pathobiont is less clear, a recent meta-analysis suggests that this pathotype could be involved in its pathogenesis (18). Both *in vitro* and *in vivo* assays helped explain the molecular basis of AIEC pathogenicity in CD (9, 19). AIEC mechanisms to cross the mucus layer include the secretion of bacterial proteases (20, 21) as well as the alteration of host antimicrobial peptides (22). Adhesion and invasion to IECs occurs through the interaction between, among others, AIEC type 1 pili and the eukaryotic glycoprotein CEACAM6 (23, 24). On the other hand, flagella are crucial in mediating AIEC-induced cellular responses through their binding to IECs-toll like receptor (TLR)-5 (25). All these events end up triggering a cytokine release which, in turn, promotes intestinal epithelial permeability (26) and intestinal inflammation in compromised patients (27). AIEC are also able to invade M cells and translocate through Peyer's patches reaching the lamina propria and rapidly spreading through the mesenteric lymph nodes (28–30), and to translocate across the intestinal barrier due to tight junctions expression alteration (31). Overall, it has been demonstrated that AIEC infections affect a wide variety of host cell processes such as protein synthesis, signal transduction, cell division, and cytoskeletal function among many others (32).

AIEC identification is currently challenging, as it relies on phenotypic assays based on infected cell cultures, which are highly time-consuming. Therefore, the identification of AIEC molecular markers is of great importance since it would support detection of AIEC carriers, which is necessary to carry out epidemiological studies and to eventually establish prevention protocols (33–35). Different immortalized cell lines have been applied to assess the AIEC phenotype. The most common ones for the study of AIEC adhesion and invasion capacity are Caco2, Intestine-407 (I407), T84 and Hep2 as reviewed by Camprubí-Font et al. (36). Even though cell lines are easy to obtain, handle and expand over time, they lack important physiological features such as tissue cytoarchitecture, inter-individual variability and gut location-specific attributes. All of these limitations can be overcome by using human primary cultures. Organs or tissues isolated from their *in vivo* environment offer the advantage of providing a more physiological experimental setting due to their mimesis of the tissue of origin, phenotype and structure. Hence, infecting human colonocytes derived from patient biopsies might represent a promising strategy for studying the intestinal epithelium response to AIEC, as well as new pathogenicity mechanisms associated with this pathobiont. Such an approach could lead to the discovery of new disease biomarkers and new therapeutic targets. To our knowledge, there are few publicly available reports that analyze the interaction between enteric pathogens and human isolated IECs (23, 37–41). More recently, Sayed et al. published a study in which AIEC infection of organoid-derived 2D cultures is applied to explore host engulfment in IBD. Their research supports the suitability of human organoid-derived epithelial monolayers (ODMs) as a tool to study AIEC pathogenicity (42). Here, we deeply describe our recently developed infection method that uses colonic ODMs to examine the ability of AIECs to adhere to and invade primary human epithelial cells. This *ex vivo* cell culture exhibits an appropriate cell polarization for a more physiological-like bacteria-host cell interplay and thus represents a powerful tool for AIEC-infection studies. Throughout the next sections we will detail the entire procedure by which ODMs are obtained and lately infected with AIEC. To that end, we will also specify the performed infection-kinetics assay to determine the ideal time of infection and the bacteria/IEC ratio for this pathobiont to efficiently invade ODMs.

MATERIALS AND EQUIPMENT

Reagents

Biological Reagents

- Human Epithelial Organoid 3D Cultures (EpOCs): intestinal samples of healthy sigmoid colon with no evidence of macroscopic inflammatory lesions were obtained from subjects undergoing surgery for left-sided colorectal cancer (CRC) or routine endoscopy for CRC screening. For surgical pieces, a segment of healthy mucosa was collected at least 10 cm from the margin of the affected area. Biopsy samples showed no evidence of neoplastic lesions. However, biopsies were not specifically assessed for signs of microscopic inflammation.

Surgical or biopsy samples were immediately used for generating EpOCs. **Supplementary Table 1** shows the clinical and demographic characteristics of the subjects enrolled to develop this protocol and from which 3D cultures were obtained. EpOCs samples were used on day 5 of expansion and were distributed among different subgroups based on the experimental approaches used. Patients were recruited at the Department of Gastroenterology, Hospital Clinic Barcelona. The study protocol was approved by the Ethics Committee of the Hospital Clinic of Barcelona (registration number HCB/2016/0546).

- Cell lines: Intestine-407 – I407 – (ATCC CCL-6, RRID: CVCL_1907) cell line.
- Bacterial Strains: The AIEC strain LF82, which was isolated from a chronic ileal lesion of a patient with CD, and the non-pathogenic strain *E. coli* K12 C600 [a prototypical derived laboratory strain which has been extensively used for molecular microbiology and bacterial physiology studies since its isolation in 1954 (43)], were provided in 2006 by Prof. Arlette Darfeuille-Michaud (Université d'Auvergne, Clermont-Ferrand, France).

Primary Cell Culture Reagents

All concentrations shown here correspond to the used working concentration (WC).

- Heat inactivated – at 56°C for 30 minutes – fetal bovine serum – FBS – South American (Applied Biosystems, Foster City, CA, USA. Ref. 10270106).
- Washing medium (WM) (**Supplementary Table 2**).
- Matrigel Growth Factor Reduced Basement Membrane (Corning, NY, USA. Ref. 356231): -80°C stored bottles were thawed overnight (ON) on ice. 500 µl aliquots were prepared and frozen at -20°C for later use. Once thawed, aliquots were stored at 4°C for no longer than one week.
- Cell Recovery solution (Corning, NY, USA. Ref. 354253).
- Dissociation medium (**Supplementary Table 3**).
- Wnt3a-conditioned medium + Y (STEM+Y medium) (**Supplementary Table 4**).
- Trypan blue Solution (Gibco, Grand Island, NY, USA. Ref. 15250061).
- Differentiation medium (DIFF medium) (**Supplementary Table 5**).

Cell Line Reagents

- Trypsin-EDTA (Lonza, Basel, Switzerland. Ref. H3BE17-161E). WC: 170,000 U/L trypsin and 200mg/L EDTA.
- EMEM Complete Medium (**Supplementary Table 6**).

Bacterial Culture Reagents

- Liquid Luria-Bertani (LB) Broth (Sigma-Aldrich, Saint Louis, MO, USA. Ref. L3022).

Gentamicin Protection Assay Reagents

- Minimal media (EMEM-MM/DIFF-MM; **Supplementary Tables 7** and **8**, respectively).
- Minimal media containing 100 µg/ml of gentamicin (Lonza, Basel, Switzerland. Ref. 17-519Z).
- Ringer Solution (Scharlau, Barcelona, Spain. Ref. 06-073-500).
- LB Agar (**Supplementary Table 9**).

RNA Isolation and Quantitative Multiplex Real-Time Polymerase Chain Reaction Reagents

- TRIzol reagent (Life Technologies, Carlsbad, CA, USA. Ref. 15596018).
- Chloroform (Sigma-Aldrich, Saint Louis, MO, USA. Ref. C2432-500).
- RNeasy Kit (Qiagen, Hilden, Germany. Ref. 74106).
- High Capacity cDNA Reverse Transcription kit (Applied Biosystems, Carlsbad, CA, USA. Ref. 4368813).
- RNAse Inhibitor (Applied Biosystems, Carlsbad, CA, USA. Ref. N8080119).
- TaqMan™ Fast Universal PCR Master Mix (2X), no AmpErase™ UNG (Applied Biosystems, Carlsbad, CA, USA. Ref. 4366073).
- Nuclease Free Water (Promega, Madison, WI, USA. Ref. P1193).
- Pre-designed TaqMan Assays (Applied Biosystems, Carlsbad, CA, USA.): *MYC* (Mm00487804_m1), *MKI67* (Mm01278617_m1), *AXIN2* (Hs00610344_m1), *TJP3 (*Hs00274276_m1*), TFF3* (Hs00902278_m1), *MUC2* (Hs03005094_m1), *LGR5* (Hs00173664_m1), *FYN* (Hs00176628_m1), *CDCA7* (Hs00230589_m1), *ZG16* (Hs00380609_m1), *TLR3* (Hs01551078_m1), *TLR4* (Hs00152939_m1), *CCL20* (Hs01011368_m1), *CXCL1* (Hs00605382_gH), *CXCL2* (Hs00601975_m1), *ANPEP* (Hs00952642_m1), *FABP2* (Hs01573164_g1), *AQP8* (Hs00154124_m1), *CA1* (Hs01100176_m1), *CHGA* (Hs00154441_m1), *CEACAM7* (Hs03988977_m1), *OCLN* (Hs00170162_m1), *PHGDH* (Hs01106330_m1), *CYP1B1* (Hs00164383_m1), (all of them conjugated with FAM dye) and *ACTB* (endogenous control; Ref. 4310881E) with VIC dye.

Immunostaining Assay Reagents

- Paraformaldehyde aqueous solution – PFA – (Electron Microscopy Sciences, Hatfield, PA, USA. Ref. 15710. WC: 4%.
- Glycine (Sigma-Aldrich, Saint Louis, MO, USA Ref. G7126). WC: 20 mM.
- Bovine serum albumin – BSA – (Sigma-Aldrich, Saint Louis, MO, USA Ref. T8787). WC: 1%.
- Primary antibodies: mouse anti-EpCAM (1:100; Dako, Denmark. Ref. M0804), rabbit anti-E-Cadherin (1:100, Cell Signaling Technology, Danvers, MA, USA. Ref. 3195S), mouse anti-KI67 (1:100, Leica, Wetzlar, Germany. Ref. NCL_L-KI67_MM1), rabbit anti-MUC2 (1:250, Santa Cruz Biotechnology, Dallas, TX, USA. Ref. sc-15334), mouse anti-VILLIN (1:100; Dako, Denmark. Ref. M3637) all diluted in 1% BSA.
- Secondary antibodies: anti-mouse Cy3 (1:400, Jackson ImmunoResearch, Cambridge, UK. Ref. 115-165-205. RRID: AB_2338694) and anti-rabbit Alexa 488 (1:400, Jackson ImmunoResearch, Cambridge, UK. Ref. 111-545-144. RRID: AB_2338052) all diluted in 1% BSA.
- 4′,6-diamidino-2-phenylindole (DAPI) (diluted 1:10000 in DPBS, Invitrogen, Carlsbad, CA, USA. Ref. D1306).

- Alexa Fluor™ 555 Phalloidin (diluted 1:40 in 1%BSA; Invitrogen, Carlsbad, CA, USA. Ref. A34055).
- Mounting medium: glycerol (Sigma. Ref. G5516-500). WC: 80%.

Other Reagents

- Dulbecco phosphate-buffered saline – DPBS – (Gibco, Grand Island, NY, USA. Ref. 14190-169).
- Triton X-100 (Sigma-Aldrich, Saint Louis, MO, USA. Ref. T8787).
- Distilled H_2O.
- CellTox™ Green Cytotoxicity Assay (Promega, Madison, WI, USA. Ref. G8741).
- Digitonin (Sigma-Aldrich, Saint Louis, MO, USA., Ref. D141). WC: 100 µg/ml.

Equipment

Consumables

- 1.5 ml tubes (Eppendorf, Hamburg, Germany. Ref. 211-2130).
- 1.5 ml tubes RNAse free (Invitrogen, Carlsbad, CA, USA Ref. AM12400).
- Falcon 15ml Sterile Disposable Conical Centrifuge Tubes (BD Biosciences, San Jose, CA, USA. Ref. 352096).
- Falcon 50ml Sterile Disposable Conical Centrifuge Tubes (BD Biosciences, San Jose, CA, USA. Ref. 352070).
- Filtered pipette tips – 10 µl, 20 µl, 200 µl, 1000 µl – (VWR International Eurolab, Barcelona, Spain. Refs. 732-1148/732-1150/732-1153/732-1154).
- Serological pipettes: 5, 10, 25 ml and 50 ml (VWR International Eurolab, Barcelona, Spain. Refs. 357543/357551/357535/734-1740).
- Scalpels (VWR, International Eurolab, Barcelona, Spain. Ref. SWAN6608).
- Microscope slides (DDBiolab, Barelona, Spain. Ref. 37519).
- KOVA® Glasstic Slide 10 With Counting Grids (Kova, Garden Grove, CA, USA. Ref. 87144E).
- BD Emerald 5 ml syringes (BD Biosciences, San Jose, CA, USA. Ref. 1026307731).
- BD Microlance® 3 21Gx1" 0.8mmx25mm (BD Biosciences, San Jose, CA, USA. Ref. 301156).
- MicroAmp™ Optical Adhesive Film (Applied Biosystems, Foster City, CA, USA. Ref. 4311971).

Plates and Flasks

- 48-well plates (Corning, NY, USA. Ref. 3548).
- 24-well plates (Jet Biofil, Guangzhou, China. Ref. TCP-011-024).
- µ-Slide 8 Well ibiTreat: #1.5 polymer coverslip, tissue culture treated, sterilized (IBIDI, Gräfelfing, Germany. Ref. 80826).
- T25 and T75 tissue culture flasks (BioLab, Barcelona, Spain. Refs. 55400/55402).
- 120x120mm Petri dishes (Corning, NY, USA. Ref. GOSSBP124-05).
- Microplate 96 well qPCR FAST THERMAL CYCLING (Applied Biosystems, Foster City, CA, USA. Ref. 4346907).

Lab Equipment

- Vortex mixer.
- Thermo Scientific™ NanoDrop™ One^C Microvolume UV-Vis Spectrophotometer Precision Scale.
- Veriti 96-well Thermal Cycler (Applied Biosystems).
- Benchtop shaker (BOECO Mini-Rocker Shaker MR-1).
- Benchtop refrigerated centrifuge (for 1.5 ml, 15 ml and 50 ml conical tubes).
- Inverted microscope (Olympus X51 Inverted Microscope).
- Fluorescence Inverted Microscope Nikon S Ti.
- Cell incubator (37°C, 5% CO_2).
- Biosafety hood.
- Autoclave.
- Spectrophotometer.
- ABI PRISM 7500 Fast RT-PCR System (Applied Biosystems).
- Leica TCS_SP5 scanning spectral confocal microscope (Leica Microsystems, Germany) equipped with an DMI 6000 inverted fluorescence microscope, blue diode (405nm), Argon (488nm), diode pumped solid state (561nm) lasers and a Apochromat 63X oil immersion objective (NA 1.4).
- Zeiss LSM880 laser scanning spectral confocal microscope (Carl Zeiss, Jena, Germany) equipped with an Axio Observer 7 inverted microscope, blue diode (405nm), Argon (488nm), diode pumped solid state (561nm) and HeNe (633nm) lasers and a Plan Apochromat 63X oil (NA 1.4) immersion objective lenses.

Other Equipment

- Micropipettes and Pipettor.
- Tube racks.
- Refrigerated racks.
- Aluminum foil.
- Cell-counter.
- Forceps.
- Scissors.
- Spectrophotometer Cuvettes.

Software Equipment

- Image processing software (Image J Fiji, https://imagej.net/Fiji).
- Data software analysis Graphpad Prism 5 (GraphPad Software, http://www.graphpad.com/).

METHODS

Our prime aim was to develop a new model of infection using primary human intestinal epithelium. For that purpose, ODMs were generated from EpOCs and differentiated (d-ODMs) before being infected by *E. coli*.

In this section we will accurately describe the optimized protocol for ODM generation from EpOCs, ODM differentiation and AIEC infection of d-ODMs to evaluate AIEC's invasive capacity in differentiated primary epithelial cells.

Organoid-Derived Monolayer (Timing ⏲ 4d)

Generation of Organoid-Derived Monolayers

EpOCs were generated as previously described (44, 45). Briefly, crypts were isolated from intestinal samples after an incubation of 45' with 8mM EDTA at 4°C. Crypts were then embedded in 25 µl of Matrigel and covered with 250 µl of STEM medium (**Supplementary Table 4** – modified without Y). After 2-3 days, the crypt culture was mechanically dissociated to single cells using a dispase-based solution (**Supplementary Table 3**) and expanded at a 1:3 dilution. EpOCs were used after 5 days of expansion to generate ODMs as detailed below. Prior to EpOCs dissociation, 48-well plates were pre-coated with a thin layer of diluted (1:20) Matrigel in DPBS to promote cell adhesion. A volume of 150 µl/well was added and plates were incubated at room temperature (RT) for 1h. Excess Matrigel was discarded and the diluted-Matrigel layer was covered with Advanced DMEM/F12 medium and kept at RT until immediate use. Alternatively, coated plates were stored at 4°C covered in DPBS for up to 7 days.

Δ CRITICAL. Based on our experience, every EpOCs drop contains around 40,000-100,000 cells. Thus, depending on the final number of single cells needed for the invasion assay, a determined number of EpOCs drops will be used at the starting point.

To generate ODMs from EpOCs, the protocol was as follows:

(1) Matrigel drops containing EpOCs were washed with cold DPBS and collected in Cell Recovery solution (300 µl/well) at 4°C for 40 minutes. Every 5-10 minutes, cell suspensions were gently inverted upside-down.

(2) 4-5 ml of washing medium (WM) (**Supplementary Table 2**) were added, and the cell suspensions were centrifuged at 400*g* for 4 minutes at 4°C.

(3) Supernatant was discarded and the pellet was resuspended in Dissociation Medium (**Supplementary Table 3**) followed by 15-20 minutes of incubation at 37°C. On average, 5 ml Dissociation Medium were used for every 20-25 Matrigel drops.

(4) After organoid release, cells were mechanically disaggregated using a 5 ml syringe with a 21G needle until the cells were totally dissociated (20-50 strokes were conducted depending on the sample (**Figure 1A**)). To evaluate the extent to which EpOCs were dissociated to single cells, microscope observation was performed. If required, additional rounds of 10-20 strokes followed by microscope observation were performed until complete cell dissociation was reached.

(5) Cells were centrifuged at 800*g* at 4°C for 4 minutes and washed with 5 ml of WM after supernatant removal. This step was repeated twice.

(6) The remaining pellet was resuspended in 1-2 ml of WM for manual cell counting:

a. Cells (10 µl) were diluted 1:1 with Trypan blue Solution.

b. 10 µl of the cell suspension was loaded into a Glasstic Slide 10 With Counting Grids and the cell number was estimated according to the manufacturer's recommendations. The mortality rate (% of dead cells over the total number of cells) was usually below 10%.

(7) Single cells were again centrifuged, and the pellet was resuspended in the required volume of STEM+Y medium (**Supplementary Table 4**) to achieve $2x10^5$ cells/well/250 µl.

(8) Cells were seeded on Matrigel pre-coated 48-well plates and incubated for 24h at 37°C 5% CO_2 (**Figure 1B**).

Differentiation of Organoid-Derived Monolayers

After incubation, ODMs were induced to differentiation. To this end, STEM + Y medium was discarded and ODMs were washed with DPBS and Advanced DMEM/F12 medium (300 µl/well) at RT to remove dead cells. DIFF medium (250 µl/well) (**Supplementary Table 5**) was then added and ODMs were incubated at 37°C 5% CO_2 for an additional 48h.

Under these conditions, the differentiated monolayer (d-ODMs) reached 100% confluence 1-2 days after differentiation (**Figure 2A**). Therefore, the period between cells seeding and infection was 72h (cells were incubated for 24h after seeding and before differentiation, and 48h after differentiation and before infection).

Quantitative Multiplex Real-Time Polymerase Chain Reaction and Immunofluorescence

Δ FOR SYSTEM SET UP ONLY. The methodology described in this section was only utilized during optimization and until the protocol we established was entrenched (**Figure 1C**).

RT-qPCR

Both ODMs and d-ODMs were harvested in Trizol for RNA extraction (**Supplementary Table 1 Group 1**) and isolation using the RNeasy Kit. RNA was transcribed to cDNA at a final concentration of 250 ng/50 µl using the reverse transcriptase High-Capacity cDNA RT kit with RNase inhibitor. Reverse transcription was performed using a Programmable Thermal Cycler for 10 minutes at 25°C followed by 2 hours at 37°C. Quantitative Multiplex Real-time PCR (qPCR) was then conducted to characterize the monolayer gene expression pattern in ODMs versus d-ODMs. qPCR 96-well microplates contained a .volume of 10 µl/well (1 µl cDNA+0.5 µl each TaqMan Assay diluted in TaqMan Fast Universal PCR Master Mix and H_2O). Target genes were amplified and quantified using *ACTB* as the endogenous control. PCR reaction was run in the ABI PRISM 7500 Fast RT-PCR System using the following program: a holding stage for 20 seconds at 95°C and a cycling stage for 3 minutes at 95°C and 30 seconds at 60°C during 40 cycles. Target gene expression values relative to *ACTB* were expressed as arbitrary units (AU) following this formula:

$$AU = 2^{-(\text{Ct target gene} - Ct\ ACTB)} \times 1000$$

Immunofluorescence Staining

Monolayer cultures (both ODMs and d-ODMs, **Supplementary Table 1 Group 3**) seeded in µ-Slide 8 Well ibiTreat chambers

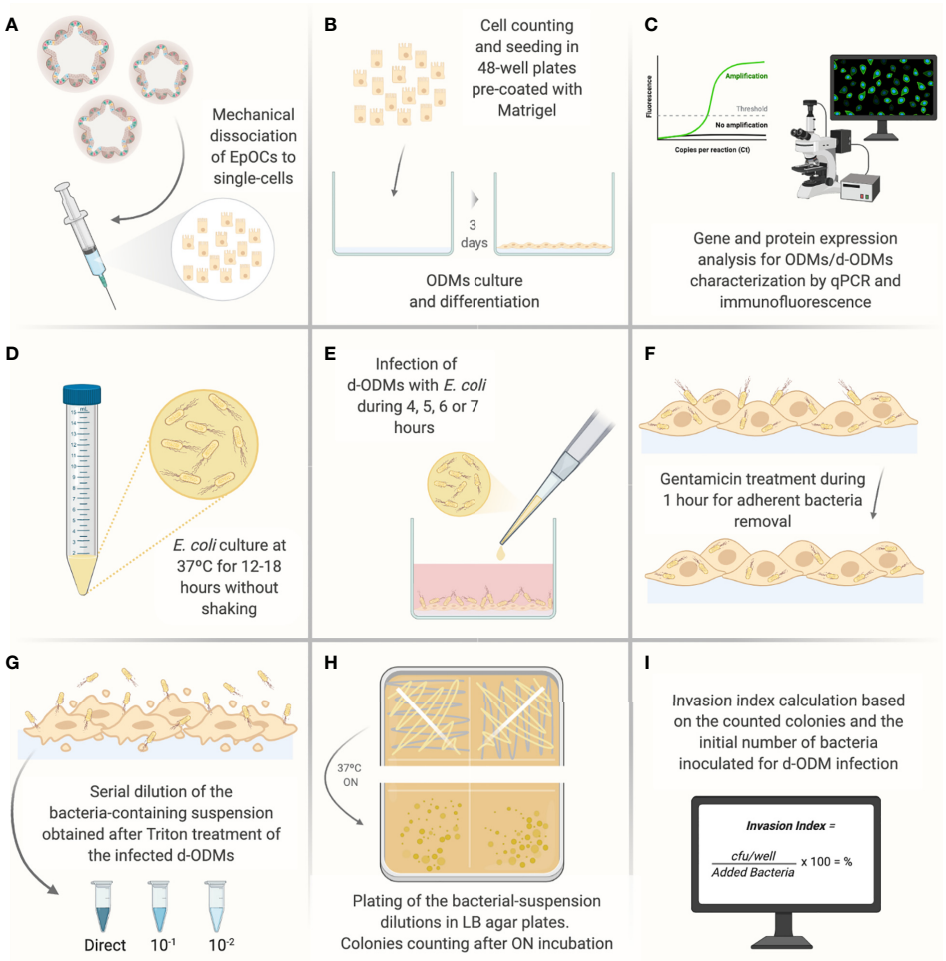

FIGURE 1 | Illustrated experimental workflow of the most critical steps of the d-ODMs-*E. coli* infection protocol. **(A)** Mechanical dissociation of EpOCs with the help of a 5 ml syringe with a 21G needle until achievement of single-cells. **(B)** Single-cell counting and seeding ($2x10^5$ cells/well on pre-coated 48-well plates with diluted Matrigel (1:20). Cells were incubated until ODM formation for further differentiation. **(C)** Characterization of ODMs and d-ODMs by qPCR and immunostaining (only during the protocol set-up). **(D)** ON growth of *E. coli* LF82 and K12 strains were grown in liquid LB. **(E)** Infection of d-ODMs with *E. coli* strains performed by gently releasing the drop. Infection times were from 4-7 hours. **(F)** Gentamicin (100 µg/ml) addition for 1 hour to eliminate adherent bacteria. **(G)** Cell treatment with 1% Triton X-100 to facilitate intracellular bacteria release. The bacterial suspension was then serially diluted and seeded. **(H)** ON incubation of bacterial dilutions in LB agar plates. **(I)** After colony counting, the Invasion Index for each strain was determined. This figure was created using BioRender.com.

(for optimal image acquisition) were processed for immunofluorescent staining as follows:

(1) After two DPBS washes, the cell monolayer was fixed with 2% PFA (1:1 4% PFA + DPBS) for 5 minutes at RT and then with 4% PFA for 10 minutes at RT.

(2) Cells were washed three times with DPBS: 1st fast; 2nd and 3rd 5 minutes at RT.

Δ **CRITICAL**. STOP POINT – Cells were stored at 4°C covered in DPBS (300 µl) or were immediately used for staining.

(3) 250 µl of 20mM Glycine was added for 10 minutes at RT to reduce background staining.

(4) DPBS washes were conducted as described in step (2).

(5) For permeabilization, 250 µl of 0.25% Triton X100 were added for 20 minutes at RT.

(6) Cells were then washed 3 additional times – 5 minutes each – with DPBS.

(7) To block non-specific binding, 250 µl of 1% BSA was applied and incubated at RT for 30-45 minutes.

(8) Primary antibodies (150-200 µl/well) – EpCAM, E-Cadherin, MUC2, Villin or KI67 – were added at the specified dilutions (in 1% BSA) and incubated ON at 4°C.

(9) After 3 DPBS washes (as in step 6), cells were incubated with 150-200 µl/well of the secondary antibodies – Anti-mouse Cy3 and Anti-rabbit 488 – at the specified dilutions (see *Materials* section) in 1% BSA for 1h of incubation at RT. Cells were washed 3x with DPBS at RT as described in step 6.

(10) For DNA counterstaining, DAPI (250 µl/well) was added and incubated at RT for 10 minutes. Washes were repeated as in step 6.

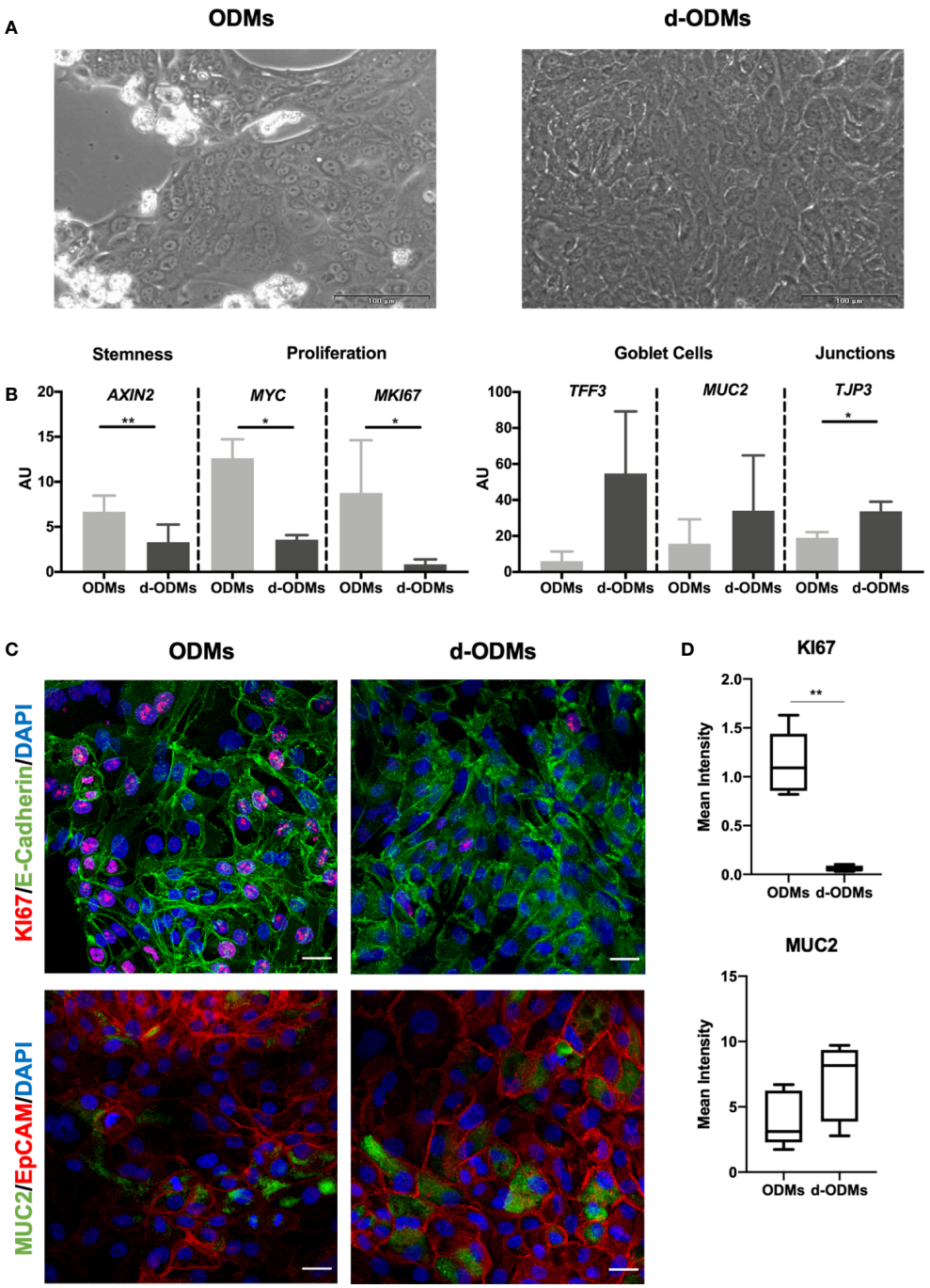

FIGURE 2 | Organoid-Derived Monolayers (ODMs) characterization. **(A)** ODMs (left panel) 24 hours after seeding showed a confluence of around 70-80% and d-ODMs (right panel) 48 hours after differentiation, showed 100% confluence. **(B)** Gene expression analysis of ODMs and d-ODMs (n = 5 for each culture type). *AXIN2, MYC, MKI67, TFF3*, *MUC2* and *TJP3* genes were analyzed by qPCR to determine their expression levels in ODM vs. d-ODMs. A paired t-test was performed to examine statistically different expression patterns between the two groups (ODMs/d-ODMs). A P value of <0.05 was considered statistically significant. *AXIN2*: **indicates P = 0.0012. *MYC*: *indicates P = 0.0135. *MKI67*: *indicates P = 0.0335. *TJP3*: *indicates P = 0.0365. **(C)** Protein expression analysis by immunofluorescence. KI67 and MUC2 were analyzed to confirm the proliferation and differentiation status of both ODMs and d-ODMs. E-Cadherin and EpCAM were used as epithelial cell-wall markers. DAPI was used to counterstain the cell nuclei. Scale bars: 25 µm. Images are representative of n = 3 independent experiments performed with samples from two different donors. **(D)** Box-plot distribution of the fluorescent signal of KI67 and MUC2 proteins in ODMs and d-ODMs, expressed as Mean Intensity. Fluorescence was quantified in 5 different fields per sample. A paired t-test was performed to examine statistically different expression patterns between the two groups (ODMs/d-ODMs). A P value of <0.05 was considered statistically significant. KI67: **indicates P = 0.0013.

(11) Finally, 200 µl/well of mounting medium (80% Glycerol in DPBS) were added. Samples were stored at 4°C for subsequent fluorescent microscope observation.

Δ CRITICAL. After adding the secondary antibodies, cells were kept in the dark.

Δ CRITICAL. For short-term storage, stained cells were kept at 4°C or at -20°C for up to 6 months.

AIEC Infection of Differentiated Organoid-Derived Monolayer (Timing ◴ 3d)

Bacterial Strains

Prior to infection, LF82 and *E. coli* K12 strains were cultured in 1.5 ml of LB Broth and incubated for 12-18 hours at 37°C without shaking (**Figure 1D**).

Reference Model of Infection

The I407 cell line, originally employed for AIEC-pathotype identification (6), was used as the reference method of the gentamicin protection assay in order to ensure that the bacterial strains ON cultures show the expected phenotype. Cells were passaged every 2-3 days *via* 5-minute incubation with 1 ml of Trypsin-EDTA after a washing step with DPBS. After collection, cells were centrifuged at 500*g* for 5 minutes and 20°C. Pelleted cells were resuspended in EMEM complete medium (**Supplementary Table 6**) and seeded in T75 flasks. Twenty-four hours before infection, $4x10^5$cells/well were plated on 24-well plates.

The assay was performed at Multiplicity of Infection (MOI) 10, as described previously (46, 47). Infection lasted 3 hours followed by 1 hour of gentamycin treatment. During the entire procedure, EMEM-MM (**Supplementary Table 7**) was employed. Invasive ability was quantified as the percentage of the intracellular bacteria from the initial inoculum (4×10^6 cfu/ml):

$$\text{I-INV}\,(\%) = \left(\text{intracell. bacteria}/4\times10^6\right)\times 100$$

Δ FOR SYSTEM SET UP ONLY. This model of infection was only performed until establishment of the d-ODM-based gentamicin protection assay.

d-ODM-Based Gentamicin Protection Assay

d-ODM Cell Counting

To infect cells with a determined MOI, it is crucial to know the exact number of cells seeded as a monolayer at the time of infection. In our particular case, we seeded $2x10^5$ EpOCs-derived single cells/well in 48-well plates based on previous experience (data not published), although this may need to be adjusted by each lab as culture conditions can vary slightly. To monitor the number of cells present in the plate at 100% confluency, experiments were performed seeding the above number of cells/well and counting cells present in d-ODM prior to infection. This step proved decisive in order to adjust the needed inoculum of bacteria and achieve the desired MOI. Briefly, d-ODMs were washed with DPBS to remove non-attached cells. Trypsin-EDTA (150 µl) was added to the culture for 10-15 minutes at 37°C 5% CO_2. Detached cells were collected and resuspended in Advanced DMEM/F12 + 10% FBS. These last two steps were repeated until complete cell-detachment was achieved. Cells were centrifuged at 800*g* for 4min and at 4°C and resuspended in 200 µl of Advanced DMEM/F12 + 10% FBS for cell counting as explained in a previous section (see the *ODM generation* section).

Δ CRITICAL. It is important to not exceed the 10-15 minutes incubation with Trypsin-EDTA in order to prevent cell death.

On average, we recovered approximately $1.8x10^5$ cells/well prior to infection (**Supplementary Figure 1**), which is close to the number of cells initially seeded. Notice that these numbers may have to be adjusted by each lab, as mentioned above.

For the infection assay, two different MOI – 20 and 100 – were assessed on d-ODM-based assays.

Thus, d-ODM counted-cells ($1.8x10^5$ cells/well) were multiplied 20- or 100-times to determine the bacterial colony forming units (cfu)/ml required for reaching each MOI value. In our case, $3{,}6x10^6$ or 18 $x10^6$ *E. coli* cfu/ml were needed.

Δ CRITICAL. Working at a confluence as close as possible to 100%, is essential to ensure the optimal ratio of bacterial cells/eukaryotic cells in order to reach the desired MOI.

Bacterial Optical Density and Colony Forming Unit Adjustment

The study of the *E. coli* growth curve in LB allowed us to estimate the cfu/ml at every measured Optical Density (OD) (**Supplementary Figure 2**). Prior to infection, ON bacterial cultures (both from LF82 and K12 strains) were adjusted to OD = 0.1, corresponding to $1.6x10^8$ cfu/ml. This OD was chosen since it represents an adequate inoculum volume for the infection assay for both of the assessed MOIs. The bacterial suspension was prepared following these steps:

(1) ON bacterial cell suspensions (500 µl) were diluted 1:1 with LB medium and 1 ml was transferred to a cuvette.

(2) The OD was measured with a spectrophotometer at a wavelength (λ) of 600 nm.

(3) OD adjustment was achieved in accordance with the following formula:

$$iV = fOD\ \ (0.1)\times fV/(mOD)\times\ \ 2$$

iV; Initial Volume (required volume for the ON culture)
fOD; Final OD (0.1 in this case)
fV; Final Volume (1 ml)
mOD; Measured OD

(4) The calculated iV and DIFF-MM (**Supplementary Table 8**) up to 1 ml total volume were added to a 1.5 ml tube.

ODM Infection and Gentamicin Protection Assay

As already mentioned, LF82 and K12 strains were used as positive (invasive) and negative (non-invasive) control, respectively. Infection was performed using d-ODMs generated from 7 different subjects (**Supplementary Table 1 Group 2**) as the starting material. Every experiment was conducted in duplicate.

DIFF medium was discarded from 100% confluent d-ODMs; cells were washed twice with DPBS at RT (500 µl/well) and fresh DIFF-MM was added (500 µl/well). Then, the corresponding

volume of OD 0.1 bacterial suspension (**Table 1**) was inoculated to reach each assessed MOI by gently releasing the drop (**Figure 1E**). Infected d-ODMs were incubated for 4, 5, 6 or 7 hours at 37°C 5% CO_2 for the complete infection-kinetics study. At the end of each time point, cells were washed 3 times with DPBS at RT – as explained above – and DIFF-MM containing 100 µg/ml of gentamicin was added for 1 additional hour (**Figure 1F**) in order to remove the extracellular bacterial cells. Three more DPBS washes at RT were required after gentamicin treatment. 1% Triton X-100 (250 µl/well) was added to d-ODMs to release the internalized bacteria. Vigorous pipetting to generate bubbles was required to efficiently detach and break the eukaryotic cell membranes (**Figure 1G**).

Δ CRITICAL. The Triton X-100 step should not take longer than 30 minutes in order to avoid bacterial cell death.

Invasion Index

To be able to count cfu/ml, the bacterial suspension resulting from the Triton X-100 treatment was serially diluted in Ringer Solution (**Figure 1G**). Dilutions of 10^{-1} and 10^{-2}, as well as the non-diluted samples, were plated (25 µl) in LB agar plates (**Supplementary Table 9**) and incubated ON at 37°C.

♦ **TIP**. 120x120mm square plates were used to plate up to 4 different dilutions. Plating was performed with the pipette-tip itself immediately after inoculation. The inoculum was streaked homogeneously through the plate-section (**Figure 1H**).

Δ CRITICAL. For a homogeneous mixture of bacterial dilutions, vortexing solutions is highly recommended.

Grown colonies in each dilution were only taken into consideration when the counting was between 15 - 150 (**Figure 1I**).

Intracellular bacteria

$$= \frac{\Sigma\ colonies}{(0.025\ \times\ (n_1 + 0.1\ \ x\ \ n_2)\ \times\ DF)}\ \times\ well\ \ volume\ \ (0.25)$$

$$= cfu/well$$

n_1 = number of plates at the more concentrated dilution
n_2 = number of plates at the less concentrated dilution
DF = dilution factor of the more concentrated dilution

Once the number of cfu/well was obtained, the invasion index (%) was calculated considering the amount of bacteria initially inoculated to d-ODMs:

$$Invasion\ \ Index = \frac{Intracellular\ \ bacteria}{Inoculated\ \ Bacteria\ \dagger}\ \times\ 100 = \%$$

†: in this context, $3.6x10^6$ for MOI 20 or $18\ x10^6$ for MOI 100.

TABLE 1 | Adjustment of the added bacterial-culture volume to the d-ODM culture depending on the tested MOI.

MOI 20	MOI 100
Number of d-ODM-cells: 180,000	Number of d-ODM-cells: 180,000
Final cfu/ml (fC): 3,600,000	Final cfu/ml (fC): 18,000,000
Final volume/well (fV): 500 µl	Final volume/well (fV): 500 µl
Initial cfu/ml (iC): $1.6x10^8$	Initial cfu/ml (iC): $1.6x10^8$
Added volume ($_{add}$V): **11.25 µl**	Added volume ($_{add}$V): **56.25 µl**

As previously described by Darfeuille-Michaud et al., who studied AIEC infection by using immortalized cell lines (6), we considered a strain to be invasive when the Invasion Index was > 0.1%

Fluorescent Cyto-staining and CellTox Green Cytotoxicity Assay

Notice that even though the techniques detailed herein are not mandatory, they were performed to obtain a deeper understanding of the results obtained from the AIEC infection of d-ODM (see *Anticipated Results* section).

Fluorescent Cyto-Staining

To visualize the bacterial internalization, LF82- and K12-infected monolayer cultures (at 5 hours of infection followed by 1 hour of gentamicin treatment (5 + 1) and MOI 100) seeded in µ-Slide 8 Well ibiTreat chambers, were processed for fluorescent cyto-staining. This procedure was identical to that used for ODM/d-ODM characterization until step (7) of the Immunofluorescence Staining section. After incubation with the blocking solution, 150-200 µl/well of Phalloidin diluted 1:40 in 1% BSA was added for staining of the actin filaments. After 1-hour incubation at RT, cells were washed 3x with DPBS at RT as in step 6 (see *Immunofluorescence Staining* section). DAPI (250 µl/well) was then added and the protocol continued as described in steps 10 and 11. The assay was performed with cells obtained from 3 different subjects (**Supplementary Table 1 Group 3**).

CellTox Green Cytotoxicity Assay

The protocol for d-ODMs cytotoxicity assessment corresponded to that recommended by the manufacturer. Briefly, after the infection assay, infected and non-infected d-ODMs were incubated with the CellTox reagent (1:1, 150 µl DIFF-MM + 150 µl CellTox) previously diluted according to the manufacturer's instructions (1:500 in Assay Buffer). After ≥15 minutes of incubation at 37°C in the dark, cultures were observed using a fluorescence microscope. A positive control of cell death was included by adding 100 µg/ml of digitonin in the uninfected d-ODM for 1 hour.

Data and Statistical Analysis

Quantitative data are expressed as the standard error of the mean (SEM). A paired t-test was performed to examine statistically different expression patterns between 2 groups, and a 2-way ANOVA test to examine statistical significance in multiple group data sets, followed by a Tukey test correction for multiple testing. A p-value of <0.05 was considered statistically significant. Data were analyzed using Graphpad Prism 8 (version 8.2.1).

ANTICIPATED RESULTS

Establishment of Differentiated Human Intestinal Epithelial Monolayer Cultures

The intestinal crypt is organized so that the stem-cell compartment resides at the bottom, thereby protected from the luminal content, while the differentiated and surface epithelium is more directly in

contact with the microbiota and its metabolites. In order to develop a model that would more closely resemble the type of upper crypt epithelium that is more susceptible to bacterial interactions and based on previous results from our lab (48, 49), we used a monolayer of differentiated epithelial cells derived from epithelial organoid cultures (d-ODMs).

First, we aimed to determine the optimal culture conditions for the ODMs to acquire a differentiated phenotype while reaching an appropriate confluence (100%) for the AIEC invasion assay. Based on previous experiments by our lab, we seeded $2x10^5$ single cells/well. On day 1, cells created clusters that alternated with empty areas, while on day 3, the monolayers reached 100% confluence, the requirement for AIEC infection (**Figure 2A**). Under these conditions, cells were collected and counted, obtaining an average of approximately $1.8x10^5$ cells/well (**Supplementary Figure 1**). Once the d-ODM number of cells at ~100% confluency was determined, we confirmed the differentiated phenotype of the monolayer by measuring key genes and proteins whose expression changes dramatically upon epithelial stem cell differentiation (38, 50).

As shown in **Figure 2B**, mRNA levels of *AXIN2*, *MYC* and *MKI67*, (the first, marker of stemness and the two last, markers of proliferation), were significantly higher in ODMs compared to d-ODMs. On the other hand, transcriptional levels of the differentiation markers *TFF3* and *MUC2*, showed an up-regulation, despite not statistically significant, in d-ODMs compared to ODMs. Similarly, *TJP3*, representative marker of epithelial cell junctions, was significantly up-regulated in d-ODM. Other markers included in the analysis (**Supplementary Figure 3**) confirmed the differentiated phenotype of the d-ODM culture (48).

Although using transcriptional analysis to easily screen cultures for their differentiation status – or other phenotypic features – is valuable, protein staining of the intact 2D cultures would help evaluate not just protein expression but also localization within the cell monolayer.

As an example, here we determined the protein expression of KI67, MUC2 and Villin by immunofluorescence. **Figure 2C** and **Supplementary Figure 4A** show representative images from 3 independent experiments. In agreement with the differentiated phenotype achieved in d-ODMs, KI67 was markedly decreased while MUC2 and Villin were increased compared to ODMs. These results were confirmed by fluorescence quantification analysis (**Figure 2D** and **Supplementary Figure 4B**).

Finally, to prove that the 2D culture exhibited an appropriate cell polarization, orthogonal views of MUC2 and Villin were analyzed (**Supplementary Figure 5**), showing a marked up-regulation of these two differentiation markers at the apical side of the d-ODM.

Altogether, both approaches demonstrated that primary cells derived from human EpOCs can establish a stable monolayer that preserves the intestinal identity thus mimicking the tissue of origin. Moreover, we achieved a differentiated and polarized phenotype in the d-ODMs at optimal confluence for the AIEC-infection study.

AIECs Can Invade d-ODMs

To the date, the characteristics and pathogenicity of AIECs have been studied so far by employing immortalized cell lines (36). Here, we studied the capability of AIECs to interact and invade a primary intestinal monolayer culture. First, we designed a kinetics infection assay to determine the time course of bacterial entry and/or intracellular survival in our culture system. To verify the strains' invasiveness capacity, I407 cell line was used as the reference method of the gentamicin protection assay. Both invasion assays (d-ODM and I407 infection) were carried out in parallel; thus, the *E. coli* ON cultures used for their infection were the same for each experiment performed. Results represented in **Supplementary Figure 6** show an INV-I% in I407 cells of 0.99 ± 0.225 and 0.0025 ± 0.00094 for the LF82 and K12 strains, respectively. These results were in agreement with previously published data (6, 46). Therefore, we conducted an infection-kinetics study to examine AIEC-d-ODMs infection by determining the percentage of internalized bacteria every hour for 7 hours of infection followed by 1 hour of gentamicin treatment as detailed in the previous sections. The assessed MOIs were 20 and 100. As shown in **Figures 3A, B**, we could quantitatively prove that the AIEC LF82 strain was able to invade d-ODMs, while the non-invasive *E. coli* strain (K12) showed an invasion index (INV-I%) below the established background (<0.1%). Moreover, LF82 showed a time-dependent increment of the INV-I%, and thus of the invasion capacity and/or intracellular multiplication in the AIEC-reference strain. Nevertheless, this capability was significantly higher compared to the K12 strain, both at 6 and 7 hours after infection for MOI 20 (**Figure 3A**) and at all time points for MOI 100 (**Figure 3B**). In fact, 5 hours of infection followed by 1 hour of gentamicin treatment at MOI 100 showed the greatest difference; the LF82 INV-I% measured almost 13 times greater than the K12 INV-I%. This occurred despite the fact that all INV-I % were lower at MOI 100 than at MOI 20. Furthermore, working with a greater number of bacteria/cell (higher MOI) ensured a remarkable reproducibility over time with highly consistent numbers of internalized bacteria in every experiment performed (**Figure 3C**). Nevertheless, this does not ensure higher INV-I%; in fact, this proved to be higher when the MOI was lower, as shown in **Figures 3A, B**. Maintenance of the d-ODMs cells' viability throughout all of the timepoints was observed *via* the CellTox Green assay (data not shown).

By staining the eukaryotic actin filaments (**Figure 4**), we confirmed the presence of high amounts of intracellular LF82 bacteria in the majority of those cells that formed the d-ODMs compared to the K12 strain.

In summary, we demonstrated the capacity of AIECs to invade the epithelial cells of d-ODMs. Thus, we present here a method that can be applied in multiple AIEC-IEC cross-talk studies, not only to discover new AIEC pathogenic mechanisms and host implicated molecules, but also, and more relevantly, to establish a possible starting point for further clinically oriented applications.

ADVANTAGES AND DISADVANTAGES

In the following section we will highlight which, in our opinion, are the most noteworthy advantages and disadvantages that this protocol presents. By doing so, we can focus on its practicality and try to overcome its limitations.

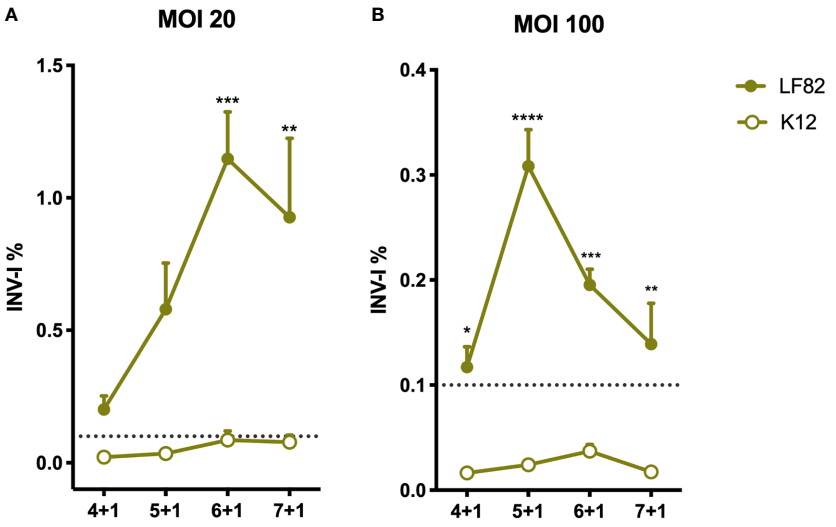

C

		K12		LF82		
		Mean	SEM (±)	Mean	SEM (±)	Adjusted p-value
MOI 20	4+1	0.021	0.0028	0.2012	0.0510	0.9824
	5+1	0.0346	0.0114	0.5794	0.1742	0.1401
	6+1	0.0856	0.0345	1.1468	0.1773	**0.0002**
	7+1	0.0782	0.026	0.9266	0.2980	**0.0033**
MOI 100	4+1	0.0164	0.0048	0.1172	0.0193	**0.0300**
	5+1	0.0242	0.0017	0.3084	0.0348	**<0.0001**
	6+1	0.0372	0.0063	0.1954	0.0148	**0.0001**
	7+1	0.0174	0.0049	0.139	0.0388	**0.0048**

FIGURE 3 | Graphic representation of *E. coli* LF82 and K12 invasion indexes on d-ODMs. INV-I% of both *E. coli* strains (n = 5 for each represented point in the graph) at MOI 20 **(A)** and 100 **(B)** relative to the increasing infection time points. The dashed line represents the established threshold (0,1) over which *E. coli* strains were considered to be invasive. The error bars correspond to the SEM. **(C)** Mean, SEM and adjusted p-values obtained by a 2-way ANOVA test to examine statistical significance between LF82 and K12 INV-I% for each infection timepoint. This analysis was followed by a Tukey test correction for multiple testing. A P value of <0.05 was considered statistically significant, and it is highlighted in bold.

Advantages

- Working with samples isolated from their natural surroundings (the human intestine in this case), preserves the cytoarchitecture and most of the intercellular connections and interactions. Moreover, it also provides the option to consider the interindividual variability that exists between different subjects.
- Working with ODMs and d-ODMs offers accessibility to the IECs-apical side, contrary to 3D-organoid structures which may be required for infectious models.
- We also demonstrate its great reproducibility, a highly relevant feature when one considers the differences between individuals and their responses to microbes.
- Given the fact that ODMs and d-ODMs can be generated from potentially any individual, including patients suffering from IBD, this method offers the possibility of testing personalized treatment approaches.

Disadvantages

- Time-consuming. EpOCs and ODM cultures are time intensive. Nonetheless, once the system is set up, organoid-derived single cells can be more rapidly obtained, shortening the time required for the entire procedure.
- Costly. EpOCs and ODM cultures could remain unaffordable for some research groups due to the high costliness of most of the reagents that are required.
- Access to patient specimens is required.
- Sample-to-sample variability might lead to differences in the number of cells obtained from every EpOCs drop. This might

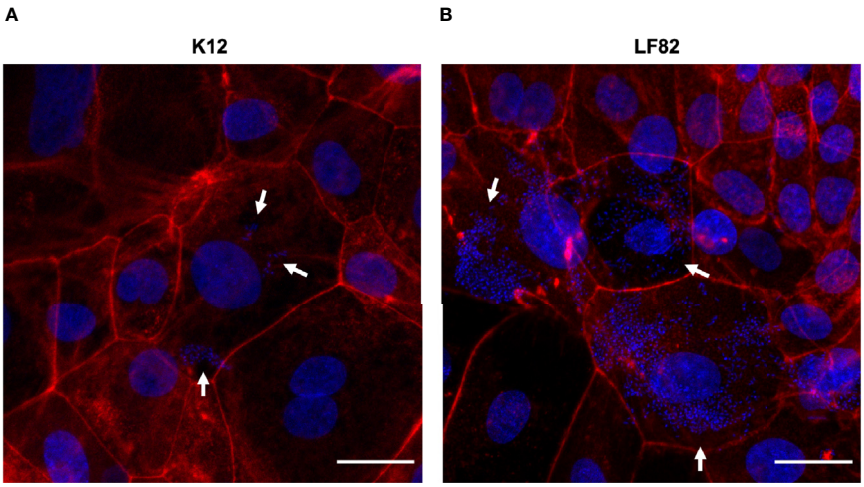

FIGURE 4 | *E. coli* LF82 and K12 invasion of d-ODMs as determined by the gentamicin protection assay. Phalloidin staining was performed to visualize the non-invasive control strain K12 **(A)** and the invasive LF82 **(B)** in d-ODMs after 5 hours of infection and 1 hour of gentamicin treatment at MOI 100. Phalloidin marked the eukaryotic actin filaments while DAPI bound to the DNA of both epithelial and bacterial cells. White arrows show bacterial localization inside the IECs. Scale bars: 25 µm. Images are representative of n = 3 independent experiments performed with samples from two different donors.

be an important limiting aspect that should be considered when applying the method described here.

DISCUSSION

In this manuscript we describe the steps required to develop a novel and reproducible human intestinal epithelial model for the study of enteric bacterial infections, particularly AIEC-related infections. Our model takes into consideration the variability of human biological responses to any pathogens, something that other models based on the use of cell lines cannot fully address (41, 51). Indeed, one of the main advantages of working with *ex vivo* primary cultures (as we mentioned in the previous section) is that these might offer a more physiological view of the host's response to AIEC infections. However, unpredictable biological variability could hinder the obtainment of the necessary cell concentration at the starting point. In that context, establishing an accurate and standardized protocol is crucial to facilitating reproducibility and enabling results comparisons. In our case, reproducibility was assessed first, by testing the gene and protein expression levels of the 2D cultures derived from the different donors. Moreover, AIEC infections were carried out in duplicate, exposing those EpOCs-derived d-ODMs from seven different individuals to *E. coli*. This validation approach is of great importance in host-pathogen interaction studies, considering the real differences in infection susceptibility among individuals and the divergence in host responses to a pathogen (39).

While a more extensive characterization of the d-ODM at protein level would add robustness to our culture system, our results suggest that ODMs and d-ODMs preserve the characteristics of the intestinal epithelium *in vivo*, resembling cells at the base and top of colonic crypts, respectively. Determining the number of cells that form the monolayer at the time of infection is a crucial step to better adjusting the working conditions in order to (1) achieve the optimal differentiated phenotype of the monolayer cultures, and (2) to properly adjust the number of exposed bacterial cells to the d-ODMs (MOI), which can greatly affect the results.

AIEC infection of d-ODMs was performed at different time points to analyze and select the best condition for achieving high reproducibility of infection and maximum specificity (lowest infection by non-invasive *E. coli*). Over time, increasing amounts of invasive bacteria were detected, with higher values evident when smaller amounts of bacteria (MOI 20) were added to the culture at the starting point. Based on this finding, we concluded that adding more bacteria does not directly correlate with higher invasion values. Similar results were obtained by Boudeau et al. in 1999 with Hep-2 cells (46). A 5-fold increase in the inoculum only represented an increase of 2.06 ± 0.7–fold (mean value of the fold-change increase for each timepoint) in intracellular bacteria. As d-ODMs cells were verified as viable with the CellTox Green assay, differences in the invasion indices were related to the initial inoculum. We believe that the d-ODMs can harbor a limited number of intracellular bacteria and, therefore, upon a given quantity of initial inoculum the invasion index will be lower. Even so, working with higher bacterial loads ensures a remarkable reproducibility of the results. This observation is not only valid for the invasive LF82 strain but also for the non-invasive control, K12.

Another observation concerns the dramatic decrease in the invasion index at the longest time of infection on LF82 INV-I% for both MOI 20 and 100. Other authors have similarly reported a decrease in the intracellular bacteria 4 hours after infection in mouse embryonic fibroblasts and HeLa, Hep-2 and I407 cell lines (52). Initially, we hypothesized that this event might be a consequence of eukaryotic cell death due to the bacterial infection process. Based to this assumption, when the initial

bacterial load was higher (MOI 100), eukaryotic cells would have begun dying at earlier time points. Nonetheless, using the CellTox Green assay we observed that infected cells viability was maintained over time (data not shown). Although AIECs are capable of evading IECs and macrophage-related stress responses in order to eliminate intracellular pathogens (6, 7, 46), decreases in the intracellular bacteria could reflect the capacity of IECs to restrict AIEC replication after a certain infection period (52). Testing the intracellular-bacteria viability at each time point would help confirm our hypothesis. It would also be interesting to determine, using this model, the presence of intracellular AIEC cells with a persistent phenotype; i.e. viable bacteria in a non-replicating state (53).

Similar strategies have been applied to study the interaction between AIEC, or other enteric pathogens and *E. coli* pathotypes, and human isolated IECs (23, 37–39, 41) and there is a recent and relevant publication in which organoid-derived 2D cultures are infected with AIEC (42). Nonetheless, this report does not include a detailed description of the steps taken to optimize infection efficacy. In contrast, our focus was to describe the steps required to obtain optimal ODM from EpOCs, that can be used as a model of primary epithelial cell infection with different *E. coli* strains. In particular, we go over the optimized steps from cell counting prior to infection to ODMs differentiation, and from infection kinetics to MOI testing. To the best of our knowledge, this is the first publicly accessible protocol that demonstrates the capacity of AIEC, compared to a non-invasive strain, to infect human primary IECs in a 2D configuration. Nonetheless, in our study we did not evaluate the impact of AIEC infection on epithelial cells including expression of bacterial sensing molecules, tight junctions, or immune response secreted proteins (54, 55). Such studies deserve further attention and will help elucidate how the epithelium differentially responds to invasive compared to non-invasive *E. coli*.

In conclusion, we can report the successful development of a human primary organoid-derived epithelial monolayer model of infection. Further application of this model, such as growing the d-ODMs in transwell-chambers in order to co-culture monolayers with AIECs and other human intestinal cell types (56) or the generation of d-ODMs derived from IBD patients, might lead not only to the development of a more comprehensive approach for studying the interaction of AIECs with the human gut, but also to a better understanding of the pathophysiology underlying inflammatory intestinal disorders.

DATA AVAILABILITY STATEMENT

The original contributions presented in the study are included in the article/**Supplementary Material**. Further inquiries can be directed to the corresponding author.

ETHICS STATEMENT

The studies involving human participants were reviewed and approved by Ethic Committee of the Hospital Clinic of Barcelona with the registration number HCB/2016/0546. The patients/participants provided their written informed consent to participate in this study.

AUTHOR CONTRIBUTIONS

AM, ID, AS, and MM-M designed the study. AM designed and conducted the experiments, acquired and analyzed the data, performed the biostatistics analysis, and wrote the manuscript. ID, designed and conducted experiments. MM-P and ME collected samples and provided technical support. QB-R provided technical support. ER recruited patients and collected samples. ID, AS, and MM-M supervised the experiments, analyzed data, and reviewed the manuscript. All authors contributed to the article and approved the submitted version.

FUNDING

AM was supported by the Programa Estatal de Investigación, Desarrollo e Innovación del Ministerio de Economía, Industria y Competitividad, co-funded by the European Social Fund (ESF) under grant agreement number FPI BES-2016-076642. ID is funded by the Horizon 2020 Framework Programme (EU for Research and Innovation H2020), Grant 720905. QB-R was supported by the Programa d'Ajuts per a Investigadors en Formació de la Universitat de Girona – IFUdG 2019/21. AS is funded by the Centro de Investigación Biomédica en Red de Enfermedades Hepáticas y Digestivas (CIBEREHD) and Grant RTI2018- 096946-B-I00 from the Ministerio de Ciencia, Innovación y Universidades, Spain. MM-M is funded by the Spanish Ministry of Economy and Competitiveness through project SAF2017-82261-P, which is co-funded by the European Regional Development Fund.

ACKNOWLEDGMENTS

We thank the Advanced Optical Microscopy Unit at the Universitat de Barcelona for their support, the Endoscopy and Pathology Departments at Hospital Clinic Barcelona and the Biobank Facility at the Institut d'Investigacions Biomèdiques August Pi i Sunyer (IDIBAPS) for providing us with the samples required to conduct this study, and all of the volunteers for their selfless participation. We also thank Carla Camprubí-Font, Carlos Ratia, Victoria Ballén and Mar Cordero-Alba for technical support, and Joe Moore for editorial assistance.

SUPPLEMENTARY MATERIAL

The Supplementary Material for this article can be found online at: https://www.frontiersin.org/articles/10.3389/fimmu.2021.646906/full#supplementary-material

REFERENCES

1. Delmas J, Dalmaso G. Richard Bonnet. Escherichia coli: The Good, the Bad and the Ugly. *Clin Microbiol* (2015) 04. doi: 10.4172/2327-5073.1000195
2. Christofi T, Panayidou S, Dieronitou I, Michael C, Apidianakis Y. Metabolic output defines Escherichia coli as a health-promoting microbe against intestinal Pseudomonas aeruginosa. *Sci Rep* (2019) 9:14463. doi: 10.1038/s41598-019-51058-3
3. Boudeau J, Glasser A-L, Julien S, Colombel J-F, Darfeuille-Michaud A. Inhibitory effect of probiotic Escherichia coli strain Nissle 1917 on adhesion to and invasion of intestinal epithelial cells by adherent-invasive E. coli strains isolated from patients with Crohn's disease. *Aliment Pharmacol Ther* (2003) 18:45–56. doi: 10.1046/j.1365-2036.2003.01638.x
4. Huebner C, Ding Y, Petermann I, Knapp C, Ferguson LR. The probiotic Escherichia coli Nissle 1917 reduces pathogen invasion and modulates cytokine expression in Caco-2 cells infected with Crohn's disease-associated E. coli LF82. *Appl Environ Microbiol* (2011) 77:2541–4. doi: 10.1128/AEM.01601-10
5. Glasser A-L, Boudeau J, Barnich N, Perruchot M-H, Colombel J-F, Darfeuille-Michaud A. Adherent Invasive Escherichia coli Strains from Patients with Crohn's Disease Survive and Replicate within Macrophages without Inducing Host Cell Death. *Infection Immun* (2001) 69:5529–37. doi: 10.1128/IAI.69.9.5529-5537.2001
6. Darfeuille-Michaud A, Boudeau J, Bulois P, Neut C, Glasser A-L, Barnich N, et al. High prevalence of adherent-invasive Escherichia coli associated with ileal mucosa in Crohn's disease. *Gastroenterology* (2004) 127:412–21. doi: 10.1053/j.gastro.2004.04.061
7. Ossa JC, Ho NK, Wine E, Leung N, Gray-Owen SD, Sherman PM. Adherent–invasive Escherichia coli blocks interferon-γ-induced signal transducer and activator of transcription (STAT)-1 in human intestinal epithelial cells. *Cell Microbiol* (2013) 15:446–57. doi: 10.1111/cmi.12048
8. Darfeuille-Michaud A, Neut C, Barnich N, Lederman E, Di Martino P, Desreumaux P, et al. Presence of adherent Escherichia coli strains in ileal mucosa of patients with Crohn's disease. *Gastroenterology* (1998) 115:1405–13. doi: 10.1016/S0016-5085(98)70019-8
9. Palmela C, Chevarin C, Xu Z, Torres J, Sevrin G, Hirten R, et al. Adherent-invasive *Escherichia coli* in inflammatory bowel disease. *Gut* (2018) 67:574–87. doi: 10.1136/gutjnl-2017-314903
10. Baumgart M, Dogan B, Rishniw M, Weitzman G, Bosworth B, Yantiss R, et al. Culture independent analysis of ileal mucosa reveals a selective increase in invasive Escherichia coli of novel phylogeny relative to depletion of Clostridiales in Crohn's disease involving the ileum. *ISME J* (2007) 1:403–18. doi: 10.1038/ismej.2007.52
11. Sasaki M, Sitaraman S, Babbin B, Gerner-Smidt P, Ribot E, Garrett N, et al. Invasive Escherichia coli are a feature of Crohn's disease. *Lab Invest* (2007) 87:1042–54. doi: 10.1038/labinvest.3700661
12. Martinez-Medina M, Aldeguer X, Lopez-Siles M, González-Huix F, López-Oliu C, Dahbi G, et al. Molecular diversity of Escherichia coli in the human gut: new ecological evidence supporting the role of adherent-invasive E. coli (AIEC) in Crohn's disease. *Inflammation Bowel Dis* (2009) 15:872–82. doi: 10.1002/ibd.20860
13. Raso T, Crivellaro S, Chirillo MG, Pais P, Gaia E, Savoia D. Analysis of Escherichia coli isolated from patients affected by Crohn's disease. *Curr Microbiol* (2011) 63:131–7. doi: 10.1007/s00284-011-9947-8
14. Negroni A, Costanzo M, Vitali R, Superti F, Bertuccini L, Tinari A, et al. Characterization of adherent-invasive Escherichia coli isolated from pediatric patients with inflammatory bowel disease. *Inflammation Bowel Dis* (2012) 18:913–24. doi: 10.1002/ibd.21899
15. Dogan B, Scherl E, Bosworth B, Yantiss R, Altier C, McDonough PL, et al. Multidrug resistance is common in Escherichia coli associated with ileal Crohn's disease. *Inflammation Bowel Dis* (2013) 19:141–50. doi: 10.1002/ibd.22971
16. Conte MP, Longhi C, Marazzato M, Conte AL, Aleandri M, Lepanto MS, et al. Adherent-invasive Escherichia coli (AIEC) in pediatric Crohn's disease patients: phenotypic and genetic pathogenic features. *BMC Res Notes* (2014) 7:748. doi: 10.1186/1756-0500-7-748
17. Céspedes S, Saitz W, Del Canto F, De la Fuente M, Quera R, Hermoso M, et al. Genetic Diversity and Virulence Determinants of Escherichia coli Strains Isolated from Patients with Crohn's Disease in Spain and Chile. *Front Microbiol* (2017) 8:639. doi: 10.3389/fmicb.2017.00639
18. Nadalian B, Yadegar A, Houri H, Olfatifar M, Shahrokh S, Aghdaei HA, et al. Prevalence of the pathobiont adherent-invasive Escherichia coli and inflammatory bowel disease: a systematic review and meta-analysis. *J Gastroenterol Hepatol* (2020). doi: 10.1111/jgh.15260
19. Agus A, Massier S, Darfeuille-Michaud A, Billard E, Barnich N. Understanding Host-Adherent-Invasive Escherichia coli Interaction in Crohn's Disease: Opening Up New Therapeutic Strategies. *BioMed Res Int* (2014) 2014:e567929. doi: 10.1155/2014/567929
20. Dharmani P, Srivastava V, Kissoon-Singh V, Chadee K. Role of Intestinal Mucins in Innate Host Defense Mechanisms against Pathogens. *J Innate Immun* (2009) 1:123–35. doi: 10.1159/000163037
21. McGuckin MA, Lindén SK, Sutton P, Florin TH. Mucin dynamics and enteric pathogens. *Nat Rev Microbiol* (2011) 9:265–78. doi: 10.1038/nrmicro2538
22. McPhee JB, Small CL, Reid-Yu SA, Brannon JR, Le Moual H, Coombes BK. Host defense peptide resistance contributes to colonization and maximal intestinal pathology by Crohn's disease-associated adherent-invasive Escherichia coli. *Infect Immun* (2014) 82:3383–93. doi: 10.1128/IAI.01888-14
23. Barnich N, Carvalho FA, Glasser A-L, Darcha C, Jantscheff P, Allez M, et al. CEACAM6 acts as a receptor for adherent-invasive E. coli, supporting ileal mucosa colonization in Crohn disease. *J Clin Invest* (2007) 117:1566–74. doi: 10.1172/JCI30504
24. Carvalho FA, Barnich N, Sivignon A, Darcha C, Chan CHF, Stanners CP, et al. Crohn's disease adherent-invasive Escherichia coli colonize and induce strong gut inflammation in transgenic mice expressing human CEACAM. *J Exp Med* (2009) 206:2179–89. doi: 10.1084/jem.20090741
25. Mimouna S, Gonçalvès D, Barnich N, Darfeuille-Michaud A, Hofman P, Vouret-Craviari V. Crohn disease-associated Escherichia coli promote gastrointestinal inflammatory disorders by activation of HIF-dependent responses. *Gut Microbes* (2011) 2:335–46. doi: 10.4161/gmic.18771
26. Shawki A, McCole DF. Mechanisms of Intestinal Epithelial Barrier Dysfunction by Adherent-Invasive Escherichia coli. *Cell Mol Gastroenterol Hepatol* (2016) 3:41–50. doi: 10.1016/j.jcmgh.2016.10.004
27. Bretin A, Lucas C, Larabi A, Dalmasso G, Billard E, Barnich N, et al. AIEC infection triggers modification of gut microbiota composition in genetically predisposed mice, contributing to intestinal inflammation. *Sci Rep* (2018) 8:12301. doi: 10.1038/s41598-018-30055-y
28. Hase K, Kawano K, Nochi T, Pontes GS, Fukuda S, Ebisawa M, et al. Uptake through glycoprotein 2 of FimH + bacteria by M cells initiates mucosal immune response. *Nature* (2009) 462:226–30. doi: 10.1038/nature08529
29. Chassaing B, Rolhion N, de Vallée A, Salim SY, Prorok-Hamon M, Neut C, et al. Crohn disease–associated adherent-invasive E. coli bacteria target mouse and human Peyer's patches *via* long polar fimbriae. *J Clin Invest* (2011) 121:966–75. doi: 10.1172/JCI44632
30. Vazeille E, Chassaing B, Buisson A, Dubois A, de Vallée A, Billard E, et al. GipA Factor Supports Colonization of Peyer's Patches by Crohn's Disease-associated Escherichia Coli. *Inflammation Bowel Dis* (2016) 22:68–81. doi: 10.1097/MIB.0000000000000609
31. Wine E, Ossa JC, Gray-Owen SD, Sherman PM. Adherent-invasive Escherichia coli, strain LF82 disrupts apical junctional complexes in polarized epithelia. *BMC Microbiol* (2009) 9:180. doi: 10.1186/1471-2180-9-180
32. Mirsepasi-Lauridsen HC, Vallance BA, Krogfelt KA, Petersen AM. Escherichia coli Pathobionts Associated with Inflammatory Bowel Disease. *Clin Microbiol Rev* (2019) 32:e00060–18. doi: 10.1128/CMR.00060-18
33. Martinez-Medina M, Garcia-Gil LJ. Escherichia coli in chronic inflammatory bowel diseases: An update on adherent invasive Escherichia coli pathogenicity. *World J Gastrointest Pathophysiol* (2014) 5:213–27. doi: 10.4291/wjgp.v5.i3.213
34. Camprubí-Font C, Lopez-Siles M, Ferrer-Guixeras M, Niubó-Carulla L, Abellà-Ametller C, Garcia-Gil LJ, et al. Comparative genomics reveals new single-nucleotide polymorphisms that can assist in identification of adherent-invasive Escherichia coli. *Sci Rep* (2018) 8:2695. doi: 10.1038/s41598-018-20843-x
35. Lee JG, Han DS, Jo SV, Lee AR, Park CH, Eun CS, et al. Characteristics and pathogenic role of adherent-invasive Escherichia coli in inflammatory bowel disease: Potential impact on clinical outcomes. *PloS One* (2019) 14:e0216165. doi: 10.1371/journal.pone.0216165

36. Camprubí-Font C, Martinez-Medina M. Why the discovery of adherent-invasive Escherichia coli molecular markers is so challenging? *World J Biol Chem* (2020) 11:1–13. doi: 10.4331/wjbc.v11.i1.1
37. Jarry A, Crémet L, Caroff N, Bou-Hanna C, Mussini JM, Reynaud A, et al. Subversion of human intestinal mucosa innate immunity by a Crohn's disease-associated E. coli. *Mucosal Immunol* (2015) 8:572–81. doi: 10.1038/mi.2014.89
38. VanDussen KL, Marinshaw JM, Shaikh N, Miyoshi H, Moon C, Tarr PI, et al. Development of an enhanced human gastrointestinal epithelial culture system to facilitate patient-based assays. *Gut* (2015) 64:911–20. doi: 10.1136/gutjnl-2013-306651
39. Rajan A, Vela L, Zeng X-L, Yu X, Shroyer N, Blutt SE, et al. Novel Segment- and Host-Specific Patterns of Enteroaggregative Escherichia coli Adherence to Human Intestinal Enteroids. *mBio* (2018) 9:e02419–17. doi: 10.1128/mBio.02419-17
40. Poletti M, Arnauts K, Ferrante M, Korcsmaros T. Organoid-based models to study the role of host-microbiota interactions in IBD. *J Crohns Colitis* (2020). doi: 10.1093/ecco-jcc/jjaa257
41. Roodsant T, Navis M, Aknouch I, Renes IB, van Elburg RM, Pajkrt D, et al. A Human 2D Primary Organoid-Derived Epithelial Monolayer Model to Study Host-Pathogen Interaction in the Small Intestine. *Front Cell Infect Microbiol* (2020) 10:272. doi: 10.3389/fcimb.2020.00272
42. Sayed IM, Suarez K, Lim E, Singh S, Pereira M, Ibeawuchi S-R, et al. Host engulfment pathway controls inflammation in Inflammatory Bowel Disease. *FEBS J* (2020) 287:3967–88. doi: 10.1111/febs.15236
43. Appleyard RK. Segregation of New Lysogenic Types during Growth of a Doubly Lysogenic Strain Derived from Escherichia Coli K12. *Genetics* (1954) 39:440–52.
44. Jung P, Sato T, Merlos-Suárez A, Barriga FM, Iglesias M, Rossell D, et al. Isolation and *in vitro* expansion of human colonic stem cells. *Nat Med* (2011) 17:1225–7. doi: 10.1038/nm.2470
45. Sato T, Stange DE, Ferrante M, Vries RGJ, Van Es JH, Van den Brink S, et al. Long-term expansion of epithelial organoids from human colon, adenoma, adenocarcinoma, and Barrett's epithelium. *Gastroenterology* (2011) 141:1762–72. doi: 10.1053/j.gastro.2011.07.050
46. Boudeau J, Glasser AL, Masseret E, Joly B, Darfeuille-Michaud A. Invasive ability of an Escherichia coli strain isolated from the ileal mucosa of a patient with Crohn's disease. *Infect Immun* (1999) 67:4499–509. doi: 10.1128/IAI.67.9.4499-4509.1999
47. Camprubí-Font C, Ewers C, Lopez-Siles M, Martinez-Medina M. Genetic and Phenotypic Features to Screen for Putative Adherent-Invasive Escherichia coli. *Front Microbiol* (2019) 10:108:108. doi: 10.3389/fmicb.2019.00108
48. Dotti I, Mora-Buch R, Ferrer-Picón E, Planell N, Jung P, Masamunt MC, et al. Alterations in the epithelial stem cell compartment could contribute to permanent changes in the mucosa of patients with ulcerative colitis. *Gut* (2017) 66:2069–79. doi: 10.1136/gutjnl-2016-312609
49. Ferrer-Picón E, Dotti I, Corraliza AM, Mayorgas A, Esteller M, Perales JC, et al. Intestinal Inflammation Modulates the Epithelial Response to Butyrate in Patients With Inflammatory Bowel Disease. *Inflammatory Bowel Dis* (2019) 26:43–55. doi: 10.1093/ibd/izz119
50. Jung P, Sommer C, Barriga FM, Buczacki SJ, Hernando-Momblona X, Sevillano M, et al. Isolation of Human Colon Stem Cells Using Surface Expression of PTK7. *Stem Cell Rep* (2015) 5:979–87. doi: 10.1016/j.stemcr.2015.10.003
51. Liu Y, Chen Y-G. 2D- and 3D-Based Intestinal Stem Cell Cultures for Personalized Medicine. *Cells* (2018) 7:225. doi: 10.3390/cells7120225
52. Lapaquette P, Glasser A-L, Huett A, Xavier RJ, Darfeuille-Michaud A. Crohn's disease-associated adherent-invasive E. coli are selectively favoured by impaired autophagy to replicate intracellularly. *Cell Microbiol* (2010) 12:99–113. doi: 10.1111/j.1462-5822.2009.01381.x
53. Demarre G, Prudent V, Schenk H, Rousseau E, Bringer M-A, Barnich N, et al. The Crohn's disease-associated Escherichia coli strain LF82 relies on SOS and stringent responses to survive, multiply and tolerate antibiotics within macrophages. *PloS Pathog* (2019) 15:e1008123. doi: 10.1371/journal.ppat.1008123
54. Eaves-Pyles T, Allen CA, Taormina J, Swidsinski A, Tutt CB, Eric Jezek G, et al. Escherichia coli isolated from a Crohn's disease patient adheres, invades, and induces inflammatory responses in polarized intestinal epithelial cells. *Int J Med Microbiol* (2008) 298:397–409. doi: 10.1016/j.ijmm.2007.05.011
55. Elatrech I, Marzaioli V, Boukemara H, Bournier O, Neut C, Darfeuille-Michaud A, et al. Escherichia coli LF82 differentially regulates ROS production and mucin expression in intestinal epithelial T84 cells: implication of NOX1. *Inflammation Bowel Dis* (2015) 21:1018–26. doi: 10.1097/MIB.0000000000000365
56. Noel G, Baetz NW, Staab JF, Donowitz M, Kovbasnjuk O, Pasetti MF, et al. A primary human macrophage-enteroid co-culture model to investigate mucosal gut physiology and host-pathogen interactions. *Sci Rep* (2017) 7:45270. doi: 10.1038/srep45270

Conflict of Interest: The authors declare that the research was conducted in the absence of any commercial or financial relationships that could be construed as a potential conflict of interest.

frontiers in Pharmacology

ORIGINAL RESEARCH
published: 20 April 2021
doi: 10.3389/fphar.2021.644387

Berberine-Loaded Carboxylmethyl Chitosan Nanoparticles Ameliorate DSS-Induced Colitis and Remodel Gut Microbiota in Mice

Luqing Zhao[1], Xueying Du[2], Jiaxin Tian[2], Xiuhong Kang[1], Yuxin Li[1], Wenlin Dai[3], Danyan Li[1], Shengsheng Zhang[1] and Chao Li[2]**

[1]Digestive Disease Center, Beijing Hospital of Traditional Chinese Medicine, Capital Medical University, Beijing, China, [2]State Key Laboratory of Chemical Resource Engineering, Beijing University of Chemical Technology, Beijing, China, [3]Center for Applied Statistics, Institute of Statistics and Big Data, Renmin University of China, Beijing, China

OPEN ACCESS

Edited by:
Lixin Zhu,
The Sixth Affiliated Hospital of Sun Yat-sen University, China

Reviewed by:
Crystal Naudin,
Emory University, United States
Mei Tu,
Jinan University, China
Zhaoxiang Bian,
Hong Kong Baptist University, Hong Kong

***Correspondence:**
Shengsheng Zhang
zhangshengsheng@bjzhongyi.com
Chao Li
lichao@mail.buct.edu.cn

Specialty section:
This article was submitted to Gastrointestinal and Hepatic Pharmacology, a section of the journal Frontiers in Pharmacology

Received: *21 December 2020*
Accepted: *01 March 2021*
Published: *20 April 2021*

Citation:
Zhao L, Du X, Tian J, Kang X, Li Y, Dai W, Li D, Zhang S and Li C (2021) Berberine-Loaded Carboxylmethyl Chitosan Nanoparticles Ameliorate DSS-Induced Colitis and Remodel Gut Microbiota in Mice. Front. Pharmacol. 12:644387. doi: 10.3389/fphar.2021.644387

Inflammatory bowel disease (IBD) is a refractory disorder characterized by chronic and recurrent inflammation. The progression and pathogenesis of IBD is closely related to oxidative stress and irregularly high concentrations of reactive oxygen species (ROS). A new oxidation-responsive nano prodrug was constructed from a phenylboronic esters-modified carboxylmethyl chitosan (OC-B) conjugated with berberine (BBR) that degrades selectively in response to ROS. The optimized micelles exhibited well-controlled physiochemical properties and stability in a physiological environment. OC-B-BBR micelles could effectively encapsulate the anti-inflammatory drug berberine and exhibit ideal H_2O_2-triggered release behavior as confirmed by *in vitro* drug loading and release studies. The *in vivo* anti-inflammatory effect and regulation of gut microbiota caused by it were explored in mice with colitis induced by dextran sodium sulfate (DSS). The results showed that OC-B-BBR significantly ameliorated colitis symptoms and colon damage by regulating the expression levels of IL-6 and remodeling gut microbiota. In summary, this study exhibited a novel BBR-loaded Carboxylmethyl Chitosan nano delivery system which may represent a promising approach for improving IBD treatment.

Keywords: berberine, nanoparticles, colitis, drug delivery, gut microbiota

INTRODUCTION

Inflammatory bowel disease (IBD) is a refractory gastrointestinal disorder characterized by chronic and recurrent inflammation. Ulcerative colitis (UC) and Crohn's disease (CD) are the two main forms of IBD (Kaser et al., 2010). IBD has a high incidence in the United States (more than 1 million) and in Western Europe (2.5 million), and has evolved into a widespread disease with increasing prevalence all over the world (Kaplan, 2015). The pathogenesis of IBD is still not fully understood, but it is mainly considered to be associated with environmental factors, host genetic susceptibility, changes in intestinal flora and intestinal epithelial barrier dysfunction, and other factors (Zundler and Neurath, 2015). Oxidative stress plays an essential role in the pathogenesis and progression of IBD (Tian et al., 2017), and leads to excessive ROS accumulation. Biopsies from patients with IBD demonstrate abnormally high levels of ROS at the site of the lesion, with mucosal ROS concentrations increasing from 10- to 100-fold (Simmonds et al., 1992; Lih-Brody et al., 1996).

Although there is no clear evidence of a relationship between IBD and mortality, there is no doubt that IBD has an adverse impact on the quality of life of patients. Many drugs are available for the treatment of UC including 5-Aminosalicylic acid, steroids, immunosuppressant, probiotics, biological agents, herbal medicines, and so on. Ulcerative colitis can be cured with FMT in patients who do not respond to other more accessible treatments. However, IBD is difficult to cure permanently at present. Taking medicine inevitably brings about many adverse reactions and consumes a lot of medical resources (Shivaji et al., 2019; Wilke et al., 2020).

Berberine (BBR) is an isoquinoline alkaloid, often used as an antidiarrheal, derived from the rhizome of *Coptis chinensis* ("Huang-Lian" in Chinese) of the Ranunculaceae family. Recently, BBR and its derivatives have been examined for use in IBD treatment (Massironi et al., 2013; Wakuda et al., 2013). It is worth noting that BBR may alleviate intestinal inflammation through different mechanisms. It seems to be related to the regulation of the Treg/Th17 balance by modifying gut microbiota (Cui et al., 2018). In addition, BBR could identify bitter taste receptors on intestinal Tuft cells and activate IL-25-ILC2-IL-13 immune pathway to impair damaged intestinal tract by promoting differentiation of intestinal stem cells (Xiong et al., 2021). There is also a broad space to improve the efficacy and bioavailability of BBR. For example, its absolute bioavailability has been reported to be less than 1% (Chae et al., 2008; Chen et al., 2011) and the plasma level of BBR is very low, although the significant pharmacological effects of BBR have been observed in clinic (Hua et al., 2007).

A targeted drug delivery system can ensure that the drug is released only at the intestinal inflammation site instead of healthy tissue. Targeting and selectivity are achieved by the abnormally high concentration of ROS in the inflammation site (Wilson et al., 2010; Zhang et al., 2016). Because the nanosized targeted delivery system will mainly accumulate in the inflamed part of the intestine, it is considered to be an excellent idea for the treatment of IBD (Lamprecht et al., 2001). Santos' group reported a nano-in-micro composite to achieve an oxidation-responsive delivery of rifaximin (RIF) for IBD treatment. RIF mediates changes in epithelial cell physiology and reduces bacterial attachment and internalization, and also antagonized the effects of tumor necrosis factor-α on intestinal epithelial cells by activating pregnane X receptor, which inhibits nuclear factor-κB-mediated proinflammatory mediators and induces detoxification genes. RIF-loaded nanoparticles have been prepared by phenylboronic esters-modified dextran (OxiDEX). Under physiologically relevant H_2O_2 concentrations, the nanoparticles exhibited a high degree of H_2O_2-responsive degradation ability and controlled drug release (Bertoni et al., 2018). Nanoparticles are likely to adjust the properties of drugs, such as stability, solubility, and release ability, and their surface is easily modified to introduce targeting ligands, and even adjust surface characteristics, including surface charge and adhesion properties. Consequently, we here proposed a functional prodrug micelle as an inflammation-targeted drug, which was comprised of BBR covalent linked to biocompatible carboxylmethyl chitosan by aryl boronic ester as responsive linker. This nanosystem was adopted so that chitosan-based prodrug micelles could effectively deliver berberine to inflamed tissue by ROS responsive mechanism, improving its bioavailability in the specific site (**Figure 1**). Compared with the RIF-loaded delivery system, BBR in the current system was covalently linked to the carrier by unique catechol group, which can precisely achieve ROS-responsive and prevent the premature release of drugs in the delivery process. The synthesis and physiochemical properties of polymeric OC-B-BBR were explored to optimize micelle structure. The ability of the system to release berberine in physiological and simulated ROS overexpression medium was also investigated. *In vivo* anti-inflammatory effect and regulation of gut microbiota by it were explored in mice with colitis induced by dextran sodium sulfate (DSS), which showed features in common with ulcerative colitis in humans.

MATERIALS AND METHODS

Materials

Carboxylmethyl chitosan (OC, Mw = 37 kDa, degree of deacetylation = 88.7%) was purchased from Macklin. Berberine (BBR) was purchased from Saen Chemical Technology Co., Ltd. The Spectra/Por 1 dialysis membrane (MWCO: 3,500) was purchased from Spectrum Laboratories. All the other reagents and solvents were provided by Beijing Chemical Reagent Co., Ltd. and used without further purification. A Bruker AV-400 nuclear magnetic resonance spectroscope was used to record all NMR spectra at 400 MHz in $CDCl_3$ (unless otherwise specified). An Agilent 6540 UHD Q-TOF MS (analyzed ions up to m/z 6,000) equipped with a gas nebulizer probe was used to record data of High-resolution mass spectra (HRMS). DSS was purchased from MP Biomedicals Co., Ltd. TNF-α and IL-6 enzyme-linked immunosorbent assay (ELISA) kits were purchased from Wuhan servicebio technology Co., Ltd. TGF-β and IL-23 ELISA kits were purchased from Multisciences (LIANKE) Biotech Co., Ltd.

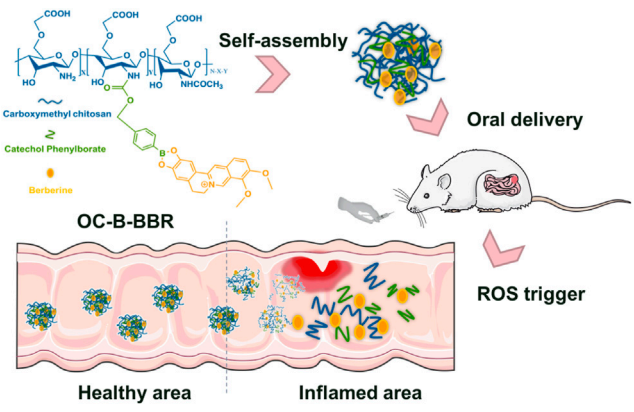

FIGURE 1 | The schematic presentation of OC-B-BBR prodrug micelles structure and their inflamed-selective anti-inflammatory drug delivery by ROS-triggered mechanism.

Preparation of OC-B-BBR Micelles

Phloroglucinol (2.5 g, 19.8 mmol) was dissolved in 60% H_2SO_4 (50 ml) and stirred at room temperature until the raw materials were completely dissolved to form a colorless solution. Berberine (2.5 g, 7.4 mmol) was added to the above solution, and the mixture was stirred at 95°C for 15 min. Then the reaction was transferred to the saturated NaCl solution and stirred at room temperature for 2 h. The solution was filtered, and the filter cake was dissolved with methanol. The resulted solution was concentrated *in vacuo* and washed by ethyl acetate for twice. The solution was then filtered again, upon which the compound demethyleneberberine was obtained as a dark red solid (yield 90%). 1H-NMR (400Mz, DMSO-d_6): δ/ppm = 3.105–3.136 (t, 2H, - CH_2), 4.070 (s, 3H, - CH_3), 4.095 (s, 3H, - CH_3), 4.898–4.929 (t, 2H, - CH_2), 6.884 (s, H, Ph-H), 7.557 (s, H, Ph-H), 8.052–8.075 (d, H, Ph-H), 8.173–8.196 (d, H, Ph-H), 8.768 (s, H, Ph-H), 9.432 (bs, H, -OH), 9.857 (s, H, Ph-H), 10.246 (bs, H, -OH).

We dissolved carboxymethyl chitosan (OC, 128 mg, 0.24 mmol) and 0.2 ml of tetramethylguanidine in 15 ml deionized water, then stirred the mixture for 30 min 4-nitrophenyl [4-(4,4,5,5-tetramethyl-1,3,2-dioxaborolan-2-yl) phenyl]methyl ester (NBC, 0.2 g, 0.501 mmol) was dissolved in 5 ml THF, which was added dropwise to the above mixture at 25°C. After the reaction was finished, the solution was dialyzed against water for 2 days. The product OC-B was obtained by lyophilization.

The OC-B-BBR micelles were prepared using dialysis method. In brief, OC-B (20 mg) was dissolved in 8.4 ml deionized water and saturated $NaHCO_3$ was added to adjust pH = 8. Then 3 ml DMA was added to the above solution with stirring for 10 min at room temperature. 10 mg of demethyleneberberine dissolved in methanol (2 ml) were slowly added to the mixture, then stirred for 8 h at 25°C. The resulting solution was dialyzed against water/methanol (1,000 : 2, v/v) for 2 days (molecular weight cut off 3,500 Da) to remove by-products, and then lyophilized to obtain a dry reddish brown flocculent product of OC-B-BBR micelles (60 mg).

Characterization of Physiochemical Properties

Gel permeation chromatography (GPC) (TDK 302, Viscotek, USA) was used to determine the molecular weight distribution of the analytes, in which the mobile phase was water. A Zetasizer Nano instrument (Zetaplus, Brookhaven, USA) and a HeeNe laser (633 nm) were used to measure the particle size of micelles by dynamic light scattering (DLS) to collect optical measurements. All analytes were suspended in pH 7.4 PBS at a concentration of 1 mg mL^{-1} in DLS measurement. S-4700 cold field emission scanning electron microscope (SEM, Hitachi, Japan) was used to analyze the surface morphology of polymeric products and obtain SEM images. Double-sided tape was used to mount the sample for SEM to the metal post, and a thin layer of gold was sputtered under vacuum. For zeta potential measurement, a Nano-ZS ZEN3600 particle sizer (Malvern Instruments) was used.

The encapsulation efficiency (EE) and loading capacity (LC) of OC-B-BBR micelle were depicted as **Eqs. 1** and **2**, respectively.

$$EE(\%) = \frac{\text{weight of Barberine in micelle}}{\text{weight of Barberine feed}} \times 100\% \quad (1)$$

$$LC(\%) = \frac{\text{weight of encapsulated Berberine}}{\text{total weight of micelle}} \times 100\% \quad (2)$$

In Vitro Drug Release of Micelles

A dialysis membrane was used to evaluate the release of OC-B-BBR micelles under sink conditions. For simulated ROS released study, H_2O_2 with different concentrations was added into phosphate-buffer solution (PBS, pH 7.4) as the release media. In brief, 2 mg of OC-B-BBR micelles (DS = 13.1%) were kept in a dialysis bag (MWCO: 3.5 kDa), sealed and placed in 200 ml of release medium, and continuously shook at 100 rpm at 37°C. 1 ml of buffer solution was collected at various time intervals, and 1 ml of fresh medium was added in time after each collection. The cumulative amounts of berberine were determined by Waters Alliance HPLC (UV-detector, λ = 360 nm, C-18 column, eluent: 0.2% phosphoric acid in water: acetonitrile (36:64, v/v), flow rate: 1.0 ml min^{-1}).

Animal Experiments and Dosage Information

Animal experiments were designed according to ARRIVE 2.0 Guideline. C57BL/6 J mice aged 6–8 weeks were obtained from the SPF (Beijing) Biotechnology Co., Ltd (permission number: SCXK (jing) 2019–0,010). The mice were cultured under standard conditions (temperature of 20–26°C, relative humidity of 40–70%, light-dark cycle of 12/12 h, clean bedding, free access to water, and standard dry pellet diet). After a week of adaptive feeding, the mice were randomly divided into four groups, with eight mice in each group. The groups were as follows: 1) Control group, continually fed water alone for 10 days; 2) DSS group, colitis was induced with 3% DSS, which was added to their drinking water for 6 days, on the fourth day, started to use normal saline for gavage for 7 days; 3) OC-B-BBR group, colitis was induced with 3% DSS, which was added to their drinking water for 6 days, on the fourth day, started to use nano-berberine for gavage (30 mg kg^{-1}·d^{-1}) for 7 days; 4) Mesalazine group, colitis was induced with 3% DSS for 6 days, on the fourth day, started to use mesalazine for gavage (100 mg kg^{-1}) for 7 days.

Animal studies were performed according to the NIH Guide for the Care and Use of Laboratory Animals and were approved by Animal Care and Use Committee of Beijing Hospital of traditional Chinese Medicine, Capital Medical University.

Disease Activity Index (DAI)

The body weight, stool viscidity, and fecal occult blood were observed daily, and the DAI (Yan et al., 2018) of the mice were measured, including body weight loss (the percentage of weight loss relative to the initial body weight, where 0 score = none, 1 score = 1%–5%, 2 score = 5%–10%, 3 score = 10%–20%, 4 score => 20%),

stool viscidity (0 score = normal, 2 score = loose, 4 score = diarrhea), and fecal occult blood (0 score = no blood, 1 score = +, 2 score = ++, 3 score = +++, 4 score = gross bleeding). DAI = (body mass index + stool viscidity + bleeding)/3.

Sample Collection and Measurement

Colons and spleens were excised from sacrificed mice, and then the length of colons and weight of the spleens were measured. The spleen index = wet weight of the spleen (mg)/the bodyweight (g). Feces were collected for 16 S ribosomal RNA (16SrRNA) analysis. Portions of the colon were fixed in 10% formalin and then embedded in paraffin sections for hematoxylin-eosin (H&E) staining. A portion of that colon was store at -80°Cfor ELISA analysis.

Intestinal Mucosal Injury Index Analysis

The colons were dissected to observe the damages on intestinal mucosa. The extent of the damage was graded by colonic mucosa damage index (CMDI) (Yan et al., 2018), scored as follows: 0, no injury to the colonic mucosa; 1, the surface of intestinal mucosa is smooth, no erosion or ulcer, but with mild hyperemia and edema; 2, has congestion and edema, the mucosa is coarse and granular, with erosion or intestinal adhesion; 3, necrosis and ulcers appeared on the surface of intestinal mucosa, which also has high congestion and edema (the maximum longitudinal diameter of the ulcer is shorter than 1.0 cm), moreover, the intestinal wall surface has necrosis and inflammation or the hyperplasia of intestinal wall; and 4, the maximum longitudinal diameter of ulcer is longer than 1.0 cm, or with total intestinal wall necrosis more severe than 3 points.

Histological Analysis

H&E stained sections of colonic tissue was determined by two independent, blinded investigators following a scoring system for inflammation-associated histological changes in the colon (Wirtz et al., 2007). The scoring system for inflammation-associated histological changes in the colon was: 0, No evidence of inflammation; 1, Low level of inflammation with scattered infiltrating mononuclear cells (1–2 foci); 2, Moderate inflammation with multiple foci; 3, High level of inflammation with increased vascular density and marked wall thickening; and 4, Maximal severity of inflammation with transmural leukocyte infiltration and loss of goblet cells.

ELISA Analysis

Levels of TNF-α (purchased from Wuhan servicebio technology Co., Ltd.), IL-6 (purchased from Wuhan servicebio technology Co., Ltd.), TGF-β (purchased from Multisciences (LIANKE) Biotech Co., Ltd.), and IL-23 (purchased from Multisciences (LIANKE) Biotech Co., Ltd.) in colon tissue were quantified using ELISA kits according to the instructions.

16SrNA Analysis

Magpure stool DNA KF kit B (Magen, China) was used to extract genomic DNA from feces. 30ng of qualified genomic DNA samples and corresponding fusion primers were used to configure the PCR reaction system. The v3-v4 region of 16 S rRNA of genomic DNA was amplified by setting the PCR reaction parameters. The PCR products were purified with agencourt ampure XP magnetic beads, dissolved in elusion buffer, labeled, and completed the establishment of the library. Agilent 2,100 Bioanalyzer was used to detect the fragment range and concentration of the library. According to the size of inserted fragments, hiseq platform was selected for sequencing. After getting off the machine, the data were filtered, and the reads were spliced into tags through the overlap relationship between reads. Under the given similarity, tags were aggregated into out, and the OTU representative sequences were compared with the database by RDP classifer (V2.2) software for species annotation, and the confidence threshold was set to 0.6. Based on OTU and annotation results, species complexity analysis, species diversity analysis, and correlation analysis were carried out.

Statistical Analysis

Multiple groups were compared by one-way analysis of variance (ANOVA). *t*-test or Mann-Whitney *U*-test was used to compare the two groups. Data were expressed as mean ± standard deviation (SD). $p < 0.05$ was considered statistically significant.

RESULTS

Design and Synthesis of Berberine Nanomicelle

Carboxylmethyl chitosan was chosen as a carrier to improve solubility and biocompatibility of micelles for drug delivery. Stimuli-responsive phenyl borate ester as a linker conjugated berberine to carboxylmethyl chitosan by effective aminolysis reaction. The synthesis route of the nanocarrier OC-B-BBR was depicted in **Supplementary Scheme S1**. Initially, NBC was prepared according to previous reports (Jourden and Cohen, 2010; Chung et al., 2018), as a key intermediate for linking glycol chitosan and berberine. Phenyl boronate moiety was linked to 2-NH_2 on carboxylmethyl chitosan by aminolysis, and subsequently borate ester was then easily hydrolyzed under alkaline conditions to give OC-B. A simple strategy was proposed to conjugate berberine by its unique catechol structure. The exposed boronic acid group can spontaneously react with catechol in water to form stable borate ester (OC-B-BBR). The successful synthesis of OC-B-BBR nanocarrier was confirmed by 1H NMR spectra. The characterization of OC and OC-B was also presented as controls to better assign the proton signals of berberine in OC-B-BBR (**Supplementary Figures S1–S3**). The amphiphilic OC-B-BBR conjugates readily formed self-assembled micelles in an aqueous environment. In mild excess ROS environment, the stimuli-responsive borate ester was broken to release berberine molecules.

Physicochemical Properties of Micelles

The physiochemical properties of nanocarriers should be carefully considered to achieve target special delivery of the particles. The primary concerns, including degree of substitute (DS), particle size, encapsulation efficiency (EE), and loading capacity (LC), were determined as shown in **Table 1**. The feed

TABLE 1 | Physiochemical properties of OC, OC-NBC, and OC-B-BBR.

Samples	M_w (Da) ± SD	M_n (Da) ± SD	M_w/M_n ± SD	Particle size (nm) ± SD	PDI[b] ± SD	EE (%)[c] ± SD	LC (%)[d] ± SD
OC	37,695 ± 1,348	17,127 ± 1,123	2.2 ± 0.2	-[a]	-	-	-
OC-NBC	54,985 ± 2,350	22,982 ± 2,140	2.4 ± 0.3	222.7 ± 26.4	0.42 ± 0.12	-	-
OC-NBC-BBR	17,049 ± 929	14,497 ± 827	1.2 ± 0.1	230.2 ± 18.1	0.22 ± 0.09	67.5 ± 4.4	13.1 ± 1.6

[a]*no data.*
[b]*polydispersity index.*
[c]*Encapsulation efficiency, see section Materials and Methods for calculation.*
[d]*Loading capacity, see section Materials and Methods for calculation.*

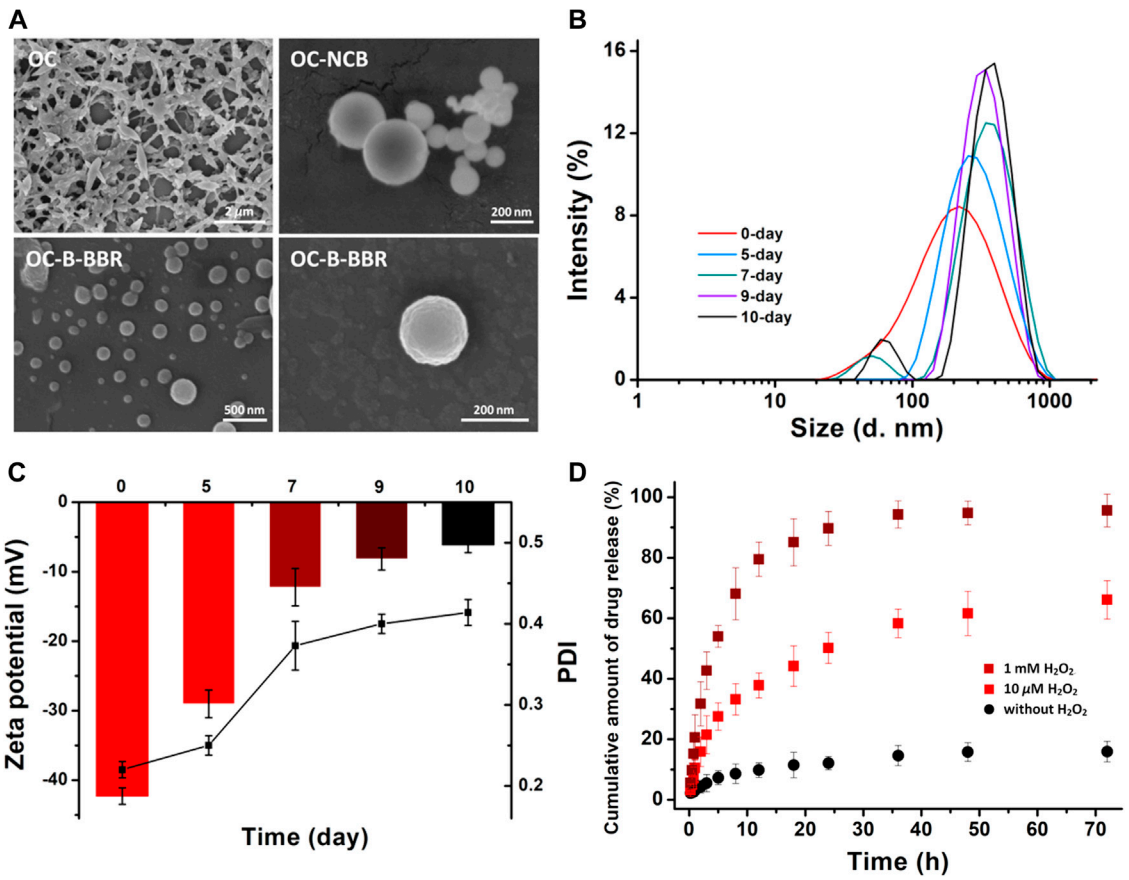

FIGURE 2 | (A) SEM images of the different polymers. **(B)** The changes in OC-B-BBR nanoparticle size in pH 7.4 medium. **(C)** The changes in surface charges and PDI **(D)** *In vitro* drug release profiles of berberine. The OC-B-BBR micelle was incubated in pH = 7.4 buffer without H_2O_2 (black dot), 10 μM H_2O_2 (red square), and 1 mM H_2O_2 (wine square), as measured through HPLC.

ratio of the reaction was changed to adjust the DS of berberine, which can greatly affect the self-assembly behavior and hydrophilic-lipophilic balance of the micelles. Phenyl boronic ester was firstly grafted to OC with different DSs ranged from 10.08 to 26.02%, and the mean diameters of the micelles, measured by DLS, were in the 120–140 nm range. The poor solubility of berberine and reactivity of phenolic hydroxyl (alcoholic hydroxyl was more likely to react with phenylboric acid), to a large extent, limited the increase of DS. The optimized OC-B-BBR (DS = 13.6%) was used to evaluate the subsequent drug release and *in vivo* anti-inflammatory efficacy.

The nanoscale morphology of the obtained structure was shown by electron microscope images. As shown in **Figure 2A** by SEM measurement, OC and blank OC-B were spherical nanoparticles (about 100 nm) and cross-linked. The micelles of OC-B-BBR maintained good microsphere morphology, as shown in **Figure 2A** in different scales. The average particle size of the nanoparticles was about 130 nm, and slightly larger than the

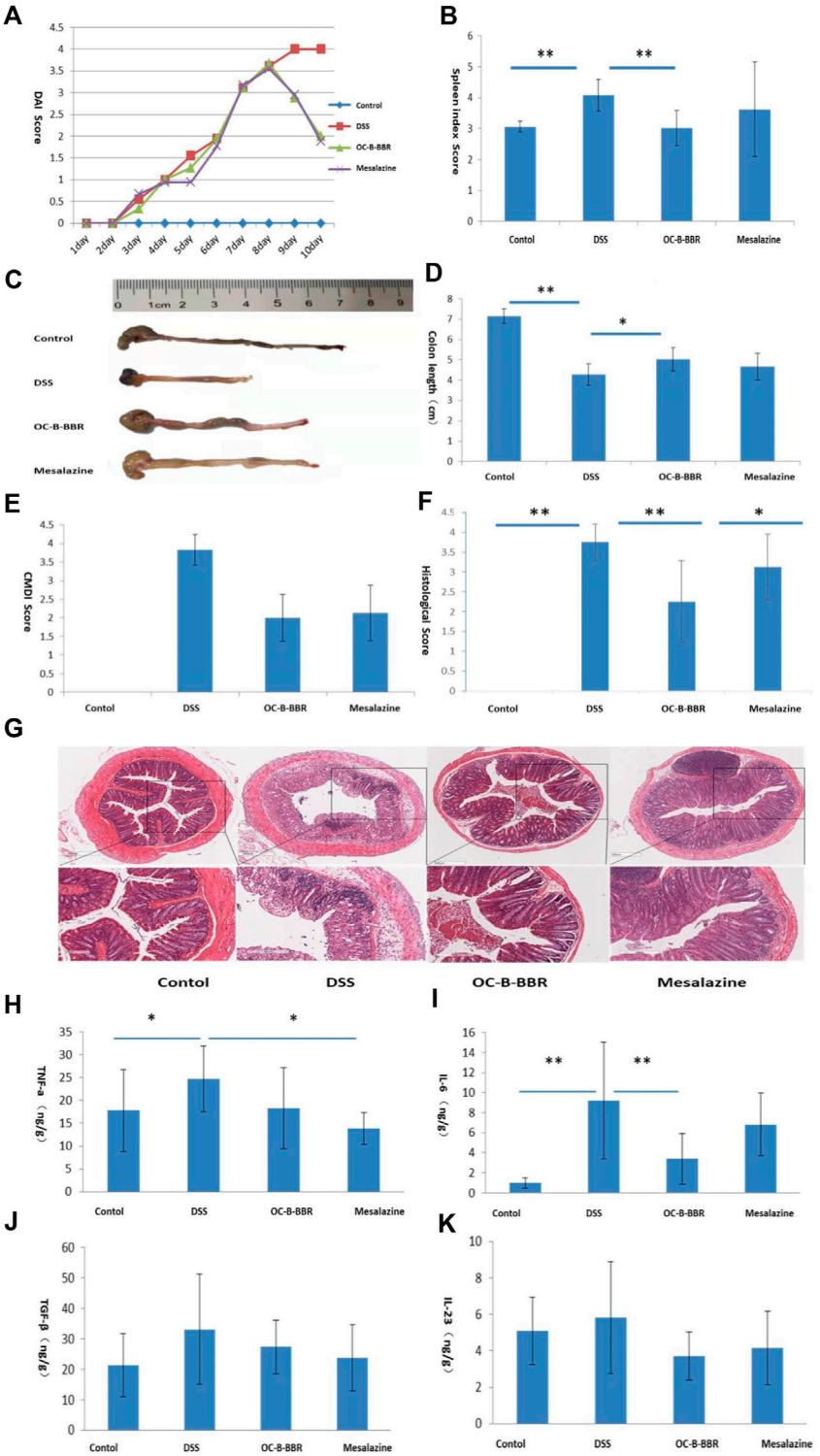

FIGURE 3 | OC-B-BBR ameliorated DSS-induced colitis in mice. Results represent mean ± SD; n = 8, *$p < 0.05$; **$p < 0.01$. **(A)** disease activity indexes (DAI); **(B)** Spleen index; **(C)** Colon picture; **(D)** Colon length; **(E)** Colonic mucosa damage index (CMDI) score; **(F)** Histological score; **(G)** H&E staining of sections displayed colonic tissue damage and leukocyte infiltration, ×4 and ×10; **(H)** TNF-α; **(I)** IL-6; **(G)** TGF-β; **(K)** IL-23.

carrier OC-B. The change trends of particle size measured by DLS were basically the same as that measured by SEM. For the specific data of particle size, the DLS results were slightly larger than the SEM results. This was mainly because the structure was in a hydrated state during DLS measurement, which made the size of the structure larger.

Subsequently, the stabilities of OC-B-BBR micelles were monitored on the basis of variation in sizes and surface charges. In pH = 7.4 medium, the micelles showed insignificant changes in size and a negligible decrease in zeta potential in 5 days (**Figures 2B,C**), suggesting the good stability of the micelles that was essential for a prolonged blood half-life *in vivo*.

In Vitro Drug Release Profile

The drug release profiles in physiological and simulated ROS environment were explored. As shown in **Figure 2D** without H_2O_2, less than 20% berberine was released in 72 h incubation at pH 7.4, indicating that the micelles had satisfactory stability around physiological conditions. When 10 μM H_2O_2 was added in the micelles system, 50% of berberine was collected in 24 h incubation, indicating the ROS-sensitivity of OC-B-BBR micelles. At least 65% of the drugs were released over the tested time. The same assays were performed again with 1 mM H_2O_2 incubation, and the rate of berberine release sharply increased. More than 90% of the drugs can be released in 24 h incubation, showing the sensitivity to excess ROS. The sustained and thorough release indicated that the nanomicelles have a favorable response ability in inflamed tissues with high levels of ROS, which promoted drug delivery efficacy.

OC-B-BBR Showed a Potential Role in Ameliorating the Colitis Induced by DSS in Mice

To study the effect of OC-B-BBR in colitis, five parameters, DAI, colon length, spleen index, CMDI score, and histological score, were evaluated. Mice in the DSS group presented more severe colitis than mice in the OC-B-BBR group, as evidenced by a significant increasing of DAI (**Figure 3A**) and spleen index ($p < 0.01$) (**Figure 3B**), and shortening of the colon ($p < 0.05$) (**Figures 3C,D**). The damage on intestinal mucosa by visual inspection in the DSS group presented significantly higher congestion and edema, more serious erosion or intestinal adhesion, bigger ulcers, and higher CDMI score ($p < 0.01$) (**Figure 3E**) compared with the OC-B-BBR group. Similarly, the inflammatory cell infiltration and histological score of H&E staining sections of colon tissue in the DSS group were significantly higher compared with the OC-B-BBR group ($p < 0.01$) (**Figures 3F,G**). There were no significant differences between the OC-B-BBR and mesalazine group in the DAI, colon length, spleen index, or CMDI score. The histological scores of the OC-B-BBR group were significantly lower than that of the mesalazine group ($p < 0.05$). Above all, OC-B-BBR could effectively ameliorate DSS-induced colitis in mice and may have potential advantages over mesalazine.

OC-B-BBR Suppressed the Secretion of Some Inflammatory Cytokines in DSS-Induced Mice

Excessive production of proinflammatory cytokines lead to the progression and exacerbation of colitis. To understand the anti-inflammatory effect of OC-B-BBR, we measured the levels of proinflammatory cytokines in the colon homogenates by ELISA. The results showed that the levels of TNF-α and IL-6 were significantly increased after DSS-induced ($p < 0.05$ or $p < 0.01$). The increase of IL-6 was significantly reduced by OC-B-BBR treatment ($p < 0.01$), while the increase of TNF-α was significantly reduced by mesalazine treatment ($p < 0.05$). There were no significant differences of TGF-β and IL-23 in the four groups (**Figures 3H–K**).

OC-B-BBR Modified Gut Microbiota

α-diversity analysis reflected the richness and diversity of microbial communities, including a series of statistical analysis indexes. The Chao and ACE indexes are used to estimate the microbial richness, while Shannon index is used to estimate the microbial diversity. The ACE index of DSS group was significantly lower than that of the normal group, of which the OC-B-BBR group and mesalazine group were significantly increased ($p < 0.05$) (**Figure 4A**). Although the Chao index did not increase significantly, the increase in species richness was demonstrated to some extent (**Figure 4A**). Shannon index showed no significant difference among the four groups (**Figure 4A**). No apparent clustering was observed in principal component analysis (PCA) (**Figure 4B**) or principal coordinate analysis (PCoA) (**Figure 4B**) among the normal group, DSS group, OC-B-BBR group, or mesalazine group.

At phylum level, the compositions of gut microbiota in each group were shown in **Figure 4C**. Compared with the normal group, the relative abundance of Bacteroidetes, Deferribacteres, and Proteobacteria in the DSS group increased significantly, while the relative abundance of Firmicutes and Verrucomicrobia decreased significantly ($p < 0.05$ or $p < 0.01$) (**Figures 4D,E**). Compared with the DSS group, the relative abundance of Firmicutes increased significantly in the OC-B-BBR group, while the relative abundance of Proteobacteria decreased ($p < 0.05$) (**Figure 4F**). There was no significant difference between the DSS group and mesalazine group (**Figure 4G**).

At genus level, the compositions of gut microbiota in each group were shown in **Figure 4H**. Compared with the normal group, the relative abundance of *Bacteroides*, *Escherichia*, *Helicobacter*, and so on increased significantly in the DSS group, while the relative abundance of Akkermansia and Coprococcus decreased significantly ($p < 0.05$ or $p < 0.01$) (**Figure 4I**). Compared with DSS group, the relative abundance of *Bacteroides* and *Escherichia* decreased significantly in the OC-B-BBR group ($p < 0.05$) (**Figure 4J**). There was no significant difference between the DSS group and mesalazine group (**Figure 4K**).

LEfSe linear discriminant analysis (LDA) was used to discriminate the significant different species (LDA>4, $p < 0.05$). The higher the LDA score, the greater effect of the

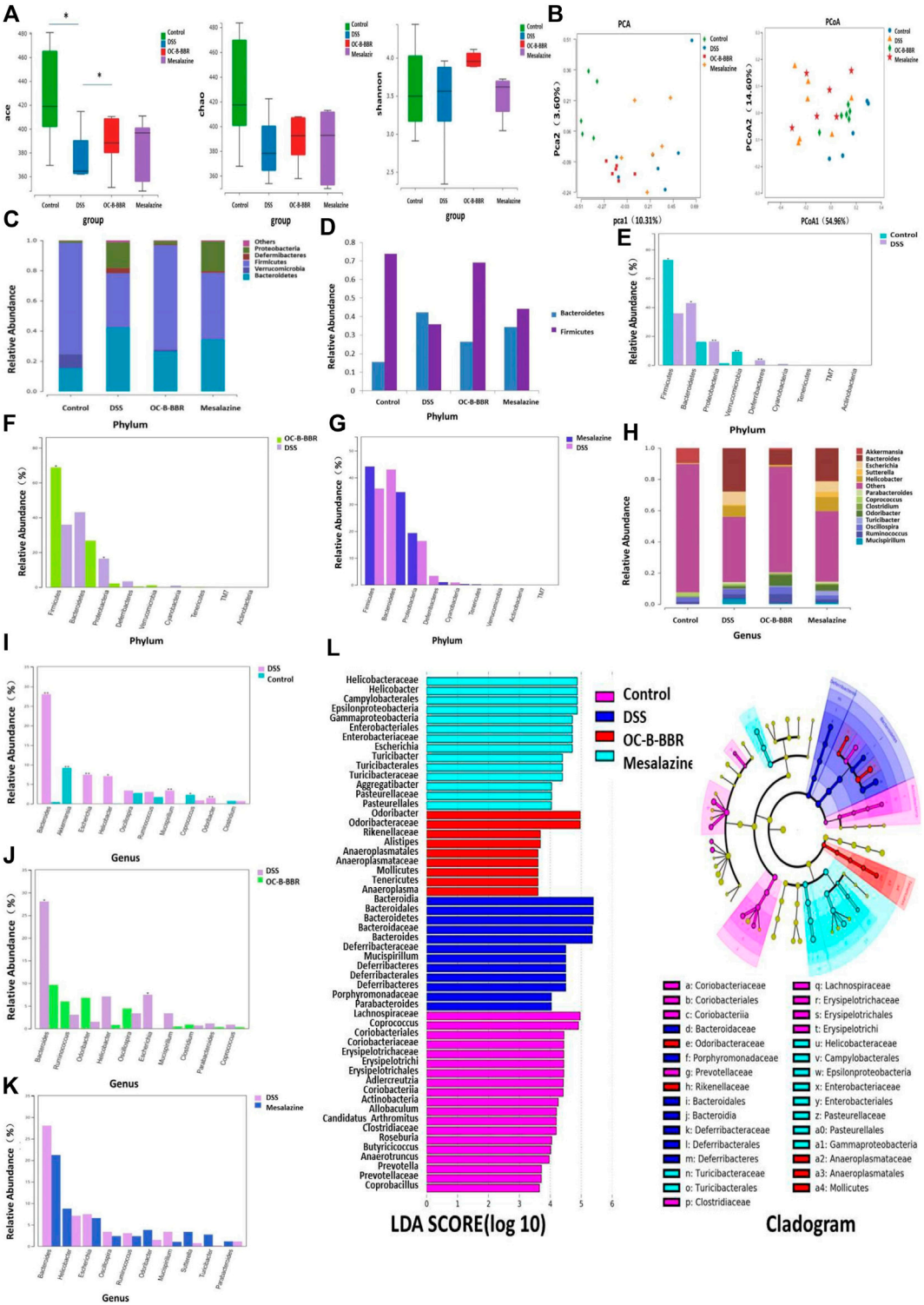

FIGURE 4 | (A) α-Diversity estimated by ACE, Chao, and Shannon indexs,*$p < 0.05$; **(B)** PCA score and PCoA score plots; **(C)** Gut microbiota composition at phylum level in each group; **(D)** Firmicutes/Bacteroidetes ratio at phylum level in each group; **(E)** The proportions of key species at phylum level, Normal group vs DSS group; **(F)** The proportions of key species at phylum level, OC-B-BBR group vs DSS group; **(G)** The proportions of key species at phylum level, Mesalazine group vs DSS group; **(H)** Gut microbiota composition at genus level in each group; **(I)** The proportions of key species at genus level, Normal group vs DSS group; **(J)** The proportions of key species at genus level, OC-B-BBR group vs DSS group; **(K)** The proportions of key species at genus level, Mesalazine group vs DSS group; **(L)** LDA score and LEfSe taxonomic cladogram.

relative abundance of species on the difference. There were significant differences in the composition of key species among the four groups. A LEfSe taxonomic cladogram represented key bacterial alterations. Different colors of purple, blue, red, and green respectively represent the NC, model, OC-B-BBR, and mesalazine groups. Each small circle at different taxonomic levels represents a taxon at that level, and the diameter of the small circle is proportional to the relative abundance (**Figure 4L**).

DISCUSSION

Chinese herbal medicine treatment of inflammatory bowel disease has a long history in China and around the world (Zhao et al., 2017). However, due to the low content of active ingredients and oral bioavailability, the further improvement of the curative effect of Chinese herbal medicine is limited. The development of targeted drug delivery based on nano technology presents a new approach for natural drugs extracted from Chinese herbal medicine in the treatment of IBD.

Chitosan is a natural polymer of living organisms, which provides a basis for the construction of functional polymer biomaterials with biological properties and unique physicochemical properties, biocompatibility, and biodegradability. In particular, through the controlled functionalization of some simple borate parts, we can obtain an intelligent system for specific site drug delivery with certain required response characteristics, such as ROS response (Maji et al., 2015). Herein, based on ROS responsiveness, we designed a new type of chitosan nanocarrier to achieve targeted drug delivery to inflammation sites. The ROS responsive group, which can effectively deliver the encapsulated BBR to the inflammatory site by ROS-triggered release in the microenvironment of oxidative stress, was formed by the self-assembly of amphiphilic carboxymethyl chitosan and phenylborate side groups. The selectivity of phenylborate as the linker was mainly due to its ROS responsiveness and biocompatibility, as well as convenient conjugation with drugs *via* catechol moiety. Many natural anti-inflammatory drugs contained catechol, such as quercetin and rutin. Thus, the current design provided a realistic and general strategy for constructing catechol-based responsive nanodrug delivery system.

Dynamic light scattering (DLS) was used to evaluate the size and polydispersity index (PDI) of the OC-B-BBR micelles. The hydrodynamic average size was about 220 nm, with a relatively similar particle size distribution of 0.22 (**Table 1**). However, in the case of the empty nanocarrier OC-B, the detected particle size distribution was slightly wider at 0.42, due to the weak hydrophobicity in the core without drugs. This result was consistent with the observation on SEM. In the subsequent stability tests, the relatively intact micelles were obtained in a few days by DLS and zeta potential analysis, which provided a vital guarantee for stable drug delivery before reaching the inflammatory site.

Here our results showed that OC-B-BBR alleviated DSS-induced colitis in mice. Compared with the DSS group, after OC-B-BBR treatment the DAI score and spleen index was decreased, the colon length was increased, and the damage to the colon (congestion, edema, erosion, ulcer or inflammatory cell infiltration etc) was reversed. A particular concern was that histological scores were significantly lower in the OC-B-BBR group than in the mesalazine group, while there were no significant differences between the two groups on other indicators. This showed that for histological healing OC-B-BBR may have had potential advantages over mesalazine. Histological deep healing is the highest goal of clinical treatment for IBD patients. A recent systematic review and meta-analysis revealed that patients who achieved endoscopic and histological remission have a significantly lower risk of clinical relapse than patients who achieved clinical remission (Yoon et al., 2020). The proinflammatory cytokines levels correlate with the severity of colitis. Our results showed that OC-B-BBR treatment inhibited the release of IL-6, while mesalazine treatment inhibited the release of TNF-α. It suggests that OC-B-BBR and mesalazine may exert anti-inflammatory effects through different pathways.

The pathogenesis of IBD is complicated and not clear. It is now accepted that a complex interplay of genetic and environmental factors and gut microbiota lead to abnormal immune responses and chronic colitis (Nishida et al., 2018). Compared with healthy people, IBD patients had less bacteria with anti-inflammatory capacities and more bacteria with inflammatory capacities (Peterson et al., 2008). The most recognized changes were a decrease in the diversity of the intestinal microbial community, a decrease in abundance of Firmicutes, and increases in abundance of Proteobacteria and Bacteroidetes (Manichanh et al., 2006; Walker et al., 2011). Our results showed that OC-B-BBR increased the community richness of gut microbiota decreased by DSS induction. At phylum and genus level, compared with the DSS group, the relative abundance of Firmicutes was increased, while the relative abundance of Proteobacteria, *Bacteroides*, and *Escherichia* was decreased in the OC-B-BBR group. In the DSS group, the ratio of Firmicutes and Bacteroidetes was inverted, and OC-B-BBR treatment was shown to restore its normal trend. OC-B-BBR treatment shifted the microbiome toward a "healthy" phenotype. The relative abundance of species in the mesalazine group were not significantly different from the DSS group. OC-B-BBR may attenuate DSS-induced colitis by modulating the composition of bacterial communities. In future studies, we need to explore the mechanism of OC-B-BBR inhibiting inflammation by regulating gut microbiota.

CONCLUSIONS

In summary, BBR was conjugated to carboxylmethyl chitosan by aryl boronic ester, giving a potential ROS responsive for an effective delivery of drugs to the inflammatory tissue. OC-B-BBR as carboxylmethyl chitosan nanomicelles were prepared and characterized, which ameliorates DSS-induced colitis and remodels gut microbiota. The novel natural drug nano delivery system may represent a promising approach for improving IBD treatment.

DATA AVAILABILITY STATEMENT

The original contributions presented in the study are included in the article/**Supplementary Material**, further inquiries can be directed to the corresponding authors.

ETHICS STATEMENT

The animal study was reviewed and approved by the Animal Care and Use Committee of Beijing Hospital of traditional Chinese Medicine, Capital Medical University.

AUTHOR CONTRIBUTIONS

LZ, SZ, and CL conceived and designed the experiments. XD, XK, and YL performed the experiments. XD, JT, and WD contributed to the data analysis. LZ guided the animal experiment work. LZ and JT wrote the article and DL assisted in this work. SZ and CL drafted and revised the manuscript. All authors read and approved the final manuscript.

FUNDING

This study was financially supported by the National Natural Science Foundation of China (No. 81973764, 21572018); Joint Project of BRC-BC (Biomedical Translational Engineering Research Center of BUCT-CJFH) (XK 2020–06); Beijing Science and technology project (No.z181100001718218); Beijing Nova Program (Z201100006820119) from Beijing Municipal Science and Technology Commission.

SUPPLEMENTARY MATERIAL

The Supplementary Material for this article can be found online at: https://www.frontiersin.org/articles/10.3389/fphar.2021.644387/full#supplementary-material.

REFERENCES

Bertoni, S., Liu, Z., Correia, A., Martins, J. P., Rahikkala, A., Fontana, F., et al. (2018). pH and reactive oxygen species-sequential responsive nano-in-micro composite for targeted therapy of inflammatory bowel disease. *Adv. Funct. Mater.* 28 (50), 1806175. doi:10.1002/adfm.201806175

Chae, H. W., Kim, I. W., Jin, H. E., Kim, D. D., Chung, S. J., and Shim, C. K. (2008). Effect of ion-pair formation with bile salts on the *in vitro* cellular transport of berberine. *Arch. Pharm. Res.* 31 (1), 103–110. doi:10.1007/s12272-008-1127-4

Chen, W., Miao, Y.-Q., Fan, D.-J., Yang, S.-S., Lin, X., Meng, L.-K., et al. (2011). Bioavailability study of berberine and the enhancing effects of TPGS on intestinal absorption in rats. *AAPS PharmSciTech* 12 (2), 705–711. doi:10.1208/s12249-011-9632-z

Chung, C. Y. S, Timblin, G. A., Saijo, K., and Chang, C. J. (2018). Versatile histochemical approach to detection of hydrogen peroxide in cells and tissues based on puromycin staining. *J. Am. Chem. Soc.* 140 (9), 6109–6121. doi:10.1021/jacs.8b02279

Cui, H., Cai, Y., Wang, L., Jia, B., Li, J., Zhao, S., et al. (2018). Berberine regulates Treg/Th17 balance to treat ulcerative colitis through modulating the gut microbiota in the colon. *Front. Pharmacol.* 9, 571. doi:10.3389/fphar.2018.00571

Hua, W., Ding, L., Chen, Y., Gong, B., He, J., and Xu, G. (2007). Determination of berberine in human plasma by liquid chromatography-electrospray ionization-mass spectrometry. *J. Pharm. Biomed. Anal.* 44 (4), 931–937. doi:10.1016/j.jpba.2007.03.022

Jourden, J. L., and Cohen, S. M. (2010). Hydrogen peroxide activated matrix metalloproteinase inhibitors: a prodrug approach. *Angew. Chem. Int. Ed. Engl.* 49 (38), 6795–6797. doi:10.1002/ange.201003819

Kaplan, G. G. (2015). The global burden of IBD: from 2015 to 2025. *Nat. Rev. Gastroenterol. Hepatol.* 12 (12), 720–727. doi:10.1038/nrgastro.2015.150

Kaser, A., Zeissig, S., and Blumberg, R. S. (2010). Inflammatory bowel disease. *Annu. Rev. Immunol.* 28, 573–621. doi:10.1146/annurev-immunol-030409-101225

Lamprecht, A., Schäfer, U., and Lehr, C. M. (2001). Size-dependent bioadhesion of micro- and nanoparticulate carriers to the inflamed colonic mucosa. *Pharm. Res.* 18 (6), 788–93. doi:10.1023/A:1011032328064

Lih-Brody, L., Powell, S. R., Collier, K. P., Reddy, G. M., Cerchia, R., Kahn, E., et al. (1996). Increased oxidative stress and decreased antioxidant defenses in mucosa of inflammatory bowel disease. *Dig. Dis Sci* 41 (10), 2078–2086. doi:10.1007/BF02093613

Maji, T., Banerjee, S., Biswas, Y., and Mandal, T. K. (2015). Dual-stimuli-responsive l-serine-based zwitterionic UCST-type polymer with tunable thermosensitivity. *Macromolecules* 48 (14), 4957–4966. doi:10.1021/acs.macromol.5b01099

Manichanh, C., Rigottier-Gois, L., Bonnaud, E., Gloux, K., Pelletier, E., Frangeul, L., et al. (2006). Reduced diversity of faecal microbiota in Crohn's disease revealed by a metagenomic approach. *Gut* 55 (2), 205–211. doi:10.1136/gut.2005.073817

Massironi, S., Rossi, R. E., Cavalcoli, F. A., Della Valle, S. D., Fraquelli, M., and Conte, D. (2013). Nutritional deficiencies in inflammatory bowel disease: therapeutic approaches. *Clin. Nutr.* 32 (6), 904–910. doi:10.1016/j.clnu.2013.03.020

Nishida, A., Inoue, R., Inatomi, O., Bamba, S., Naito, Y., and Andoh, A. (2018). Gut microbiota in the pathogenesis of inflammatory bowel disease. *Clin. J. Gastroenterol.* 11 (1), 1–10. doi:10.1007/s12328-017-0813-5

Peterson, D. A., Frank, D. N., Pace, N. R., and Gordon, J. I. (2008). Metagenomic approaches for defining the pathogenesis of inflammatory bowel diseases. *Cell Host Microbe* 3 (6), 417–427. doi:10.1016/j.chom.2008.05.001

Shivaji, U. N., Sharratt, C. L., Thomas, T., Smith, S. C. L., Iacucci, M., Moran, G. W., et al. (2019). Review article: managing the adverse events caused by anti-TNF therapy in inflammatory bowel disease. *Aliment. Pharmacol. Ther.* 49 (6), 664–680. doi:10.1111/apt.15097

Simmonds, N. J., Allen, R. E., Stevens, T. R. J., Niall, R., Van Someren, M., Blake, D. R., et al. (1992). Chemiluminescence assay of mucosal reactive oxygen metabolites in inflammatory bowel disease. *Gastroenterology* 103 (1), 186–196. doi:10.1016/0016-5085(92)91112-H

Tian, T., Wang, Z., and Zhang, J. (2017). Pathomechanisms of oxidative stress in inflammatory bowel disease and potential antioxidant therapies. *Oxidative Med. Cell Longevity* 2017, 4535194. doi:10.1155/2017/4535194

Wakuda, T., Azuma, K., Saimoto, H., Ifuku, S., Morimoto, M., Arifuku, I., et al. (2013). Protective effects of galacturonic acid-rich vinegar brewed from Japanese pear in a dextran sodium sulfate-induced acute colitis model. *J. Funct. Foods* 5 (1), 516–523. doi:10.1016/j.jff.2012.10.010

Walker, A. W., Sanderson, J. D., Churcher, C., Parkes, G. C., Hudspith, B. N., Rayment, N., et al. (2011). High-throughput clone library analysis of the mucosa-associated microbiota reveals dysbiosis and differences between inflamed and non-inflamed regions of the intestine in inflammatory bowel disease. *BMC Microbiol.* 11, 7. doi:10.1186/1471-2180-11-7

Wilke, T., Groth, A., Long, G. H., Tatro, A. R., and Sun, D. (2020). Rate of adverse events and associated health Care costs for the management of inflammatory bowel disease in Germany. *Clin. Ther.* 42 (1), 130–143. doi:10.1016/j.clinthera.2019.11.012

Wilson, D. S., Dalmasso, G., Wang, L., Sitaraman, S. V., Merlin, D., and Murthy, N. (2010). Orally delivered thioketal nanoparticles loaded with TNF-α-siRNA target inflammation and inhibit gene expression in the intestines. *Nat. Mater.* 9 (11), 923–8. doi:10.1038/nmat2859

Wirtz, S., Neufert, C., Weigmann, B., and Neurath, M. F. (2007). Chemically induced mouse models of intestinal inflammation. *Nat. Protoc.* 2 (3), 541–546. doi:10.1038/nprot.2007.41

Xiong, X., Cheng, Z., Wu, F., Hu, M., Liu, Z., Dong, R., et al. (2021). Berberine in the treatment of ulcerative colitis: a possible pathway through Tuft cells. *Biomed. Pharmacother.* 134, 111129. doi:10.1016/j.biopha.2020.111129

Yan, Y. X., Shao, M. J., Qi, Q., Xu, Y. S., Yang, X. Q., Zhu, F. H., et al. (2018). Artemisinin analogue SM934 ameliorates DSS-induced mouse ulcerative colitis via suppressing neutrophils and macrophages. *Acta Pharmacol. Sin* 39 (10), 1633–1644. doi:10.1038/aps.2017.185

Yoon, H., Jangi, S., Dulai, P. S., Boland, B. S., Prokop, L. J., Jairath, V., et al. (2020). Incremental benefit of achieving endoscopic and histologic remission in patients with ulcerative colitis: a systematic review and meta-analysis. *Gastroenterology* 159 (4), 1262–1275.e7. doi:10.1053/j.gastro.2020.06.043

Zhang, Q., Tao, H., Lin, Y., Hu, Y., An, H., Zhang, D., et al. (2016). A superoxide dismutase/catalase mimetic nanomedicine for targeted therapy of inflammatory bowel disease. *Biomaterials* 105, 206–221. doi:10.1016/j.biomaterials.2016.08.010

Zhao, L., Zhang, S., and He, P. (2018). Mechanistic understanding of herbal therapy in inflammatory bowel disease. *Curr. Pharm. Des.* 23 (34), 5173–5179. doi:10.2174/1381612823666171010124414

Zundler, S., and Neurath, M. F. (2015). Immunopathogenesis of inflammatory bowel diseases: functional role of T cells and T cell homing. *Clin. Exp. Rheumatol.* 33 (4 Suppl 92), S19–S28. PMID: 26458165

Conflict of Interest: The authors declare that the research was conducted in the absence of any commercial or financial relationships that could be construed as a potential conflict of interest.

frontiers in Pharmacology

REVIEW
published: 26 April 2021
doi: 10.3389/fphar.2021.651813

Natural-Derived Polysaccharides From Plants, Mushrooms, and Seaweeds for the Treatment of Inflammatory Bowel Disease

*Cailan Li[1], Guosong Wu[2], Hualang Zhao[3], Na Dong[3], Bowen Wu[3], Yujia Chen[3] and Qiang Lu[3]**

[1]Department of Pharmacology, Zunyi Medical University, Zhuhai Campus, Zhuhai, China, [2]Pharmacy Department, Baiyun Branch of Nanfang Hospital of Southern Medical University, Guangzhou, China, [3]Department of Pharmaceutical Sciences, Zunyi Medical University, Zhuhai Campus, Zhuhai, China

Inflammatory bowel disease (IBD) is a chronic inflammatory disease impairing the gastrointestinal tract, and its incidence and prevalence have been increasing over time worldwide. IBD greatly reduces peoples' quality of life and results in several life-threatening complications, including polyp, toxic colonic dilatation, intestinal perforation, gastrointestinal bleeding, and cancerization. The current therapies for IBD mainly include drugs for noncritical patients and operation for critical patients. However, continuous use of these drugs causes serious side effects and increased drug resistance, and the demand of effective and affordable drugs with minimal side effects for IBD sufferers is urgent. Natural-derived polysaccharides are becoming a research hotspot for their therapeutic effects on IBD. This study focuses on the research progress of various natural polysaccharides from plants, seaweeds, and mushrooms for the treatment of IBD during recent 20 years. Regulation of oxidative stress, inflammatory status, gut microbiota, and immune system and protection of the intestinal epithelial barrier function are the underlying mechanisms for the natural-derived polysaccharides to treat IBD. The excellent efficacy and safety of polysaccharides make them promising candidates for IBD therapy.

Keywords: inflammatory bowel disease, polysaccharides, therapeutic effects, action mechanism, plants, mushrooms, seaweeds

OPEN ACCESS

Edited by:
Ning-Ning Liu,
Shanghai Jiao Tong University, China

Reviewed by:
Rinaldo Pellicano,
Molinette Hospital, Italy
Jianye Yuan,
Longhua Hospital Shanghai University of Traditional Chinese Medicine, China

****Correspondence:***
Qiang Lu
luqiang@zmu.edu.cn

Specialty section:
This article was submitted to Gastrointestinal and Hepatic Pharmacology, a section of the journal Frontiers in Pharmacology

Received: *11 January 2021*
Accepted: *22 March 2021*
Published: *26 April 2021*

Citation:
Li C, Wu G, Zhao H, Dong N, Wu B, Chen Y and Lu Q (2021) Natural-Derived Polysaccharides From Plants, Mushrooms, and Seaweeds for the Treatment of Inflammatory Bowel Disease. Front. Pharmacol. 12:651813. doi: 10.3389/fphar.2021.651813

INTRODUCTION

Inflammatory bowel disease (IBD) includes two chronic idiopathic inflammatory diseases: Crohn's disease (CD) and ulcerative colitis (UC), which have become prevalent all over the world (Ananthakrishnan et al., 2019). According to statistics, the prevalence of IBD is the highest in North America, Europe, and Oceania, which exceeded 0.3% of the population (Ng et al., 2017). In contrast, the incidence and prevalence of IBD in Asia and Africa was relatively rare (Kaplan and Ng, 2016; Kaplan and Ng, 2017). However, with westernized diet and lifestyle, a wave of rapidly rising incidence has followed (Mak et al., 2020). The annual direct and indirect expenses associated with IBD are assessed to be as high as €4.6–5.6 billion in Europe and US$6 billion in the United States of America (Kaplan, 2015).

IBD is a chronic inflammatory disease of the gastrointestinal tract, which is characterized by long course, difficulty in curing, low quality of life, and high risk of canceration (Sairenji et al.,

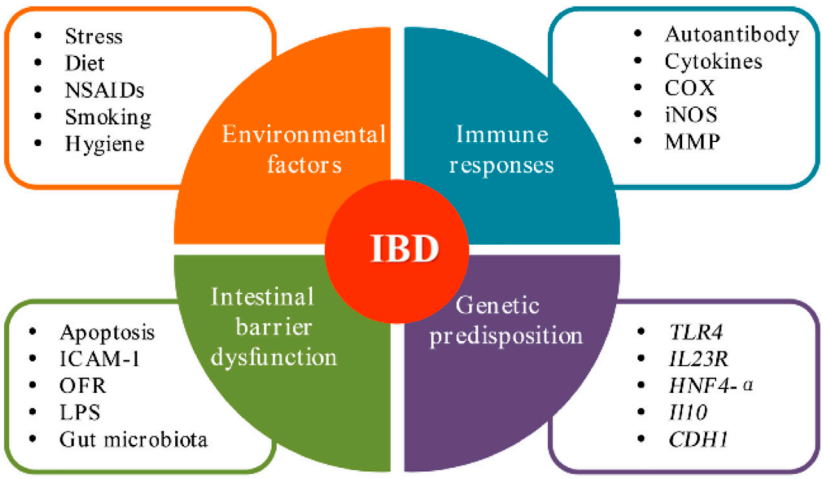

FIGURE 1 | Current overview on the pathogenesis of IBD.

TABLE 1 | Current drugs and their disadvantages for the treatment of IBD.

Type	Drug	Limitation	Reference
5-amino salicylic acids	Balsalazide Sulfasalazine Mesalazine Olsalazine	There are certain adverse reactions such as diarrhea, stomachache, nausea, and emesis. The new-type 5-amino salicylic acids including mesalazine and olsalazine are expensive	Caprilli et al. (2009); Rosenberg and Peppercorn (2010)
Glucocorticoids	Hydrocortisone Prednisone BDP Budesonide	Short-term treatment has a good effect, while long-term application may lead to adverse reactions such as moon-shaped face, weakened immunity, and acne, whose efficacy and safety are difficult to be guaranteed	Ren et al. (2015); Rosenberg and Peppercorn (2010)
Immunosuppressants	Azathioprine 6-mercapopurine Cyclosporine A	The effect takes a long time. The mechanism of action will lead to the inhibition of the body's normal immune response. Long-term application may cause liver and kidney damage	Falasco et al. (2002); Mao et al. (2017)
Biologicals	Infliximab Adalimumab	These drugs also have some adverse reactions and are expensive	Danese et al. (2014); Freeman (2012)

2017). At present, IBD has been listed as one of the modern refractory diseases by the World Health Organization. The main clinical symptom of IBD is bloody diarrhea, abdominal pain, hematochezia and emesis; some patients have extraintestinal manifestations, such as arthritis, iridocyclitis, hepatosis, and eye and skin lesion (Vavricka et al., 2015; Ribaldone et al., 2019). No sex predominance exists in IBD, and the peak age of disease onset is between ages 17 and 40 years (Kotze et al., 2020). Although the cause of IBD remains unknown, studies have provided evidence that the pathogenesis (**Figure 1**) of IBD is multifactorial, mainly including genetic predisposition, epithelial barrier defects, dysregulated immune responses, and environmental factors (Guan, 2019; Li C. L. et al., 2020). Modern medical therapy for patients with IBD mainly involves aminosalicylic acids, glucocorticoids, immunosuppressants, and biological agents, which can control its symptoms (Eberhardson et al., 2019). However, many disadvantages (**Table 1**) are increasingly prominent, such as severe side effects, easy recurrence, increased drug resistance, and high price (Moreau and Mas, 2015). Therefore, scientists are constantly devoting themselves to the development of more safe and effective drugs for treating IBD.

Polysaccharides are polymeric carbohydrates consisting of at least 10 monosaccharides with glycoside bonds (Ferreira et al., 2015). They range in structure from linear to highly branch. Generally, there are more than 100 monosaccharides in polysaccharides, and even as many as thousands, with great different properties (Yu et al., 2018). Polysaccharides are not only the supporting tissues and storage nutrients of animals and plants but also possess rich physiological activities, such as immune regulation (Tabarsa et al., 2020), antitumor (Khan et al., 2019), anti-oxidation (Ma et al., 2020), and so on. Notably, a large number of studies have shown that polysaccharides from different sources exerted significant inhibitory effects on IBD (**Figure 2**). In this study, the research progress of natural polysaccharides for the treatment of IBD was reviewed. It is hoped that it will provide inspiration for

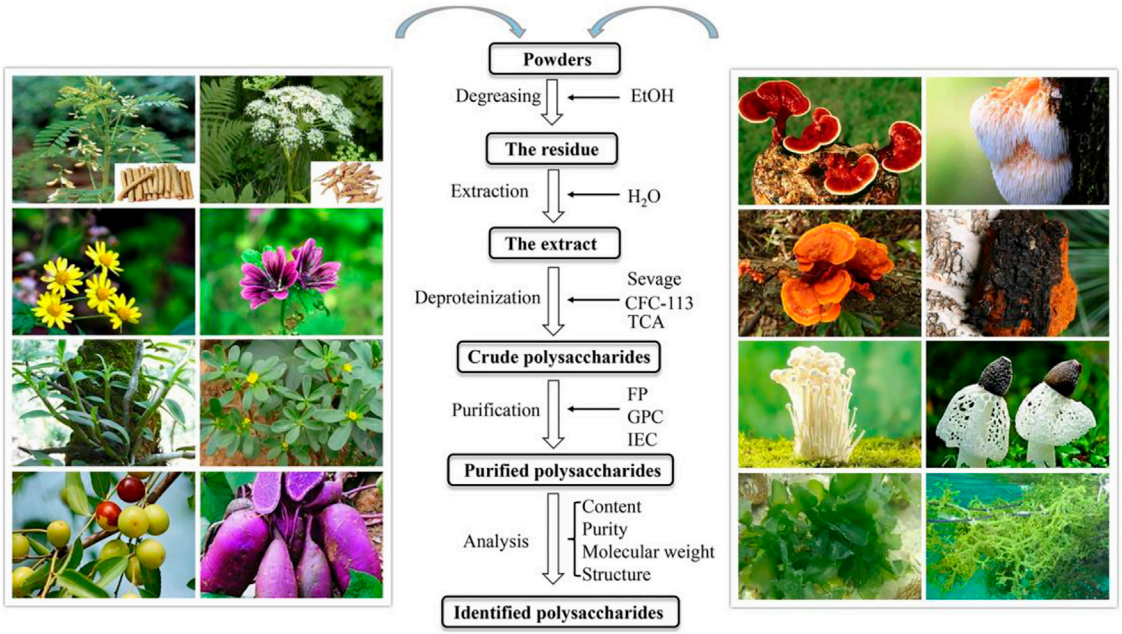

FIGURE 2 | Glance at the natural sources of polysaccharides for the treatment of IBD in the past decades and the essential steps on the isolation and purification of them.

the researchers to design, research, and develop new drugs for IBD therapy.

METHODS

To identify the studies related to the effect and mechanism of natural-derived polysaccharides against IBD, we referred to the published articles in the following academic databases from the creation date to August 2020: Google Scholar, Web of Science (WOS), PubMed, and Embase. In the literature retrieval, the following search terms were adopted in combination ("polysaccharide" OR "polysaccharose") AND ("inflammatory bowel disease" OR "IBD," "ulcerative colitis" OR "colitis" OR "ulcer colitis" OR "UC," OR "Crohn's disease" OR "CD"). All articles with abstracts were considered.

After searching, the acquired articles were carefully screened. First, the articles on the effect and mechanism of natural-derived polysaccharides against IBD were initially selected through reading the titles and abstracts. Second, for the articles that cannot be identified through preliminary screening, the full text was further examined. Finally, all articles that fit the topic were imported into EndNote as the supporting resources of this review.

POLYSACCHARIDES FROM PLANTS

Due to the wide variety, large amount, and easy access, terrestrial plants have always been the most important natural resources for human survival. The original sources of food and medicine for humans also mainly come from terrestrial plants. At present, the researches on bioactive components mainly focus on edible and medicinal plants (Atanasov et al., 2015). Significantly, there are many studies on plant polysaccharides against IBD. **Tables 2**, **3** listed the chemical and pharmacological information of polysaccharides from plants for the treatment of IBD, respectively.

Astragalus membranaceus

A. membranaceus belongs to the Leguminosae family and is one of the most commonly used Chinese herb medicine in China. It has many pharmacological effects, such as immune regulation, antitumor, antivirus, and so on (Fu et al., 2014). Polysaccharides, triterpenoids, and flavonoids are the three main active components of *A. membranaceus* (Jin et al., 2014). Lv et al. (2017) prepared a polysaccharide APS from *A. membranaceus* and evaluated the therapeutic roles of APS and delineated the possible molecular mechanisms in the DSS-induced mouse colitis model. The results demonstrated that APS treatment observably improved colitis-related clinical signs and pathological damage of colon caused by DSS exposure. Moreover, APS could also significantly inhibit the intestinal inflammation response through downregulating the colonic mRNA expression and release of pro-inflammatory mediators, including TNF-α, IL-1β, and IL-6, and reducing the MPO activity. In addition, APS treatment was observed to block NF-κB activation by suppressing the phosphorylation of NF-κB p65. Overall, these found implied that APS could serve as a natural therapeutic approach for the treatment of IBD.

TABLE 2 | Monosaccharide composition, molecular weight, and main glycosidic bond of polysaccharides from natural sources.

Name	Source	Monosaccharide composition	M.W. (Da)	Main glycosidic bond	Reference
Polysaccharides from edible and medicinal plants					
APS	Roots of *Astragalus membranaceus*	Rha, Glc, Gal, and Ara in a ratio of 1.00: 18.45:3.53:7.11	NA	NA	Lv et al. (2017)
SP1-1	Roots of *Scutellaria baicalensis*	Man, Rib, GluA, Glc, Xyl, and Ara in a ratio of 2.14:3.61:1.00:2.86:5.98:36.39	4.56×10^5	NA	Cui et al. (2019)
ASP	Roots of *Angelica sinensis*	GluA, Glc, Ara, and Gal in a ratio of 1.00: 1.70:1.85:5.02	8.00×10^4	(1→3)-linked Gal*p*, (1→6)-linked Gal*p*, and 2-OMe-(1→6)-linked Gal*p*	Cheng et al. (2020)
DOPS	Stems of *Dendrobium officinale*	Man, Glc, and Ara in a ratio of 5.55: 1.00:0.12	3.94×10^5	(1→4)-linked *β*-D-mannopyranosyl residues and *β*-D-glucopyranosyl residues	Liang et al. (2018)
CP	Flowers of *Chrysanthemum morifolium*	NA	NA	NA	Tao et al. (2017, 2018)
PLS	Fruits of *Morinda citrifolia*	GalA, Gal, Ara, Rha, and Man in a ratio of 29.10:30.90:31.00:5.40:3.60	NA	NA	Batista et al. (2020)
WJPs	Sarcocarps of *Ziziphus jujuba*	Glc, Ara, GalA, and Gal in a ratio of 38.59: 23.16:17.64:10.44	NA	NA	Yue et al. (2015)
ALP-1	Roots of *Arctium lappa*	Fru and Glc	5.12×10^3	(2→1)-β-D-fructofuranose	Wang Y. et al. (2019)
MSP	Aerial parts of *Malva sylvestris*	Gal, Glc, UA, Ara, and Rha in a ratio of 4.00: 5.00:14.00:6.00:1.00	1.30×10^6	NA	Hamedi et al. (2016)
HMFO	Roots of *Cynanchum wilfordii*	Glc, Ara, Gal, Rha, and GalA	$0.12–5.20 \times 10^5$	NA	Cho et al. (2017)
PP	Rootstocks of *Rauvolfia verticillata*	GalA, Gal, Ara, Rha, Glc, and Man in a ratio of 51.00:6.80:7.10:2.60:31.30:0.70	$0.50–3.00 \times 10^5$	NA	Miao et al. (2019)
POLP	Aerial parts of *Portulacae oleracea*	NA	NA	NA	Wang et al. (2018), Wang Z. et al. (2020)
OP	Fruits of *Vaccinium oxycoccos*	GalA, Rha, Ara, Glc, and Gal in a ratio of 82.00:1.50:8.00:5.00:3.00	$1.00–3.00 \times 10^5$	NA	Popov et al. (2006)
ASPP	Tubers of *Ipomoea batatas*	Rha, Ara, Xyl, Man, and Glc in a ratio of 2.80:1.90:1.00:7.60:53.30	1.80×10^5	1,4-linked Glc*p*	Sun et al. (2020)
MAP	Fruits of *Malus/ domestica*	GalA and Gal	$0.50–1.00 \times 10^4$	NA	Li et al. (2017)
Polysaccharides from edible mushrooms					
GLP	*Ganoderma lucidum*	NA	1.03×10^5	1,6-lnked *β*-D-Glc*p*	Xie et al. (2019)
HECP	*Hericium erinaceus*	Glc, Gal, Ara, Xyl, Rha, and Man in a ratio of 76.71:14.26:4.04:2.57:1.32:1.14	8.67×10^4	NA	Ren et al. (2018)
EP-1	*Hericium erinaceus*	Glc, Man, Gal	3.10×10^3	(1→3)-linked glucan	Wang D. D. et al. (2019)
CMP33	*Poria cocos*	NA	15.23×10^4	(1→3)-linked glucose	Liu X. F. et al. (2018)
IOP	*Inonotus obliquus*	Man, Rha, Glc, Gal, Xyl, and Ara in a ratio of 9.20:4.40:46.60:11.50:11.10:4.30	NA	NA	Chen et al. (2019)
DIP	*Dictyophora indusiata*	Glc	5.36×10^5	β-(1→3)-D-glucan	Wang Y. L. et al. (2019)
PPS	*Pycnoporus sanguineus*	Glc, Man, and Gal	3.29×10^4	NA	Li M. X. et al. (2020)
FVP	*Flammuliana velutipes*	Glc, Man, and Gal in a ratio of 56.20:29.70: 14.10	5.48×10^4	NA	Zhang et al. (2020)
LEP	*Lachnum* YM130	Man and Gal in a ratio of 3.80:1.00	1.31×10^6	NA	Zong et al. (2020)
Polysaccharides from seaweeds					
GBP	*Gracilaria birdiae*	Gal and AnGal	$0.38–2.60 \times 10^6$	→4–3,6–anhydro–α–L–Gal*p* (1→3) β–D–Gal*p* 1→ segments	Brito et al. (2014)
ULP	*Ulva lactuca*	Rha, Xyl, Glc, and UA	NA	NA	Zhu et al. (2017)
ECP	*Eucheuma cottonii*	Gal	NA	NA	Sudirman et al. (2018)
BMP	*Blidingia minima*	Rha, Xyl, GluA, and Glc	NA	NA	Song et al. (2019)

Scutellaria baicalensis

S. baicalensis is a species of the flowering plant in the *Lamiaceae* family. Its dried roots have been used for over 2,000 years as a traditional Chinese medicine known as *Huang-Qin* (Zhao et al., 2016). Cui et al. (2019) obtained a purified polysaccharide SP1-1 from *S. baicalensis*, and found that SP1-1 administration can effectively improve DSS-induced colitis by reducing DAI scores, colonic lesions, and MPO activity. SP1-1 significantly suppressed the production of pro-inflammatory cytokines TNF-α, IL-1β, and IL-18 in the serum and colon of DSS-induced colitis mice and LPS-induced THP-1 derived macrophages. In addition, SP1-1 remarkably

TABLE 3 | Summary of the mechanisms of polysaccharides from natural sources in the treatment of IBD.

Name	Source	Model	Mechanism of action	Reference
Polysaccharides from edible and medicinal plants				
APS	*Astragalus membranaceus*	DSS-induced C57BL/6 mice	Downregulation: TNF-α, IL-1β, IL-6, MPO, and NF-κB p-p65	Lv et al. (2017)
SP1-1	*Scutellaria baicalensis*	DSS-induced C57BL/6 mice; LPS-stimulated THP-1 cells	Upregulation: p65 (cytoplasm) and p-p65 (cytoplasm); downregulation: MPO, p-IKKα, -IKKβ, p-IκBα, p65 (nucleus), p-p65 (nucleus), NLRP3, caspase-1, cleaved caspase-1, IL-1β, pro-IL-1β, IL-18, and pro-IL-18	Cui et al. (2019)
ASP	*Angelica sinensis*	DSS-induced BALB/c mice; LPS-stimulated Caco-2 cells	Upregulation: ZO-1, occludin, claudin-1, and Bcl-2; downregulation: MPO, IL-6, IL-1β, TNF-α, Bax, and caspase-3	Cheng et al. (2020)
DOPS	*Dendrobium officinale*	DSS-induced BALB/c mice; LPS-stimulated NCM460 cells	Upregulation: IL-10; downregulation: IL-1β, IL-6, IL-18, TNF-α, IFN-γ, NLRP3, ASC, caspase1, and β-arrestin1	Liang et al. (2018)
CP	*Chrysanthemum morifolium*	TNBS-induced SD rats	Upregulation: IL-4, IL-10, IL-13, SOD, *Firmicutes*/*Bacteroidetes*, *Butyricicoccus*, *Clostridium*, *Lactobacillus*, *Bifidobacterium*, *Lachnospiraceae,* and *Rikenellaceae*; downregulation: MPO, TNF-α, IL-1β, IL-6, IF-17, IL-23, IFN-γ, MDA, TLR4, p65, p-p65, STAT3, p-STAT3, JAK2, *Escherichia, Enterococcus*, and *Prevotella*	Tao et al. (2017, 2018)
PLS	*Morinda citrifolia*	HOAc-induced Swiss mice	Upregulation: GSH; downregulation: MPO, MDA, NO_3/NO_2, and COX-2	Batista et al. (2020)
WJPs	*Ziziphus jujuba*	TNBS-induced SD rats; TNF-α-stimulated Caco-2 cells	Upregulation: occludin, claudin-1, claudin-4, ZO-1, p-AMPK, and p-ACC; downregulation: TNF-α, IL-1β, IL-6, and MPO	Yue et al. (2015)
ALP-1	*Arctium lappa*	DSS-induced ICR mice	Upregulation: IL-10, IgA, *Firmicutes, Ruminococcaceae, Lachnospiraceae, and Lactobacillus*; downregulation: IL-1β, IL-6, TNF-α, *Proteobacteria*, *Alcaligenaceae*, *Staphylococcus*, and *Bacteroidetes*	Wang Y. et al. (2019)
HMFO	*Cynanchum wilfordii*	DSS-induced BALB/c mice; LPS-stimulated RAW264.7 cells	Downregulation: MPO, PGE_2, NO, TNF-α, IL-6, iNOS, COX-2, p-p65, p-IκBα, p-IKK α/β, p-JNK, p-ERK, and p-p38	Cho et al. (2017)
PP	*Rauvolfia verticillata*	DSS-induced BALB/c mice	Upregulation: IκBα; downregulation: MPO, TNF-α, IL-6, p65, ERK, JNK, and p38	Miao et al. (2019)
POLP	*Portulacae oleracea*	DSS-induced Kunming mice	Upregulation: IL-10, IκBα, and NF-κB p65 (cytoplasm); downregulation: TNF-α, IL-1β, IL-6, IL-18, PGE_2, Bcl-2, survivin, p-STAT3, COX-2, and NF-κB p65 (nucleus)	Wang et al. (2018), Wang Z. et al. (2020)
OP	*Vaccinium oxycoccos*	HOAc-induced A/HeJ mice	Downregulation: MDA	Popov et al. (2006)
ASPP	*Ipomoea batatas*	DSS-induced ICR mice	Upregulation: AA, PA, BA, and *Firmicutes*; downregulation: TNF-α, IL-1β, IL-6, *Bacteroidetes*, *Proteobacteria*, and *Actinobacteria*	Sun et al. (2020)
MAP	*Malus domestica*	DSS-induced ICR mice	Upregulation: IL-22BP; downregulation: IL-22, p-STAT3, Bcl-2, and cyclin D1	Li et al. (2017)
Polysaccharides from edible mushrooms				
GLP	*Ganoderma lucidum*	DSS-induced Wistar rats	Upregulation: TA, AA, PA, BA, *Ruminococcus_1*, *Ccl5, Cd3e, Cd8a, Il21r, Lck, and Trbv*; downregulation: *Escherichia–Shigella*, *Ccl3, Gro, Il11, Mhc2, and Ptgs*	Xie et al. (2019)
HECP	*Hericium erinaceus*	DSS-induced C57BL/6 mice	Upregulation: T-SOD and *Bacteroidetes*; downregulation: NO, MDA, MPO, IL-6, IL-1β, TNF-α, COX-2, iNOS, p-p65/p65, p-IκBα/IκBα, pAkt/Akt, p-p38/p38, p-ERK/ERK, p-JNK/JNK, *Verrucomicrobia*, *Actinobacteria*, *Arthrobacter* spp., *Methylibium* sp., *Succinivibrio* sp., *Desulfovibrio* sp., and *Akkermansia muciniphila*	Ren et al. (2018)
EP-1	*Hericium erinaceus*	HOAc-induced SD rats H_2O_2-induced Caco-2 cells	Upregulation: MMP, SOD, OCR, ATP, Bcl-2, AA, PA, BA, VA, IBA, IVA, GPR41, GPR43, and IgM; downregulation: MDA, TNF-α, IL-1, IL-6, ROS, p-p65, p65, caspase-3, and C3	Shao et al. (2019); Wang D. D. et al. (2019)
CMP33	*Poria cocos*	TNBS-induced Kunming mice	Upregulation: IL-4, IL-10, and DHT; downregulation: MPO, MDA, TNF-α, IL-6, L-1β, IL-12, IFN-γ, IL-2, IL-17, Hmgcs2, Fabp2, Hp, B4galnt2, B3gnt6, Sap, Ca1, and oleic acid	Liu X. F. et al. (2018)
IOP	*Inonotus obliquus*	DSS-induced BALB/c mice	Upregulation: ZO-1, occludin, IL-4, IL-10, GATA-3, Foxp3, and p-STAT6; downregulation: p-STAT1, p-STAT3, IFN-γ, IL-17, T-bet, and ROR-γt	Chen et al. (2019)
DIP	*Dictyophora indusiata*	DSS-induced C57BL/6 mice	Upregulation: GSH, HO-1, IL-10, Bcl-2, TJP1, and IRF4; downregulation: MDA, MPO, TNF-α, IL-6, IL-1β, IL-18, NLRP3, p-IκBα, p-STAT3, Bax, IRF5, and CD86	Wang Y. L. et al. (2019)
PPS	*Pycnoporus sanguineus*	DSS-induced BALB/c mice	Upregulation: ZO-1, E-cadherin, PCNA, Th1, MCP-1β, ULK1, LC3 I, p62, Beclin-1, and LC3 II; downregulation: LPS, Proportions of Th cells, Th2, Th17, Treg, MPO, IL-10, IL-12p40, IL-15, IL-17, and LC3 II/I	Li M. X. et al. (2020)

(Continued on following page)

TABLE 3 | (*Continued*) Summary of the mechanisms of polysaccharides from natural sources in the treatment of IBD.

Name	Source	Model	Mechanism of action	Reference
FVP	*Flammuliana velutipes*	DSS-induced SD rats	Upregulation: SOD, AA, PA, BA, IVA, and VA; downregulation: MPO, NO, DAO, TLR4, NF-κB, and p-p65	Zhang et al. (2020)
LEP	*Lachnum* YM130	DSS-induced ICR mice	Upregulation: ZO-1, occludin, claudin-1, E-cadherin, claudin-3, claudin-7, MUC1, MUC2, TFF3, Relmβ, Reg3β, Reg3γ, PPARγ, CAT, SOD, T-AOC, IRE1α, XBP1; downregulation: TNF-α, IL-1β, IL-6, iNOS, COX-2; NO, PGE_2; NF-κB p-p65, p-IκBα, p-STAT3 MPO, Ly6G; $CD4^+IL\text{-}10^+$, F4/80, NLRP3, ASC, caspase-1, Bip, ATF6, PERK, CHOP, C-Cas3, MDA, nitrotyrosine, and NOx	Zong et al. (2020)
Polysaccharides from seaweeds				
GBP	*Gracilaria birdiae*	TNBS-induced Wistar rats	Upregulation: GSH; downregulation: IL-1β, TNF-α, MPO, MDA, and NO_3/NO_2	Brito et al. (2014)
ULP	*Ulva lactuca*	DSS-induced C57BL/6 mice	Upregulation: GSH, GPx, and Se; downregulation: MPO, IL-6, TNF-α, iNOS, COX-2, CD68, NF-κB p-p65, and p-IκBα	Zhu et al. (2017)
ECP	*Eucheuma cottonii*	DSS-induced BALB/c mice	Upregulation: IL-10; downregulation: TNF-α, IL-1β, and IL-6	Sudirman et al. (2018)
BMP	*Blidingia minima*	DSS-induced C57BL/6J mice and IPEC-J2 cells	Upregulation: ZO-1, occludin, claudin-1, IL-10, and DAO; downregulation: MPO, EPO, ET-1, TNF-α, IL-1β, p-NF-κB, p-IκBα, and p-AKT	Song et al. (2019)

decreased the colonic $CD11b^+$ macrophage infiltration. Meanwhile, SP1-1 treatment effectively inhibited the activation of the NF-κB pathway through reducing phosphorylation of IKKα, IKKβ, and IκBα, and inhibiting the translocation of NF-κB p65 from cytoplasm to nucleus. Furthermore, the elevated expression of NLRP3, caspase-1, cleaved caspase-1, IL-1β, pro-IL-1β, IL-18, and pro-IL-18 in DSS treated mice was mitigated by SP1-1, resulting in the inactivation of NLRP3 inflammasome. These data implied that the anti-inflammatory effect of SP1-1 against DSS-induced colitis was closely related to its inhibition of NLRP3 inflammasome and NF-κB signaling pathways. SP1-1 may be served as a novel candidate drug to treat IBD in future.

Angelica sinensis

A. sinensis belongs to the Umbelliferae family, which has been traditionally used in Chinese medicinal formulation for a long time and is also commonly used as a dietary supplement in Europe and America (Wei et al., 2016). Polysaccharides are a class of phytochemicals in *A. sinensis*, which have been proved to have many pharmacological activities (Jin et al., 2012). Cheng et al. (2020) extracted an acidic polysaccharide ASP (**Figure 3A**) from *A. sinensis* and investigated the protective effects of ASP on DSS-induced colitis. Results showed that ASP observably attenuate the severity of colitis symptoms manifested as the reduction of weight loss, DAI score, and colon length shortening induced by DSS. Furthermore, the mRNA expressions of pro-inflammatory cytokines (TNF-α, IL-6, and IL-1β) and MPO activity caused by DSS were strikingly inhibited by ASP treatment. ASP also improved the colonic barrier function *via* enhancing the expressions of TJs proteins (ZO-1, occludin, and claudin-1) and decreasing cell membrane permeability in LPS-stimulated Caco-2 cell. In addition, ASP could significantly mitigate intestinal epithelium cell apoptosis and promote proliferation through upregulating Bcl-2 protein expression and downregulating Bax and caspase-3 levels in colon tissues of DSS-induced colitis mice. Collectively, these results manifested that ASP can be a potential natural ingredient for the treatment of IBD.

Dendrobium officinale

D. officinale, a precious plant of the Orchidaceae family, possesses extremely high medicinal and edible values. It has been broadly applied to treat gastrointestinal diseases in China for thousand years, which was the earliest recorded in Shennong's Classic of Materia Medica (Tang et al., 2017). Liang et al. (2018) obtained a heteropolysaccharide DOPS (**Figure 3B**) from *D. officinale*, and found DOPS could obviously ameliorate the clinical symptoms, reduce mortality, and relieve pathological damage of colon in colitis mice induced by DSS. Interestingly, DOPS treatment pronouncedly regulated the imbalance of pro-/anti-inflammatory mediators through reducing the production of pro-inflammatory cytokines (TNF-α, IL-6, IL-1β, IL-18, and IFN-γ) and augmenting the anti-inflammatory IL-10 level, and thus descending the ratio of pro-/anti-inflammatory cytokines. In addition, DOPS could significantly inhibit the expression of NLRP3, ASC, caspase1, and β-arrestin1 in DSS-induced colitis mice and LPS-stimulated NCM460 cells. In summary, these data indicated that DOPS administration exhibited a therapeutic effect on DSS-induced experimental colitis in mice, which was probably associated with the suppression of NLRP3 inflammasome activation and β-arrestin1 signaling pathway, and the subsequent expression of pro-inflammatory cytokines. DOPS is expected to be a potential candidate component for the treatment of inflammatory diseases like IBD in the future.

Chrysanthemum morifolium

C. morifolium, a medicinal and edible plant of the Asteraceae family, has been broadly applied in clinical practice for thousands of years in China and Korea (Tao et al., 2016). Tao et al. (2017), Tao et al., (2018) abstracted polysaccharides from *C. morifolium* and found that CP possessed pronouncedly protective effects on

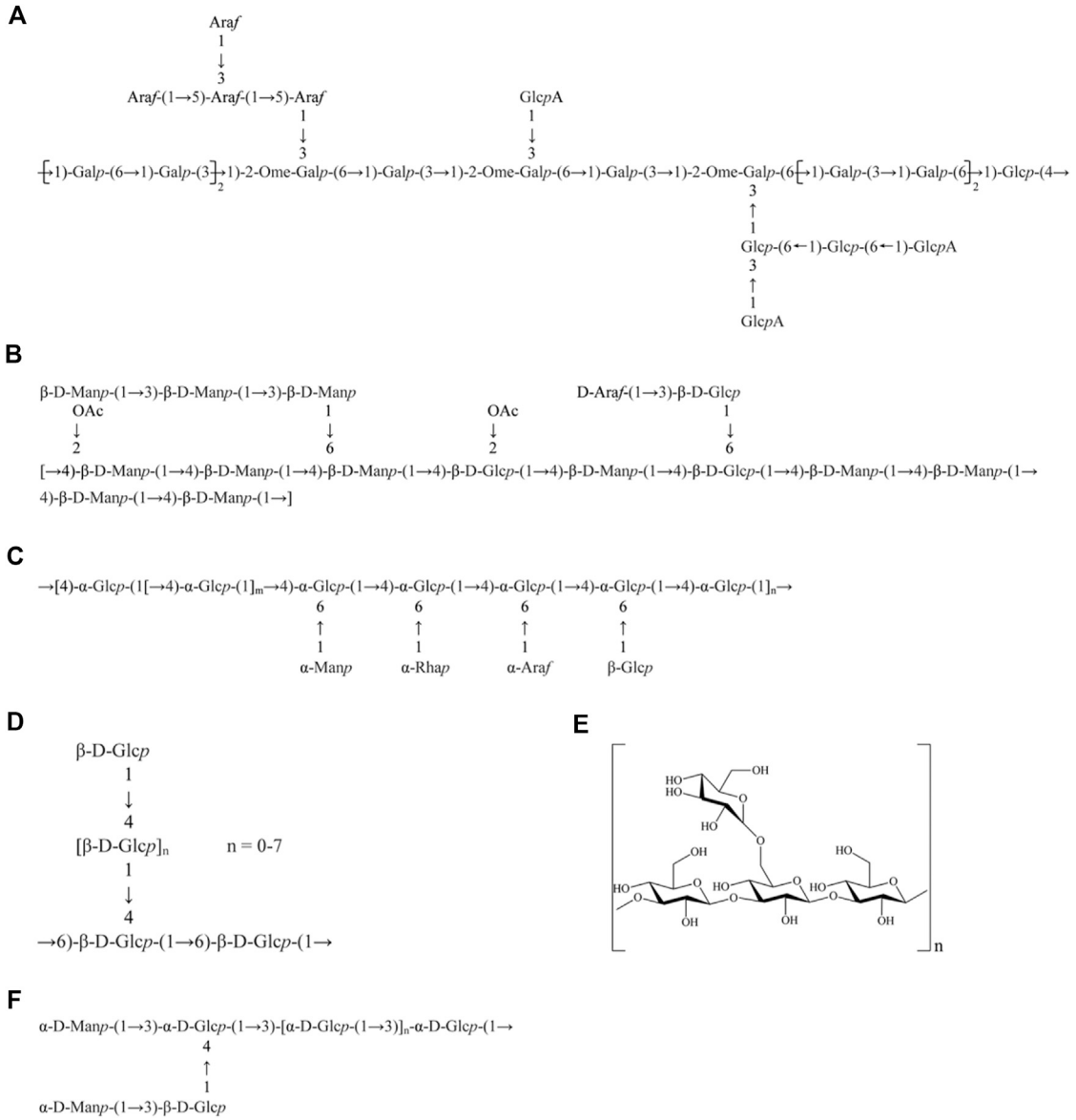

FIGURE 3 | Chemical structures of polysaccharides from natural sources for the treatment of IBD. **(A)** ASP from *Angelica sinensis*; **(B)** DOPS from *Dendrobium officinale*; **(C)** ASPP from *Ipomoea batatas*; **(D)** GLP from *Ganoderma lucidum*; **(E)** DIP from *Dictyophora indusiata*; and **(F)** EP-1 from *Hericium erinaceus*.

TNBS-induced colitis in rats. CP administration could significantly enhance the production of anti-inflammatory mediators IL-4, IL-10, and IL-13 while decreased the secretion of pro-inflammatory factors, including TNF-α, IL-1β, IL-6, IL-17, IL-23, and IFN-γ. Moreover, CP inhibited oxidative stress by increasing the SOD level and reducing the MDA content. Further mechanistic study illustrated that the anti-inflammatory roles of CP might be related to blocking the activation of NF-κB/TLR4 and IL-6/JAK2/STAT3 signaling pathways by inhibiting the mRNA levels of NF-κB, TLR4, IL-6, JAK2, and STAT3, and the protein expression of NF-κB p65, p-p65, TLR4, JAK2, STAT3, and p-STAT3 in colonic tissues of TNBS-induced colitis rats. Additionally, 16S rRNA sequencing analysis result revealed that CP remarkably raised the ratio of *Firmicutes*/*Bacteroidetes*, and elevated microbial diversity and community richness in rats with colitis. The relative abundance of pathogens (*Escherichia, Enterococcus,* and *Prevotella*) was downregulated, while the levels of probiotics including *Butyricicoccus*, *Clostridium*, *Lactobacillus*, *Bifidobacterium*, *Lachnospiraceae,* and *Rikenellaceae* were increased after CP treatment. Correlation analysis demonstrated that the gut microflora was correlated closely with the expression of cytokines, and they interacted with each other to modulate immune function. In conclusion, CP could alleviate IBD by regulating intestinal microecological balance and maintaining immune homeostasis, which promote the curative drug development of IBD.

Morinda citrifolia

M. citrifolia, commonly known as noni, belongs to the Rubiaceae family and is a native tropical shrub in Southeast Asia. It has been used in traditional medicine for more than 2,000 years. Nowadays, *M. citrifolia* attracted the attention of researchers from the pharmaceutical and food industry for different therapeutic purposes (Almeida et al., 2019). Batista et al. (2020) extracted polysaccharides (PLS) from the fruits of *M. citrifolia*. PLS was found to ameliorate the intestinal damage and MPO activity in acetic acid–induced colitis. PLS significantly reduced oxidative damage by increasing the GSH level and decreasing the content of MDA and NO_3/NO_2. Moreover, PLS could prominently inhibit the expression of TNF-α, IL-1β, and COX-2. This result demonstrated that PLS exhibited an anti-inflammatory effect against colitis by mitigating inflammatory response and oxidative stress in the inflamed colon, suggesting PLS possessed therapeutic potential against inflammatory diseases like IBD.

Ziziphus jujuba

Z. jujuba, also called jujube, is a thorny, rhamnaceous deciduous plant broadly distributed in northern China. Its fruits are much admired for their high nutritional and medicinal values (Gao et al., 2013). Yue et al. (2015) abstracted a crude polysaccharide WJPs from wild jujube sarcocarp and investigated the therapeutic roles of WJPs on TNBS-induced colitis rats and TNF-α-stimulated Caco-2 cells. Results showed that WJPs could observably ameliorate the severity of colitis and attenuate mucosal injury in colitis rats. In addition, WJPs mitigated the intestinal inflammatory response by inhibiting the levels of TNF-α, IL-1β, IL-6, and MPO activity. Furthermore, WJPs was found to improve the intestinal epithelial barrier function as WJPs could significantly reverse TNF-α-induced increase of FD-4 flux and decrease of TER in Caco-2 cells, and upregulate the expression of TJs proteins (ZO-1, occludin, claudin-1, and claudin-4) in colonic tissues of rats with TNBS-induced colitis. Further mechanistic study revealed that WJPs remarkably induced activation of the AMPK pathway through upregulation of the phosphorylation of AMPK and ACC *in vivo* and *in vitro*. Taken together, WJPs possess prominently protective effect on colitis, at least partly through enhancing intestinal barrier function, and suppressing inflammation response. WJPs may be used as a promising candidate to meet the medication needs of IBD.

Arctium lappa

A. lappa, also called burdock, is a medicinal and edible plant belonging to the Asteraceae family. It is mainly distributed in China and Western Europe and traditionally used to treat various diseases. Nowadays, *A. lappa* is regarded as a valued source for secondary metabolites, which exhibits many biological activities and pharmacological functions (Gao et al., 2018). Wang Y. et al. (2019) extracted a water-soluble polysaccharide ALP-1 from *A. lappa* and applied the DSS-induced mice model to assess the protective effect of ALP-1 on colitis. The results revealed that ALP-1 could dramatically increase anti-inflammatory cytokine IL-10 and alleviate pro-inflammatory mediator (IL-1β, IL-6, and TNF-α) levels in colon and serum of colitis mice. Moreover, the reduced level of IgA caused by DSS exposure was notably increased after ALP-1 treatment. In addition, compared with the DSS-induced colitis group, ALP-1 treatment remarkably enhanced the relative abundance of probiotics, including *Firmicutes*, *Ruminococcaceae*, *Lachnospiraceae,* and *Lactobacillus*, while descended the levels of pathogen, such as *Proteobacteria*, *Alcaligenaceae*, *Staphylococcus,* and *Bacteroidetes*. In conclusion, the research showed that the anti-colitis effect of ALP-1 may be associated with the regulation of gut microbiota structure and the imbalance of inflammatory cytokines. ALP-1 may be applied as a dietary supplement agent for patients with IBD.

Malva sylvestris

M. sylvestris, known as common mallow, belongs to the Malvaceae family. It is a medicinal and edible plant that mainly grows in Europe, North Africa, and Asia. Studies have proved that *M. sylvestris* possess beneficial gastrointestinal effects (Gasparetto et al., 2012). Polysaccharides are reported to be the major active components of *M. sylvestris*. Hamedi et al. (2016) found that the isolated polysaccharide MSP from *M. sylvestris* could effectively ameliorate macroscopic and microscopic parameters and inhibit inflammation symptoms of colitis, which exhibited obviously a protective effect against IBD induced by acetic acid in rats.

Cynanchum wilfordii

C. wilfordii belongs to the Asclepiadaceae family and is mainly distributed in Korea, Japan, and China. Its underground roots are traditionally used for the treatment of gastrointestinal diseases (Jiang et al., 2011). Cho et al. (2017) prepared a crude polysaccharide HMFO from *C. wilfordii*, and explored the anti-inflammatory effects and underlying mechanisms of HMFO in DSS-induced mouse colitis and LPS-stimulated RAW 264.7 cells. Results showed that HMFO dramatically relieved the pathological characteristics and histological damage of colitis, reduced MPO activity, and inhibited the production of pro-inflammatory factors TNF-α and IL-6 in the colon of colitis mice. Furthermore, HMFO significantly downregulated the expression of iNOS, COX-2, and phosphorylated NF-κB in mice. *In vitro*, HMFO sharply mitigated several cytokines and enzymes associated with inflammation, including NO, PGE_2, TNF-α, IL-6, iNOS, and COX-2. Further mechanism study revealed that HMFO blocked the activation of NF-κB and MAPK signaling pathways by retarding the phosphorylation of NF-κB p65, IκBα, IKK α/β, p38, ERK, and JNK. These results speculated that HMFO is a promising remedy to treat IBD.

Rauvolfia verticillata

R. verticillata belongs to the Apocynaceae family and is mainly distributed in China and Vietnam. Its roots and leaves are used for medicinal purposes including treating hypertension, hyperthermia, insomnia, and so on (Hong et al., 2012). Miao et al. (2019) obtained a pectic polysaccharide PP from the rootstocks of *R. verticillata* and found that PP treatment attenuated the overall physical activity, DAI, and

morphological damage in DSS-treated colitis mice. Meanwhile, PP dramatically reduced TNF-α, IL-6, and MPO activity. Furthermore, the down-regulated IκBα level and up-regulated expression of NF-κB p65, ERK, JNK, and p38 caused by DSS exposure were reversed by PP treatment. In short, these findings strongly suggested that PP can inhibit the colonic inflammation *via* suppressing NF-κB and MAPK pathways, providing a scientific basis for the application of PP as an effective therapeutic agent for the treatment of IBD.

Portulacae oleracea

P. oleracea belongs to the Portulacaceae family and is a widespread edible and medicinal plant for alleviating various diseases (Iranshahy et al., 2017). Wang et al. (2018), Wang Z. et al. (2020) acquired a polysaccharide POLP from *P. oleracea* and found that POLP could relieve DSS-induced clinical symptoms and improve histopathological damage. The levels of pro-inflammatory factors TNF-α, IL-1β, IL-6, IL-18, and PGE_2 were markedly decreased, whereas the secretion of anti-inflammatory mediator IL-10 was increased after POL administration. Moreover, POLP sharply upregulated the IκBα protein expression, inhibited the translocation of NF-κB p65 from cytoplasm to nucleus, and downregulated the NF-κB p65 related proteins (including Bcl-2 and survivin) in DSS-treated mice. In addition, POLP significantly suppressed the COX-2 protein expression and the phosphorylation of STAT3. Thus, it was speculated that POLP exhibited excellent protective effects on IBD, and the mechanisms were closely associated with the inhibition of NF-κB and STAT3/COX-2 pathways.

Vaccinium oxycoccos

V. oxycoccos, also called European cranberry, is a plant belongs to the Ericaceae family. Its fruits are a valuable source of antioxidants and other biologically active substances (Jurikova et al., 2019). Popov et al. (2006) extracted a pectic polysaccharide OP from *V. oxycoccos* and found that the colonic macroscopic damage score and total injury area were obviously relieved in the OP treatment group compared with those of the 5% acetic acid–induced colitis group. OP has shown to reduce the MPO activity in colon tissue and increase the mucus content. Moreover, OP pretreatment can significantly reduce the colon MDA level. OP has also been found to suppress inflammation, which is estimated by preventing vascular permeability. In addition, the adhesion of peritoneal neutrophils and macrophages was mitigated after OP administration. Overall, OP has a therapeutic effect on acetic acid–induced colitis in mice. The protective effect of OP may be related to the inhibition of neutrophil infiltration and antioxidant.

Ipomoea batatas

I. batatas, a plant belongs to the Convolvulaceae family, is generally called purple sweet potato for purple flesh and treated as a nutritionally rich food (Mohanraj and Sivasankar, 2014). Sun et al. (2020) abstracted a novel alkali-soluble polysaccharide ASPP (**Figure 3C**) from *I. batatas*, and assessed the protective effects of ASPP on DSS-induced colitis in mice. The results demonstrated that ASPP improved the immune organ (spleen and thymus) indices and alleviated the colonic pathological damage. In addition, the levels of pro-inflammatory cytokines, including TNF-α, IL-1β, and IL-6 in colonic tissue and serum were significantly inhibited by ASPP treatment. ASPP could also elevate the SCFAs production, such as AA, PA, and BA in DSS-induced mice. Moreover, the 16S rRNA sequencing result suggested that ASPP regulated the compositions of gut microbiota in DSS-induced colitis mice by increasing the relative abundance of *Firmicutes* and reducing the levels of *Bacteroidetes*, *Proteobacteria*, and *Actinobacteria*. In conclusion, ASPP diminished intestinal inflammation through mitigating pro-inflammatory factors and modulating the gut microbiota structure of DSS-induced colitis mice.

Malus pumila

M. pumila belongs to the Rosaceae family, and its fruits (namely apple) have very high nutritional values for containing abundant minerals and vitamins. Meanwhile, apples contain a variety of phytochemicals with bioactivity (Boyer and Liu, 2004). Li et al. (2017) extracted a polysaccharide MAP from *M. pumila* and applied a DSS-induced mouse colitis, MCA-38 cell line, and DC2.4 cell to investigate the anti-inflammatory properties and underlying mechanisms of MAP. Results showed that MAP significantly ameliorated intestinal toxicity caused by DSS in mice, and suppressed the proliferation of MCA-38 cells. Besides, MAP treatment remarkably increased IL-22BP levels, while inhibited the expression of IL-22, p-STAT3, Bcl-2, and cyclin D1 *in vivo* and *in vitro*. In short, these data indicated that MAP was likely to exert a protective effect on colitis *via* modulating the expression and function of IL-22 and IL-22BP, which provided a theoretical basis for apples used to prevent colitis.

POLYSACCHARIDES FROM MUSHROOMS

Mushrooms are fungi that generally live on dead trees. According to statistics, there are more than 2000 kinds of edible mushrooms in the world, including about 700 kinds of mushrooms with medicinal value. Edible mushroom is one of the important sources of nutrients in people's daily life, and its factory cultivation is an emerging sunrise industry in the 21st century. Meanwhile, due to the richness of various active components, mushrooms are increasingly appreciated for their health and medicinal value (Roupas et al., 2012). There have been several polysaccharides from this source and have shown evident efficacy for IBD. **Tables 2**, **3** listed the chemical and pharmacological information of polysaccharides from mushrooms in the treatment of IBD, respectively.

Ganoderma lucidum

G. lucidum, called *Ling-Zhi* in Chinese and Reishi in Japanese, is a famous medicinal mushroom growing on dead wood. Its main components are polysaccharides and triterpenes, which have various pharmacological activities, such as immunomodulation, antitumor, and anti-oxidation (Ahmad,

2018; Lu et al., 2020). Xie et al. (2019) reported that a polysaccharide GLP (**Figure 3D**) from *G. lucidum* remarkably reduced DSS-induced DAI scores and augmented SCFAs levels (including TA, AA, PA, and BA). Moreover, GLP effectively regulated the intestinal microbiota structure by increasing the amount of prebiotics (e.g., *Ruminococcus_1*) and reducing some pathogens (e.g., *Escherichia–Shigella*). Transcriptional analysis indicated that GLP regulated the expression of genes enriched in inflammation-related KEGG pathways, such as elevating *Ccl5*, *Cd3e*, *Cd8a*, *Il21r*, *Lck,* and *Trbv*, and decreasing the levels of *Ccl3*, *Gro, Il11*, *Mhc2,* and *Ptgs2*, resulting in improvement of immunity and reduction of inflammation and colonic carcinoma risk. Therefore, these results demonstrated that GLP ameliorated DSS-induced colitis and may have potential application prospects in the remission of IBD.

Hericium erinaceus

H. erinaceus, a kind of edible and medicinal mushroom, is commonly used to prevent and treat gastrointestinal disorders (Friedman, 2015). Ren et al. (2018) isolated a polysaccharide HECP from *H. erinaceus*, and found that HECP obviously improved DSS-induced clinical symptoms and pathological damage. HECP ameliorated oxidative damage through inhibiting the levels of NO, MDA, and MPO, and increasing the T-SOD activity. HECP could also suppress the development of inflammation *via* inhibiting COX-2, iNOS, and phosphorylation of NF-κB (p65 and IκBα), MAPK (p38, ERK, and JNK), and PI3K/AKT (AKT) signaling pathways in colon tissues of DSS-induced colitis mice. As a consequence, the mRNA expression and levels of pro-inflammatory cytokines, including TNF-α, IL-6, and IL-1β, were dramatically suppressed after HECP treatment. Moreover, HECP could regulate gut microbiota dysbiosis, manifested as the reduction of *Verrucomicrobia* and *Actinobacteria*, elevation of *Bacteroidetes*, and subsequently the decrease of some bacterial species, including *Arthrobacter* spp., *Methylibium* sp., *Succinivibrio* sp., and *Akkermansia muciniphila* and the enhancement of *Desulfovibrio* sp. in fecal sample, resulting in microbiota composition close to that of normal mice and prevent intestinal barrier damage caused by DSS. Taken together, HECP exhibited an important protective effect on DSS-induced colitis in mice, at least partly through the modulation of oxidative stress, inflammation-related cytokines and signaling pathways, and gut microbiota dysbiosis, indicating HECP can serve as a potential dietary nutrient against IBD in the future.

Another purified polysaccharide EP-1 (**Figure 3F**) was extracted from *H. erinaceus*, and research showed that EP-1 observably relieved the clinical symptoms and colonic mucosa damage in acetic acid–induced colitis rats. EP-1 effectively regulated the gut microbial structure, increased the levels of SCFAs (including AA, PA, BA, VA, IBA, and IVA), GPR41, and GPR43. EP-1 treatment could also upregulate SOD activity, downregulate MDA and ROS production, and thus inhibit oxidative damage both in acetic acid–induced colitis mice and in H_2O_2-induced Caco-2 cells. Consequently, the mitochondria integrity and function were remarkably improved, indicated by the elevated levels of MMP, OCR, and ATP. Furthermore, EP-1 was found to exhibit an appreciable anti-inflammatory effect, which was closely associated with the blockade of NF-κB pathways by decreasing the expression of NF-κB p-65 and p-p65 in colonic tissue and subsequently reducing the production of pro-inflammatory cytokines TNF-α, IL-1, and IL-6 in rat serum. EP-1 also exerted an immunoregulation effect through increasing the IgM content and decreasing the C3 level. Additionally, EP-1 treatment inhibited intestinal epithelial cells apoptosis by increased Bcl-2 and decreasing caspase-3 activation (Shao et al., 2019; Wang D. D. et al., 2019). Overall, these results proved that EP-1 shows potential for the development of novel functional foods and drugs to treat IBD.

Poria cocos

P. cocos, an edible and pharmaceutical fungus, is widely applied in the formulation of tea supplements, cosmetics, and functional foods (Rios, 2011). Polysaccharides are the major component of *P. cocos*, which have aroused wide attention on the structural features and pharmacological activities (Jia et al., 2016). A novel polysaccharide CMP33 was abstracted from *P. cocos*. Animal experiment found that after the administration of CMP33, the elevated mortality rate, DAI scores, MPO activity, and macro- or microscopic histopathological score induced by TNBS in mice were remarkably mitigated (Liu X. F. et al., 2018). Furthermore, CMP33 significantly reduced the release of pro-inflammatory cytokines (TNF-α, IL-6, L-1β, IL-12, IFN-γ, IL-2, and IL-17), whereas triggered anti-inflammatory factors IL-4 and IL-10 in the colon tissue and serum of colitis mice. Besides, CMP33 could effectually abrogate lipid peroxidation by decreasing MDA content in TNBS-induced colitis mice. iTRAQ-based proteomics revealed that CMP33 exhibited anti-inflammation effect by decreasing seven proteins (B3gnt6, B4galnt2, Ca1, Fabp2, Hmgcs2, Hp, and Sap). Additionally, GC-TOF-MS-based metabolomics data suggested that oleic acid and DHT might be the targets of CMP33. Collectively, these results indicated that CMP33 exhibited an important protective effect on colitis in mice.

Inonotus obliquus

I. obliquus, the most promising medicinal fungus, grows on the birch trunks at low latitude in Europe and North America. Studies have shown that polysaccharides of *I. obliquus* may potentially be used for treating many diseases including tumors, diabetes, and colitis (Duru et al., 2019). *I. obliquus* polysaccharide (IOP) administration was reported to strikingly relieve DSS-induced chronic murine intestinal inflammatory symptoms (Chen et al., 2019). IOP treatment could significantly ameliorate DAI and the mucosa damage, where increase the TJs proteins ZO-1 and occludin in colon tissues. IOP could also upregulate the expression of Treg and Th2 and downregulate Th17 and Th1 in colon tissues, spleen, and mesenteric lymph nodes, resulting in reducing the mRNA levels of IFN-γ, IL-17, T-bet, and ROR-γt, and enhancing that of IL-4, IL-10, GATA-3, and Foxp3. Moreover, the elevated p-STAT1 and p-STAT3 and reduced p-STAT6 in DSS-induced mice were dramatically reversed by IOP. Taken together, these results demonstrated that IOP

regulated the balance of Th1/Th2 and Th17/Treg through modulating the JAK-STAT pathway in DSS-induced colitis mice, suggesting IOP as a potential natural effective therapeutic agent or options for IBD.

Dictyophora indusiata

D. indusiata, a saprophytic fungus of bamboo forest, has been one of the most popular edible mushrooms for its edible values and medicinal functions (Habtemariam, 2019). Wang Y. L. et al. (2019) extracted a purified polysaccharide DIP (**Figure 3E**) from *D. indusiata*, and investigated the anti-colitis effect and underlying mechanism of DIP in DSS-treated mice. Results showed that DIP could ameliorate colitis manifested as the reduction of clinical DAI scores, spleen index, and colonic histpathologic damage induced by DSS. Immunofluorescence staining illustrated that DIP significantly increased the colonic TJP1 protein expression, resulting in repairing epithelium barrier function. DIP could also relieve intestine oxidative stress by decreasing the MDA content and increasing the expression of GSH and HO-1 in the colonic tissue. Meanwhile, DIP treatment remarkably regulated inflammation responses through upregulating the anti-inflammatory cytokine IL-10 level and downregulating MPO activity and the release of pro-inflammatory cytokines TNF-α, IL-6, IL-1β, and IL-18 in DSS-induced colitis. DIP treatment was found to block the NF-κB, STAT3, and NLRP3 pathways *via* reducing the expression of NLRP3, p-IκBα, and p-STAT3, which may be responsible for the anti-inflammatory mechanism of DIP on colitis. Additionally, DIP could modulate macrophage subset through promoting DSS-induced IRF4 protein expression and inhibiting IRF5 and CD86 protein levels. Furthermore, DIP significantly inhibited DSS-induced apoptosis, which was associated with an upregulation of Bcl-2 expression and downregulation of Bax expression and TUNEL positive nuclei in colonic tissues. In conclusion, these results indicated that DIP exerted an obvious anti-colitis efficacy by reducing oxidative stress and inflammation, inhibiting key inflammatory signaling pathways, and regulating the macrophage subset. DIP could be served as a functional food or nutraceutical agent for the treatment of IBD.

Pycnoporus sanguineus

P. sanguineus is a saprophytic fungus, which is widely applied in industry and medicine all over the world. Li M. X. et al. (2020) extracted a polysaccharide PPS from *P. sanguineus* and found that PPS could alleviate the colitis induced by DSS, which is manifested by reducing DAI, colon shortening, colonic MPO activity, and serum LPS concentration. PPS could effectively restored intestinal barrier function by increasing the expression of ZO-1, E-cadherin, and PCNA. Moreover, PPS significantly descended the proportions of Th cells and its subsets (Th2, Th17, and Treg), increased Th1 level, and suppressed the secretion of several inflammation-related cytokines, including IL-10, IL-15, IL-17, and IL-12p40 while increased chemokine MCP-1β. In addition, PPS mitigated the colitis-induced autophagy *via* downregulating the LC3 II/I ratio and upregulating the expression of ULK1, LC3 II, LC3 I, p62, and Beclin-1. This study revealed that PPS could relieve Th cell-associated inflammatory response, inhibit autophagy, and restore the intestinal barrier function, which might hold an important clinical implication for the treatment of IBD.

Flammulina velutipes

F. velutipes is a well-known edible mushroom and widely consumed all over the world. Previous studies suggested that polysaccharides are the major component of *F. velutipes* and possess various bioactivities (Dong et al., 2020). Zhang et al. (2020) extracted a water-soluble polysaccharide FVP from *F. velutipes*, and found that FVP treatment could improve the DSS-induced colitis manifestations and epithelial mucous damage *in vivo*. The MPO and NO released by neutrophils in colonic inflammatory tissues were significantly inhibited by FVP. FVP also exhibited antioxidant capacity *via* decreasing the plasma DAO level, increasing intestinal SOD activity in DSS-induced colitis mice. Furthermore, FVP was found to show a favorable anti-inflammatory effect through downregulating the expression of TLR4, NF-κB, and NF-κB p-p65, resulting in suppression of the TLR4/NF-κB signaling pathway. Meanwhile, FVP could modulate the intestinal microbial dysbiosis and enhance the production of SCFAs (including AA, PA, BA, IVA, and VA). In summary, these results can promote the potential utilization of FVP as a functional food ingredient therapeutic for IBD.

Lachnum YM130

Lachnum sp. is a genus of higher fungi with extremely high bioactivity value, which grows throughout Asia, America, and Europe. Zong et al. (2020) found that *Lachnum* YM130 polysaccharide (LEP) could remarkably alleviate clinical symptoms, colonic pathological damage, and inflammatory cell infiltration in DSS-induced colitis mice. Compared to the DSS-induced model group, the levels of MPO, Ly6G, F4/80 macrophage, and $CD4^{+}IL\text{-}10^{+}$ were significantly decreased in the LEP treatment group, suggesting LEP can inhibit the infiltration of inflammatory cells. LEP treatment also improved intestinal barrier integrity through increasing the expression of TJs proteins (including ZO-1, occludin, claudin-1, E-cadherin, claudin-3, and claudin-7), enhancing antimicrobial proteins expression Reg3β and Reg3γ, and upregulating the mRNA levels of mucus layer protective proteins, such as MUC1, MUC2, TFF3, and Relmβ. Moreover, LEP treatment strikingly inhibited the expression of inflammatory cytokines, including TNF-α, IL-1β, IL-6, NO, PGE_2, iNOS, and COX-2 in colonic tissue of DSS-treated mice. Mechanistically, LEP treatment was found to block the activation of PPARγ/NF-κB and STAT3 pathways by upregulating PPARγ expression and retarding the phosphorylation of NF-κB p65, IκB, and STAT3 in DSS-induced colitis. LEP treatment also sharply downregulated the protein levels of NLRP3, ASC, caspase-1, and IL-1β in colonic tissues, thus inhibiting NLRP3 inflammasome activation. In addition, DSS-induced promotion of MDA, nitrotyrosine, and NOx levels and decrease of SOD, CAT, and T-AOC activities were significantly reversed after LEP administration. Meanwhile, the ER stress markers IRE1α and XBP1 were evidently elevated, whereas Bip, ATF6, PERK, CHOP, and C-Cas3 were descended in the LEP treatment group as compared with that

in the DSS-induced colitis group. Overall, these results demonstrated that LEP possessed pronounced anti-colitis capacity and its mechanism might be tightly associated with protecting intestinal mucosal barrier function, suppressing inflammatory response, ER stress, and oxido-nitrosative stress.

POLYSACCHARIDES FROM SEAWEEDS

Seaweed is an indispensable part of the marine ecosystem with many kinds, large quantity, and fast propagation. Moreover, it is also a rich and valuable resource for human beings, which plays an important role in functional food, food additives, marine drugs, organic fertilizer, bioenergy, and many other fields (Venkatesan et al., 2015). There are some studies on the treatment of IBD with polysaccharide from seaweeds, which have attracted extensive attention of researchers. **Tables 2**, **3** listed the chemical and pharmacological information of polysaccharides from seaweeds in the treatment of IBD, respectively.

Gracilaria birdiae

G. birdiae is a kind of red algae, which is used to produce agar in Brazil with important economic value. In the past few years, the structure and bioactivity of *G. birdiae* polysaccharide have been widely studied (Souza et al., 2012). Brito et al. (2014) isolated an agar-type polysaccharide from *G. birdiae* and found that GBP treatment significantly ameliorated intestinal macroscopic and microscopic damage caused by TNBS in rats. In addition, it could also decrease the levels of pro-inflammatory cytokines IL-1β and TNF-α and MPO activity. Additionally, PLS relieved TNBS-caused oxidative stress injury manifested as the upregulation of the GSH level and reduction of MDA and NO_3/NO_2 concentration in the colonic mucosa. Together, this data concluded that GBP has a protective effect on intestinal epithelial damage by mitigating inflammatory cell infiltration, pro-inflammatory cytokine release, and oxidative stress.

Ulva lactuca

U. lactuca is a kind of green giant algae, which participates in the destructive green tide observed all over the world. However, *U. lactuca* has been found to contain commercially valuable constituents including bioactive compounds, food or biofuel (Dominguez and Loret, 2019). Zhu et al. (2017) prepared selenium nanoparticles decorated with *U. lactuca* polysaccharide ULP with average size ~130 nm. ULP treatment exhibited a prominent protective effect on DSS-induced acute colitis in mice. ULP could suppress macrophage infiltration by decreasing the colonic CD68 level. Moreover, ULP markedly attenuated oxidative stress damage *via* increasing the colonic GSH, GPx, and Se levels and reducing the generation of MDA. In addition, ULP exerted a strong effect on mitigating the mRNA expression and levels of inflammatory markers, including IL-6, TNF-α, iNOS, and COX-2 in DSS-induced colitis mice and in LPS-stimulated BMDMs. Mechanistically, ULP pretreatment was found to suppress the inactivation of the NF-κB signaling pathway *via* retarding the phosphorylation of NF-κB p65 and IκBα *in vivo* and *in vitro*. Altogether, these data indicated that ULP supplementation might be a potential therapeutic candidate for preventing inflammatory diseases, like IBD.

Eucheuma cottonii

The edible red algae *E. cottonii* is largely cultivated due to carrageenan production. Meanwhile, it is rich in active constituents, such as polyphenols, steroids, and polysaccharides (Namvar et al., 2012). Sudirman et al. (2018) extracted crude polysaccharides ECP from *E. cottonii* and found that after treatment for 7 days, ECP could remarkably ameliorate DSS-induced colitis by alleviating weight loss and colonic mucosa injury and reducing the ratio of colon weight and length. Additionally, ECP also dramatically decreased the levels of pro-inflammatory mediators TNF-α, IL-1β, and IL-6 in serum and increased the anti-inflammatory cytokine IL-10 level in colon tissue of DSS-treated mice. This result revealed that ECP exhibited a pronouncedly effect on colitis, which might be used to a promising candidate for the treatment of IBD in the future.

Blidingia minima

B. minima is prevalent along many coastlines since these green algae originate in areas with large differences in seawater salinity and freshwater tidal areas. Song et al. (2019) extracted polysaccharides from *B. minima*, and conducted the *in vitro* and *in vivo* experiments to investigate the anti-inflammatory effect of BMP through using DSS-treated intestinal epithelial cells (IPEC-J2 cells) and C57BL/6J mice, respectively. Results illustrated that BMP exhibited a remarkably anti-inflammatory effect on DSS-stimulated cells. Additionally, BMP noticeably ameliorated colitis symptoms, and improved colonic infiltration by reducing the levels of MPO and EPO in the colonic tissue. BMP treatment restored the colonic barrier functions by upregulating the expression of TJs proteins (ZO-1, occludin, and claudin-1) and DAO activity, and downregulating the ET-1 level in DSS-treated mice. Moreover, the mRNA expression and production of pro-inflammatory cytokines TNF-α and IL-1β were mitigated, while anti-inflammatory factor IL-10 was enhanced after BMP treatment. Furthermore, the phosphorylated protein levels of NF-κB, IκBα, and AKT in colonic tissue were all decreased by BMP supplementation. These results indicated that BMP was endowed with a pronounced anti-inflammatory property, and its mechanism might be intimately associated with the inhibition of NF-κB and AKT pathways.

DISCUSSION AND CONCLUSION

With the progress of civilization, people's lifestyles and eating habits have also undergone tremendous changes. The diet structure is changing to a high-fat, low-fiber pattern, which has a negative impact on the body, decreases immunity, and makes people susceptible to diseases and pathogenic bacteria. Early IBD was prevalent in western countries. However with globalization and changes in lifestyle, the incidence of IBD is

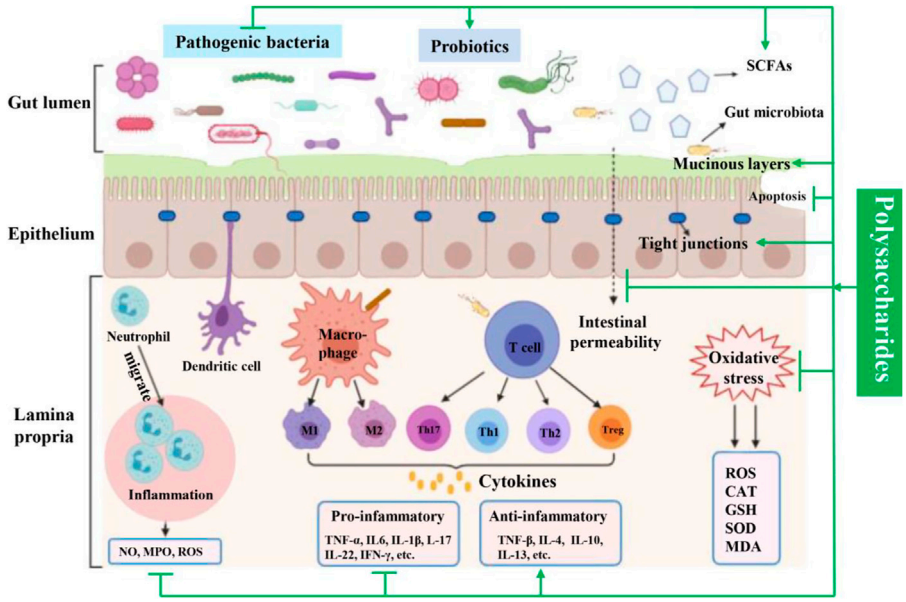

FIGURE 4 | Involved mechanisms of natural-derived polysaccharides in the treatment of IBD (promotion and inhibition).

rapidly increasing in Asian countries such as India and China (Mak et al., 2020). Current strategies for IBD therapy are mainly synthetic drugs intervention, which is accompanied by a wide range of side effects. For centuries, polysaccharides, as a natural product, are endowed with various beneficial treatment effects, such as immunomodulatory, anti-inflammatory, antioxidant, and bacteriostasis, with no or fewer toxicity, making them one of the novel therapeutic agents or optimal candidate drugs for treating IBD. In this review article, for the first time, we present the investigations conducted in this field since the beginning of this century, mainly focusing on polysaccharides from plants, edible mushrooms, and seaweeds that exert ameliorative effects against experimental IBD and related properties along with their mechanisms of action (**Figure 4**).

Intestinal epithelium, located at the junction of intestinal microbiota and lymphoid tissue, plays a key role in mucosal formation and defense against luminal antigens, endotoxins, and pro-inflammatory mediators. The barrier defects are considered as the first event during IBD pathological progression, resulting in increasing intestinal permeability, and ultimately leading to a severe inflammatory response in intestinal tissues (Luo et al., 2020). Mucinous layer, consists of mucins (mainly including MUC1 and MUC2) released by epithelial goblet cells, is the first line of defense against the invasion of pathogens. TJs proteins (including ZO-1, ZO-2, occludin, and claudin1), located between the adjacent intestinal epithelial cells, are an essential mechanical barrier, which plays a crucial role in the regulation of intestinal epithelial barrier integrity and intestinal permeability (Li C. L. et al., 2020; Zhao et al., 2020). In IBD patients, decreased expression of TJs and mucins were observed, which are currently emerged as a novelty effective target for IBD therapy. In this review, we found that the expression of TJs proteins and mucins proteins was reduced by DSS or TNBS exposure. However, this change was reversed after polysaccharides treatment, such as ASP, WJPs, LEP, and BMP.

In addition to TJs changes, increased epithelial cell apoptosis may also lead to intestinal barrier dysfunction (Dong et al., 2015). Under physiological conditions, the life span of intestinal epithelial cells is relatively short. Apoptosis caused by programmed cell death is a carefully controlled process, which is essential for maintaining normal barrier function (Yuan et al., 2015; Butkevych et al., 2020). However, excessive epithelial cell apoptosis can damage the intestinal barrier function and is related to the initiation and development of IBD (Wang W. et al., 2020). The Bcl-2 family plays a vital role in the apoptosis pathway, and Bcl-2 is an apoptosis suppressor molecule involved in protection against oxidative stress-induced apoptosis and maintenance of cell survival. Conversely, Bax is an apoptosis-promoting gene. The ratio of Bax/Bcl-2 determines cell growth or apoptosis (Jia et al., 2015). Additionally, Caspase-3 is an important downstream transducer in most types of cells. It plays an important role in the initiation of apoptosis by cleavage of cell substrates (Gansukh et al., 2019). In the current review, we found that the expression of Bax and caspase-3 was significantly downregulated, whereas the expression of Bcl-2 was upregulated by multiple polysaccharides treatment, such as ASP, MAP, EP-1, and DIP, leading to a decrease of Bax/Bcl-2 ratio. These results elucidated that these polysaccharides exerted a certain anti-apoptotic effect in DSS- or acetic acid–induced UC mice, which promote the recovery of intestinal barrier defects.

Abnormal chronic inflammation is one of the pivotal clinical symptoms of IBD (Na et al., 2019). In the presence of persistent inflammation, strong colonic inflammation was developed, accompanied with augmented levels of pro-inflammatory mediators (e.g., TNF-α, IL-1β, and IL-6) and descended production of anti-inflammatory cytokines (e.g., IL-4, IL-10, and IL-13), causing increase of intestinal permeability and impairment

of mucosal barrier function. Among them, pro-inflammatory mediators could promote the immune inflammatory response through activating Th cells, triggering neutrophil migration and inducing intracellular signal transduction. Inversely, anti-inflammatory cytokines could ameliorate the development of colitis clinically (Lee et al., 2020). Therefore, regulating the balance of pro-inflammatory and anti-inflammatory cytokines is a crucial therapeutic strategy to suppress the inflammatory process. In the current review, the up-regulated release of pro-inflammatory mediators, such as TNF-α, IL-6, IFN-γ, IL-1β, and IL-18, and the down-regulated levels of anti-inflammatory factors, such as IL-4, IL-10, and IL-13, in colitis mice were dramatically inhibited by polysaccharides from edible and medicinal plants (e.g., APS, DOPS, and ASPP), edible mushrooms (e.g., HECP, EP-1, and IOP), and seaweeds (e.g., ECP, BMP, and GBP). MPO activity, a marker of the inflammatory response in damaged tissues, was also decreased. Further mechanism study manifested that their anti-inflammatory effect was mainly associated with the blockage of major inflammatory signaling pathways including NF-κB, MAPK, IL-6/JAK2/STAT3, PI3K/AKT, and NLRP3 inflammasome pathways.

In addition, oxidative stress in intestinal mucosa has been regarded as a key event during the pathological progression of IBD (Piechota-Polanczyk and Fichna, 2014). Excessive inflammatory cytokines could induce oxidative stress and nitrosative stress by irritating ROS and RNS production systems, which in turn further aggravates the immune inflammation, resulting in tissue damage and deterioration of patient's condition (Saber et al., 2019). In the development of IBD, ROS-generating processes are sharply elevated, consequently causing intestinal epithelial cell injury (Mei et al., 2020). Therefore, the anti-oxidative stress approach is one of the crucial strategies in treating IBD. In the experimental IBD model, excessive oxidative stress was observed as the increased contents of ROS, MDA, NO_3/NO_2, decreased levels of SOD, CAT, and T-AOC. However, after the treatment of polysaccharide, such as PLS, HECP, EP-1, and LEP, these changes could significantly be reversed.

Gut microbiota, approximately 100 trillion microorganisms, is a large bacterial community that colonizes in the intestine, which plays a substantial role in regulating the intestinal structure and intestinal permeability, and its dysbiosis is closely related to the IBD (Stange and Schroeder, 2019). In the case of IBD, the richness and diversity of intestinal microbiota were strikingly reduced in comparison with healthy individuals. Moreover, the abundance of pathogenic bacteria, such as *Escherichia*, *Enterococcus*, and *Prevotella* was increased while the ratio of *Firmicutes* to *Bacteroidetes* decreased dramatically (Liu W. et al., 2018). In the present review, we found that natural polysaccharides, including CP, ALP-1, ASPP, and HECP prominently increased the diversity of intestinal flora and modulated the gut microbiota community close to that of normal mice.

In addition, SCFAs, mainly including AA, PA, BA, and VA, are the major fermentation products of prebiotic metabolism in the gut lumen, which plays a crucial function in intestinal homeostasis (Sun et al., 2017). Notably, AA and BA can activate GPR41 and GPR43 and suppress histone deacetylase to exhibit the anti-inflammatory effect (Kobayashi et al., 2017). In colonic tissues of IBD patients, the contents of BA, AA and so on, were significantly decreased (Macia et al., 2015). Thus, the regulation of SCFAs production has also become a promising therapeutic target for IBD treatment. Interesting, in the present review, it showed that the decreased proportions of AA, BA, PA, and TA in colon of the disease model group were remarkably upregulated by polysaccharides treatment, including ASPP, GLP, EP-1, and FVP.

In summary, this article firstly summarizes the therapeutics effect of polysaccharides derived from plants, mushrooms, and seaweeds and shows how these polysaccharides exhibited prominently and beneficial effects in attenuate colonic inflammation. Multiple factors are involved in their protective effects on IBD, including the alleviation of the intestinal barrier destruction *via* increasing TJs proteins and mucus layer protective proteins and reducing epithelial cell apoptosis, modulation of gut microbiota, reduction of excessive oxidative stress, and inhibition of aberrant inflammatory response, inflammatory cells infiltration, and MPO activity through blocking NF-κB, MAPK, IL-6/JAK2/STAT3, PI3K/AKT, and NLRP3 inflammasome signaling pathways. In conclusion, these findings provided a solid scientific basis for utilization of natural polysaccharides from plants, mushrooms, and seaweeds as promising candidates for IBD therapy. Further clinical and preclinical studies to reveal the molecular mechanisms are needed to promote the clinical translation of natural polysaccharides for IBD.

AUTHOR CONTRIBUTIONS

All authors have contributed to the writing, design, and preparation of figures. The senior authors CL and QL have carried out coordination of efforts.

FUNDING

This study was financially supported by the National Natural Science Foundation of China (No. 82003771) and Science and Technology Foundation of Guizhou Province (No. QKHPTRC(2018)5772-021 & QKHJC-ZK(2021)YB525).

REFERENCES

Ahmad, M. F. (2018). *Ganoderma lucidum*: persuasive biologically active constituents and their health endorsement. *Biomed. Pharmacother.* 107, 507–519. doi:10.1016/j.biopha.2018.08.036

Almeida, É. S., Oliveira, D., and Hotza, D. (2019). Properties and applications ofMorinda citrifolia(noni): a review. *Compr. Rev. Food Sci. Food Saf.* 18 (4), 883–909. doi:10.1111/1541-4337.12456

Ananthakrishnan, A. N., Kaplan, G. G., and Ng, S. C. (2019). Changing global epidemiology of inflammatory bowel diseases: sustaining health care delivery into the 21st century. *Clin. Gastroenterol. Hepatol.* 18 (6), 1252–1260. doi:10.1016/j.cgh.2020.01.028

Atanasov, A. G., Waltenberger, B., Pferschy-Wenzig, E. M., Linder, T., Wawrosch, C., Uhrin, P., et al. (2015). Discovery and resupply of pharmacologically active plant-derived natural products: a review. *Biotechnol. Adv.* 33 (8), 1582–1614. doi:10.1016/j.biotechadv.2015.08.001

Batista, J. A., Magalhães, D. d. A., Sousa, S. G., Ferreira, J. d. S., Pereira, C. M. C., Lima, J. V. d. N., et al. (2020). Polysaccharides derived from *Morinda citrifolia*

Linn reduce inflammatory markers during experimental colitis. *J. Ethnopharmacology* 248, 112303. doi:10.1016/j.jep.2019.112303

Boyer, J., and Liu, R. H. (2004). Apple phytochemicals and their health benefits. *Nutr. J.* 3, 1–15. doi:10.1186/1475-2891-3-5

Brito, T. V., Neto, J. P. R. P., Prudêncio, R. S., Batista, J. A., Júnior, J. S. C., Silva, R. O., et al. (2014). Sulfated-polysaccharide fraction extracted from red algae *Gracilaria birdiae* ameliorates trinitrobenzenesulfonic acid-induced colitis in rats. *J. Pharm. Pharmacol.* 66 (8), 1161–1170. doi:10.1111/jphp.12231

Butkevych, E., de Sa, F. D. L., Nattramilarasu, P. K., and Bucker, R. (2020). Contribution of epithelial apoptosis and subepithelial immune responses in campylobacter jejuni-induced barrier disruption. *Front. Microbiol.* 11, 344. doi:10.3389/fmicb.2020.00344

Caprilli, R., Cesarini, M., Angelucci, E., and Frieri, G. (2009). The long journey of salicylates in ulcerative colitis: the past and the future. *J. Crohn's Colitis* 3 (3), 149–156. doi:10.1016/j.crohns.2009.05.001

Chen, Y. F., Zheng, J. J., Qu, C., Xiao, Y., Li, F. F., Jin, Q. X., et al. (2019). Inonotus obliquus polysaccharide ameliorates dextran sulphate sodium induced colitis involving modulation of Th1/Th2 and Th17/Treg balance. *Artif. Cell Nanomedicine, Biotechnol.* 47 (1), 757–766. doi:10.1080/21691401.2019.1577877

Cheng, F., Zhang, Y., Li, Q., Zeng, F., and Wang, K. P. (2020). Inhibition of dextran sodium sulfate-induced experimental colitis in mice by *Angelica sinensis* polysaccharide. *J. Med. Food* 23 (6), 584–592. doi:10.1089/jmf.2019.4607

Cho, C. W., Ahn, S., Lim, T. G., Hong, H. D., Rhee, Y. K., Yang, D. C., et al. (2017). *Cynanchum wilfordii* polysaccharides suppress dextran sulfate sodium-induced acute colitis in mice and the production of inflammatory mediators from macrophages. *Mediat. Inflamm.* 2017, 3859856. doi:10.1155/2017/3859856

Cui, L., Wang, W., Luo, Y., Ning, Q., Xia, Z., Chen, J., et al. (2019). Polysaccharide from Scutellaria baicalensis Georgi ameliorates colitis via suppressing NF-κB signaling and NLRP3 inflammasome activation. *Int. J. Biol. Macromolecules* 132, 393–405. doi:10.1016/j.ijbiomac.2019.03.230

Danese, S., Fiorino, G., Peyrin-Biroulet, L., Lucenteforte, E., Virgili, G., Moja, L., et al. (2014). Biological agents for moderately to severely active ulcerative colitis. *Ann. Intern. Med.* 160 (10), 704–711. doi:10.7326/m13-2403

Dominguez, H., and Loret, E. P. (2019). *Ulva lactuca*, a source of troubles and potential riches. *Mar. Drugs* 17 (6), 357. doi:10.3390/md17060357

Dong, J. N., Wang, H. G., Zhao, J., Sun, J., Zhang, T. H., Zuo, L. G., et al. (2015). SEW2871 protects from experimental colitis through reduced epithelial cell apoptosis and improved barrier function in interleukin-10 gene-deficient mice. *Immunol. Res.* 61 (3), 303–311. doi:10.1007/s12026-015-8625-5

Dong, Y. T., Pei, F., Su, A. X., Sanidad, K. Z., Ma, G. X., Zhao, L. Y., et al. (2020). Multiple fingerprint and fingerprint-activity relationship for quality assessment of polysaccharides from *Flammulina velutipes*. *Food Chem. Toxicol.* 135, 110944. doi:10.1016/j.fct.2019.110944

Duru, K. C., Kovaleva, E. G., Danilova, I. G., and Bijl, P. (2019). The pharmacological potential and possible molecular mechanisms of action ofInonotus obliquusfrom preclinical studies. *Phytotherapy Res.* 33 (8), 1966–1980. doi:10.1002/ptr.6384

Eberhardson, M., Hedin, C. R. H., Carlson, M., Tarnawski, L., Levine, Y. A., and Olofsson, P. S. (2019). Towards improved control of inflammatory bowel disease. *Scand. J. Immunol.* 89 (3), e12745. doi:10.1111/sji.12745

Falasco, G., Zinicola, R., and Forbes, A. (2002). Immunosuppressants in distal ulcerative colitis. *Alimentpharm. Ther.* 16 (2), 181–187. doi:10.1046/j.1365-2036.2002.01170.x

Ferreira, S. S., Passos, C. P., Madureira, P., Vilanova, M., and Coimbra, M. A. (2015). Structure-function relationships of immunostimulatory polysaccharides: a review. *Carbohydr. Polym.* 132, 378–396. doi:10.1016/j.carbpol.2015.05.079

Freeman, H. J. (2012). Colitis associated with biological agents. *Wjg* 18 (16), 1871–1874. doi:10.3748/wjg.v18.i16.1871

Friedman, M. (2015). Chemistry, nutrition, and health-promoting properties ofHericium erinaceus(Lion's Mane) Mushroom Fruiting Bodies and Mycelia and Their Bioactive Compounds. *J. Agric. Food Chem.* 63 (32), 7108–7123. doi:10.1021/acs.jafc.5b02914

Fu, J., Wang, Z. H., Huang, L. F., Zheng, S. H., Wang, D. M., Chen, S. L., et al. (2014). Review of the Botanical Characteristics, Phytochemistry, and Pharmacology ofAstragalus membranaceus(Huangqi). *Phytother. Res.* 28 (9), 1275–1283. doi:10.1002/ptr.5188

Gansukh, E., Mya, K. K., Jung, M., Keum, Y. S., Kim, D. H., and Saini, R. K. (2019). Lutein derived from marigold (*Tagetes erecta*) petals triggers ROS generation and activates Bax and caspase-3 mediated apoptosis of human cervical carcinoma (HeLa) cells. *Food Chem. Toxicol.* 127, 11–18. doi:10.1016/j.fct.2019.02.037

Gao, Q. H., Wu, C. S., and Wang, M. (2013). The jujube (*Ziziphus jujuba* Mill.) fruit: A review of current knowledge of fruit composition and health benefits. *J. Agric. Food Chem.* 61 (14), 3351–3363. doi:10.1021/jf4007032

Gao, Q., Yang, M. B., and Zuo, Z. (2018). Overview of the anti-inflammatory effects, pharmacokinetic properties and clinical efficacies of arctigenin and arctiin from *Arctium lappa* L. *Acta Pharmacol. Sin.* 39 (5), 787–801. doi:10.1038/aps.2018.32

Gasparetto, J. C., Martins, C. A. F., Hayashi, S. S., Otuky, M. F., and Pontarolo, R. (2012). Ethnobotanical and scientific aspects of *Malva sylvestris* L.: a millennial herbal medicine. *J. Pharm. Pharmacol.* 64 (2), 172–189. doi:10.1111/j.2042-7158.2011.01383.x

Guan, Q. A. (2019). Comprehensive review and update on the pathogenesis of inflammatory bowel disease. *J. Immunol. Res.* 2019, 7247238. doi:10.1155/2019/7247238

Habtemariam, S. (2019). The Chemistry, Pharmacology and therapeutic potential of the edible mushroom *Dictyophora indusiata* (*Vent ex. Pers.*) Fischer (Synn. *Phallus indusiatus*). *Biomedicines* 7 (4), 98. doi:10.3390/biomedicines7040098

Hamedi, A., Rezaei, H., Azarpira, N., Jafarpour, M., and Ahmadi, F. (2016). Effects of *Malva sylvestris* and its isolated polysaccharide on experimental ulcerative colitis in rats. *J. Evid. Based Complement. Altern Med* 21 (1), 14–22. doi:10.1177/2156587215589184

Hong, B., Gao, J., Wu, J., and Zhao, C. J. (2012). Chemical constituents from *Rauvolfia verticillata* and bioactivities research. *Chem. Nat. Compd.* 48 (2), 276–280. doi:10.1007/s10600-012-0220-6

Iranshahy, M., Javadi, B., Iranshahi, M., Jahanbakhsh, S. P., Mahyari, S., Hassani, F. V., et al. (2017). A review of traditional uses, phytochemistry and pharmacology of *Portulaca oleracea* L. *J. Ethnopharmacology* 205, 158–172. doi:10.1016/j.jep.2017.05.004

Jia, G., Wang, Q., Wang, R., Deng, D. N., Xue, L., Shao, N. Y., et al. (2015). Tubeimoside-1 induces glioma apoptosis through regulation of Bax/Bcl-2 and the ROS/Cytochrome C/Caspase-3 pathway. *Onco Targets Ther.* 8, 303–311. doi:10.2147/OTT.S76063

Jia, X. J., Ma, L. S., Li, P., Chen, M. W., and He, C. W. (2016). Prospects of *Poria cocos* polysaccharides: Isolation process, structural features and bioactivities. *Trends Food Sci. Tech.* 54, 52–62. doi:10.1016/j.tifs.2016.05.021

Jiang, Y., Choi, H. G., Li, Y., Park, Y. M., Lee, J. H., Kim, D. H., et al. (2011). Chemical constituents of *Cynanchum wilfordii* and the chemotaxonomy of two species of the family Asclepiadacease, *C. wilfordii* and *C. auriculatum*. *Arch. Pharm. Res.* 34 (12), 2021–2027. doi:10.1007/s12272-011-1203-z

Jin, M. L., Zhao, K., Huang, Q. S., and Shang, P. (2014). Structural features and biological activities of the polysaccharides from *Astragalus membranaceus*. *Int. J. Biol. Macromolecules* 64, 257–266. doi:10.1016/j.ijbiomac.2013.12.002

Jin, M. L., Zhao, K., Huang, Q. S., Xu, C. L., and Shang, P. (2012). Isolation, structure and bioactivities of the polysaccharides from *Angelica sinensis* (Oliv.) Diels: A review. *Carbohydr. Polym.* 89 (3), 713–722. doi:10.1016/j.carbpol.2012.04.049

Jurikova, T., Skrovankova, S., Mlcek, J., Balla, S., and Snopek, L. (2019). Bioactive compounds, antioxidant activity, and biological effects of european cranberry (*Vaccinium oxycoccos*). *Molecules* 24 (1), 24. doi:10.3390/molecules24010024

Kaplan, G. G., and Ng, S. C. (2016). Globalisation of inflammatory bowel disease: perspectives from the evolution of inflammatory bowel disease in the UK and China. *Lancet Gastroenterol. Hepatol.* 1 (4), 307–316. doi:10.1016/s2468-1253(16)30077-2

Kaplan, G. G., and Ng, S. C. (2017). Understanding and preventing the global increase of inflammatory bowel disease. *Gastroenterology* 152 (2), 313–321. doi:10.1053/j.gastro.2016.10.020

Kaplan, G. G. (2015). The global burden of IBD: from 2015 to 2025. *Nat. Rev. Gastroenterol. Hepatol.* 12 (12), 720–727. doi:10.1038/nrgastro.2015.150

Khan, T., Date, A., Chawda, H., and Patel, K. (2019). Polysaccharides as potential anticancer agents-A review of their progress. *Carbohydr. Polym.* 210, 412–428. doi:10.1016/j.carbpol.2019.01.064

Kobayashi, M., Mikami, D., Kimura, H., Kamiyama, K., Morikawa, Y., Yokoi, S., et al. (2017). Short-chain fatty acids, GPR41 and GPR43 ligands, inhibit TNF-

α-induced MCP-1 expression by modulating p38 and JNK signaling pathways in human renal cortical epithelial cells. *Biochem. Biophysical Res. Commun.* 486 (2), 499–505. doi:10.1016/j.bbrc.2017.03.071

Kotze, P. G., Underwood, F. E., Damião, A. O. M. C., Ferraz, J. G. P., Saad-Hossne, R., Toro, M., et al. (2020). Progression of inflammatory bowel diseases throughout Latin America and the Caribbean: a systematic review. *Clin. Gastroenterol. Hepatol.* 18 (2), 304–312. doi:10.1016/j.cgh.2019.06.030

Lee, Y., Sugihara, K., Gillilland, M. G., Jon, S., Kamada, N., and Moon, J. J. (2020). Hyaluronic acid-bilirubin nanomedicine for targeted modulation of dysregulated intestinal barrier, microbiome and immune responses in colitis. *Nat. Mater.* 19 (1), 118–126. doi:10.1038/s41563-019-0462-9

Li, C. L., Ai, G. X., Wang, Y. F., Lu, Q., Luo, C., Tan, L. H., et al. (2020). Oxyberberine, a novel gut microbiota-mediated metabolite of berberine, possesses superior anti-colitis effect: Impact on intestinal epithelial barrier, gut microbiota profile and TLR4-MyD88-NF-κB pathway. *Pharmacol. Res.* 152, 104603. doi:10.1016/j.phrs.2019.104603

Li, M. X., Luo, T., Huang, Y., Su, J. Y., Li, D., Chen, X. H., et al. (2020). Polysaccharide from Pycnoporus sanguineus ameliorates dextran sulfate sodium-induced colitis via helper T cells repertoire modulation and autophagy suppression. *Phytotherapy Res.* 34 (10), 2649–2664. doi:10.1002/ptr.6695

Li, Y. H., Fan, L., Tang, T. L., Tang, Y., Xie, M., Zeng, X. C., et al. (2017). Modified apple polysaccharide prevents colitis through modulating IL-22 and IL-22BP expression. *Int. J. Biol. Macromolecules* 103, 1217–1223. doi:10.1016/j.ijbiomac.2017.05.172

Liang, J., Chen, S. X., Chen, J. H., Lin, J. Z., Xiong, Q. P., Yang, Y. Q., et al. (2018). Therapeutic roles of polysaccharides from Dendrobium Officinaleon colitis and its underlying mechanisms. *Carbohydr. Polym.* 185, 159–168. doi:10.1016/j.carbpol.2018.01.013

Liu, W., Zhang, Y., Qiu, B., Fan, S. J., Ding, H. F., and Liu, Z. H. (2018). Quinoa whole grain diet compromises the changes of gut microbiota and colonic colitis induced by dextran Sulfate sodium in C57BL/6 mice. *Sci. Rep.* 8 (1), 14916. doi:10.1038/s41598-018-33092-9

Liu, X. F., Yu, X. T., Xu, X. F., Zhang, X. J., and Zhang, X. W. (2018). The protective effects of *Poria cocos*-derived polysaccharide CMP33 against IBD in mice and its molecular mechanism. *Food Funct.* 9 (11), 5936–5949. doi:10.1039/c8fo01604f

Lu, J. H., He, R. J., Sun, P. L., Zhang, F. M., Linhardt, R. J., and Zhang, A. Q. (2020). Molecular mechanisms of bioactive polysaccharides from *Ganoderma lucidum* (Lingzhi), a review. *Int. J. Biol. Macromolecules* 150, 765–774. doi:10.1016/j.ijbiomac.2020.02.035

Luo, X. P., Yue, B., Yu, Z. L., Ren, Y. J., Zhang, J., Ren, J. Y., et al. (2020). Obacunone protects against ulcerative colitis in mice by modulating gut microbiota, attenuating TLR4/NF-κB signaling cascades, and improving disrupted epithelial barriers. *Front. Microbiol.* 11, 497. doi:10.3389/fmicb.2020.00497

Lv, J., Zhang, Y. H., Tian, Z. Q., Liu, F., Shi, Y., Liu, Y., et al. (2017). *Astragalus* polysaccharides protect against dextran sulfate sodium-induced colitis by inhibiting NF-κB activation. *Int. J. Biol. Macromolecules* 98, 723–729. doi:10.1016/j.ijbiomac.2017.02.024

Ma, J. S., Liu, H., Han, C. R., Zeng, S. J., Xu, X. J., Lu, D. J., et al. (2020). Extraction, characterization and antioxidant activity of polysaccharide from *Pouteria campechiana* seed. *Carbohydr. Polym.* 229, 115409. doi:10.1016/j.carbpol.2019.115409

Macia, L., Tan, J., Vieira, A. T., Leach, K., Stanley, D., Luong, S., et al. (2015). Metabolite-sensing receptors GPR43 and GPR109A facilitate dietary fibre-induced gut homeostasis through regulation of the inflammasome. *Nat. Commun.* 6, 6734. doi:10.1038/ncomms7734

Mak, W. Y., Zhao, M., Ng, S. C., and Burisch, J. (2020). The epidemiology of inflammatory bowel disease: East meets west. *J. Gastroenterol. Hepatol.* 35 (3), 380–389. doi:10.1111/jgh.14872

Mao, E. J., Hazlewood, G. S., Kaplan, G. G., Peyrin-Biroulet, L., and Ananthakrishnan, A. N. (2017). Systematic review with meta-analysis: Comparative efficacy of immunosuppressants and biologics for reducing hospitalisation and surgery in Crohn's disease and ulcerative colitis. *Aliment. Pharmacol. Ther.* 45 (1), 3–13. doi:10.1111/apt.13847

Mei, Y., Wang, Z. H., Zhang, Y. F., Wan, T., Xue, J. C., He, W., et al. (2020). FA-97, a new synthetic caffeic acid phenethyl ester derivative, ameliorates DSS-induced colitis against oxidative stress by activating Nrf2/HO-1 pathway. *Front. Immunol.* 10, 2969. doi:10.3389/fimmu.2019.02969

Miao, X. P., Sun, X. N., Li, Q. S., Cui, L. J., Wang, X. Y., Zhuang, G. F., et al. (2019). Pectic polysaccharides extracted from Rauvolfia verticillata (Lour.) Baill. var. hainanensis Tsiang ameliorate ulcerative colitis via regulating the MAPK s and NF -κB pathways in dendritic cells. *Clin. Exp. Pharmacol. Physiol.* 46 (1), 48–55. doi:10.1111/1440-1681.13026

Mohanraj, R., and Sivasankar, S. (2014). Sweet Potato (*Ipomoea* batatas[L.] Lam) - A Valuable Medicinal Food: A Review. *J. Med. Food* 17 (7), 733–741. doi:10.1089/jmf.2013.2818

Moreau, J., and Mas, E. (2015). Drug resistance in inflammatory bowel diseases. *Curr. Opin. Pharmacol.* 25, 56–61. doi:10.1016/j.coph.2015.11.003

Na, Y. R., Stakenborg, M., Seok, S. H., and Matteoli, G. (2019). Macrophages in intestinal inflammation and resolution: a potential therapeutic target in IBD. *Nat. Rev. Gastroenterol. Hepatol.* 16 (9), 531–543. doi:10.1038/s41575-019-0172-4

Namvar, F., Mohamed, S., Fard, S. G., Behravan, J., Mustapha, N. M., Alitheen, N. B. M., et al. (2012). Polyphenol-rich seaweed (*Eucheuma cottonii*) extract suppresses breast tumour via hormone modulation and apoptosis induction. *Food Chem.* 130 (2), 376–382. doi:10.1016/j.foodchem.2011.07.054

Ng, S. C., Shi, H. Y., Hamidi, N., Underwood, F. E., Tang, W., Benchimol, E. I., et al. (2017). Worldwide incidence and prevalence of inflammatory bowel disease in the 21st century: a systematic review of population-based studies. *The Lancet* 390 (10114), 2769–2778. doi:10.1016/s0140-6736(17)32448-0

Piechota-Polanczyk, A., and Fichna, J. (2014). Review article: the role of oxidative stress in pathogenesis and treatment of inflammatory bowel diseases. *Naunyn-schmiedeberg's Arch. Pharmacol.* 387 (7), 605–620. doi:10.1007/s00210-014-0985-1

Popov, S. V., Markov, P. A., Nikitina, I. R., Petrishey, S., Smirnov, V., and Ovodov, Y. S. (2006). Preventive effect of a pectic polysaccharide of the common cranberryVaccinium oxycoccosL. on acetic acid-induced colitis in mice. *Wjg* 12 (41), 6646–6651. doi:10.3748/wjg.v12.i41.6646

Ren, K., Yuan, H. J., Zhang, Y. J., Wei, X., and Wang, D. (2015). Macromolecular glucocorticoid prodrug improves the treatment of dextran sulfate sodium-induced mice ulcerative colitis. *Clin. Immunol.* 160 (1), 71–81. doi:10.1016/j.clim.2015.03.027

Ren, Y. L., Geng, Y., Du, Y., Li, W., Lu, Z. M., Xu, H. Y., et al. (2018). Polysaccharide of *Hericium erinaceus* attenuates colitis in C57BL/6 mice via regulation of oxidative stress, inflammation-related signaling pathways and modulating the composition of the gut microbiota. *J. Nutr. Biochem.* 57, 67–76. doi:10.1016/j.jnutbio.2018.03.005

Ribaldone, D. G., Pellicano, R., and Actis, G. C. (2019). The gut and the inflammatory bowel diseases inside-out: Extra-intestinal manifestations. *Minerva Gastroenterol. Dietol.* 65 (4), 309–318. doi:10.23736/S1121-421X.19.02577-7

Ríos, J. L. (2011). Chemical Constituents and Pharmacological Properties ofPoria cocos. *Planta Med.* 77 (7), 681–691. doi:10.1055/s-0030-1270823

Rosenberg, L. N., and Peppercorn, M. A. (2010). Efficacy and safety of drugs for ulcerative colitis. *Expert Opin. Drug Saf.* 9 (4), 573–592. doi:10.1517/14740331003639412

Roupas, P., Keogh, J., Noakes, M., Margetts, C., and Taylor, P. (2012). The role of edible mushrooms in health: Evaluation of the evidence. *J. Funct. Foods* 4 (4), 687–709. doi:10.1016/j.jff.2012.05.003

Saber, S., Khalil, R. M., Abdo, W. S., Nassif, D., and El-Ahwany, E. (2019). Olmesartan ameliorates chemically-induced ulcerative colitis in rats via modulating NFκB and Nrf-2/HO-1 signaling crosstalk. *Toxicol. Appl. Pharmacol.* 364, 120–132. doi:10.1016/j.taap.2018.12.020

Sairenji, T., Collins, K. L., and Evans, D. V. (2017). An update on inflammatory bowel disease. *Prim. Care Clin. Off. Pract.* 44 (4), 673–692. doi:10.1016/j.pop.2017.07.010

Shao, S., Wang, D. D., Zheng, W., Li, X. Y., Zhang, H., Zhao, D. Q., et al. (2019). A unique polysaccharide from *Hericium erinaceus* mycelium ameliorates acetic acid-induced ulcerative colitis rats by modulating the composition of the gut microbiota, short chain fatty acids levels and GPR41/43 respectors. *Int. Immunopharmacology* 71, 411–422. doi:10.1016/j.intimp.2019.02.038

Song, W., Li, Y., Zhang, X. L., and Wang, Z. L. (2019). Potent anti-inflammatory activity of polysaccharides extracted from *Blidingia minima* and their effect in a mouse model of inflammatory bowel disease. *J. Funct. Foods* 61, 103494. doi:10.1016/j.jff.2019.103494

Souza, B. W. S., Cerqueira, M. A., Bourbon, A. I., Pinheiro, A. C., Martins, J. T., Teixeira, J. A., et al. (2012). Chemical characterization and antioxidant activity of sulfated polysaccharide from the red seaweed *Gracilaria birdiae*. *Food Hydrocolloids* 27 (2), 287–292. doi:10.1016/j.foodhyd.2011.10.005

Stange, E. F., and Schroeder, B. O. (2019). Microbiota and mucosal defense in IBD: an update. *Expert Rev. Gastroenterol. Hepatol.* 13 (10), 963–976. doi:10.1080/17474124.2019.1671822

Sudirman, S., Hsu, Y. H., He, J. L., and Kong, Z. L. (2018). Dietary polysaccharide-rich extract from *Eucheuma cottonii* modulates the inflammatory response and suppresses colonic injury on dextran sulfate sodium-induced colitis in mice. *PLoS One* 13 (10), e0205252. doi:10.1371/journal.pone.0205252

Sun, J., Chen, H., Kan, J., Gou, Y. R., Liu, J., Zhang, X., et al. (2020). Anti-inflammatory properties and gut microbiota modulation of an alkali-soluble polysaccharide from purple sweet potato in DSS-induced colitis mice. *Int. J. Biol. Macromolecules* 153, 708–722. doi:10.1016/j.ijbiomac.2020.03.053

Sun, M. M., Wu, W., Liu, Z. J., and Cong, Y. Z. (2017). Microbiota metabolite short chain fatty acids, GPCR, and inflammatory bowel diseases. *J. Gastroenterol.* 52 (1), 1–8. doi:10.1007/s00535-016-1242-9

Tabarsa, M., You, S., Yelithao, K., Palanisamy, S., Prabhu, N. M., and Nan, M. (2020). Isolation, structural elucidation and immuno-stimulatory properties of polysaccharides from Cuminum cyminum. *Carbohydr. Polym.* 230, 115636. doi:10.1016/j.carbpol.2019.115636

Tang, H. X., Zhao, T. W., Sheng, Y. J., Zheng, T., Fu, L. Z., and Zhang, Y. S. (2017). *Dendrobium officinale* Kimura et Migo: A review on its ethnopharmacology, phytochemistry, pharmacology, and industrialization. *Evid. Based Compl. Altern. Med.* 2017, 7436259. doi:10.1155/2017/7436259

Tao, J. H., Duan, J. A., Jiang, S., Feng, N. N., Qiu, W. Q., and Ling, Y. (2017). Polysaccharides from *Chrysanthemum morifolium* Ramat ameliorate colitis rats by modulating the intestinal microbiota community. *Oncotarget* 8 (46), 80790–80803. doi:10.18632/oncotarget.20477

Tao, J. H., Duan, J. A., Jiang, S., Guo, J. M., Qian, Y. Y., and Qian, D. W. (2016). Simultaneous determination of six short-chain fatty acids in colonic contents of colitis mice after oral administration of polysaccharides from *Chrysanthemum morifolium* Ramat by gas chromatography with flame ionization detector. *J. Chromatogr. B* 1029-1030, 88–94. doi:10.1016/j.jchromb.2016.07.002

Tao, J. H., Duan, J. A., Zhang, W., Jiang, S., Guo, J. M., and Wei, D. D. (2018). Polysaccharides from *Chrysanthemum morifolium* Ramat ameliorate colitis rats via regulation of the metabolic profiling and NFκB/TLR4 and IL-6/JAK2/STAT3 signaling pathways. *Front. Pharmacol.* 9, 746. doi:10.3389/fphar.2018.00746

Vavricka, S. R., Schoepfer, A., Scharl, M., Lakatos, P. L., Navarini, A., and Rogler, G. (2015). Extraintestinal manifestations of inflammatory bowel disease. *Inflamm. Bowel Dis.* 21 (8), 1982–1992. doi:10.1097/mib.0000000000000392

Venkatesan, J., Lowe, B., Anil, S., Manivasagan, P., Kheraif, A. A. A., Kang, K. H., et al. (2015). Seaweed polysaccharides and their potential biomedical applications. *Starch - Stärke* 67 (5), 381–390. doi:10.1002/star.201400127

Wang, D. D., Zhang, Y. Q., Yang, S., Zhao, D. Q., and Wang, M. X. (2019). A polysaccharide from cultured mycelium of *Hericium erinaceus* relieves ulcerative colitis by counteracting oxidative stress and improving mitochondrial function. *Int. J. Biol. Macromolecules* 125, 572–579. doi:10.1016/j.ijbiomac.2018.12.092

Wang, W., Zhang, F. R., Li, X. Y., Luo, J., Sun, Y., Wu, J., et al. (2020). Heat shock transcription factor 2 inhibits intestinal epithelial cell apoptosis through the mitochondrial pathway in ulcerative colitis. *Biochem. Biophysical Res. Commun.* 527 (1), 173–179. doi:10.1016/j.bbrc.2020.04.103

Wang, Y. L., Ji, X. M., Yan, M. L., Chen, X., Kang, M. Z., Teng, L. P., et al. (2019). Protective effect and mechanism of polysaccharide from *Dictyophora indusiata* on dextran sodium sulfate-induced colitis in C57BL/6 mice. *Int. J. Biol. Macromolecules* 140, 973–984. doi:10.1016/j.ijbiomac.2019.08.198

Wang, Y., Zhang, N. F., Kan, J., Zhang, X., Wu, X. N., Sun, R., et al. (2019). Structural characterization of water-soluble polysaccharide from *Arctium lappa* and its effects on colitis mice. *Carbohydr. Polym.* 213, 89–99. doi:10.1016/j.carbpol.2019.02.090

Wang, Z., Liang, Y. N., Zhang, D. B., Wu, X., Yu, J. G., Zhang, Z., et al. (2020). Protective effects of polysaccharide extracted from *Portulacae oleracea* L. on colitis induced by dextran sulfate sodium. *J. Med. Food* 23 (2), 125–131. doi:10.1089/jmf.2019.4414

Wang, Z., Wang, L., Wu, X., Pan, Y. L., Xie, P., Pei, G., et al. (2018). Polysaccharide extracted from *Portulacae oleracea* L. exerts protective effects against dextran sulfate sodium-induced colitis through inhibition of NF-kappa B. *Am. J. Transl. Res.* 10 (8), 2502–2510. doi:10.3390/nu10060791

Wei, W. L., Zeng, R., Gu, C. M., Qu, Y., and Huang, L. F. (2016). Angelica sinensis in China-A review of botanical profile, ethnopharmacology, phytochemistry and chemical analysis. *J. Ethnopharmacology* 190, 116–141. doi:10.1016/j.jep.2016.05.023

Xie, J. L., Liu, Y. X., Chen, B. H., Zhang, G. W., Ou, S. Y., Luo, J. M., et al. (2019). *Gonoderma lucidum* polysaccharide improves rat DSS-induced colitis by altering cecal microbiota and gene expression of colonic epithelial cells. *Food Nutr. Res.* 63, 1559. doi:10.29219/fnr.v63.1559

Yu, Y., Shen, M. Y., Song, Q. Q., and Xie, J. H. (2018). Biological activities and pharmaceutical applications of polysaccharide from natural resources: A review. *Carbohydr. Polym.* 183, 91–101. doi:10.1016/j.carbpol.2017.12.009

Yuan, B. S., Zhou, S. P., Lu, Y. K., Liu, J., Jin, X. X., Wan, H. J., et al. (2015). Changes in the expression and distribution of claudins, increased epithelial apoptosis, and a mannan-binding lectin-associated immune response lead to barrier dysfunction in dextran sodium sulfate-induced rat colitis. *Gut Liver* 9 (6), 734–740. doi:10.5009/gnl14155

Yue, Y., Wu, S. C., Li, Z. K., Li, J., Li, X. F., Xiang, J., et al. (2015). Wild jujube polysaccharides protect against experimental inflammatory bowel disease by enabling enhanced intestinal barrier function. *Food Funct.* 6 (8), 2568–2577. doi:10.1039/c5fo00378d

Zhang, R. J., Yuan, S. J., Ye, J. F., Wang, X. D., Zhang, X. D., Shen, J., et al. (2020). Polysaccharide from *Flammuliana velutipes* improves colitis via regulation of colonic microbial dysbiosis and inflammatory responses. *Int. J. Biol. Macromolecules* 149, 1252–1261. doi:10.1016/j.ijbiomac.2020.02.044

Zhao, L., Li, M. Y., Sun, K. C., Su, S., Geng, T., and Sun, H. (2020). Hippophae rhamnoides polysaccharides protect IPEC-J2 cells from LPS-induced inflammation, apoptosis and barrier dysfunction *in vitro* via inhibiting TLR4/NF-κB signaling pathway. *Int. J. Biol. Macromolecules* 155, 1202–1215. doi:10.1016/j.ijbiomac.2019.11.088

Zhao, Q., Chen, X. Y., and Martin, C. (2016). Scutellaria baicalensis , the golden herb from the garden of Chinese medicinal plants. *Sci. Bull.* 61 (18), 1391–1398. doi:10.1007/s11434-016-1136-5

Zhu, C. H., Zhang, S. M., Song, C. W., Zhang, Y. B., Ling, Q. J., Hoffmann, P. R., et al. (2017). Selenium nanoparticles decorated with *Ulva lactuca* polysaccharide potentially attenuate colitis by inhibiting NF-κB mediated hyper inflammation. *J. Nanobiotechnol.* 15, 20. doi:10.1186/s12951-017-0252-y

Zong, S., Ye, Z. Y., Zhang, X. M., Chen, H., and Ye, M. (2020). Protective effect of *Lachnum* polysaccharide on dextran sulfate sodium-induced colitis in mice. *Food Funct.* 11 (1), 846–859. doi:10.1039/c9fo02719j

Conflict of Interest: The authors declare that the research was conducted in the absence of any commercial or financial relationships that could be construed as a potential conflict of interest.

GLOSSARY

AA Acetic acid
Akt Protein kinase B
AMPK AMP-activated protein kinase
Ara Arabinose
ASC Apoptosis-associated speck-like protein containing a CARD
ATF6 Activating transcription factor 6
ATP Adenosine triphosphate
BA Butyrate acid
Bax Bcl2-associated X protein
Bcl-2 B-cell lymphoma-2
BDP Beclomethasone dipropionate
Bip Binding immunoglobulin protein
BMDMs Bone marrow-derived macrophages
B3gnt6 Beta-1,3-N-Acetylglucosaminyltransferase 6
B4galnt2 Beta-1,4-N- acetylgalactosaminyltransferase 2
CAT Catalase
CA1 Carbonic anhydrase I
C-Cas3 Cleaved-caspase-3
Ccl3 C-C motif chemokine 3
Ccl5 C-C motif chemokine 5
Cd3e T-cell surface glycoprotein CD3 epsilon chain
Cd8a T-cell surface glycoprotein CD8 alpha chain
CDH1 Cadherin 1
CFC-113 Trichlorotrifluoroethane
CHOP C/EBP homologous protein
COX-2 Cyclooxygenase-2
C3 Complement C3
DAI Disease activity index
DAO Diamine oxidase
DHT Dihydrotestosterone
DSS Dextran sulfate sodium
EPO Eosinophil peroxidase
ER Endoplasmic reticulum
ERK Extracellular signal-regulated kinase
ET-1 Endothelin 1
EtOH Ethanol
Fabp2 Fatty acid binding protein 2
FD-4 FITC-conjugated dextran-4
Foxp3 Transcription factor forkhead box P3
FP Fractional precipitation
Fru Fructose
F4/80 Adhesion G protein-coupled receptor E1
Gal Galactose
GalA Galacturonic acid
GATA3 GATA-binding protein 3
Glc Glucose
GluA Glucuronic acid
GPC Gel permeation chromatography
GPR41 G protein-coupled receptor 41
GPR43 G protein-coupled receptor 43
GPx Glutathione peroxidase
Gro Cxcl1/2/3
GSH Glutathione
Hmgcs2 3-hydroxy-3-methylglutaryl-CoA synthase 2
HNF4-α Hepatocyte nuclear factor 4-α
HO-1 Heme oxygenase
Hp Haptoglobin
IBA Isobutyric acid
IBD Inflammatory bowel disease
ICAM-1 Intercellular adhesion molecule-1
IEC Ion-exchange chromatography
IFN-γ Interferon γ
IgA Immunoglobulin A
IgM Immunoglobin M
IκBα Inhibitor of nuclear factor-κB
IKK Inhibitor of nuclear factor-κB kinase
IL Interleukin
IL-22BP IL-22binding protein
IL-12p40 Interleukin 12B
Il21r Interleukin 21 receptor
iNOS Inducible nitric oxide synthase
IRE1α Inositol-requiring enzyme 1α
IRF4 Interferon regulatory factor 4
IRF5 Interferon regulatory factor 5
IVA Isovaleric acid
JAK2 Janus kinase 2
JNK C-Jun N-terminal kinase
Lck Lymphocyte cell-specific protein tyrosine kinase
LC3 Light chain 3
Ly6G Lymphocyte antigen 6 complex locus protein G
LPS Lipopolysaccharide
Man Mannose
MAPK Mitogen-activated protein kinases
MCP-1β Monocyte chemoattractant protein-1β
MDA Malondialdehyde

Mhc2 MHC class II antigen
MMP Mitochondrial membrane potential
MPO Myeloperoxidase
MUC1 Mucin 1
MUC2 Mucin 2
MW Molecular weight
NA Not Available
NF-κB Nuclear factor -κB
NLRP3 (NOD)-like receptor family pyrin domain containing 3
NO Nitric oxide
NOx Nitrites
NO3/NO2 Nitrate/nitrite
NSAIDs Nonsteroidal anti-inflammatory drugs
OCR Oxygen consumption rate
OFR Oxygen free radical
PA Propionic acid
p-ACC Phospho-acetyl-coA carboxylase
PCNA Proliferating cell nuclear antigen
PERK Protein kinase RNA-like ER kinase
p-ERK Phospho-extracellular signal-regulated kinase
PGE2 Prostaglandin E2
p-IκBα Phosphonated inhibitor of nuclear factor-κB
PI3K Phosphatidylinositol-3-kinase
p-JNK Phospho-c-jun N-terminal kinase
p62 Sequestosome 1
p65 Nuclear factor-κB p65
p-p38 Phospho-p38 mitogen-activated protein kinases
p-p65 Phospho-nuclear factor-κB-p65
p-STAT3 Phospho-signal transducer and activator of transcription 3
Ptgs2 Prostaglandin-endoperoxide synthase 2
Reg3β Regenerating islet-derived 3β
Reg3γ Regenerating islet-derived 3γ
Relmβ Resistin-like molecule β
Rha Rhamnose
Rib Ribose
RNS Reactive nitrogen species
ROR-γt Retinoid-related orphan nuclear receptor γt
ROS Reactive oxygen species
SCFAs Short chain fatty acids
Se Selenium
SOD Superoxide dismutase
STAT3 Signal transducer and activator of transcription 3
T-AOC Total antioxidant capacity
TCA Trichloroacetic acid
T-bet T-box protein 21
TER Transepithelial electrical resistance
TFF3 Trefoil factor 3
Th Helper T cells
TJs Tight junctions
TJP1 Tight junction protein 1
TLR4 Toll-like receptor 4
TNBS Trinitrobenzene sulfonic acid
TNF-α Tumor necrosis factor α
Trbv T-cell receptor beta chain V region;
Treg Regulatory T cell
TUNEL Terminal deoxynucleotidyl transferase-mediated dUTP nick end labeling
UA Uronic acid
ULK1 Unc51-like kinase 1
VA Valeric acid
XBP1 X-box binding protein 1
Xyl Xylose
ZO-1 Zonula occluden-1

frontiers in Pharmacology

ORIGINAL RESEARCH
published: 21 May 2021
doi: 10.3389/fphar.2021.640347

Metformin Affects Gut Microbiota Composition and Diversity Associated with Amelioration of Dextran Sulfate Sodium-Induced Colitis in Mice

*Zhiyi Liu[1,2†], Wangdi Liao[3†], Zihan Zhang[1,2], Ruipu Sun[1,2], Yunfei Luo[4], Qiongfeng Chen[4], Xin Li[3], Ruiling Lu[3] and Ying Ying[1,4,5]**

[1]Jiangxi Institute of Respiratory Disease, The First Affiliated Hospital of Nanchang University, Nanchang, China, [2]Queen Mary School, Nanchang University, Nanchang, China, [3]Departments of Gastroenterology, The First Affiliated Hospital of Nanchang University, Nanchang, China, [4]Department of Pathophysiology, Schools of Basic Medical Sciences, Nanchang University, Nanchang, China, [5]The Department of Respiratory and Critical Care Medicine, The First Affiliated Hospital of Nanchang University, Nanchang, China

OPEN ACCESS

Edited by:
Heike Wulff,
University of California, Davis,
United States

Reviewed by:
Antonella Marino Gammazza,
University of Palermo, Italy
Agata Mulak,
Wroclaw Medical University, Poland

***Correspondence:**
Ying Ying
yingying@ncu.edu.cn

[†]These authors have contributed equally to this work

Specialty section:
This article was submitted to Gastrointestinal and Hepatic Pharmacology, a section of the journal Frontiers in Pharmacology

Received: 11 December 2020
Accepted: 10 May 2021
Published: 21 May 2021

Citation:
Liu Z, Liao W, Zhang Z, Sun R, Luo Y, Chen Q, Li X, Lu R and Ying Y (2021) Metformin Affects Gut Microbiota Composition and Diversity Associated with Amelioration of Dextran Sulfate Sodium-Induced Colitis in Mice. Front. Pharmacol. 12:640347. doi: 10.3389/fphar.2021.640347

Background: Inflammatory bowel disease (IBD) is an increasingly common and globally emergent immune-mediated disorder. The etiology of IBD is complex, involving multiple factors such as immune dysregulation, environmental factors, genetic mutations, and microbiota dysbiosis, exacerbated by a lack of effective clinical therapies. Recently, studies hypothesized that dysbiosis of intestinal flora might participate in the onset of IBD. Metformin is widely used to treat type 2 diabetes and has shown beneficial effects in mouse models of IBD, although its underlying mechanisms remain poorly understood. Accumulating studies found that metformin shows beneficial effects for diabetes by affecting microbiota composition. This study explores possible regulatory effects of metformin on intestinal microecology during treatment for IBD.

Methods: Inflammation was induced using 3% Dextran Sulfate Sodium (DSS) solution to generate mice models of IBD. Metformin treatments were assayed by measuring body weights and colon lengths of mice and H&E staining to observe histological effects on colon tissue structures. Changes in bacterial community composition and diversity-related to IBD and metformin treatment were assessed by high-throughput metagenomic sequencing analysis.

Results: Metformin administration significantly ameliorated body weight loss, inhibited colon shrinking, and contributed to preserving the integrity of colon histological structures. The gut microbiota profiles revealed that the biodiversity of intestinal flora lost during inflammation was restored under metformin treatment. Metformin administration was also

Abbreviations: IBD, inflammatory bowel disease; DSS, dextran sodium sulfate; UC, ulcerative colitis; CD, crohn's disease; AMPK, 5′-adenosine mono-phosphate-activated protein kinase; H&E, hematoxylin and eosin; C group, control group; D group, DSS-induced colitis model group; MD group, metformin treatment for DSS-induced colitis group; P group, metformin pretreatment for DSS-induced colitis group; M group, metformin group; 16SrRNA, 16S ribosomal RNA; OTU, operational taxonomic unit; PBS, phosphate buffer saline; PCoA, principal coordinates analysis; PCR, polymerase chain reaction; LDA, linear discriminant analysis; LefSe, LDA effect size.

associated with decreased pathogenic *Escherichia shigella* and increased abundance of *Lactobacillus* and *Akkermansia*.

Conclusion: Metformin appears to induce anti-inflammatory effects, thus ameliorating colitis symptoms, concurrent with enrichment for beneficial taxa and restored microbial diversity, suggesting a viable strategy against IBD.

Keywords: inflammatory bowel disease, metformin, gut microbiota, anti-inflammatory effect, biodiversity

INTRODUCTION

Inflammatory bowel disease (IBD), characterized by chronic inflammatory disorders of the colon and small intestine, are common and widespread. Ulcerative colitis (UC) and Crohn's disease (CD) are the two main types of IBD, manifested with severe intestinal disorders, including diarrhea, abdominal pain, weight loss, and bloody stools (De Souza and Fiocchi, 2016). The IBD-associated immune reaction is triggered by intestinal components, especially gut microbiota, which are suspected of contributing to susceptibility to CD and UC (Ni et al., 2017). Evidence has been reported in both human and animal studies for a potential role for imbalance among gut microbiota in the pathogenic mechanisms of IBD (Matsuoka and Kanai, 2015; Nishida et al., 2018). According to clinical observations, the majority of colitis lesions in IBD patients are located in segments where gut microbes are highly concentrated, significantly associated with fecal accumulation, such as the colorectal terminal segment (Ni et al., 2017). Molecular and high-throughput sequencing analysis of gut microbiota in IBD patients has revealed changes in characteristic microbial profiles, or dysbiosis, characterized by disruption in the balance between commensal, intestinal probiotics, and opportunistic pathogens, ultimately resulting in decreased gut biodiversity (Wlodarska et al., 2015).

Metformin is a widely used drug for the treatment of type 2 diabetes, and its therapeutic mechanisms are associated with the activation of 5′-adenosine mono-phosphate-activated protein kinase (AMPK) to reduce insulin resistance. AMPK is also involved in anti-inflammatory pathways by inhibiting pro-inflammatory cytokines production (Kim et al., 2014), which suggests a therapeutic role for metformin in inflammatory disease and immune disorders. Furthermore, in diabetic and high-fat diet (HFD) rats, enrichment for a beneficial intestinal bacterial community was observed with long-term metformin treatment. The abundance of short-chain fatty acid-producing bacteria increased significantly, and the level of *Lactobacillus*, *Prevotella*, and A*kkermansia muciniphila* was also elevated, thus improving the maintenance of metabolic processes and the homeostasis of intestinal tissue (Bauer et al., 2018).

Here, we explored the intervention effects of metformin on dysbiosis of intestinal microecology in DSS-induced colitis mice model. To this end, we histologically evaluated the degree of inflammation in intestinal tissue structures, in addition to assessing overall changes in body weight and colon length under metformin pretreatment, treatment and non-treatment conditions during DSS-induced colitis. We also profiled gut microbiota via high-throughput sequencing of the v3-v4 region of 16s ribosomal DNA (rDNA) for metagenomic analysis of microbiota composition and diversity. We report restoration of diversity under metformin treatment that was lost under inflammatory conditions and enrichment for beneficial taxa associated with ameliorated colitis symptoms following metformin administration. This work provides insight into the relationship between metformin exposure and gut microbiota in an induced mouse model of intestinal colitis and suggests a potentially viable clinical strategy for this widespread disease.

MATERIALS AND METHODS

Experimental Animals

Forty C57BL/6 male mice, aged 8–10 weeks, were purchased from the laboratory animal center of Nanchang University. The mice were housed in a sterile, ventilated room for a week at 20–25°C and given sufficient sterile food and water. All the animal protocols were approved and followed the guidelines and laws of the Animal Care Committee of Nanchang University Jiangxi Medical College (Animal protocol: NCDXSYDWFL-2015097).

Instruments and Reagents

Dextran Sodium sulfate powder (Dextran Sulfate Sodium, DSS, MW 36,000–50,000) was purchased from the MP Biomedicals company (United States). Metformin was from Sigma (Germany). TransGen AP221-02:TransStart Fastpfu DNA Polymerase (TransGen Biotech, Beijing, China), AxyPrep DNA gel extraction kit (AXYGE, United States), QuantiFluorTM-ST (Promega, United States), TruSeqTM DNA Sample Prep Kit (Illumina, United States).

A bx-41 binocular optical microscope was purchased from Olympus company (Japan), polymerase chain reaction instrument (ABI GeneAmp® 9700, ABI, United States), Embedding cassettes (Citotest Labware Manufacturing Co., Ltd., China), KD-TS3D tissue processor (KEDEE, United States).

Induction of Experimental Intestinal Bowel Disease

The procedures of disease induction were carried out as follows. The C57BL/6 male mice were given sterile drinking water for acclimation 7 days before induction of colitis. Then forty mice were randomly divided into five groups (as shown in **Table 1**): 1) control group (C group) receiving sterile drinking water and PBS intraperitoneal

TABLE 1 | Grouping and time of medication.

Groups\Time(days)	Day 0	Day 1~3	Day 4~7
C group	PBS injection	Sterile water + PBS injection	Sterile water + PBS injection
D group	PBS injection	DSS solution + PBS injection	DSS solution + PBS injection
MD group	PBS injection	DSS solution + PBS injection	DSS solution + metfromin injection
P group	Metformin injection	DSS solution + metformin injection	DSS solution + metformin injection
M group	PBS injection	Sterile water + metformin injection	Sterile water + metformin injection

Note: C = Control, D = DSS group, MD = DSS + Metformin, P = DSS + pre-Metformin, M = Metformin.

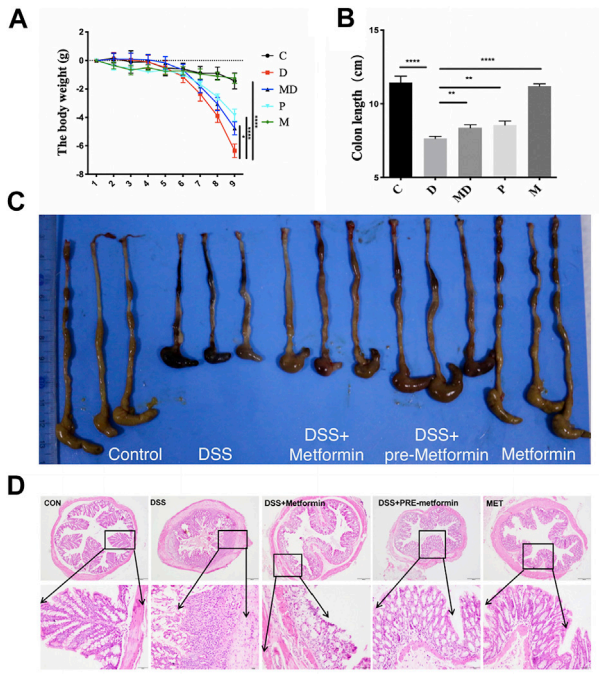

FIGURE 1 | Metformin prevents DSS-induced colitis in mice. C57BL/6 mice were divided into five groups and induced acute colitis by giving 3% DSS. The mice were treated with intraperitoneal PBS or metformin (150 mg/kg/day) daily. **(A)** The body weight changes during the colitis induction process. Significance was tested by Two-way ANOVA. $^{*}p < 0.05$ $^{****}p < 0.0001$, $n = 8$. **(B)** The colon length of each group. The Significance was analyzed by student t-test (mean ± SEM, $n = 8$), $^{**}p < 0.01$, $^{***}p < 0.001$. **(C)** The representative macroscopic image of mice colon. **(D)** Histology analyzed the severity of colitis in DSS with H&E staining. Representative images are shown. Overview: 100 ×; magnification: 400 ×, Scale bar = 100 μm and 20 μm.

injection. 2) DSS-induced colitis model group (D group) receiving PBS intraperitoneal injection. 3) metformin treatment for DSS-induced colitis (MD group) receiving metformin intraperitoneal injection (150 mg/kg/day) 3 days after disease induction. 4) metformin pretreatment for DSS-induced colitis group (P group) receiving metformin injection (150 mg/kg/day) one day before disease induction. 5) metformin group (M group) receiving sterile water and intraperitoneal injection of metformin (150 mg/kg/day). The weight of each mouse was measured daily at the same time. At eight days after giving 3% DSS solution, the mice were sacrificed, and the length of the colons above 5 mm from the end of the rectum was measured and recorded. After rinsed by PBS solution, the colons were divided into the upper, middle, and lower segments, and the middle parts were collected. The feces samples were rapidly collected from the end of the colon and stored in −80°C refrigerator.

Histopathological Analysis

The colon tissues were fixed in 4% formalin solution for 24 h and then washed thoroughly with PBS solution, dehydrated, and embedded in paraffin. The tissues were cut into 4 μm slices by lycra slicer and stained with H&E stain. Finally, the tissue sections were observed and photographed at 100x and 400x magnification with an optical microscope.

Gut Microbiota Analysis

The feces samples kept in dry ice was sent to Shanghai Majorbio Biopharm Technology Co., Ltd., for DNA extraction and sequencing. The gut microbiota DNA was extracted from lumenal stools, and PCR reactions amplified the fragments of 16s rDNA v3-v4 region with TransStart Fastpfu DNA Polymerase (AP221-02), and the final products were quantified by QuantiFluorTM-ST (Promega, Beijing, China). The DNA was collected by AxyPrep DNA gel extraction kit (AxyPrep Co., Ltd.). Then, the purified DNA products were processed by TruSeqTM DNA Sample Prep Kit and sequenced by Illumina Miseq. The sequencing data were spliced, quality controlled to obtain an optimized sequence with FLASH (v1.2.11). Moreover, subsequently, the bacterial sequences were clustered by Uparse (v7.0.1090) on the level of OTU (Operational Taxonomic Units) that classifies bacteria with 97% similarity of 16 s gene sequences. The OTU abundance table was conducted for subsequent biogenetic analysis.

The alpha diversity of observed OTU level and Shannon index were analyzed on the platform of the Majorbio cloud. Beta diversity analysis based on the Bray Curtis distance and Weighted unifrac algorithm was presented by the Principal coordinate analysis (PCoA) figure, and Adonis calculated the difference between groups. The linear discriminant analysis effect size (LEfSe) analysis was performed to represent the biomarkers of samples on different taxonomic levels using the LDS score to estimate the influence of richness on the extent of the difference.

Statistical Analysis

The data and statistical analysis were conducted by GraphPad Prism (v.8.2.1). The results of the quantitative analysis were presented by mean ± standard error of the mean (SEM). The significant differences were evaluated either by unpaired Student's *t*-test, two-way analysis of variance and by Wilcoxon

rank-sum method or Mann-Whitney U test for non-parametric data. $p < 0.05$ indicates statistical significance. Asterisks used to indicate significance correspond with: $^{*}p < 0.05$, $^{**}p < 0.01$, $^{***}p < 0.001$.

RESULTS

Metformin Ameliorates General Symptoms and Histopathological Change in DSS-Induced Colitis Mice

Prior to investigating a potential relationship between metformin and microbiota in the amelioration of UC and IBD, we first examined the effects of metformin treatment on C57BL/six mouse body weight and colon length. The weights of individual mice were measured daily during the colitis induction period (**Figure 1A**). The body weights of the control (C) and metformin-treated healthy mice (M) similarly showed a slight but non-significant decrease during the first two days of treatment but remained stable over the remaining period of model establishment. In contrast, the DSS-induced colitis (D) and DSS-induced colitis with metformin treatment (MD) groups did not show any apparent weight loss until the third day, at which point the D group exhibited a dramatic weight reduction following DSS administration, while the MD group showed significant alleviation of colitis-associated weight loss ($p < 0.05$). The mice that received metformin pretreatment (P) showed slight weight loss but had delayed occurrence and a smaller range of weight loss compared with the D group ($p < 0.0001$).

These changes in body weight due to DSS were reflected by a marked decrease in colon lengths of induced colitis mice (**Figure 1B**). The colons of the C and M mice were the longest among these five groups, significantly longer than those of the D group ($p < 0.0001$). In addition, metformin treatment (M) and pretreatment (p) significantly inhibited colon shortening compared with untreated colitis (D) mice ($p < 0.01$) but did not show complete restoration of the colon length to that of non-colitis mice. These results show that metformin administration can counteract colitis's negative impacts on body weight and colon length in DSS-induced colitis mice.

To better understand the changes associated with colitis and metformin treatment at the cellular level in colon tissue, we conducted a histological evaluation of each treatment group (**Figure 1D**). To this end, colon sections from each of the five groups were sampled at the eighth day after giving DSS solution, processed by H&E staining, and observed by light microscopy. At 100X magnification, we observed that the intestinal layer and glands of the D group exhibited substantially greater inflammatory cell infiltration in the mucosal epithelium and lamina propria, loss of glandular parts, and hypertrophy of the colon wall compared to that of C and M groups. In the MD and p groups, the muscular layers were more intact, and the arrangement of intestinal glands appeared relatively healthy. Under 400X magnification, we found that the mucosal columnar epithelium and goblet cells in the gut glands were severely damaged, and the architectures of both crypt and villus were disrupted in the colons of D group mice. In sharp contrast with MD and p groups after metformin treatment, the inflammatory cells were significantly decreased, and more intact mucosal epithelium was observed. Moreover, more significant alleviation of inflammation was observed among P group mice, with a large number of goblet cells and longer, well-organized glands. These results together indicate that metformin protects the histological architecture of the colon and ameliorate pathological damages during the process of colitis induction.

Metformin Restores Biodiversity of Gut Microbiota in Induced-Colitis Mice

In light of the apparent damage associated with colitis and the effects of metformin treatment, we evaluated differences in gut microbial diversity among the treatment groups. The results of observed-OTU index analysis showed that the M group had the highest diversity of OTUs, which was significantly greater than that of the other four groups ($p < 0.05$) (**Figure 2A**). However, there was no significant difference in either the observed-OTU or Shannon Alpha diversity indexes between the MD group and D groups (**Figures 2A,B**), although the trend indicated increasing diversity of intestinal flora after metformin treatment. Meanwhile, p group mice showed considerable restoration of bacterial diversity with longer metformin treatment courses and were significantly different from the D group ($p < 0.05$) (**Figure 2A**).

The results of OTU-level principal component analysis (PCA) revealed differences in Beta diversity, an indicator of group similarity calculated by the Bray_Curtis distance and Weighted_unifrac algorithms, among these groups (**Figures 2D,C**). The C and M groups shared a large overlapping area that suggested a large number of bacteria were shared between these two groups, whereas the biological composition of gut microbiota was significantly changed in the D group. Clustering patterns of the MD and P groups revealed that they became more similar to the C group following metformin treatment, while the difference between the P and C groups was smaller than that between the MD and C groups. These results indicate that metformin treatment does not affect healthy microbiota diversity but can restore the diversity of mice with induced colitis.

Metformin Restores Gut Microbiota Composition of Induced-Colitis Colons

We then conducted LEfSe analysis to identify differentially enriched microbiota within each group that could potentially serve as biomarkers for colitis in the gut. This analysis showed that at the phylum level, the M group was significantly associated with *Bacteroidetes*, D group with *Proteobacteria*, MD group with *Firmicutes*, and the P group with *Actinobacteria* (**Figures 3A,B**). Analysis of phylum-level (other <0.01) community composition showed that

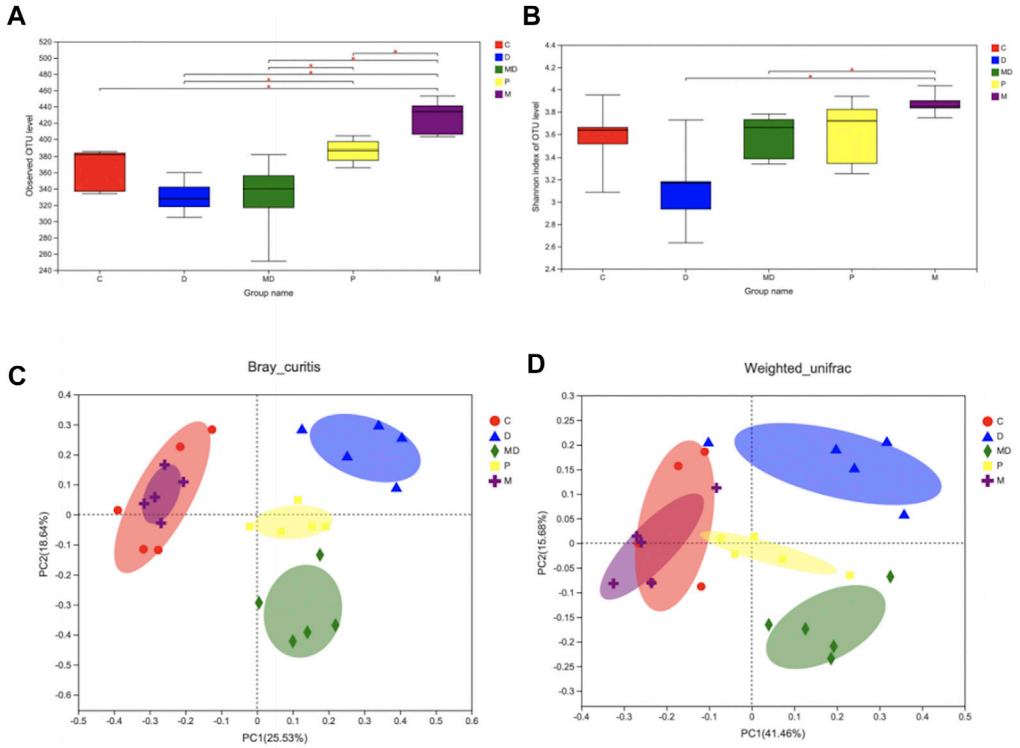

FIGURE 2 | Metformin restores the species diversity and richness of gut microbiota in DSS-induced colitis. **(A)** The Alpha-diversity index is based on observe-OTU of intestinal flora within each group. **(B)** The Alpha-diversity index is based on Shannon of intestinal flora within each group. **(C)** Beta-diversity (PCoA analysis based on Bray_curitis). **(D)** Beta-diversity (PCoA analysis based on Weighted_unifrac). Significance was tested by Wilcoxon rank-sum method. (Data are presented as mean ± SEM.*$p < 0.05$. C = Control, D = DSS + PBS injection, MD = DSS + Metformin injection, P = pre-Metformin injection, M = only Metformin injection).

Bacteroidetes, *Firmicutes*, *Proteobacteria*, *Verrucomicrobia*, and *Actinobacteria* accounted for the largest proportions of phyla in all groups (**Figure 3C**). Community barplot analysis of genus-level (other <0.01) also showed that *Escherichia-Shigella*, *Lactobacillus,* and *Akkermansia* and *Ricknellaceae* taxa which are potentially associated with IBD pathogenesis and therapeutic effects of metformin, were varied among D, MD, and P groups (**Figure 3D**). Further analysis of the relative abundance of individual taxa revealed that the C and M groups shared a similar proportion of these four bacteria (**Figures 3E–H**). However, compared with the C group, the D group showed a significant increase in *Escherichia-Shigell*a, although the growth of this genus was inhibited in the MD and P groups. The relative abundances of *Lactobacillus*, *Akkermansia, and Ricknellaceae* were significantly reduced in the D group compared with control mice but exhibited a substantial increase after treatment with metformin. The pretreatment group also showed significantly higher levels of *Lactobacillus, Akkermansia, and Ricknellaceae* than those of the D group ($p < 0.01$). These results together suggest that disruption of colon community composition by colitis, resulting in over-representation of disease-associated taxa, can be restored by metformin treatment to a similar composition as that of a healthy colon environment.

DISCUSSION

In this study, we examined the potential inflammatory disease therapeutic metformin for its effects on diversity and composition of colon microbiota in a DSS-induced mouse model of IBD. We confirmed that induced colitis disrupted the architecture of the intestinal epithelium and subsequently enriched the guts of these mice for bacterial taxa associated with inflammatory disease. Our results showed that treatment with metformin did not disrupt the microbiota composition or diversity of healthy mice. Moreover, metformin administration, either before or after the induction of colitis, resulted in amelioration of physical symptoms and also partially restored microbiota composition and diversity to more closely resemble that of healthy, non-colitis mice. Notably, we identified several enriched phyla that were indicative of specific treatments or disease states. Most notably, we observed the differential prevalence of genera that were significantly associated with disease, such as *Escherichia* sp., which were absent from healthy mice but enriched in colitic mice, *Lactobacillus*, which were prevalent in healthy and metformin-treated mice, and *Akkermansia*, which was absent in colitic mice but restored in metformin-treated mice. We also found high amounts of *Ricknellaceae*, which were specifically enriched during and after colitis, and *Turicibacter*, which were absent from the healthy controls. Our findings provide useful insights

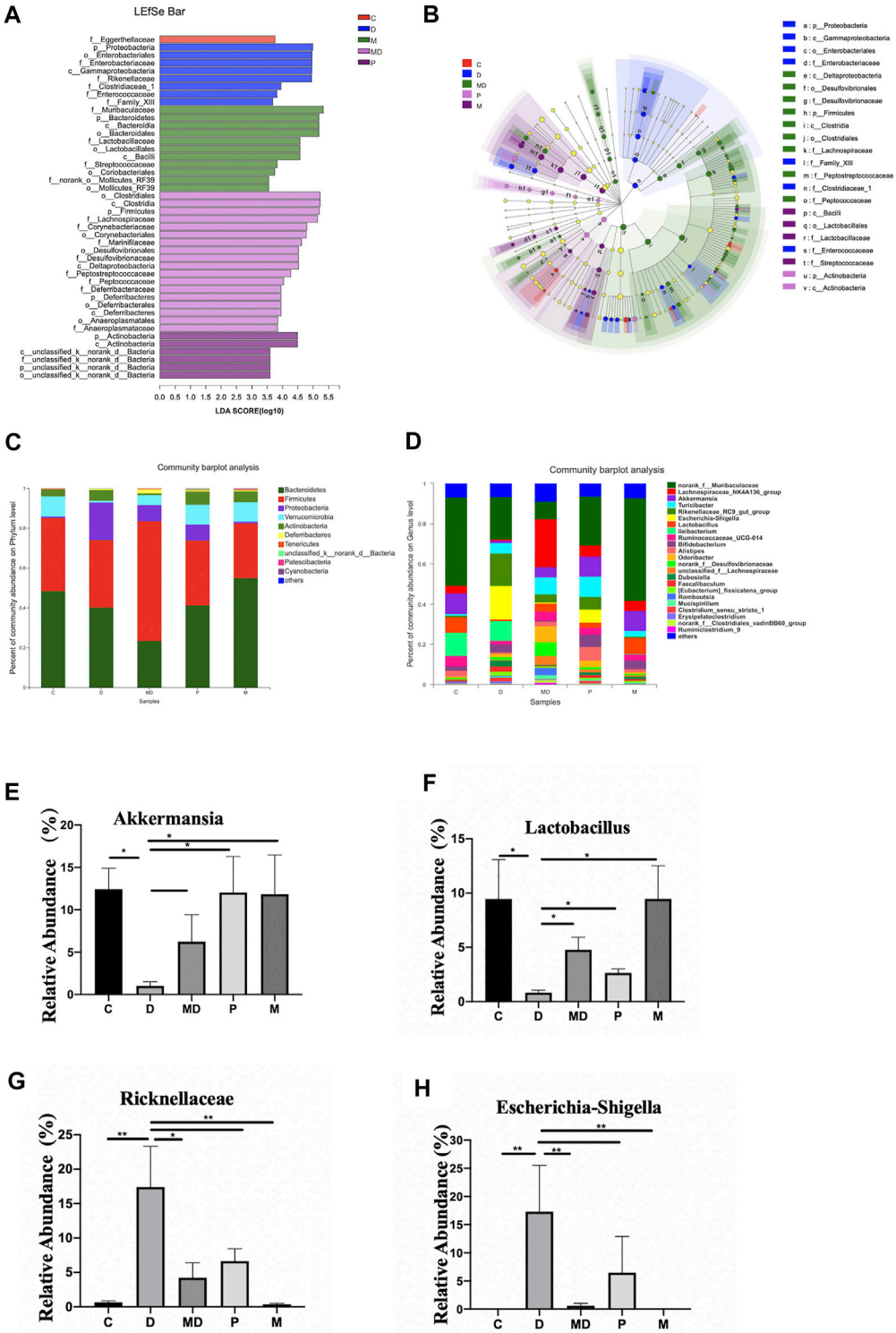

FIGURE 3 | Metformin exerts regulatory effects on the balance of some inflammation-related bacteria proportion and the overall composition of the community. **(A)** The bar plot of differential microbiota distribution among different groups based on LDA value. **(B)** The cladogram of differential microbiota on the level from Phylum to Family among different groups. **(C)** The bar plot of community composition on the Phylum level. **(D)** The bar plot of community composition on the Genus level. **(E)** The relative abundance of *Escherichia shigella* **(F)** *Lactobacillus* **(G)** *Akkermansia* **(H)** *Ricknellaceae* within each group. The *p*-value was calculated by the Mann-Whitney *U* test. **p* < 0.05, ***p* < 0.01. C = Control, D = DSS group. MD = DSS + Metformin, P = DSS + pre-Metformin, M = Metformin.

into the effects of metformin on enrichment for gut bacteria associated with healthy colon conditions during treatment for IBD.

Phenotypic examination of the induced-colitis mice confirmed that body weight and colon length were both reduced by colitis and that intestinal glands had severe infiltration by inflammatory cells infiltration, disrupted intestinal crypts, and depletion of goblet cells. These symptoms of dysbiosis in the gut microenvironment have been previously associated with pathogenic taxa (Ni et al., 2017), which are both enriched by inflammatory conditions, and also contribute to the disease progression. Intestinal microbiota has been shown to participate in interaction networks resulting in the formation of a protective barrier that can suppress excessive immune responses and ensure the integrity of the intestinal tract (Wu et al., 2020). Previous work in a mouse model of IBD has shown that metformin administration can attenuate inflammation and exert protective effects on the intestinal barrier (Lee et al., 2015). Moreover, a recent longitudinal cohort study found that long-term use of metformin provided prophylactic effects against IBD in type 2 diabetes mellitus patients (Tseng, 2020). Metformin may potentially preserve the community composition of healthy state gut microbiota through proposed anti-inflammatory mechanisms, including inhibition of pro-inflammatory cytokines production (Xue et al., 2016), activation of AMPK (Bułdak et al., 2016), improved insulin resistance (Viollet et al., 2012), or up-regulation of postbiotic (short-chain fatty acid and vitamin D) production. However, much further investigation is required to establish a causative relationship between metformin administration and restoration of healthy microbiota in IBD patients.

We next focused on the beneficial effects of metformin on the diversity of intestinal flora. The alpha diversity index at the OTU level indicated that metformin treatment leads to increased richness and diversity of gut microbiota, which ameliorated the dominance of fewer, inflammation-associated taxa, and hence the low bacterial biodiversity of colitic mice. We observed an increasing trend but no significant difference in alpha diversity between the D and MD groups, and this might indicate that the influence of metformin to restore gut biodiversity may also rely on other contributing factors, such as treatment time, diet. For example, our diversity analysis of the P group showed that a longer treatment course or a prophylactic treatment with metformin facilitated the recovery of biodiversity. This finding is consistent with that reported by Zhang and colleagues, who found metformin effect to increase microbial diversity in diabetic mice (Zhang et al., 2019). Nevertheless, mice fed with a high-fat diet exhibited had reduced microbial diversity after metformin administration, whereas mice fed with chow and treated with metformin did not experience a significant change in gut biodiversity (Zhang et al., 2015). One possible explanation for these variations in the effects of metformin is that metformin can ostensibly shift microbial diversity toward ecological equilibrium, as proposed by Elbert and co-workers, but in a manner dependent on other factors such as disease or diet since metformin did not appear to shift the diversity of healthy communities (Elbere et al., 2018).

Several specific pathogens reported to induce or exacerbate IBD-associated diseases, e.g., *Mycobacterium paratuberculosis* (Crohn's disease) (Zarei-Kordshouli et al., 2019) or *Fusobacterium nucleatum (ulcerative colitis)* (Chen et al., 2020), are likely to outcompete and subsequently reduce the abundance of beneficial microbiota that bind to epithelial receptors for survival, such as *Lactobacillus* and butyrate-producing bacteria (e.g., *Faecalibacterium prausnitzii*) (Takaishi et al., 2008; Eppinga et al., 2016). Under healthy conditions, these beneficial taxa help stabilize intestinal flora by inhibiting pathogen colonization, promoting mucus production, and enhancing immune response (Wlodarska et al., 2015). We observed the loss of several potentially beneficial taxa, as well as enrichment for other poorly understood, and potentially pathogenic OTUs, from colitic mice. At the phylum level, IBD patients have characteristically reduced ratios of obligate anaerobes such as *Firmicute* and *Bacteroidetes*, but enriched levels of facultative anaerobes, especially *Proteobacteria* and *Actinobacteria* (Matsuoka and Kanai, 2015). Consistent with these prior studies, we observed a significantly higher abundance of *Proteobacteria*, especially *Escherichia-Shigella* associated with the untreated (D) colitis group, which has been correlated with relapse of Crohn's disease in other studies (Bai and Ouyang, 2006; Cantó et al., 2019). However, we also observed increased *Firmicute abundance* in the treated (MD) colitis group, strongly suggesting that metformin may help restore taxa associated with health conditions. However, whether and how metformin promotes colonization of specific taxa requires much more in-depth investigation.

In this study, we also found that the relative abundances of few probiotics were significantly enriched in response to metformin treatment (and especially in the pretreatment group), such as that of *Akkermansia,* which has been reported by similar previous studies (Guo et al., 2017). This commensal species reportedly inhibits enteric disease development by maintaining the integrity of the mucosal barrier through mucin degradation, which leads to the freshening of the mucosa, prevention of pathogen establishment, and a clean environment conducive to physiological function (Everard et al., 2013). Moreover, *Akkermansia* administration also reportedly contributed to the prevention of weight loss and inflammatory responses associated with IBD (Bian et al., 2019). Similarly, *Lactobacillus* sp. abundance decreased in the diseased group but was restored after metformin treatment, which was consistent with the previously observed effect of metformin (Zhang et al., 2019). However, in contrast with *Akkermansia*, pretreatment had no apparent positive effects on *Lactobacillus* abundance compared with direct treatment. Interestingly, we found that *Ricknellaceae* abundance increased after metformin treatment, consistent with fluctuations related to *Ilex kudingcha* and 2-O-β-D-glucopyranosyl-L-ascorbic acid treatment of DSS-induced colitis. (Huang et al., 2019; Wan

et al., 2019), although its relationship with colitis requires further investigation.

In marked contrast with these non-pathogens, *Escherichia shigella*, a common, opportunistic, causative agent for diarrhea(Kotloff et al., 2013), was suppressed after metformin administration. *Escherichia shigella* may enhance the side effects of metformin, and 20–30% of patients with long-term metformin treatment had moderately increased abundance of *E. shigella* abundance, associated with mild diarrhea, in agreement with its enrichment in pretreated mice that had longer metformin courses (Elbere et al., 2018). However, we found that *E. shigella* was not significantly enriched in metformin-treated healthy mice, nor did these mice display diarrhea. In fact, E. *shigella* abundance decreased in diseased mice following metformin treatment, indicating that the relationship between metformin and this pathogen warrants closer scrutiny, perhaps under isolated, *in vitro* conditions.

CONCLUSION

In conclusion, our study showed the effects of metformin on intestinal flora during treatment for IBD, especially highlighting the restoration of microbial diversity and enrichment in the relative abundance of specific taxa. These effects on gut microbiota appear to be related to anti-inflammatory effects required for the alleviation of the symptom of DSS-induced colitis. Therefore, we propose that metformin is a strong potential candidate for IBD therapy, and further investigation of metformin-induced changes in gut microbiota and its anti-inflammatory effects should be investigated to clarify its molecular interactions the gut.

DATA AVAILABILITY STATEMENT

The data generated in this article can be found here: https://www.ncbi.nlm.nih.gov/sra/PRJNA682001.

ETHICS STATEMENT

The animal study was reviewed and approved by the Animal Care Committee of Nanchang University Jiangxi Medical College.

AUTHOR CONTRIBUTIONS

ZL, ZZ, YL, RS, and QC contributed to carry out the research. ZL analyzed data and prepared the manuscript. YY and WL designed the study. RL and XL supervised the experiments. ZL and YY edited the manuscript.

FUNDING

This study was supported by the National Natural Science Foundation of China (No. 81960110), Nanchang University Students' Innovation and Entrepreneurship Training Program (No. 2020CX299).

ACKNOWLEDGMENTS

This work included ZL's dissertation at the Queen Mary University of London. We thank Giulia De *Falco*, Zhimin Tang, Yang Liu for their guidance and advice.

REFERENCES

Bai, A.-P., and Ouyang, Q. (2006). Probiotics and Inflammatory Bowel Diseases. *Postgrad. Med. J.* 82, 376–382. doi:10.1136/pgmj.2005.040899

Bauer, P. V., Duca, F. A., Waise, T. M. Z., Rasmussen, B. A., Abraham, M. A., Dranse, H. J., et al. (2018). Metformin Alters Upper Small Intestinal Microbiota that Impact a Glucose-SGLT1-Sensing Glucoregulatory Pathway. *Cel Metab.* 27, 101–117. doi:10.1016/j.cmet.2017.09.019

Bian, X., Wu, W., Yang, L., Lv, L., Wang, Q., Li, Y., et al. (2019). Administration of Akkermansia Muciniphila Ameliorates Dextran Sulfate Sodium-Induced Ulcerative Colitis in Mice. *Front. Microbiol.* 10, 2259. doi:10.3389/fmicb.2019.02259

Bułdak, Ł., Machnik, G., Bułdak, R. J., Łabuzek, K., Bołdys, A., and Okopień, B. (2016). Exenatide and Metformin Express Their Anti-inflammatory Effects on Human Monocytes/macrophages by the Attenuation of MAPKs and NFκB Signaling. *Naunyn. Schmiedebergs. Arch. Pharmacol.* 389, 1103-1115. doi:10.1007/s00210-016-1277-8

Cantó, E., Zamora, C., Garcia-Planella, E., Gordillo, J., Ortiz, M. A., Perea, L., et al. (2019). Bacteria-related Events and the Immunological Response of Onset and Relapse Adult Crohn's Disease Patients. *J. Crohn's Colitis.* 13, 92–99. doi:10.1093/ecco-jcc/jjy138

Chen, Y., Chen, Y., Cao, P., Su, W., Zhan, N., and Dong, W. (2020). Fusobacterium Nucleatum Facilitates Ulcerative Colitis through Activating IL-17F Signaling to NF-κB via the Upregulation of CARD3 Expression. *J. Pathol.* 250, 170–182. doi:10.1002/path.5358

De Souza, H. S. P., and Fiocchi, C. (2016). Immunopathogenesis of IBD: Current State of the Art. *Nat. Rev. Gastroenterol. Hepatol.* 13, 13–27. doi:10.1038/nrgastro.2015.186

Elbere, I., Kalnina, I., Silamikelis, I., Konrade, I., Zaharenko, L., Sekace, K., et al. (2018). Association of Metformin Administration with Gut Microbiome Dysbiosis in Healthy Volunteers. *PLoS One* 13, e0204317. doi:10.1371/journal.pone.0204317

Eppinga, H., Sperna Weiland, C. J., Thio, H. B., van der Woude, C. J., Nijsten, T. E. C., Peppelenbosch, M. P., et al. (2016). Similar Depletion of ProtectiveFaecalibacterium Prausnitziiin Psoriasis and Inflammatory Bowel Disease, but Not in Hidradenitis Suppurativa. *Eccojc* 10, 1067–1075. doi:10.1093/ecco-jcc/jjw070

Everard, A., Belzer, C., Geurts, L., Ouwerkerk, J. P., Druart, C., Bindels, L. B., et al. (2013). Cross-talk between Akkermansia Muciniphila and Intestinal Epithelium Controls Diet-Induced Obesity. *Proc. Natl. Acad. Sci.* 110, 9066–9071. doi:10.1073/pnas.1219451110

Guo, X., Li, S., Zhang, J., Wu, F., Li, X., Wu, D., et al. (2017). Genome Sequencing of 39 Akkermansia Muciniphila Isolates Reveals its Population Structure, Genomic and Functional Diverisity, and Global Distribution in Mammalian Gut Microbiotas. *BMC Genomics* 18, 800. doi:10.1186/s12864-017-4195-3

Huang, K., Dong, W., Liu, W., Yan, Y., Wan, P., Peng, Y., et al. (2019). 2-O-β-d-Glucopyranosyl-l-ascorbic Acid, an Ascorbic Acid Derivative Isolated from the Fruits of Lycium Barbarum L., Modulates Gut Microbiota and Palliates Colitis in Dextran Sodium Sulfate-Induced Colitis in Mice. *J. Agric. Food Chem.* 67, 11408–11419. doi:10.1021/acs.jafc.9b04411

Kim, J., Kwak, H. J., Cha, J.-Y., Jeong, Y.-S., Rhee, S. D., Kim, K. R., et al. (2014). Metformin Suppresses Lipopolysaccharide (LPS)-induced Inflammatory Response in Murine Macrophages via Activating Transcription Factor-3 (ATF-3) Induction. *J. Biol. Chem.* 289, 23246–23255. doi:10.1074/jbc.M114.577908

Kotloff, K. L., Nataro, J. P., Blackwelder, W. C., Nasrin, D., Farag, T. H., Panchalingam, S., et al. (2013). Burden and Aetiology of Diarrhoeal Disease in Infants and Young Children in Developing Countries (The Global Enteric Multicenter Study, GEMS): A Prospective, Case-Control Study. *Lancet* 382, 209-222. doi:10.1016/S0140-6736(13)60844-2

Lee, S.-Y., Lee, S. H., Yang, E.-J., Kim, E.-K., Kim, J.-K., Shin, D.-Y., et al. (2015). Metformin Ameliorates Inflammatory Bowel Disease by Suppression of the Stat3 Signaling Pathway and Regulation of the between Th17/Treg Balance. *PLoS One* 10, e0135858–12. doi:10.1371/journal.pone.0135858

Matsuoka, K., and Kanai, T. (2015). The Gut Microbiota and Inflammatory Bowel Disease. *Semin. Immunopathol.* 37, 47–55. doi:10.1007/s00281-014-0454-4

Ni, J., Wu, G. D., Albenberg, L., and Tomov, V. T. (2017). Gut Microbiota and IBD: Causation or Correlation? *Nat. Rev. Gastroenterol. Hepatol.* 14, 573–584. doi:10.1038/nrgastro.2017.88

Nishida, A., Inoue, R., Inatomi, O., Bamba, S., Naito, Y., and Andoh, A. (2018). Gut Microbiota in the Pathogenesis of Inflammatory Bowel Disease. *Clin. J. Gastroenterol.* 11, 1–10. doi:10.1007/s12328-017-0813-5

Takaishi, H., Matsuki, T., Nakazawa, A., Takada, T., Kado, S., Asahara, T., et al. (2008). Imbalance in Intestinal Microflora Constitution Could Be Involved in the Pathogenesis of Inflammatory Bowel Disease. *Int. J. Med. Microbiol.* 298, 463–472. doi:10.1016/j.ijmm.2007.07.016

Tseng, C.-H. (2020). Metformin Use Is Associated with a Lower Risk of Inflammatory Bowel Disease in Patients with Type 2 Diabetes Mellitus. *J. Crohns. Colitis.* 15, 64, 73. doi:10.1093/ecco-jcc/jjaa136

Viollet, B., Guigas, B., Garcia, N. S., Leclerc, J., Foretz, M., and Andreelli, F. (2012). Cellular and Molecular Mechanisms of Metformin: An Overview. *Clin. Sci.* 122, 253–270. doi:10.1042/CS20110386

Wan, P., Peng, Y., Chen, G., Xie, M., Dai, Z., Huang, K., et al. (2019). Modulation of Gut Microbiota by Ilex Kudingcha Improves Dextran Sulfate Sodium-Induced Colitis. *Food Res. Int.* 126, 108595. doi:10.1016/j.foodres.2019.108595

Wlodarska, M., Kostic, A. D., and Xavier, R. J. (2015). An Integrative View of Microbiome-Host Interactions in Inflammatory Bowel Diseases. *Cell Host & Microbe* 17, 577–591. doi:10.1016/j.chom.2015.04.008

Wu, H., Rao, Q., Ma, G.-C., Yu, X.-H., Zhang, C.-E., and Ma, Z.-J. (2020). Effect of Triptolide on Dextran Sodium Sulfate-Induced Ulcerative Colitis and Gut Microbiota in Mice. *Front. Pharmacol.* 10. doi:10.3389/fphar.2019.01652

Xue, Y., Zhang, H., Sun, X., and Zhu, M.-J. (2016). Metformin Improves Ileal Epithelial Barrier Function in Interleukin-10 Deficient Mice. *PLoS One* 11, e0168670. doi:10.1371/journal.pone.0168670

Zarei-Kordshouli, F., Geramizadeh, B., and Khodakaram-Tafti, A. (2019). Prevalence of *Mycobacterium avium* Subspecies Paratuberculosis IS 900 DNA in Biopsy Tissues from Patients with Crohn's Disease: Histopathological and Molecular Comparison with Johne's Disease in Fars Province of Iran. *BMC Infect. Dis.* 19, 23. doi:10.1186/s12879-018-3619-2

Zhang, W., Xu, J.-H., Yu, T., and Chen, Q.-K. (2019). Effects of Berberine and Metformin on Intestinal Inflammation and Gut Microbiome Composition in Db/db Mice. *Biomed. Pharmacother.* 118, 109131. doi:10.1016/j.biopha.2019.109131

Zhang, X., Zhao, Y., Xu, J., Xue, Z., Zhang, M., Pang, X., et al. (2015). Modulation of Gut Microbiota by Berberine and Metformin during the Treatment of High-Fat Diet-Induced Obesity in Rats. *Sci. Rep.* 5. doi:10.1038/srep14405

Conflict of Interest: The authors declare that the research was conducted in the absence of any commercial or financial relationships that could be construed as a potential conflict of interest.

Advantages of publishing in Frontiers

OPEN ACCESS
Articles are free to read for greatest visibility and readership

FAST PUBLICATION
Around 90 days from submission to decision

HIGH QUALITY PEER-REVIEW
Rigorous, collaborative, and constructive peer-review

TRANSPARENT PEER-REVIEW
Editors and reviewers acknowledged by name on published articles

Frontiers
Avenue du Tribunal-Fédéral 34
1005 Lausanne | Switzerland

Visit us: www.frontiersin.org
Contact us: frontiersin.org/about/contact

REPRODUCIBILITY OF RESEARCH
Support open data and methods to enhance research reproducibility

DIGITAL PUBLISHING
Articles designed for optimal readership across devices

FOLLOW US
@frontiersin

IMPACT METRICS
Advanced article metrics track visibility across digital media

EXTENSIVE PROMOTION
Marketing and promotion of impactful research

LOOP RESEARCH NETWORK
Our network increases your article's readership